MODEL-BASED DETECTION IN CYBER-PHYSICAL SYSTEMS

By

Ashraf M. Tantawy

Dissertation

Submitted to the Faculty of the

Graduate School of Vanderbilt University

in partial fulfillment of the requirements

for the degree of

DOCTOR OF PHILOSOPHY

in

Electrical Engineering

December, 2011

Nashville, Tennessee

Approved:

Xenofon Koutsoukos

Gautam Biswas

Gabor Karsai

Mitchell Wilkes

Akos Ledeczi

ABSTRACT

Cyber-Physical Systems are tight integrations of computational and physical processes. Detection of abnormal behavior in cyber-physical systems is crucial for their safe and reliable operation. Model-based detection can improve the system detection performance by incorporating the system behavioral knowledge, captured by the system model, into the design process of detection systems. The components to be modeled, as well as the model complexity, are determined by the specific application and the objective of the study. Classical model-based detection systems have focused on (i) the use of simplified models for the physical system, (ii) the classical abrupt persistent faults, and (iii) the physical system while ignoring other cyber-physical system components. This dissertation addresses the following challenges in model-based detection (i) development of detailed models for physical systems, where simplified models are classically used, (ii) detection of intermittent and incipient faults in physical systems, in addition to persistent faults, and (iii) integration of the wireless communication network in the design of detection systems. These challenges are addressed as follows. First, a novel hybrid dynamical model for aircraft generators is developed to demonstrate the power of physics-based modeling. Second, a general algorithm that is based on change detection theory is developed to detect persistent, intermittent, and incipient faults. The effectiveness of the algorithm is demonstrated by real life case studies. Finally, a unified design process is developed to integrate the wireless communication network and multiple quality measures into the design process of detection systems. The design process is applied on wireless sensor networks with different communication protocols and topologies, and the performance improvement is demonstrated.

DEDICATION

To my mother, for her continuous prayer.

To my father, who was a Vanderbilt student 48 years ago.....I hope I made your dream come true.

ACKNOWLEDGEMENTS

In completion of this thesis, I would like to express my deep gratitude for my supervisor Professor Xenofon Koutsoukos for his continued advice and guidance during the different stages of my research which has made this work possible. I am also sincerely grateful for professor Gautam Biswas for his invaluable comments and support that have been a great help for developing this research. Also, I would like to thank Professor Gabor Karsai, Mitchell Wilkes, and Akos Ledeczi for their helpful comments on my research work. I am also obliged to my colleagues in ModEs lab, Heath Leblanc and Emeka Eyisi, for the various discussions that have provided me with numerous insights that have helped in this research. I would like also to show my gratitude to the ISIS administration and staff for their professionalism and precision that have been a great help in facilitating my work as a research student. Last but not least, I would like to thank Vanderbilt university librarians for being always helpful and friendly and for their sincere efforts in providing different research materials that have helped in accomplishing this thesis.

TABLE OF CONTENTS

Page

LIST OF TABLES

Page

LIST OF FIGURES

Page

Nomenclature

$\mathcal{H}_0$	Null hypothesis
$\mathcal{H}_1$	Alternative hypothesis
P_D	Probability of detection
P_F	Probability of false alarm
P_M	Probability of missed detection
BSC	Binary Symmetric Channel
CDMA	Code Division Multiple Access
CLD	Cross Layer Design
COTS	Commercial Off-The-Shelf
CPS	Cyber-Physical System
CSI	Channel State Information
CT	Current Transformer
DD	Decentralized Detection
DLC	Data Link Control
DPCT	Differential Protection Current Transformer
EPS	Electrical Power System
FDI	Fault Detection and Isolation
FDMA	Frequency Division Multiple Access
FSK	Frequency Shift Keying

GCU Generator Control Unit

GLR Generalized Likelihood Ratio

GLRT Generalized Likelihood Ratio Test

IDG Integrated Drive Generator

IID Independent and Identically Distributed

KKT Karush-Kuhn-Tucker

KVL Kirchoff's Voltage Law

LLR Log Likelihood Ratio

LR Likelihood Ratio

LRT Likelihood Ratio Test

MAC Media Access Control

MBD Model Based Diagnosis

MCS Monte Carlo Simulation

MIMO Multiple Input Multiple Output

ML Maximum Likelihood

MLE Maximum Likelihood Estimator

MVUE Minimum Variance Unbiased Estimator

NP Neyman-Pearson

OOK On/Off Keying

OSI Open System Interconnection

PAC Parallel Access Channel

PBPO Person By Person Optimization

PDF Probability Density Function

PSK Phase Shift Keying

QoI Quality of Information

QoS Quality of Service

REI Residual Energy Information

RLS Recursive Least Squares

RMS Root Mean Square

ROC Receiver Operating Characteristics

TBMA Type Based Multiple Access

TCP Transmission Control Policy

TDMA Time Division Multiple Access

UAS Unmanned Aircraft System

WSNs Wireless Sensor Networks

CHAPTER I

Introduction

Cyber-Physical Systems (CPS) are engineered systems comprising tightly-interacting physical and computational components. Detection of abnormal behavior in cyber-physical systems is crucial for their safe and reliable operation. Model-based detection can improve the system detection performance by incorporating the system behavior knowledge, captured by the system model, into the design process of detection systems. The components to be modeled, as well as the model complexity, are assessed by the specific application and the objective of the study. In this dissertation, we address three main challenges in model-based detection; (i) development of accurate physics-based models for the monitored physical system, (ii) detection of intermittent and incipient faults using statistical models, and (iii) integration of the wireless communication network in the design of detection systems with Wireless Sensor Networks (WSNs). In this chapter, we summarize the motivation behind our work, the research objectives, and the main research contributions. The chapter concludes with an organization for the rest of the dissertation.

I.1 Motivation

Cyber-Physical Systems are tight integrations of computation and physical processes. In CPS, embedded computers and networks monitor and control the physical process, usually with feedback loops [1]. CPS can be found in areas as diverse as aerospace, automotive, process control, transportation, consumer appliances, just to name a few. In CPS, the system is regarded as a network of interacting elements. Therefore, the emphasis is on studying the interaction and coordination between the physical and computational elements to increase the adaptability, efficiency, functionality, and reliability of the CPS [2].

Figure 1 shows an abstract representation of a CPS. The physical system is any plant that is required to be monitored and/or controlled. As an example, the physical system may represent

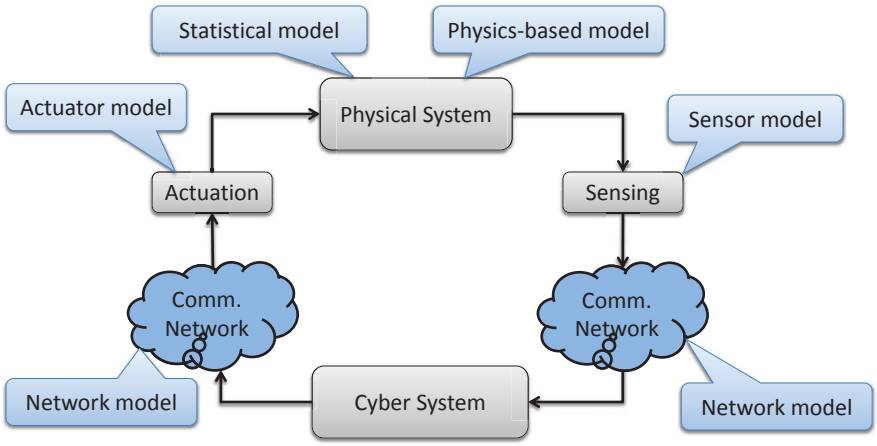

Figure 1: Cyber-Physical System

a machine, equipment, a process plant, or it may represent a geographic area in a surveillance application. The sensing function refers to the set of sensors that are installed to monitor the physical system. The cyber system is usually an embedded computer that takes as an input the sensor measurements, and calculates its output based on the programmed function. The cyber system usually acts as a controller for the physical system. Due to the increase in processing speed and the decrease in manufacturing cost of embedded systems, more functions are implemented in the cyber system. In our detection application, detection and estimation functions are usually embedded in the cyber system. If the physical system is to be manipulated, then the actuation block (motor, valve...etc.) uses the cyber system output to calculate the manipulated variable of the physical system.

Advances in communication network technologies motivated the use of wireless sensors in many applications. The deployment of wireless sensors brings new challenges to the design and optimization of CPS. Classical design of communication networks to optimize Quality of Service (QoS) measures does not necessarily result in optimal performance in terms of the given application. This is mainly because networks are designed to maximize the quantity of the information, treating all nodes equally, while CPS performance is usually determined by the quality of the information transmitted. Therefore, the communication network has to be integrated with the overall system model in the design process to optimize the application performance.

It should be highlighted that the CPS block diagram in Figure 1 is functional, i.e. it does not necessarily represent a physical separation between components. As an example, modern actuators have the control unit embedded on the actuator itself, thereby eliminating the communication network between the decision unit and the actuation element. Another theme of CPS that could be observed from Figure 1 is that it is hard to distinguish between the cyber and physical components, i.e. the tight coupling and interaction between the physical and computational elements. For example, the sensor has a physical aspect since it is in direct contact with the physical system. At the same time, modern sensors have computational and communication capabilities for local data processing and transmission to the decision unit. The same observation applies to actuators as well.

Many of the applications of CPS are mission-critical. As such, fast and accurate detection of abnormal behavior in the system is crucial for safety and reliability. Examples of abnormal behavior in Figure 1 are physical system faults, changes in the environment, sensor faults, decision unit failures, actuator faults, or communication network malfunction. In this dissertation, we focus on detecting physical system faults and changes in the environment. To optimize the detection task, a CPS has to be designed with the detection application in mind. To do that, the physical system, sensors, and the communication network components of the CPS have to be integrated in the design process of the detection system, rather than being designed independently. Model-based detection provides a framework to incorporate the behavioral knowledge of these CPS components into the design process. However, the choice of components to be modeled, and the complexity of each model is a challenging task. Accurate models that incorporate the physical system, sensors, and the communication network may be built. However, such models maybe extremely difficult to analyze, may add little insight on the system behavior, and may prove very hard to optimize for the detection task. On the other hand, careful choice of subsystem components and their interactions that are relevant to the objective of the study can lead to significant insight on the system behavior, while enhancing the detection performance.

I.2 Research Objectives

Classical model-based detection systems have the following features: (1) use of simplified models for the physical system, (2) focus on classical discrete, abrupt persistent faults, and (3) focus on the physical system while ignoring other CPS components, e.g. the communication network, in the design. The use of simplified models is usually justified by the complexity of the physical system and the lack of processing power for embedded systems to implement the model for online detection. The focus on abrupt persistent faults is promoted by industrial feedback declaring such faults as of prime interest. The communication network is usually ignored because in traditional systems, sensors and actuators are connected to the cyber system by hard-wired cables. These assumptions changed considerably in the last decade; embedded systems have ever increasing power and decreasing cost that justifies the development of more sophisticated models for the physical system to enhance the detection performance. Recent industrial reports show increasing interest in intermittent and incipient faults, as one of the causes of serious incidents in mission-critical systems [3]. Sensors with hard-wired cables are replaced in many applications by WSNs that have more flexibility, increased processing power, and reduced installation cost.

The main objective of our research is to enhance the detection performance by addressing these three new challenges:

1. Development of more detailed analytic models for physical systems, where simplified models are classically used.

2. Detection of intermittent and incipient faults in physical systems.

3. Integration of the wireless communication network in the design of detection systems

The first challenge, i.e. development of complex models, is application specific, therefore we focus on a specific physical system when addressing this challenge. For the last two challenges, we propose a general solution that is applicable on different systems, and present case studies to demonstrate our approach. Specifically, we consider the following studies to address the research challenges:

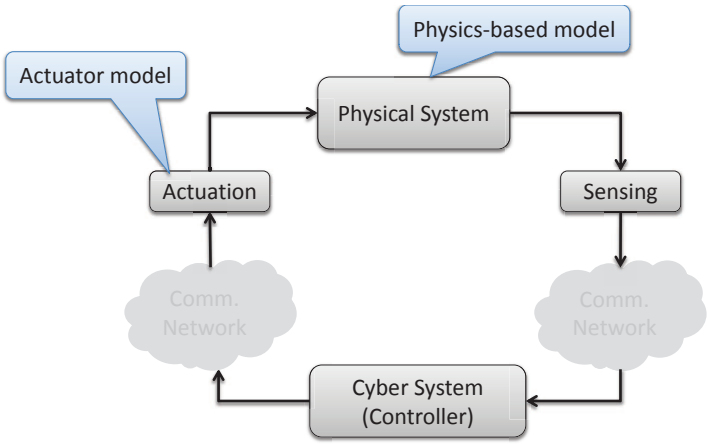

Figure 2: Focus of physics-based modeling study in CPS.

- **Physics-based Modeling for Fault Detection**. We consider physics-based modeling as a powerful modeling approach to develop accurate representation for system behavior. Physics-based modeling allows us to model and simulate different types of machine faults, which facilitates the understanding of the physics of machine failure. We use aircraft AC generators as a case study. Aircraft generators are the main source of electrical power for a number of critical systems in the aircraft. Therefore, fast and accurate fault detection and isolation are necessary for safe and reliable operation of the machine and the aircraft. In connection with Figure 1, this study involves the physical system block, sensors, the cyber system (acting as a controller), and the actuator (generator excitation unit). The communication network is not included in this study, since aircraft generators are locally monitored and controlled due to the limited size of the machine. The focus of this study is the modeling of the complete system, although general conclusions are drawn from the simulation study on how to design the decision unit. The focus of the study is demonstrated by Figure 2.

- **Statistical Modeling for Intermittent and Incipient Fault Detection**. We address the problem of intermittent and incipient fault detection using statistical modeling approaches. Statistical models are powerful in designing and tuning detection systems. Models could be constructed from real life data, simulation data, or from prior knowledge about the system. Although statistical models are less informative than physics-based models, they provide

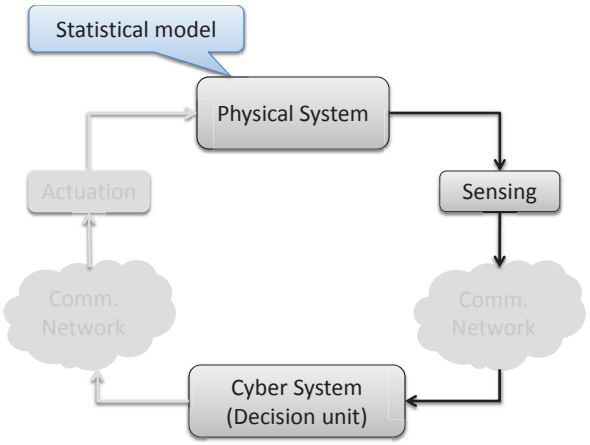

Figure 3: Focus of statistical modeling study in CPS.

tractable analysis where detection systems for intermittent faults could be designed and optimized. Often, an observer is built using physics-based models, which generates a residual signal for each sensor measurement. These residual signals are described by statistical models that are used by the decision unit for fault detection. We develop a detection algorithm that utilizes the stochastic residual signal to detect different types of faults. We apply our developed algorithm on two cases studies: (1) NASA ADAPT testbed to detect intermittent and incipient faults for DXC'10 competition [4], and (2) Fault detection for aircraft generator windings using Differential protection techniques [5]. In connection with Figure 1, this study involves the physical system block and the cyber system block, acting as a decision unit. The communication network is ignored in this study. The focus of the study is demonstrated by Figure 3.

- **Model-based Detection in Wireless Sensor Networks**. In this study, we focus on detecting a change in the physical system. As an example, this change may represent the presence of a fault in a plant, a target in a surveillance area, or a temperature change in a geographic area. In case of physical plants, the statistical model usually represents the residual signals the could be generated by embedded observers on sensor nodes. In case of geographic areas, the statistical model represents the direct measurements of sensor nodes. Both formulations are very similar, and we focus our work on monitoring geographic areas. We consider WSNs in this

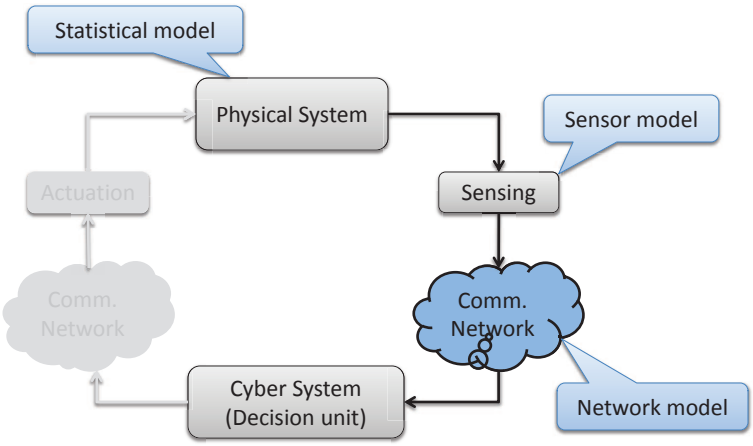

Figure 4: Focus of model-based detection in WSN study.

study and integrate the sensing and wireless communication network models into the design process of the detection system. Our main objective is to design the communication network and the decision unit in order to optimize the detection of a change in the environment. In connection with Figure 1, this study involves all the CPS components, with the exception of the actuation unit and its associated communication network, since environment manipulation is not included in the study. The focus of the study is demonstrated by Figure 4.

I.3 Contributions

We summarize our contributions as follows:

(i) **Physics-based Modeling for Fault Detection**. We develop a physics-based model for the complete brushless AC generator in Chapter III. The model incorporates the exciter generator, rectifier circuit, and the main generator in one hybrid dynamical model. Specifically, we have the following contributions:

(1) **Novel Hybrid Dynamical Model**. The developed model captures both the continuous and discrete dynamics of the system. The discrete dynamics are modeled explicitly using hybrid automata. The exciter generator continuous dynamics are modeled explicitly, and not abstracted as a voltage source as commonly assumed. The continuous dynamics for the complete system are accurately represented using state space models. The state space

model is represented in actual machine phase quantities, without any transformations that may not be valid under faulty conditions [6].

(2) **General Framework for Diode Fault Modeling and Simulation**. We show that any combination of open-circuit diode faults could be modeled with a subset of the system hybrid automaton states. We develop an algorithm to identify the valid states for each combination of diode faults.

(3) **Runtime Fault Injection**. We implement the model and simulate it in a way that facilitates injection of any parametric fault profile as well as open circuit diode faults. The fault profile for any parameter is defined as an input signal to the model. Therefore, the solver seamlessly incorporates the faulty parameter into the simulation. This eliminates the switching dynamics problem of the classical approach, where a new model is developed for each faulty behavior and implemented as a discrete state.

(4) **Development of Novel Fault Signatures for Diode Faults**. Diode faults have been recently reported as one of the most critical faults in aircraft generators [7]. We develop fault signatures for diode faults from the simulation results. The generated fault signatures reveal the discriminatory power of the electric currents in the windings installed on the rotating part.

(ii) **Statistical Modeling for Intermittent and Incipient Fault Detection**. We use the statistical modeling approach to detect different fault profiles and estimate the relevant fault parameters for a given system from the observed residual signals in Chapter IV. Specifically, we have the following contributions:

(1) **General Framework for Fault Detection**. We develop a general framework to detect and distinguish between abrupt persistent, abrupt intermittent, and incipient faults. The framework is based on the change detection theory and could be applied to any system as long as a statistical description could be obtained for the system behavior.

(2) **Closed form Solution for Gaussian/Exponential Case**. We specialize the framework to the case of Gaussian noise and exponential fault profile. We obtain closed form expressions for the estimators and a recursive expression for the fault detector.

(3) **NASA ADAPT DXC'10 Case Study**. We apply the developed framework to detect different fault types in the NASA ADAPT-Lite Electrical Power System (EPS), in the context of the DXC'10 diagnosis competition, and placed second in the contest. The EPS supplies power to the Unmanned Aircraft System (UAS) and payloads, which are necessary for successful mission completion [4].

(4) **Fault Detection for Generator Windings using Differential Protection**. We apply the developed algorithm to detect generator winding faults using differential protection techniques. This case study shows how the algorithm could be applied to a general fault model, in addition to the fault models considered in the dissertation.

(iii) **Model-based detection in Wireless Sensor Networks**. We develop an integrated model for the sensor network in a variety of sensor network configurations. We consider single hop networks with slotted ALOHA in Chapter VI, and with Time Division Multiple Access (TDMA) in Chapter VII. We study tree networks with slotted ALOHA in Chapter VIII. We use the integrated model to optimize the system design variables, and show the detection performance increase compared to classical sensor network design approaches. Specifically, we have the following contributions:

(1) **Unified Design Process**. We develop a unified design process, where the designer can choose the subsystem components to be modeled, and the model attributes, based on the performance and quality measures of the application. The design process is general and could be applied to any CPS application, not only detection applications.

(2) **Integrated Model for the Detection System**. We develop an integrated model for the wireless sensor network in detection applications. The model includes the system, sensing,

and different networking aspects. The network component captures the physical layer as well as slotted ALOHA and TDMA MAC sublayers [8].

(3) **ALOHA-TDMA Comparative Analysis**. Since TDMA and slotted ALOHA are quite common MAC protocols, we conduct a comparative study between the two implementations. We show the conditions under which each protocol achieves a better detection performance over the other. These conditions provide a guideline for the designer to choose between the two protocols based on the available system resources and design constraints.

(4) **Integration of Different Sensor Quality Measures**. We include different quality measures in the design process. In classical detection applications, only the quality of sensor information is considered. In WSN applications, the channel state information and/or the residual energy information are considered. In our design, we integrate the three quality measures into the design process [8].

(5) **Design of a Complete Transmission Control Policy**. We design a complete transmission control policy for the sensor network. The transmission control policy includes the communication rate, transmission power, and medium access control parameters for each sensor [8]. These represent the essential parameters for any sensor network that need to be specified at the time of deployment.

(6) **Non-Asymptotic Analysis**. We assume a finite number of sensor nodes, and do not resort to asymptotic analysis as commonly adapted in detection studies. Therefore, the analysis results are applicable on small-scale and large-scale sensor networks as well.

(7) **Enhanced Detection Performance**. We show that our design process results in significant detection performance improvement over the classical design approaches, where either the network is ignored altogether, or designed to satisfy performance measures that are not relevant to the application [8, 9].

(8) **Single Hop and Tree Networks**. We apply our design approach on both the classical single hop network (parallel topology), as well as the tree topology network [9].

(9) **In-Network Processing**. We consider both direct transmission of sensor observations as well as in-network processing where observations are locally quantized. We compare the two transmission schemes and describe the conditions where each scheme provides better detection performance.

I.4 Organization

The dissertation is organized as follows. Chapter II summarizes the related work. We classify the related work according to the three studies outlined in Section I.2. We first present the related work on aircraft generators modeling, simulation, and fault detection. Second, we present the related work on intermittent fault detection. Finally, we summarize the related work on detection in WSNs, with emphasis on recent studies considering different communication network constraints.

Chapter III presents the hybrid model for the aircraft power generator. First, we describe the machine and explain different system components and their function. We present a literature survey on existing modeling and fault detection techniques. We present a detailed derivation for the hybrid dynamical model, and explain how it could be used to model a variety of diode faults. We present simulation results for normal and different faulty behaviors, and we conclude by a discussion on the modeling and simulation results, and possible extensions for the model.

Chapter IV presents the statistical modeling approach for fault detection in CPS. We start by a background introduction to statistical modeling and change detection theory. We define the different types of faults to be detected, and present a general algorithm that is based on the Generalized Likelihood Ratio Test (GLRT) to detect different faults. We present two case studies; DXC'10 competition and differential protection for aircraft generator windings, where Gaussian noise is assumed. We present a closed formula for the detector and the different parameter estimators. We conclude by a discussion on possible improvements in the detection algorithm.

Chapter V introduces model-based detection in WSNs. We outline the design process that is used in Chapters VI to VIII to design both single hop and tree sensor networks for detection applications. The design process is illustrated with the example sensor network that is designed in Chapter VI.

Chapter VI is the first chapter in a series of three chapters that study model-based detection in WSNs. This chapter considers detection in parallel topology (single hop) networks that use slotted ALOHA as a Media Access Control (MAC) protocol. A detailed system model is derived that incorporates network, sensing, and energy models, with explanation for each design variable and design constraint. A nonlinear optimization problem is formulated and solved to calculate the design variables that result in optimal detection performance. The design variables define how sensors participate in the detection process and how they communicate with the decision unit. A comparative study is given between the proposed design and two classical design approaches for sensor networks. The chapter concludes with possible enhancements and extensions to the system model.

Chapter VII modifies the model presented in Chapter VI for TDMA sensor networks. A nonlinear optimization problem is formulated and solved numerically to calculate the system design variables. A comparative study is given between the proposed design and two other approaches commonly used to design sensor networks. The chapter concludes with a comparison between the optimal design of slotted ALOHA and TDMA sensor networks, highlighting the conditions under which each network outperforms the other.

Chapter VIII generalizes the system in Chapter VI for tree structure sensor networks. A detailed system model is derived and a global optimization problem is formulated. A suboptimal local approach to solve the optimization problem is proposed. A comparative study is conducted against two classical design approaches for tree networks via a numerical example. An alternative design approach with in-network processing is described and compared to the direct transmission approach. The chapter concludes with possible extensions to the presented model.

Chapter IX summarizes the contributions of the dissertation. We highlight the limitations of the proposed modeling and design approaches, and describe future directions in which the current research could be improved.

CHAPTER II

Related Work

In this chapter, we provide a literature review for model-based detection. Since most of the work in this dissertation is based on statistical models, as well as monitoring using multiple sensors, the literature review focuses on decentralized detection. We give a brief introduction to classical detection theory and its extension to decentralized detection in Section II.1.1, then the taxonomy of design concerns in decentralized detection problem is presented in Section II.1.2. Every design concern treated in the literature is discussed, in addition to the newly proposed design concerns. The literature review is then organized according to the presented taxonomy of design concerns, and the proposed extensions are highlighted during the discussion. Section II.2 briefly explains existing work on aircraft generators modeling and fault detection, while Section II.3 summarizes existing work on intermittent fault detection. The end of the chapter compares the dissertation work to existing literature.

II.1 Model-based Detection

In this section, we provide a literature review for model-based detection. Since the physical system is abstracted using a statistical model describing either the direct sensor observations or the observer residual signals, our discussion is closely related to detection theory. Since we assume multiple sensors and consider the communication network in the design process, the related work focuses on decentralized detection under different constraints and design assumptions. Throughout this section, we make references to the CPS block diagram to highlight the focus of the research work under discussion.

	$\mathcal{H}_0$ is true	$\mathcal{H}_1$ is true
Accept $\mathcal{H}_0$	Correct decision	Type II error (β) false negative (missed detection)
Accept $\mathcal{H}_1$	Type I error (α) false positive (false alarm)	Correct decision

Table 1: Errors in hypothesis testing

II.1.1 A Brief Introduction to Detection Theory

In classical detection theory (also known as hypothesis testing), an ordered sequence of observations $\mathbf{X} = (X_1, X_2, \ldots, X_n)$ is used to distinguish between two or more hypotheses. Every hypothesis, $\mathcal{H}_i$, is characterized by a Probability Density Function (PDF) $p(\mathbf{X}; \mathcal{H}_i)$ over the sample space $\mathcal{S}_{\mathbf{X}}$ of the random sequence $\mathbf{X}$. The hypothesis is called a simple hypothesis if its PDF is completely known (i.e. does not depend on any unknown parameters), otherwise the hypothesis is composite. The detection problem is to identify the decision regions R_i for every hypothesis $\mathcal{H}_i$ in the n-dimensional space of the sequence $\mathbf{X}$ [10]. Many signal processing problems in practice are binary in nature, e.g. target detection, signal detection , and fault detection, just to name a few. Therefore, we restrict ourselves to binary hypothesis testing, where the two hypotheses are designated by the null hypothesis, $\mathcal{H}_0$, and the alternative hypothesis, $\mathcal{H}_1$.

Since we have two hypotheses and two courses of actions, there are four different possibilities, summarized in Table II.1.1. Two types of faults are possible in making a decision: (1) deciding $\mathcal{H}_1$ when $\mathcal{H}_0$ is true, also called type I error or false alarm, with associated probability $P_F = P(\text{decide } \mathcal{H}_1; \mathcal{H}_0)$, and (2) deciding $\mathcal{H}_0$ when $\mathcal{H}_1$ is true, also called type II error or missed detection, and the associated probability is $P_M = P(\text{decide } \mathcal{H}_0; \mathcal{H}_1)$. It is always desired to minimize both the probability of false alarm P_F and probability of missed detection P_M (equivalently maximizing the probability of detection, P_D), however it is not possible to reduce both probabilities simultaneously. The relationship $P_D - P_F$ is widely known as the Receiver Operating Characteristics (ROC) curve [11]. To design an *optimal* detector, a suitable objective function has to be defined. Different optimality criteria have been proposed in the literature, and a complete survey is included in Section II.1.2.

In Decentralized Detection (DD), a set of sensors sample the environment independently, preprocess their measurements, and communicate their information over a network to make a final decision. The communication structure is dictated by the network topology and the detection architecture. If there is no designated fusion center, then the information is communicated between sensors in order to reach a consensus about the final decision. This scheme is referred to as *distributed detection* [12]. If, on the other hand, a single node is designated as a fusion center, then the fusion center uses the information received from different sensors to make a final decision. In this later case, communication between sensors may or may not exist depending on the application. Also, the communication is usually from sensors to the fusion center, although in some schemes a feedback from the fusion center is also possible. The configuration with a fusion center is usually referred to in the literature as *decentralized detection*, and has attracted a great deal of attention as it is, arguably, more relevant to engineering applications [13].

Interest in DD has been motivated by the availability of low cost sensors with high computational capabilities, together with advances in communication networks. This allowed the formation of sensor networks of varying topologies, which cooperate to address a common goal. The goal here is to decide on one of multiple hypotheses, using information from individual sensors. Some of the advantages of using DD is the increased reliability, extended coverage area, and reduced cost. The price paid is the loss of performance compared to centralized detection, since sensors usually submit a compressed version of their local information to reduce the communication overhead, in addition to information loss due to non-ideal communication links. Classical (also known as centralized) detection could be regarded as a special case of DD when sensors submit their *raw* observations and the communication channels are ideal with no delay or dropped information, which implies the availability of sensors' local information in real time at the fusion center.

The decentralized detection problem is a multidimensional problem with multiple degrees of freedom, as well as constraints. For example, the network topology and communication structure could be a design parameter, given a fixed message format for every sensor. Alternatively, the communication structure could be fixed and the design objective is to find the optimal sensor local decision

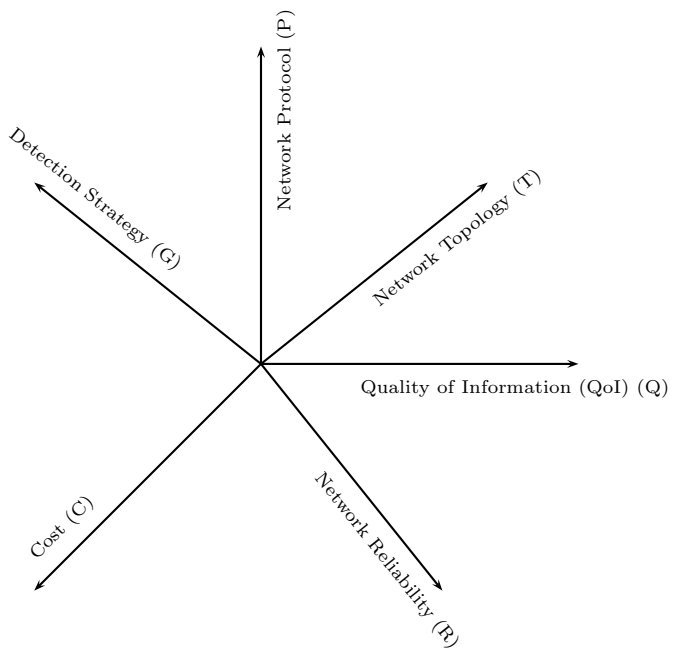

Figure 5: Decentralized detection taxonomy of related work

rules. In practical situations, some constraints are imposed on the problem formulation. The majority of research work in the DD area assumes a fixed network topology and communication structure and seeks to obtain an optimal solution for one of the system design aspects. A comprehensive definition and survey for decentralized detection multidimensional aspects is given in Section II.1.2.

II.1.2 Decentralized Detection Taxonomy

The taxonomy of design concerns in decentralized detection is shown in Figure 5. The taxonomy contains the following inter-dependent dimensions, representing the different design concerns: Quality of Information (QoI) (Q), Network Topology (T), Network Protocol (P), Detection Strategy (G), Cost (C), and Network Reliability (R). The related work is organized in this chapter in terms of these design concerns, which may represent either a design constraint, or a design objective for the decentralized detection problem. If all design concerns are given as design constraints, then the problem is to analyze the detection performance of the *completely specified system*. Throughout the discussion in this chapter, we refer to the design concerns by their abbreviation given between brackets above. In the sequel, we briefly discuss every design concern and its components.

Quality of Information (QoI)

QoI represents attributes about the data being communicated, rather than the data itself. In a sense, it is a *meta-data* about the sensor observations/decisions. The term has been used in sensor networks to differentiate between the quality of communicated data and the QoS [14]. QoS characterizes the transmission properties of the channel used between the data source and destination, and optimization of the QoS does not always result in optimization of the QoI.

In detection theory context, well-defined metrics exist for QoI, that depend on the optimality criterion used in the problem formulation. The different optimality criteria used in literature are summarized below. We follow the hypothesis testing terminology introduced in Section II.1.1

1. **Neyman-Pearson (NP) Criterion**. The objective is to maximize P_D for a fixed $P_F = \alpha$. $\mathcal{H}_0$ and $\mathcal{H}_1$ are not considered random variables in this case, and therefore, no prior information about hypotheses is required [10]. A QoI metric for this criterion is the pair (P_F, P_D).

2. **Bayesian Criterion**. For every course of action, a risk factor C_{ij} is assigned for deciding $\mathcal{H}_i$ when $\mathcal{H}_j$ is true. $\mathcal{H}_0$ and $\mathcal{H}_1$ are considered random variables with prior probabilities π_0 and π_1, respectively [10]. The objective is to minimize the expected cost or Bayesian risk defined as:

$$\mathcal{R} = E(C) = \sum_{i,j} C_{ij} P(\mathcal{H}_i, \mathcal{H}_j) = \sum_{i,j} C_{ij} P(\mathcal{H}_i|\mathcal{H}_j) P(\mathcal{H}_j) \tag{1}$$

   A QoI metric for this criterion is the Bayes risk $\mathcal{R}$. The *minimum probability of error* criterion is a special case of Bayesian criterion, where $C_{01} = C_{10} = 1$ and $C_{00} = C_{11} = 0$:

$$P_e = P(\mathcal{H}_0|\mathcal{H}_1) P(\mathcal{H}_1) + P(\mathcal{H}_1|\mathcal{H}_0) P(\mathcal{H}_0) \tag{2}$$

   Additionally, if we assume equal prior probabilities, then the detector is an ML detector. A QoI metric in the later two special cases is the probability of error P_e.

3. **Information-theoretic Criterion**. The mutual information between the true hypothesis $H = \{\mathcal{H}_0, \mathcal{H}_1\}$ and the decision $U = \{\mathcal{H}_0, \mathcal{H}_1\}$, designated by $I(H,U)$, has been proposed as an objective function to be maximized (equivalently, minimization of the conditional entropy $h(H|U)$) [15]. This criterion could be understood by analogy to the Binary Symmetric Channel (BSC) [16], where the input to the channel is the random variable H, and the output is the decision random variable U, with cross-over probabilities P_F and $(1-P_D)$, respectively. A QoI metric for this criterion is the mutual information $I(H,U)$.

4. **Relative Entropy (Kullback-Leibler Divergence)**. The relative entropy between two probability distributions $P(x)$ and $Q(x)$ that are defined over the same sample space $\mathcal{X}$ is defined as [16]:

$$D_{KL}(P \parallel Q) = \sum_{x \in \mathcal{X}} P(x) \log \frac{P(x)}{Q(x)} \tag{3}$$

The KL divergence is a measure of the distance (although not strictly a distance) between two distributions. In detection theory context, the larger the KL divergence between $P(x;\mathcal{H}_0)$ and $P(x;\mathcal{H}_1)$, the better the detection performance. Therefore, it is required to maximize the relative entropy. A QoI metric for this criterion is clearly the KL divergence.

5. **Ali-Silvey Distance (f-divergence)**. f-divergence is a function that measures the difference between two probability distributions $P(x)$ and $Q(x)$, defined over the same sample space $\mathcal{X}$. If P is absolutely continuous w.r.t. Q, then for a convex function f such that $f(1) = 0$, the f-divergence of Q from P is defined as [17]:

$$D_f(P \parallel Q) = \int_{x \in \mathcal{X}} f\left(\frac{dP}{dQ}\right) dQ \tag{4}$$

f-divergence represents a generalization of KL divergence and many other common divergences (J-divergence, Bhattacharyya bound). In general, the larger the divergence, the better the detection performance. A QoI metric for this general criterion is the divergence value.

6. **Deflection Coefficient.** It measures the difference between the two probability distributions describing the test statistic of the detector. It is given by [10]:

$$D^2 = \frac{\left(E[V;\mathcal{H}_1] - E[V;\mathcal{H}_0]\right)^2}{\mathrm{var}[V;\mathcal{H}_0]} \tag{5}$$

where V is the test statistic for the detector. We adopt the deflection coefficient as our QoI in this dissertation.

7. **Asymptotic Error Exponent**. For any feasible detection system, the probability of error (Bayesian criterion), or the probability of miss (NP criterion), decays exponentially as the sample size increases. The error exponent is defined as the rate of the exponential decay. The asymptotic error exponent is then given by:

$$a = \lim_{n\to\infty} -\frac{1}{n}\log P(n) \tag{6}$$

where $P = P_e$ or P_M and n is the sample size. In decentralized detection context, the same error exponent measure is used, where n is understood as the number of sensors. For Independent and Identically Distributed (IID) samples, the error exponent is given by the Kullback-Leibler divergence between the two distributions under each hypothesis [18].

8. **Delay for Detection**. When sensors communicate over a data communication network, information may not arrive at the destination in a timely manner. The final decision is taken upon arrival of all sensors' data, and therefore, is not taken at deterministic time intervals. The variability of the delay for detection is a result of the variability of the communication network conditions. Delay for detection is also applicable to fully distributed detection systems, where consensus algorithms are implemented to reach a final decision, in the form of the speed of convergence of the consensus algorithm. Evaluation of the decision delay is important for the complete representation of the detection quality. The delay, as a QoI metric, has been

overlooked in the literature. In Chapters VI - VIII, we consider the delay for detection as one of the sensor network design constraints.

Network Topology

The network topology refers to how sensor nodes are physically connected to each other (physical topology), and how they communicate (logical topology). Our discussion here is concerned with logical topology. The physical topology is covered under network reliability, Section II.1.2. The major network topologies in the literature are summarized below [19].

1. **Parallel Topology** (Figure 6). Sensors communicate local decisions to a common node, the fusion center. The fusion center makes a global decision U_0 using the vector of local decisions $\mathbf{U} = (U_1, U_2, \ldots, U_n)$. This is by far the most commonly used topology in the literature [20]. In some cases, a feedback from the fusion center to sensors is employed to enhance the performance, which is referred to as parallel topology with feedback.

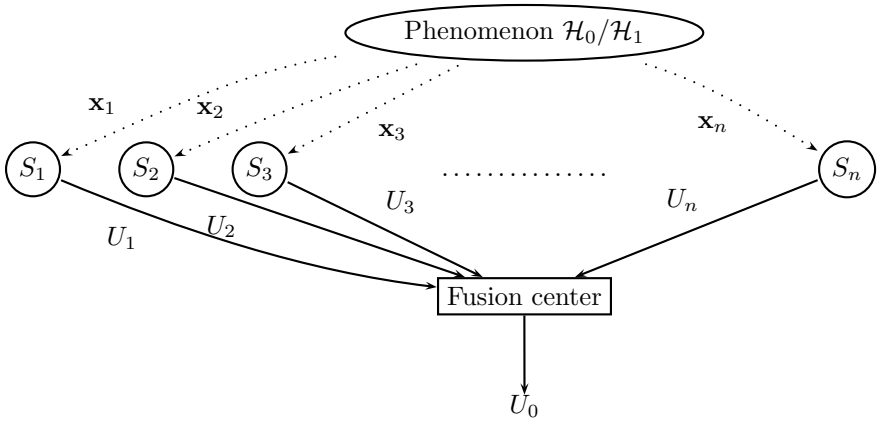

Figure 6: Parallel topology for decentralized detection. Sensors transmit their decisions to a common fusion center which makes a final global decision. No communication between sensors takes place.

2. **Serial Topology** (Figure 7). Sensors are connected in tandem, where every $(j-1)^{\text{th}}$ sensor passes its decision to the j^{th} sensor. Every sensor calculates its decision using its own observations and the decision from its predecessor (except the first sensor). The final sensor makes a global final decision U_0 [20]. In practice, the serial network suffers from reliability problems, since losing one sensor results in a loss of all information from its predecessors, and by the

same reasoning, the last sensor represents a single point of failure. Another disadvantage is that the delay accumulates through the network.

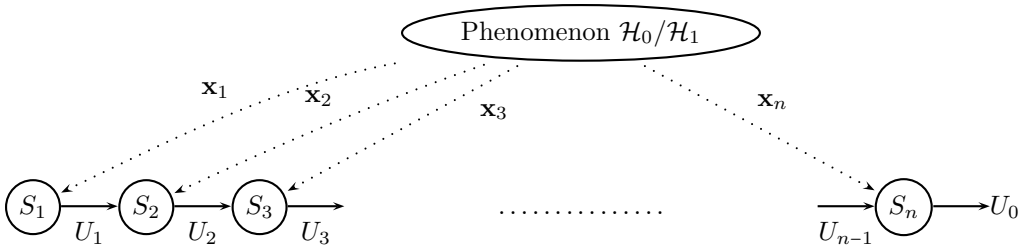

Figure 7: Serial topology for decentralized detection. Every sensor submits its decision to its successor, and the final sensor takes the final global decision.

3. **Tree topology** (Figure 8). Sensors form the leaves and intermediate nodes of a tree, where each set of sensors report their local information to their immediate parent. The tree has one root, acting as the fusion center. Intermediate nodes may or may not have access to measurements. The tree topology could be regarded as a generalization of the parallel and serial topologies, where parallel topology is a tree network with height one, and serial topology is a tree network where every parent has one and only one child. Accordingly, any result obtained for tree networks is valid as well for parallel and serial networks. However, tree networks are hard to analyze without simplifying assumptions, and little work has addressed the tree structure [20–22]. Recently, tree networks has started to regain popularity [23–25], since the tree structure possesses nice properties for WSN implementations, e.g., reliability and power conservation.

4. **Fully Connected Graph Topology**. This represents the case when every node could communicate with all other nodes. In decentralized detection applications, the graph usually represents the basic topology with link metrics representing the communication cost. The design objective is usually to form a non-redundant (loop-less) topology out of the graph, that achieves a certain performance criteria. Redundant paths may also be used if one of the design objectives is to achieve a certain reliability metric. General graphs are hard to analyze

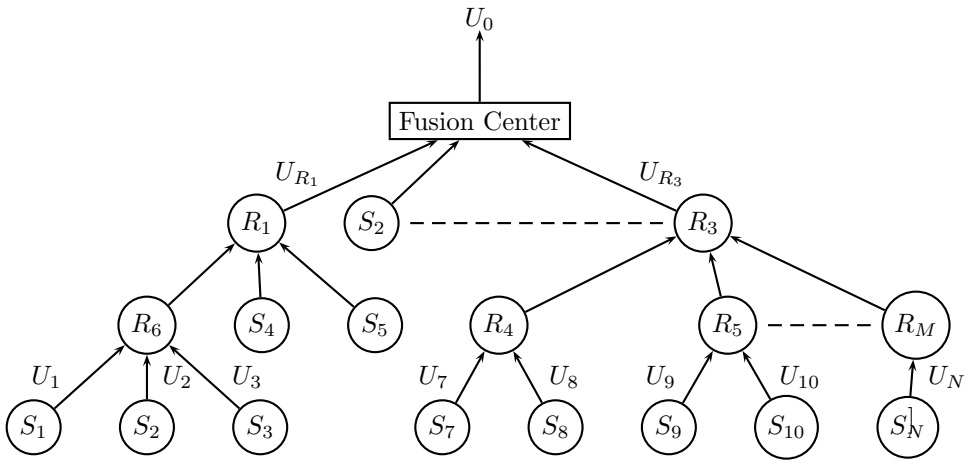

Figure 8: Tree topology for decentralized detection. Every set of sensors submit their decisions to a common parent, and the root of the tree acts as the fusion center that makes a final global decision. Tree topology is a generalization of parallel and serial topologies

using classical detection theory analysis tools, and few work has addressed the general graph topology [26–28].

5. **Fully Distributed Topology**. The majority of decentralized detection work assumes a fusion center taking a global final decision (hence, the term *decentralized*). When there is no designated fusion center, sensors communicate with each other in order to reach a local decision (maybe different across sensors), or to reach a consensus on a final decision. This later approach is termed a *fully distributed* detection, to emphasize the absence of a single fusion center [12, 29].

Network Protocol

Network protocols represent a new dimension to be explored in decentralized detection research. This dimension is a result of the fact that, in practice, WSN nodes communicate using layered network architecture (e.g. TCP/IP protocol stack, IEEE 802.15.4, OSI reference model). The main motivation behind using layered, and standard, network interfaces is to reduce the cost of deployment and to guarantee interoperability of heterogeneous network components. The majority of existing research on decentralized detection addresses only the physical layer of the protocol stack, assuming that quantized observations (representing the discrete symbol set of the communication system)

are transmitted directly using different channel encoding techniques. The viewpoint adopted is that the functionality of higher layer protocols are not needed for detection applications since they increase the delay and complexity of the system. Accordingly, higher layer protocol details have been ignored in the analysis, and joint source-channel optimization techniques have been used to enhance the performance, resulting in more restrictive designs.

Historically, custom-designed systems were traditionally built for military applications. However, in the last 20 years, the department of defense increasingly relies on "Commercial Off The Shelf" (COTS) technology in new defense systems [30]. Therefore, the foreseen future is for standardized WSNs. The advantages of assuming a layered network communication between sensor nodes is fully explored in Section II.4. In Chapters VI - VIII, we integrate the network protocol dimension with the other classical dimensions of decentralized detection in the design process.

Detection Strategy

Detection strategy refers to the collection of decision rules implemented at every node in the decentralized detection system. The decision rule, $\gamma(.)$ refers to *how information is pre-processed* at every node prior to transmission. The detection strategy is then defined by $\mathcal{G} = \{\gamma_i(.), i = 1, 2, \ldots, N\}$, where N is the number of nodes in the network. We can differentiate between two types of decision rules [20]:

1. **Local Sensor Rules**. Raw observations are processed at every sensor node to produce an intermediate decision, which may widely vary from hard decision (0/1) to being the same raw observation. This local decision is communicated with sensor nodes in order to reach a final decision (global final decision in case of a fusion center).

2. **Fusion Rules**. The collection of communicated decisions are fused together to produce a final decision. In the decentralized detection architecture with a fusion center, the fusion rule is implemented in the fusion center to produce a global final decision. In the fully distributed architecture, every sensor node implements its own fusion rule to produce a local final decision, which may approach a single final decision with other sensors using consensus algorithms.

Coupled to the detection strategy is the transmission strategy, which refers to *how the processed information is exchanged* between network nodes. The decision of whether or not to send the local decision depends on the local decision value and the transmission strategies. Efficient transmission strategies are needed to conserve sensor network energy. Some of the common transmission strategies are listed below [31]:

1. **Censoring**. In this transmission scheme, the decision space is divided into two regions; send and no send, with the local decision being transmitted only if it lies in the send region. The decision region is a design parameter often chosen to minimize detection performance loss.

2. **Sleeping**. Sensor node uses a priori knowledge about the process being monitored, together with current and past observations to decide whether the event of interest is unlikely. If the event becomes very unlikely, the sensor goes to sleep mode to conserve battery power.

3. **Reporting Detection Decisions**. In this scheme, sensor reports only if the event of interest is detected. This results in considerable energy saving if the event is very unlikely to occur. The disadvantage of this scheme in WSNs is that local sensor may fail or suffer from successive transmission failures, while assumed reporting "no event" by other nodes in the network.

Cost

The overall cost of WSN deployment is an important factor when designing the detection system. Two of the cost metrics are:

1. **Energy**. Energy is a scarce resource in WSNs, and it is always desirable to design systems achieving the performance requirements, subject to stringent energy constraints. The constraint on the energy is usually expressed in terms of power, so that the WSN lifetime could be incorporated in the design [32]. If power is a system design objective, then it is required to know the power distribution across sensor network nodes [33].

2. **Number of sensors**. Although sensor cost may not be large, the deployment of sensors in specific situations may be costly. In such scenarios, it is required to design the system with the

minimum number of sensors to achieve the required performance. In the existing literature, number of sensors metric is ignored since most of the classical analysis tools assume asymptotic regime, where number of sensors approach infinity (e.g. large deviations theory). Results using asymptotic analysis are less accurate for moderate network sizes.

Network Reliability

The WSN may suffer from different failures and degradations that directly affect the detection performance. The following represents the major reliability issues studied in literature:

1. **Channel Imperfections**. Large emphasis is put on the communication channel degradation, due to the unreliability of the wireless channel in WSN deployments. The following discrete time physical communication channel models are typical in the literature:

   (a) **Noisy Fading PAC Channel**. For a Parallel Access Channel (PAC), every sensor has a dedicated orthogonal channel to the fusion center. The output of every orthogonal channel, y, in terms of its input x is expressed as:

   $$y[n] = h[n]x[n] + w[n] \qquad n = 0, 1, \ldots \tag{7}$$

   where h is the fading envelope, and w is an additive channel noise [34].

   (b) **Noisy Fading MAC Channel**. A single Multiple Access Channel (MAC) is used between local sensors and the fusion center. For N sensors, the output of the channel in terms of its inputs is given by [35]:

   $$y[n] = \sum_{i=1}^{N} h_i[n]x_i[n] + w[n] \qquad n = 0, 1, \ldots \tag{8}$$

   (c) **MIMO Channel**. For a Multiple Input Multiple Output channel, the vector output $\mathbf{y}$ is given in terms of the input vector of decisions $\mathbf{x}$ by [33]:

$$\mathbf{y}[n] = \mathbf{H}[n]\mathbf{x}[n] + \mathbf{w}[n] \qquad n = 0, 1, \ldots \tag{9}$$

where $\mathbf{H}$ is the channel matrix and $\mathbf{w}$ is an additive noise vector.

(d) **General Probabilistic Channel**. This model is a generalization of all discrete time channel models, where the channel is modeled by the conditional probability density function of the output given the input, $p(\mathbf{y}|\mathbf{x})$ [36]. It is usually used for analysis purposes, when it is desired to derive a general result about detection with channel uncertainty. Binary Symmetric Channel model is a special case used when local sensors transmit binary decisions.

(e) **Rate-constrained Channel**. The channel is abstracted and assumed to have a reliable communication bit rate of R bps. According to information theory, this rate could be achieved by arbitrarily complex error correcting codes, as long as $R < C$, where C is the channel capacity [16]. The communication bit rate could also be regarded as a network protocol (specifically a DLC protocol) design parameter or constraint. The classification here is based on the fact that the communication rate is treated in the literature in the context of unreliable channel modeling.

(f) **Link Failure**. The communication channel may fail to deliver the transmitted information due to various reasons including physical failures, high magnitude noise, interference, and collisions. Link failure is usually modeled by a binary random variables with a fixed probability of occurrence p [37]. In a more complex failure behavior, link failure is modeled by a discrete time, binary random process.

2. **Node Failures**. Sensors may fail, either entirely producing no output, or producing incorrect outputs [38]. The criticality of the sensor failure depends on its location and role in the network. For example, in decentralized detection with a fusion center, failure of the fusion

center results in a complete system failure (if redundancy is not deployed), while losing one sensor maybe tolerable.

II.1.3 Decentralized Detection with Fixed Network Topology

Early research effort on decentralized detection has focused on obtaining the optimal detection strategies according to a pre-defined QoI, for a fixed network topology. The decentralized detection architecture with a fusion center is dominant, and the communication network between nodes is assumed ideal. Therefore, according to our original taxonomy, this research work lies along the three dimensions highlighted in Figure 9, namely quality of information as a design objective, detection strategy as a design variable, and network topology as a design constraint. In terms of the CPS block diagram, the focus of this work is highlighted in Figure 10, where the network model is not considered and the sensors are assumed with unlimited resources. The optimization problem could be summarized as:

$$\max_{G} Q(G;T) \tag{10}$$

where G is the detection strategy, Q is the quality of information, and T is the network topology. In the following, we summarize the main research results.

Bayesian Quality of Information

Research on decentralized detection is largely attributed to the seminal work of Tenney and Sandell [39]. Using an example of two binary detectors taking individual decisions, without a fusion center, the authors showed that decentralized detection formulation yields more complex behavior than centralized detection. This results from the fact that individual detectors choose their decisions to achieve a *system-wide optimization*, rather than local optimization as in classical hypothesis testing. For the statistically independent observations case, the decision strategies have been shown to be Likelihood Ratio Tests (LRTs) for each detector. However, the LR thresholds are coupled, i.e. the calculation of the threshold at each detector requires knowledge about the decision rule of the other

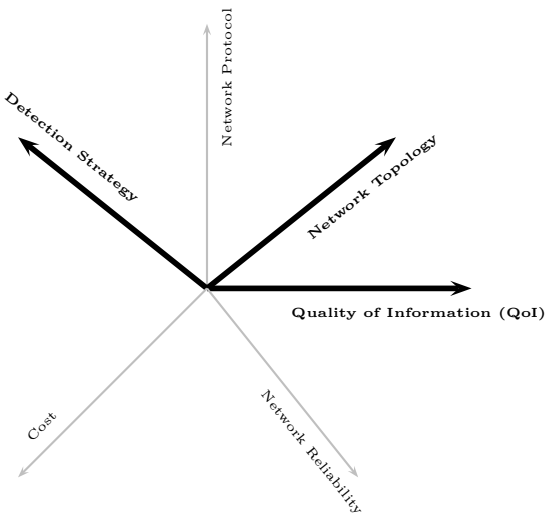

Figure 9: Early research effort has focused on finding optimal detection strategies according to a specific QoI, assuming a fixed network topology.

detectors. The solution to these coupled equations provide a *necessary*, but not sufficient condition for optimality. For the dependent observations case, the optimal solution is not an LRT in general (or equivalently, an LRT with a *data dependent threshold).*

The work in [39] was extended in a very similar way by a number of researchers for multiple hypotheses and N sensors, with a fusion center. In the following, we summarize the research results for different network topologies.

Parallel Topology The design of the entire parallel fusion network based on the Bayesian formulation is considered in [40]. A Person By Person Optimization (PBPO) has been used to find the necessary conditions for optimality of local decision rules as well as the fusion center rule. The joint optimization of local and fusion center thresholds is discussed in [41], with a further comparison between the performance of five distributed network architectures in [42]. Since the solution of the coupled threshold equations is computationally intensive, some work has been devoted to different computational algorithms, as in [43] and [44].

A rather counter-intuitive result is obtained for the case of identically distributed sensors. It would be intuitive in this case to assume that optimal decision rules are identical. However, examples

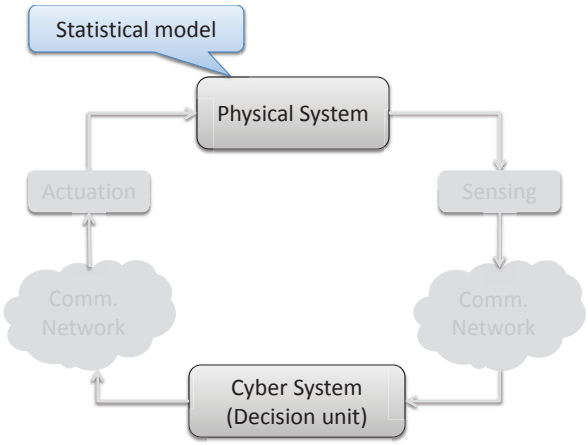

Figure 10: CPS block diagram for decentralized detection with fixed network topology

for optimal non-identical decision rules are given in [45, 46]. It has been shown, however, that the solution with identical sensors is asymptotically optimal, and that for bounded number of sensors, there is little loss of optimality [19, 47]. Accordingly, identical local decision rules are frequently assumed since this simplifies the analysis considerably.

The previous work has assumed hard decisions for local sensors, where every sensor decides either 0 for hypothesis $\mathcal{H}_0$ or 1 for hypothesis $\mathcal{H}_1$. The design of parallel fusion networks employing soft decisions (more than two quantization levels for local sensors) is considered in [48] and [49]. Both of these design approaches result in systems that perform better than the optimal hard decision systems but do not necessarily result in optimal soft decision systems. The emphasis is on tractable and efficient approaches that yield optimal or suboptimal systems.

Since the joint optimization results in difficult-to-solve equations, a number of researchers focused on the design of fusion rules, assuming fixed local sensor rules and thresholds. This later assumption is summarized by expressing the sensor quality in terms of its detection performance (P_F, P_D). The problem here is to design the optimal fusion rule $U_0 = \eta_0(\mathbf{u})$, given the vector of local sensors decisions $\mathbf{u}$. The optimal fusion rule for the case of hard, independent, local decisions is derived in [50]. The fusion of correlated decisions is considered in [51]. Contrary to the prevalent assumption that decisions arrive at the fusion center in a synchronous manner, fusion rule for asynchronous decisions is treated in [52].

Serial Topology For the serial topology, with conditionally independent observations, it has been shown that the LRT is an optimal solution [20,53]. For N sensors, $(2N-1)$ coupled equations need to be solved to determine the thresholds. A performance comparison between serial and parallel networks under Bayesian formulation is reported in [19,54,55], where it is shown that the parallel network is better than the serial network in the asymptotic sense.

Tree Topology For the tree topology, with conditionally independent observations, the analysis is carried out in a similar way to parallel and serial topologies. It is shown in [19,20,56,57] that the LRT is optimal at all tree nodes including the root node (fusion center).

Parallel Topology with Feedback In all topologies discussed before, information flows in one direction only, from local sensors to the fusion center. If it is allowed to communicate information back to local sensors, then it is possible to adapt local decision rules to enhance the performance. This approach is adapted in [58] for the parallel topology, where the fusion center reports back its global decision at time t to all local sensors, so that the future decision at time $t+1$ for every sensor is based on its local observation and the previous global decision. It is proved that the performance of the parallel topology with feedback is as good as the case with no feedback.

General Network Topology The similarity between the results for the parallel, serial, and tree topologies suggest a unified framework for detection networks. This unified approach to the analysis of general detection networks, including networks with feedback, has been studied in [22] using the Bayesian formulation. A PBPO is employed to determine the decision rule at any detector of the network.

Neyman-Pearson Quality of Information

Optimization according to NP criterion has been also studied independently. We summarize the research results for different network topologies.

Parallel Topology

For the parallel topology with binary local decisions, and conditionally independent observations, it is proved in [59] that the optimal decision rules at local sensors as well as the fusion center are LRTs. The same results have been shown to hold with multivalued (soft) local decisions in [19].

If the detection problem is for a random signal in noise, or if sensors' noise are correlated, then the conditional independence assumption fails. For conditionally dependent observations, it is shown in [60] that the optimal test at the sensors is no longer an LRT. In general, the optimal solution is intractable. It has been shown in [61] that when the observations are discrete and conditionally dependent, the optimal solution is NP-Complete. When the joint distributions of the sensor observations have a certain structure, it has been shown that the performance of certain decentralized decision rules can be easily determined [51, 62].

Serial Topology

For the serial topology (Figure 7) with binary local decisions, and conditionally independent observations, the LRT at each sensor is an optimal solution, where the LR at sensor j is computed using the sensor observation and the decision at the $(j-1)^{\text{th}}$ sensor [63]. The solution for the optimal threshold values is, in general, hard, but for the serial case, there exist algorithms that can obtain the solution with complexity that is linear in N [64]. A comparison between the parallel and serial networks is reported in [19, 20, 63].

Tree Topology

For the tree topology (Figure 8) with conditionally independent observations, it has been shown that the LRT is an optimal solution to the Neyman-Pearson problem [19]. The solution for the optimal thresholds, as in other network topologies, is generally complicated.

Hierarchical censoring for decentralized detection in WSNs is discussed in [65]. Every sensor is assumed to form its LR from its own observation and the LRs received from its children, and transmit the LR to its parent in the hierarchy. Sensors transmit the LR if the value lies in the send

region R. A simple feedback scheme is employed, where every sensor listens to transmissions from its siblings and transmits its local LR in case of one or more sensors transmitting their local LRs. The ROC curves for the system with and without feedback are compared, for different number of sensors and different probability of sensor transmissions (representing power consumption).

Information-theoretic Quality of Information

Optimization according to information-theoretic criterion has been studied in [15], where the mutual information between the true hypothesis and the decision is proposed as an objective function to be maximized. For the parallel topology, and using PBPO, the optimal decision rules have been shown to be LRTs.

Fully Distributed Topology

All network topologies studied before assume the existence of a fusion center that takes a global final decision. Some work in the literature studies the fully distributed network topology, where sensors communicate with each other and individually take a decision. Two architectures exist, the first allows different local decisions among sensors, while the second assumes a single final decision taken by all sensors. The later is usually referred to as a *consensus* decision.

An example of different local decisions is the work in [12], where the fully distributed hypothesis testing problem is studied. Every sensor is assumed to communicate an intermediate decision to all other sensors in the network, and takes a final decision based on its own observation and decisions received from other sensor nodes. It has been shown that all decision rules are LRT with coupled thresholds, under the IID assumption for sensor observations.

A very similar approach to [12] is studied in [29], using a consensus approach. Instead of letting every local sensor decide differently, sensors rebroadcast their decisions several times until reaching a consensus on a final global decision. Two approaches are proposed, a greedy approach where each sensor makes an optimum decision at each round based on its current data, and n^{th} root approach, where the decision reached by the consensus is constrained to match the centralized decision case,

sacrificing the speed of consensus. Both approaches have been shown to reach consensus with probability one.

As communication to all nodes may overload the communication network, limited local communication with neighboring nodes is assumed in [66], and therefore represents a trade off between isolated local sensor decisions architecture and the global decision architecture, where all sensors communicate to a fusion center. Every local sensor communicates with its neighboring nodes only, and the detection problem is recast into a distributed estimation problem solved by diffusion-based Recursive Least Squares (RLS) algorithms.

Summary

To summarize, for IID observations, the LRT is a PBPO detection strategy at all sensor network nodes, for a variety of network topologies. LRT thresholds are coupled, due to the system-wide objective function, and their calculations are computationally intensive. For dependent observations, finding the optimal detection strategy is an intractable problem.

The literature on decentralized detection is very rich, and it is hard to refer to all published work. For more details about the results in this section, the reader is referred to [19, 20, 67, 68] and the references therein.

II.1.4 Decentralized Detection Integrating Network Reliability

The previous work assumes ideal communication network between nodes. With the deployment of WSNs, this assumption becomes far from the reality. In response, research work shifts the focus to analyze detection networks with different node and channel impairments. According to our taxonomy, this research lies along the four dimensions highlighted in Figure 11, namely quality of information as a design objective, detection strategy as a design variable, and network topology and network reliability as design constraints. In terms of the CPS block diagram, the focus of this work is highlighted in Figure 12. The physical layer of the communication network is considered, while the sensors are assumed with unlimited resources. The optimization problem could be summarized

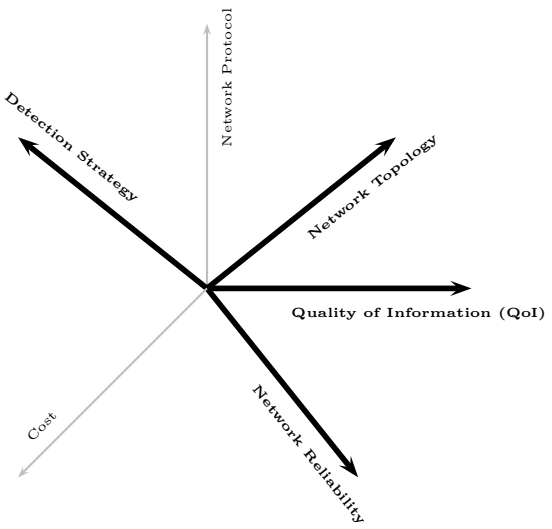

Figure 11: As a result of WSN deployment, a new dimension to decentralized detection research, network reliability, has been added to include network impairments in the analysis.

as:

$$\max_{G} Q(G; T, R) \tag{11}$$

where G is the detection strategy, Q is the quality of information, T is the network topology, and R is the network reliability measure.

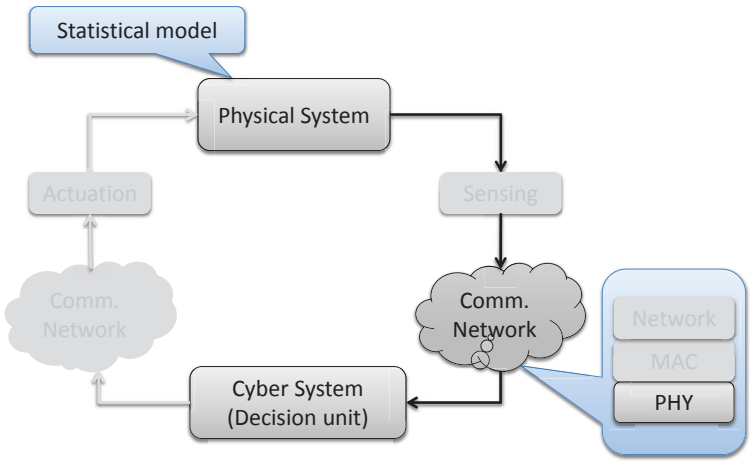

Figure 12: CPS block diagram for decentralized detection integrating network reliability

In the following, we summarize the main research results.

Rate-constrained Channels

For the parallel topology with rate-constrained channel, the following contributions have been made:

Battacharyya distance QoI The design of local quantizers to maximize the Battacharyya distance (a special case of Ali-Silvey distance) is studied in [48]. Parallel topology is assumed, with every communication link between sensor i and the fusion center having a restricted information rate R_i. The channels are assumed error-free, and therefore the provided information rate could be regarded as the *reliable* bit rate below the channel capacity, achieved by proper channel encoding and decoding techniques. Every local sensor then has 2^{R_i} quantization levels. A cyclic optimization algorithms is proposed to find the optimal quantizers.

Neyman-Pearson QoI Decentralized detection under PAC communication constraints is studied in [69]. The channel constraint is in the form of the maximum bit rate allowed for each sensor, which is expressed as a constraint on the probability of false alarm, P_F. The optimization problem is formulated in terms of the new channel constraints, and solved numerically. A randomization test is proposed to mitigate the performance loss.

Bayesian QoI Decision fusion in sensor networks with communication constraints over MAC is considered in [70]. In contrast to most of the literature in the field, where asymptotic analysis or information theoretic performance measures are used to simplify the analysis and design of detection sensor networks, authors in this paper pursue a non-asymptotic approach to design the fusion center and to study the effect of the number of sensors, SNR, and local quantization on the detection performance. The channel model is an error-free MAC, with a bit rate R that constrains the total number of quantization levels for local sensors.

The decentralized detection of a deterministic signal, corrupted by additive noise, over PAC is studied in [71]. The local sensor messages are constrained to binary decisions to ensure low bandwidth requirement, and the detection performance is studied for different noise characteristics.

The work assumes little knowledge about the noise probabilistic behavior, in contrast to the classical assumption of complete knowledge about data distribution under each hypothesis.

A slightly different problem for DD over MAC is treated in [72]. Instead of the usual assumption of fixed number of sensors and quantization levels for every sensor, authors assume that the number of sensors L, and the quantization levels per sensor D_l are design parameters. The MAC channel is characterized by a maximum reliable transmission rate R. The main result shows that having R identical sensors, each sending one bit of information, is optimal, subject to a constraint on the data distribution w.r.t. the two hypotheses. The results are obtained using asymptotic analysis to evaluate the Chernoff information (error exponent).

Noisy Fading Channels

For the parallel and tree topologies with noisy fading channels, the following contributions have been made:

Neyman-Pearson QoI Decision fusion over noisy fading PAC is considered in [34], where it is assumed that local sensors submit binary decisions $u_k \in \{+1, -1\}$, representing the two hypotheses, according to a predefined local mapping rules. Optimal LR fusion rule is derived, and different suboptimal fusion rules are proposed and compared. The optimal decision rule requires instantaneous knowledge about Channel State Information (CSI), which may be costly for resource-constrained sensor networks. A LR decision rule that requires only knowledge about channel *statistics* instead of instantaneous CSI is proposed in [73]. A very similar problem for the multi-hop wireless sensor networks is treated in [74]. A summary for the channel-aware approach for distributed detection is given in [13].

Asymptotic Error Exponent QoI The impact of fading channels and channel errors on the performance of different fusion rules is studied in [75]. Local sensors quantize their observations to binary decisions and transmit them, using a basic binary modulation scheme such as Frequency Shift Keying (FSK), Phase Shift Keying (PSK), and On/Off Keying (OOK), on parallel independent

links that are either slowly Rayleigh fading, or non-fading with BSC model. Large deviations theory is also used to derive the asymptotic error exponent for each fusion rule:

The asymptotic analysis of detection performance over one type of MAC, namely *Type-Based* MAC (TBMA) is studied in [76] (The scheme is also known as a single slot multiaccess communication). It is shown that detection over TBMA has superior performance to TDMA, FDMA, and CDMA schemes, regarding bandwidth and detection performances. The same MAC model is used in [35] to study the decentralized inference problem (detection and estimation), where asymptotic analysis is used.

Decentralized detection in relay sensor networks is studied in [77]. Sensors are assumed to broadcast their log LR to neighboring relay nodes, which combines LR from different sensors and send it to the fusion center. This scheme is different than tree networks in that leaf nodes communicate their decisions to multiple parents. Asymptotic error exponent is derived for two cases of sensor placement, with ideal and fading channels. It has been shown that the error exponent approaches in the limit the parallel fusion network case, when the number of relay nodes approaches infinity.

General Probabilistic Channel

For the parallel topology with a general probabilistic channel model, the following results have been obtained:

Bayesian QoI The optimality of the LRT for local sensor decision rules in PAC is proved in [78]. Sensors are assumed to submit binary decisions, U_i, over separate parallel channels, characterized by $p(Y_i|U_i)$, where Y_i is the output of the channel for sensor i at the fusion center. The system is optimized according to the minimum probability of error criterion, expressed in terms of the probabilistic channel model. PBPO is carried out to derive the optimal local decision rules. The results are generalized in [79] for dependent noisy channels.

Decentralized detection over noisy PAC, modeled as Binary Symmetric Channels is studied in [80], where authors suggest a selective DD strategy, where some links are eliminated if their channel error probability exceeds a certain threshold. Multi-layer detection is also proposed, where

an intermediate layer of relaying nodes is introduced between local sensors and the fusion center. Numerical simulations show the superiority of the multi-layer architecture over the single layer architectures.

Neyman-Pearson QoI Decentralized detection over MAC for arbitrary number of quantization levels is considered in [36]. The objective is to design the local quantizers, given the MAC probabilistic model, according to NP and Bayesian criteria. PBPO is carried out to find the optimal solutions.

Link Failures

A slightly different network architecture is proposed in [81], where a multi-level parallel decision fusion system is deployed. Leaf nodes submit their decisions to all upper layer nodes in the hierarchy, which in turn make their decision and transmit to the next upper layer and so on. The system performance is studied under link failures with two decision strategies; ignore missing strategy, and substitute missing strategy. It has been proved that ignore missing strategy achieves superior performance over substitution strategy, since the later does not add new information to the decision process.

Node Failures

The previously-described work has been focusing on channel impairments. On the other hand, decentralized detection with local sensor failures has attracted some attention. This problem is closely related to decentralized detection with channel errors, when BSC model is assumed, since the channel error and the local sensor fault are modeled in the same way.

Decision fusion with local sensor failures is considered in [82], where local sensors may fail and produce an incorrect decision. The failure impact on the performance is studied using asymptotic analysis, due to the difficulty of obtaining closed form solutions. The work is extended in [38] for parallel and serial network topologies, where the optimal local decision rule is derived and shown

to be a LRT. An algorithm for the numerical solution of the resulting coupled equations is also presented.

Summary

To summarize, the main objective of the research work presented in this section is to study the effect of different communication network impairments on the decentralized detection performance. In some work, detection strategies are assumed, and the objective is to analyze the performance. In other work, optimal detection strategy according to a pre-defined QoI is derived.

II.1.5 Decentralized Detection Integrating Cost Constraints

The cost of deployment of a sensor network is an important design constraint that has not been addressed in the previously discussed work. Recently, the focus of research effort has been the design of decentralized detection systems subject to cost constraints. As sensor power is critical for the lifetime of the WSN, the cost is expressed mainly in terms of average or total power consumption. According to our taxonomy, this research lies along the five dimensions highlighted in Figure 13, namely quality of information and cost as design objectives, detection strategy and cost as design variables, and network reliability and network topology as design constraints. In terms of the CPS block diagram, the focus of this work is highlighted in Figure 14. The energy constraint is added to the analysis in addition to the physical channel model. The optimization problem could be formulated using the following alternatives:

$$\max_{G} Q(G;T,R,C) \text{ subject to } C \leq c \tag{12}$$

$$\max_{C} Q(C;T,R,G) \text{ subject to } C \leq c \tag{13}$$

$$\min_{G} C(G;T,R) \text{ subject to } Q \geq q \tag{14}$$

where G is the detection strategy, Q is the quality of information, T is the network topology, R is the network reliability measure, and C is the deployment cost.

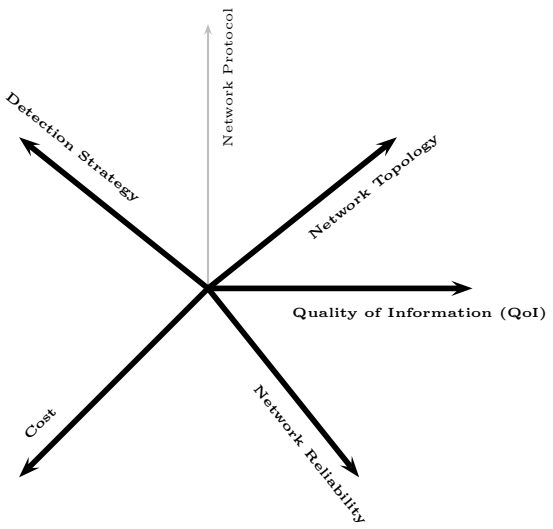

Figure 13: As the cost of WSN deployment becomes a significant factor in decentralized detection systems, a new dimension, cost, has been added to include cost constraints in the analysis.

The expected power is usually expressed as a function of the transmission mapping, e.g., assuming local sensor observations Y and local mapping rule $\gamma(Y)$, the expected power could be expressed as:

$$P(\mathcal{H}_0)E_0[|\gamma(Y)|^2] + P(\mathcal{H}_1)E_1[|\gamma(Y)|^2]$$

where $E_0[.]$ and $E_1[.]$ are the expectations w.r.t. the distributions $p(y;\mathcal{H}_0)$ and $p(y;\mathcal{H}_1)$, respectively. In the following, we summarize the main research results obtained for the parallel topology.

Noisy Fading MAC/PAC Channel

The binary decentralized detection problem, where the network is subject to a joint power constraint is studied in [83]. A parallel access channel, corrupted by additive noise is assumed between every sensor and the fusion center. Large deviations theory is used to show that having identical sensors is asymptotically optimal.

The impact of fading on decentralized detection in power constrained WSNs is studied in [84]. A parallel access channel, that is subject to fading, is assumed between every sensor and the fusion center. Using local transmission mapping rules $\gamma(Y)$, the fusion center receives degraded information

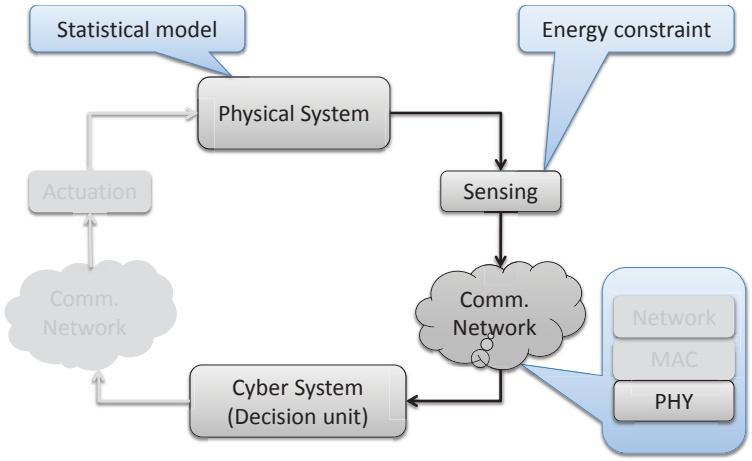

Figure 14: CPS block diagram for decentralized detection with cost constraints

of the form $U = \theta\gamma(Y) + W$, where Θ is the channel gain, and W is an additive noise. Under a power constraint of the form $\sum_{l=1}^{L} f(\gamma_l) \leq A$, it has been shown that using identical functions at all sensor nodes is asymptotically optimal. The results are established using large deviation theory.

Distributed detection over MAC, using unquantized analog communication, is studied in [85]. Two types of power constraints are considered: average power constraint, where individual sensors have no power limit, and total power constraint. Unquantized analog communication is assumed and large deviations theory is used to estimate the error exponent and quantify the performance.

Decentralized detection with censoring sensors under energy constraints is studied in [86]. Optimal decision strategies in Bayesian, NP, and Ali-Silvey sense have been shown to be LRT.

MIMO Channel

Detection over MIMO channels is considered in [33] under individual and total power budget constraints. The objective is to distribute a total transmitter power budget among local sensors, in a way that maximizes a performance metric, chosen to be the J-divergence between the two densities under each hypothesis. Optimal power budget allocation is obtained by numerical solution to the constrained optimization problem, for both the general MIMO channel case, and the orthogonal channel as a special case. It is shown that the proposed power allocation can use as little as 25% of the total power used by equal power allocation.

In a similar problem formulation to [33], authors in [87] study the detection performance for the orthogonal channels special case, using the J-divergence performance metric. Authors introduce two new concepts termed as detection outage and detection diversity, to quantify the long-term system performance in the presence of slow fading for the communication channels.

To summarize, the main problem addressed is to optimize the detection performance subject to a power budget constrain, or conversely to optimize the power allocation subject to a constraint on the detection performance. Since the problem is multi-dimensional, assumptions have to be made to make the analysis tractable. Network topology, channel model, and partial assumption about the detection strategy are usually assumed to simplify the analysis.

II.1.6 Decentralized Detection: A Cross-Layer Approach

The research work discussed so far has focused on the design of physical layer aspects of the sensor node, specifically, quantization and channel encoding techniques. The network details between sensor nodes and the fusion center have been ignored. In practical applications, WSNs nodes communicate using a well-defined communication protocols, to guarantee interoperability and to reduce deployment cost. As a result, every sensor node is regarded as a data network node, implementing different layers of the communication protocol stack, and the transmitted information no longer represents the detection decisions. Rather, detection information is encapsulated in the payload of the data network packet that has overhead bits representing header, synchronization, error correction, as well as other information.

To include the networking aspect into the decentralized detection analysis, we augment the multi-dimensional problem discussed in the previous sections with the network protocol axis, as depicted in Figure 15. This addition opens up a variety of problem formulations for decentralized detection. As an example, the network protocol may be regarded as an additional design constraint to any of the problems discussed in the related work. In terms of the CPS block diagram, the focus of this work is highlighted in Figure 16. This represents the most general block diagram, where different layers of the communication network are considered, in addition to the energy constraints for sensor

nodes. There is not a single study in the literature that considers all communication layers and all constraints. Each study has a different combination of network layers and sensor constraints.

One example for optimization problems in this category would be:

$$\max_{G} Q(G; T, R, C, P) \tag{15}$$

where the objective is to find the optimal detection strategies G, given constraints on the network topology T, network reliability R, cost C, and network protocol P. Alternatively, the network protocol could be a design objective to satisfy certain QoI metric and cost constraints:

$$\max_{P} Q(P; G, T, R, C) \tag{16}$$

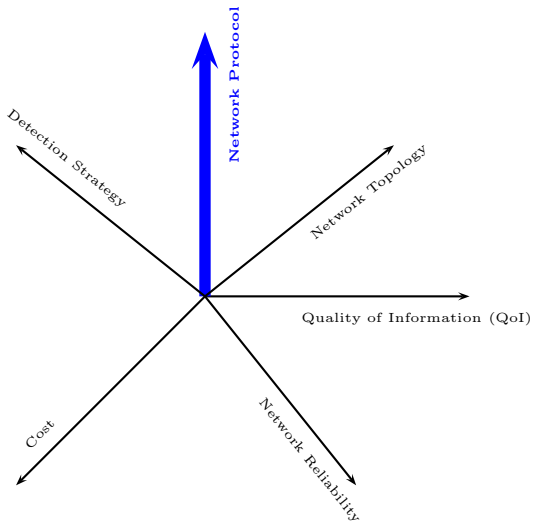

Figure 15: Practical WSNs operate with standard protocols and specifications. Networking adds a new dimension to the decentralized detection problem.

In the following, we present a few preliminary results that fit along this dimension.

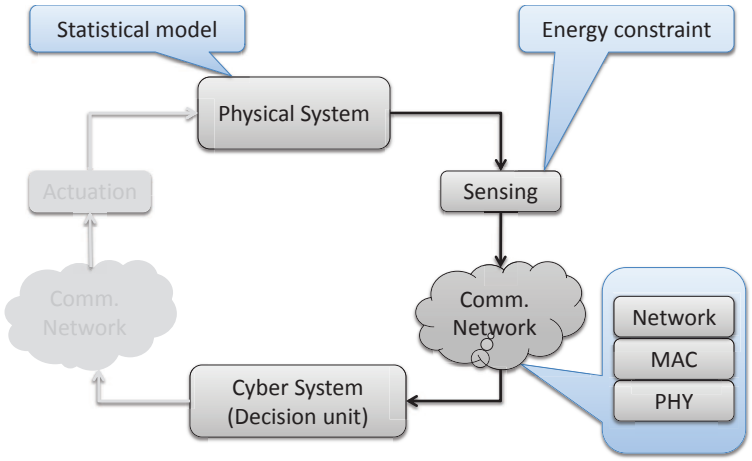

Figure 16: CPS block diagram for cross-layer design in decentralized detection

Parallel Topology

An early investigation of the decentralized detection problem with networking delays and channel errors is studied in [37]. Sensors communicate to the fusion center over PACs that have specific probability of packet loss and channel error. A PBPO local rules and fusion rule are shown to be LRTs with coupled thresholds that depend on the channels probability of packet loss and channel error. The work, however, abstracts away the communication details and assumes PAC, which is not feasible in practical WSNs. Moreover, the method is very complex and does not scale with network size.

Decision fusion over MAC is considered in [88]. Two window-based protocols are studied. The first allows messages to collide, while the second uses a simple collision resolution algorithm similar to slotted ALOHA, with dynamically updated retransmission probability. In both models, message is transmitted if a detection decision is made. The overall performance for both models are compared, and simple rules are given for assessing the conditions under which each one is preferred.

A cross-layer optimization approach is pursued in [89]. A number of K sensors transmit their observations over an independent noisy fading channels, and the observations may or may not arrive based on the channel conditions and the queue state at each sensor nodes. The fading physical channel model is coupled with a queueing model for the sensor node to evaluate the probability

that an observation will be lost. The probability of observation loss is shown to be a function of the communication rate R and the total number of sensors K. K and R are optimized to minimize the unconditional probability of error. The cross-layer approach has been shown to outperform the instantaneous and maximum throughput approaches.

Multihop Networks

Routing for DD Energy-efficient routing for signal detection in WSNs is studied in [27] for radar-like sensors that are distributed geographically to detect the presence of an object through active sensing. The paper couples the detection performance with the energy consumed in information transmission to the fusion center in a single joint optimization problem. Three different routing metrics are proposed, which trade off between the detection performance and the energy expenditure. The routing problems are formulated as combinatorial optimization programs, and solutions are provided. Simulation results are also provided to demonstrate the energy and detection performance trade-off for each proposed routing metric.

Transmission Schemes Comparison Distributed detection via multi-hop transmission in WSNs is studied in [26]. The sensor nodes and the fusion center are assumed to constitute a fully-connected graph, where every edge $e = (i, j)$ represents a wireless communication path between nodes i and j. The energy of every edge is proportional to the distance between connected nodes, $w(e) = d(i, j)^k$, where k is the path loss exponent with a typical value of 2.5 for wireless networks. The transmission structure is a spanning tree rooted at the fusion center, which minimizes the total transmission energy. The following transmission schemes are compared based on their detection performance and energy expenditure: 1) direct transmission from sensor nodes to the fusion center, 2) multihop forwarding, where intermediate nodes forward the information without processing, 3) multihop histogram fusion, where each sensor sends only the histogram (type) of its observation and its descendants, and 4) multihop LLR fusion, where intermediate nodes forms a new LR from its own observation and its descendant' LRs . The delay for detection is not considered in the paper, which results in the superior performance of multihop forwarding over direct transmission, from

the energy point of view, since both have the same detection error probability, although the fusion center has to wait more time to collect all observations to achieve the same performance of the direct transmission case. In addition, sensors are assumed to send their observations to the parent node without contention, thereby ignoring the delay encountered due to collisions if the channel access technique is MAC, or due to transmission scheduling if the channel access technique is TDMA or FDMA.

Rate Allocation for DD The problem of rate allocation in a multi-node multi-hop network used for detection applications is studied in [28]. Given a set of sensors, it is required to select the transmission rate for every sensor to maximize the QoI, represented by the probability of correct decision (alternatively minimizing the probability of error), subject to a set of constraints on the link capacities. Simulation results are provided to demonstrate the system performance.

II.2 Detection in Aircraft Synchronous Generators

In this section, we discuss the detection problem in aircraft generators. Due to the small machine size and the critical mission it performs, wireless sensors have not yet been deployed for generator monitoring and control. Detection in synchronous generators has relied on physics-based models as well as statistical models for the machine. In the following, we briefly mention existing work on generator modeling and fault detection.

Synchronous generator models have been around since the early 20^{th} century. The standard model used to represent a *single* synchronous AC generator is the dq0 model, that is based on Park's transformation [90]. Whereas the dq0 model is very useful to represent symmetric machine operations under balanced conditions, these advantages are lost when analyzing unbalanced conditions, or asymmetrical faults [91]. For these cases, the abc modeling approach is more appropriate [92].

To model the *complete* brushless generator, both synchronous generators and the rectifier circuit have to be explicitly modeled. The rectifier is composed of switching elements (diodes) which introduce discrete dynamics into the overall system behavior. The traditional way of analyzing switching circuits relies on averaging or discretization techniques to make the analysis of the circuit

more tractable [93]. To accommodate the behavior caused by diode faults, we explicitly model the diode components of the complete brushless generator. This requires the adoption of a hybrid systems modeling approach [94].

Winding faults have received considerable attention in the literature, and different approaches have been proposed for winding fault detection. Specifically, the use of search coils to measure air gap flux asymmetry has been proposed to detect inter-turn faults [95]. This requires extra equipment that may be difficult to install in existing machines. For short circuit faults, one approach is to measure the circulating current in the main armature coils [96]. This approach is dependent on the generator design and cannot be applied in general. Another approach is the injection of voltage pulses in the rotor field winding and measuring the reflected signal [97]. This technique is clearly not applicable on brushless designs where the rotor field winding is not accessible. Harmonic analysis has been proposed to detect and isolate field and armature windings inter-turn faults as well as phase to ground faults [98–100]. However, harmonic signals depend on generator construction and excitation, and change with varying loads, making the discrimination between faults and load fluctuations a difficult task.

Artificial Neural Networks (ANNs) have been proposed to diagnose internal machine faults in [101]. The difficulty with using neural networks is that they require large, comprehensive data sets that capture different modes of operation of the machine and a number of fault conditions and magnitudes to effectively classify fault conditions. Different combinations of loads, faults, fault locations and magnitudes, and current signal values are required to generate the training data sets. Unless sufficient data is available to cover a majority of these conditions, the neural network classifier will be inaccurate and it may generate incorrect results [102].

Researchers have paid less attention to the detection of rectifier diode faults when compared to winding faults. Diode faults, although not representing an immediate risk on the generating system, may develop into a condition causing machine malfunction [7]. The traditional way to detect diode faults is through harmonic analysis of the exciter generator field current [103], or by calculating a

simple ratio of the RMS main generator current to the exciter generator field current. The use of search coils in the air gap has also been proposed in [104].

In Chapter III, we model the complete Integrated Drive Generator (IDG) system and study diode fault behavior in addition to winding faults. We model the system in sufficient detail, and then develop fault signatures by understanding the physics of the failure events. Unlike existing work that relies on existing measurements or adds new equipment to measure additional signals, having a complete model for the system with faulty conditions allows the estimation of hidden states, and therefore, expands the set of signals that could be exploited for Fault Detection and Isolation (FDI).

II.3 Intermittent and Incipient Fault Detection

The interest in intermittent faults goes back to the initial days of digital circuits design. At those days, it was noticed that up to 90% of the faults in digital circuits can be estimated to be intermittent [105]. This high percentage motivated the research on modeling, analysis, and detection of intermittent faults. The models proposed are based on the two-state Markov chain, where one state represents a no-fault condition while the other state represents the fault condition. The Markov chain maybe defined as a continuous-time or discrete-time, depending on the application. For an early survey on different intermittent fault models and reliability analysis, please refer to [105].

Intermittent fault diagnosis using statistical observations has been considered in the literature. A Bayesian approach to multiple intermittent fault diagnosis has been considered in [106], where a Bayesian framework is used to calculate the posterior fault candidate probability. Intermittent fault diagnosis for scan chain, the most pervasive design for testability techniques in VLSI, is considered in [107] based on signal probability analysis. Intermittent fault diagnosis in multiprocessor systems is studied in [108], where a probabilistic model for the behavior of the intermittent processor fault is formulated and used in the fault diagnosis process.

In this dissertation, we use change detection algorithms to detect intermittent, incipient, as well as persistent faults. Change detection is a well-understood problem and several algorithms have been

proposed in the mathematical statistics literature. The two main approaches to detect a change are the weighted CUSUM algorithm and the Generalized Likelihood Ratio (GLR) algorithm [109]. Since CUSUM algorithm requires prior information about the unknown magnitude after change, it results in an integration that may not be easy to evaluate. Therefore, we choose the GLR algorithm for the work in this dissertation. Detector performance analysis and tuning follow the guidelines in [109].

Estimation of the unknown fault parameters follows the classical work on estimation theory [110]. Specifically, Maximum Likelihood (ML) estimators are used to estimate the mean time between faults and the mean fault duration. Minimum Variance Unbiased Estimators (MVUE) are used in conjunction with the linear model to estimate the slope of incipient faults.

For the differential protection case study; intermittent fault detection in aircraft generator winding, intermittent faults in aircraft generators have been reported recently as one of the causes of serious incidents to aircrafts [3]. Two of the major candidates for intermittent faults are winding and cable faults [111]. Differential protection has been successfully used in detecting persistent winding faults [99]. An adaptive threshold is typically employed to prevent unnecessary tripping of the relay due to measurement noise or current transformer saturation [112]. We extend the differential protection technique in this dissertation to detect intermittent faults in addition to the abrupt faults.

II.4 Comparison to the Research Work

The work in this dissertation spans different dimensions of model-based detection in CPS. We study physics-based modeling for aircraft generators, where we develop a detailed machine model that was not treated before in the literature. We thoroughly study the problem of intermittent fault detection and estimation, where we develop a general framework that is independent on the monitored system. Finally, for detection in WSNs, we consider all the design aspects shown in Figure 15. To do that, we pursue a model-based approach to design the wireless sensor network. The model-based approach allows us to include different quality measures for the sensor network in the design process. It allows us to integrate different system layers in one unified model, and study their interactions and effect on the global system behavior. Specifically, we consider the following:

1. **Network Reliability.** We consider the physical Channel State Information (CSI) between each sensor node and the fusion center. We model the physical channel in order to study the effect of its reliability on the overall system performance.

2. **Quality of Information.** In addition to the classical QoI measures outlined in Section II.1.2, we also consider the delay for detection as an important quality measure in uncertain wireless networking environments.

3. **Network Topology.** We consider both the parallel topology in Chapters VI and VII, and the tree topology in Chapter VIII.

4. **Network Protocol.** We include the MAC sublayer in the design process. We consider slotted ALOHA MAC protocol in Chapters VI and VIII, and TDMA transmission scheme in Chapter VII.

5. **Detection Strategy.** Our focus in this dissertation is on the integration of different system components and quality measures in one unified model, rather than the classical study of local signal processing algorithms at sensor nodes. It has been shown that most of the information provided by local observations can be compressed to very few bits and that the performance loss decays rapidly as the number of information bits per transmission increases [34, 83]. For a local sensor node implementing network functionality, the packet payload will be large enough to represent the value of the local decision rule with a high accuracy and negligible quantization error. Therefore, for analysis purposes, it can be assumed that the receiver has the same replica of the transmitted local decision. However, we consider the effect of quantization on the overall detection system performance in Chapter VIII.

6. **Cost.** To prolong the network lifetime, the energy allocated for any sensor network task should be constrained. Therefore, we consider the energy constraint in the design of the sensor network.

The focus of the research is summarized in the CPS block diagram in Figure 17, where the different components as well as the modeling approaches are shown. Unlike existing work, where only one layer

of the communication network is considered in combination with sensor constraints, we consider the physical and MAC layers, in addition to the energy constraints for the sensor network. We integrate the different layers and constraints in one unified model, and focus on the network design and resource allocation among sensors to achieve the optimal detection performance. In addition, we consider both the development of physics-based models, as well as intermittent fault detection for physical systems.

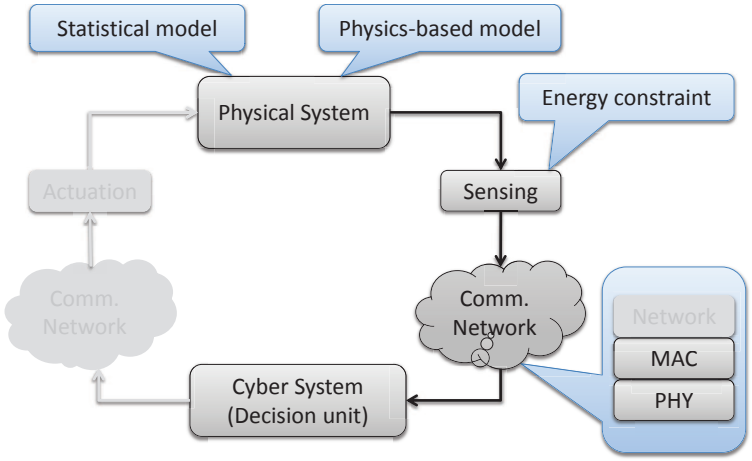

Figure 17: CPS block diagram for the research work

CHAPTER III

Aircraft Power Generators: Hybrid Modeling and Simulation for Fault Detection

In this chapter, we address the problem of physics-based modeling for fault detection. We explore the power of physics-based modeling to accurately represent the physical system behavior under both nominal and faulty conditions. We consider the Integrated Drive Generator as our case study. IDG is the main source of electrical power for a number of critical systems in aircraft. As such, fast and accurate fault detection and isolation are necessary components for safe, reliable, and efficient operation of the IDG and the aircraft. Since IDGs are complex systems, the majority of the existing fault detection and isolation techniques for the electrical subsystem (brushless generator) are based on signal analysis and heuristic methods that are derived from experience. Since model-based detection is more general and powerful in designing detection and isolation schemes, we develop in this chapter an accurate model for the brushless generator that captures the machine behavior under both nominal and faulty conditions. We exploit the hybrid modeling capability to accurately model different rectifier diode faults and rotor winding faults, reported as the most likely brushless generator faults. We simulate the hybrid model for nominal and different faulty conditions, and develop fault signatures for different machine faults [6]. In terms of the general CPS block diagram presented in Chapter I, we consider the physical system, sensors, cyber system (controller), and the actuator (exciter generator). We ignore the communication network since IDGs are usually monitored and controlled by hard-wired sensors and controllers. The scope of the study is reproduced in Figure 18.

The rest of the chapter is organized as follows: Section III.2 describes the IDG block diagram, explaining different system components and their function. Section III.3 discusses our hybrid model for the brushless generator. Section III.4 includes a discussion on modeling different types of field winding faults. Section III.5 presents a general framework to extend the generator model to include an arbitrary number of open-circuit diode faults. Section III.6 presents simulation results for normal

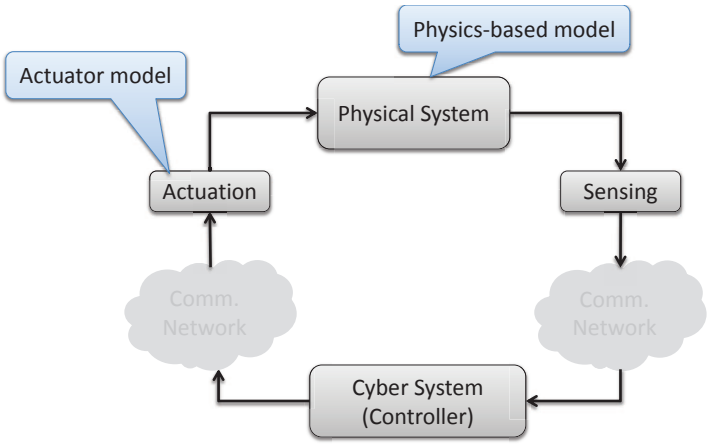

Figure 18: Focus of physics-based modeling study in CPS.

and different faulty behaviors of the machine. Section III.7 includes a discussion on modeling and simulation results, and Section III.8 concludes the work.

III.1 Introduction

The Integrated Drive Generator is the primary source for electrical power in the aircraft. The system draws its power from the main aircraft engines and comprises two synchronous generators that operate in a brushless configuration. It also includes a number of other subsystems that convert the mechanical energy into electrical energy at a pre-specified voltage and frequency. Since the machine operates in harsh environments, different components are subject to degradations and faults that can vary in terms of their critical effects on system behavior. For the electrical subsystem of the IDG, the most critical faults are winding faults and rectifier diode failures [7]. Fast and accurate Fault Detection and Isolation is a necessary component for the safe and reliable operation of the IDG, and, therefore, the aircraft.

The majority of existing techniques for FDI of synchronous generators are model-free [99–101, 113]. Some of these techniques require the installation of additional hardware, e.g., search coils, yet this may not be possible for existing IDG installations. Other techniques assume special machine designs, e.g., the ability to measure circulating current in the main armature winding, or have access to measurements that are not available in brushless designs. Harmonic analysis has been proposed

as an alternative technique to detect machine faults [100], but fault discrimination with harmonic analysis is a difficult task since different faults have similar effect on the harmonics generated in the machine windings during faulty operations.

On the other hand, Model-Based Diagnosis (MBD) techniques that utilize structural and analytic information captured in the system model provide a more general and powerful framework for designing FDI schemes [114, 115]. The distinguishing feature of MBD approach is the use of a system model that describes the laws which govern the behavior of the system for *all possible inputs*. Once a model is provided, the MBD engine should be able to detect system faults by comparing its input/output observations to the predicted behavior using the provided model. Furthermore, different models can be provided to the MBD engine for different faults, and the MBD would be able to diagnose the fault, by comparing the actual system behavior to the predicted behavior from different models [116]. An added benefit of MBD is that it provides methods for establishing the set of measurements required to discriminate among different fault types (i.e., the measurement selection problem [117]).

Despite the advantages of MBD, little work has been done in this area for brushless generators. One of the reasons is that, constructing an appropriate model for the machine is challenging due to the multiple phenomena that need to be captured by the model. In addition, the resulting model is, in general, a complex, non-linear, and time-varying model that is hard to analyze. Despite these challenges, there are some practical considerations and reasonable approximations that, if taken into account while building the model, result in a simpler model, yet with sufficient accuracy to capture the machine behavior aspects. For example, current machine implementations allow continuous operation in the linear range of the magnetic curve, except for overload conditions. Therefore, unless it is desired to study the machine behavior during overload conditions, magnetic saturation could be neglected. Also, from a practical point of view, the mechanical subsystem that regulates the speed of rotation is robust to electrical subsystem fluctuations, due to sophisticated feedback control algorithms. Therefore, the mechanical subsystem could be decoupled from the electrical

subsystem with minor loss of model accuracy. Similar approximations and practical considerations can result in system representations that are easier to analyze.

The first contribution of this work is the development of a novel *hybrid* dynamical model for the *complete* brushless AC generator, based on *phase domain* representation. The key to model-based techniques is to build an accurate model for the system. The traditional approach for modeling AC synchronous generators is based on the dq0 model, where the well-known dq transformation is applied to the state variables (winding fluxes or currents) to convert the linear time-varying system to a linear time-invariant one in the d-q frame of reference [92,118]. To obtain a time-invariant system, the transformation assumes that symmetric conditions apply to the machine model. When faults occur in the system, or a nonlinear load is connected to the machine, the conditions of symmetry are violated for the IDG exciter generator with the rectifier circuit as a load. In this case, the dq transformation does not produce a time-invariant system, therefore, the advantages of applying the transformation are lost. In general, dq0 modeling is useful only for the analysis and simulation of the normal behavior of generators, where the normal operating range is sufficient for designing generator feedback controllers. However, if it is important to study and analyze a wide variety of machine configurations and transient phenomena (especially those caused by faults), then a phase domain behavior model (with no transformations) more accurately represents the resultant behavior, and, therefore, is more useful for fault detection and isolation applications. Moreover, the phase domain representation has the advantage of handling the inherent asymmetries in the brushless design. With the goal of MBD, we focus on methods for systematically modeling and simulating a variety of nominal and faulty behaviors of the complete brushless generator.

In typical simulation studies, the focus is on the modeling of a single generator [91, 119]. The exciter generator and the rectifier circuit are represented by a constant DC voltage source. This approach is adequate for the fault-free exciter generator and rectifier circuits, but recent fault criticality analysis studies have shown that the highest priority failure modes are rotor field winding faults, rotating rectifier diode faults, and shaft bearing failures [7]. Therefore, to satisfy the need for more accurate models for FDI of the generators, we have to build models that accurately capture

the exciter generator dynamics. Since the output of the exciter generator is connected to a rectifier circuit that contains switching elements, we adopt a hybrid modeling approach, where discrete and continuous dynamics are combined, to accurately model the complete brushless AC generator under normal and faulty conditions.

The second contribution of this work is the accurate modeling of the IDG in the presence of different rectifier diode faults and winding faults, using the hybrid system modeling approach. For diode faults, a short circuit fault eventually leads to an open circuit condition, as the resultant over current burns the diode. Therefore, we only consider open circuit diode faults in this work. Field winding faults could be either parametric or structural faults, where parametric faults are characterized by a change in the magnitude of one (or more) system model parameters, while structural faults change the system configuration and cannot be represented by a system parameter magnitude change alone. We focus our attention on parametric faults to simplify the exposition in this work. However, the proposed model could be easily extended to include structural faults, by including the additional current loops in the model representation. We show that the proposed hybrid model can be effectively used to represent the brushless generator for the two fault types considered.

Our third contribution is the implementation and simulation of the hybrid system model, under normal and faulty conditions. This emphasizes the power of model-based methods to capture system dynamic behavior. Using the hybrid model, we develop fault signatures for rectifier diode faults and winding parametric faults. The fault signatures include non-measurable signals in addition to the measured terminal signals. The inclusion of non-measurable signals is unique to model-based FDI since it is possible to estimate the hidden states of the system, subject to the satisfaction of system observability conditions.

III.2 Aircraft IDG

Figure 19 illustrates the IDG system block diagram. The modeled generator operates in a 3-phase brushless configuration, with its drive end connected to a prime mover that is driven by the aircraft engine. The electrical subsystem is composed of four main components: the exciter generator, the

rectifier, the main generator (with connected load), and the Generator Control Unit (GCU). The exciter generator field current produces a magnetic field whose strength is proportional to the exciter current. The rotation of the prime mover in the magnetic field induces a 3-phase voltage in the exciter armature, which is rectified by the three-phase diode rectifier. The DC voltage current (with ripples) from the diode rectifier is then applied to the main generator field winding, which produces a 3-phase voltage in the main generator armature connected to the load. To keep the terminal voltage at (or close to) its operating value, the GCU calculates the Root Mean Square (RMS) value of the 3-phase voltages, compares it to a reference value, and regulates the field voltage of the exciter generator, using a predefined control algorithm. The exciter generator armature, rectifier, and the main generator field (enclosed in a gray dashed rectangular box) rotate with the main shaft that drives the entire brushless generator system, while the exciter field, the main generator armature, the GCU, and the load are stationary.

The mechanical subsystem is composed of the governor, which regulates the shaft speed by acting on a hydraulic unit/differential assembly. The differential unit adds or subtracts speed to drive the generator at a constant speed despite the variations of engine speed.

In this work, we model the electrical subsystem including the exciter generator, rectifier, and the main generator with connected load. To simplify the presentation, we model the governor as a simple PI controller and assume ideal hydraulic/differential assembly, where the output of the PI controller represents the mechanical torque that is applied directly to the IDG.

III.3 Brushless AC Generator Hybrid Model

Figure 20 illustrates the electrical schematic diagram for the brushless generator system (excluding the GCU). Each generator is represented by a set of magnetically coupled windings, namely the field winding (denoted by fd), the 3-phase output windings (denoted by a, b, and c), and the damper windings (denoted by kq and kd). The damper windings are used only in the main generator. The rectifier circuit is represented by a 3-phase diode bridge circuit.

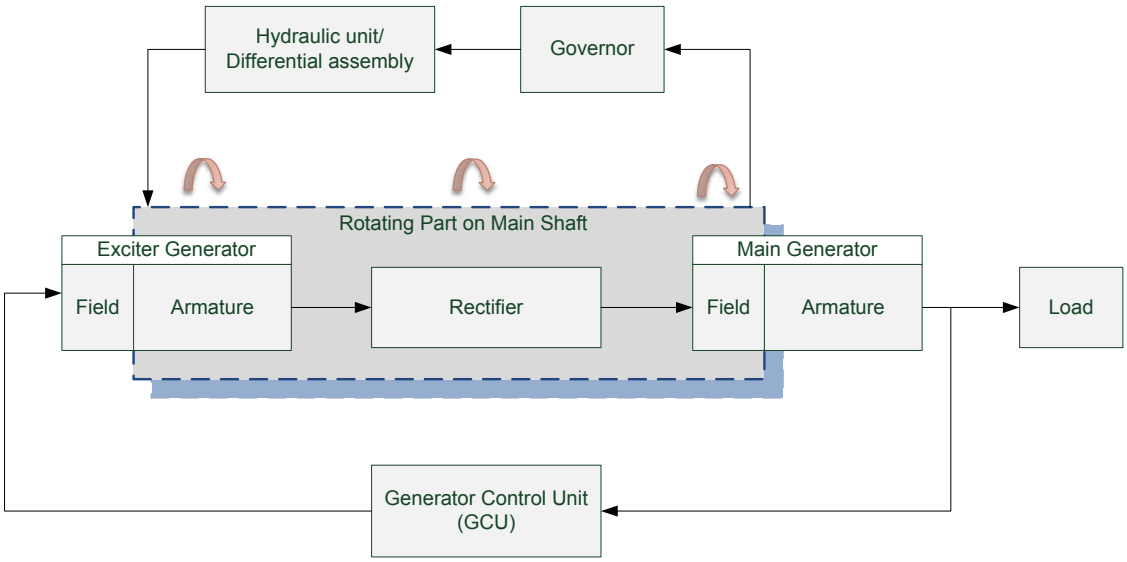

Figure 19: Integrated Drive Generator (IDG) system block diagram. The electrical subsystem includes the exciter generator, rectifier, and the main generator with connected load. It is controlled by the GCU. The mechanical subsystem includes the governor and the differential assembly. System components enclosed in the gray box rotate with the main shaft, while the remaining components are stationary, giving rise to the brushless design.

Table 2 lists a glossary of the state variables and resistance parameters used in the model, where subscript $x \in \{a, b, c, kq, fd, kd\}$ corresponds to a specific winding. To differentiate between the parameters and state variables for the exciter generator and the main generator, we use the $\hat{\cdot}$ notation, e.g. $\hat{r}_a$, for exciter generator variables. A complete glossary for model parameters is found in Tables 4 and 5.

We derive the mathematical model for the complete generating system by applying the Kirchoff's Voltage Law (KVL) equations to each winding, taking into account the magnetic coupling between the different windings. However, the rectifier circuit with its switching diodes creates multiple configurations (modes) for the system. Each mode of operation is defined by the combinations of forward and reverse-biased diodes in the rectifier, and the system behavior in each mode is defined by a set of differential equations.

We model diodes as ideal switches, acting as short circuit when forward-biased, and open circuit when reverse-biased. A detailed model for the rectifier that takes into account the conduction overlap phenomenon (arising from exciter generator inductances) would require 13 modes of operation;

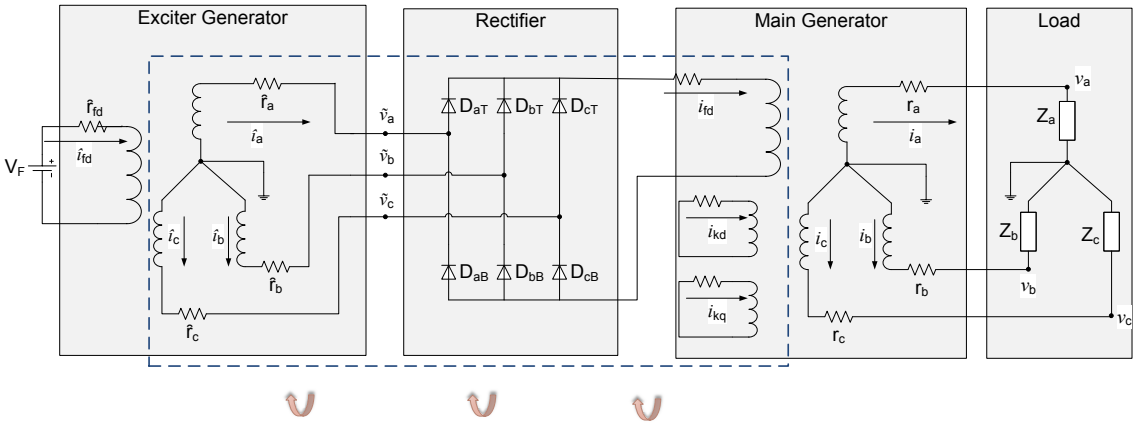

Figure 20: Brushless AC generator electrical schematic diagram

Table 2: Glossary of aircraft generator model variables

Variable	Description
i_x	Winding-x current, main generator.
$\hat{i}_x$	Winding-x current, exciter generator.
v_x	Winding-x voltage, main generator.
$\hat{v}_x$	Winding-x voltage, exciter generator.
λ_x	Winding-x flux linkage, main generator.
$\hat{\lambda}_x$	Winding-x flux linkage, exciter generator.
r_x	Winding-x resistance, main generator.
$\hat{r}_x$	Winding-x resistance, exciter generator.
ω	Electrical angular velocity.
θ_r	Angular displacement.
T_m	Mechanical input torque.
P	Number of pole pairs of the main/exciter generators.
J	Rotor inertia
D	Damping coefficient of the mechanical rotational system

six modes for the classical conduction, six modes of overlap, and one discontinuous conduction mode [120]. In this work, we ignore the conduction overlap phenomenon and model only the classical conduction modes to simplify the exposition. However, the reader should note that the impact of modeling the conduction overlap is the addition of extra modes in the hybrid model with the relevant dynamics. Therefore, the results presented here would still be applicable with a straightforward extension of the model. Table 3 lists the six classical modes of operation with their relevant terminal voltage conditions, and the forward-biased diodes (all remaining diodes are reverse-biased).

Table 3: Generator hybrid model modes of operation

Mode	Exciter Terminal Voltage Condition	Forward-biased Diodes
AB	$\hat{v}_a > \hat{v}_c > \hat{v}_b$	D_{aT} and D_{bB}
AC	$\hat{v}_a > \hat{v}_b > \hat{v}_c$	D_{aT} and D_{cB}
BC	$\hat{v}_b > \hat{v}_a > \hat{v}_c$	D_{bT} and D_{cB}
BA	$\hat{v}_b > \hat{v}_c > \hat{v}_a$	D_{bT} and D_{aB}
CA	$\hat{v}_c > \hat{v}_b > \hat{v}_a$	D_{cT} and D_{aB}
CB	$\hat{v}_c > \hat{v}_a > \hat{v}_b$	D_{cT} and D_{bB}

Figure 21 shows the corresponding system automaton with the six discrete modes and the guard conditions expressed in terms of exciter generator terminal voltages. The ignored modes of overlap would fit between every pair of the classical modes, with obvious guard conditions. As an example, an additional mode between modes AB and AC would be needed to represent the overlapping period where diodes D_{aT}, D_{bB} and D_{cB} are simultaneously forward-biased. For every discrete mode, the system evolves according to its continuous dynamics. For brevity, we present the mathematical model for mode AB only, but the dynamics of the other discrete states can be derived in a similar way.

The electrical schematic diagram for mode AB is illustrated in Figure 21. Inside the dashed box, windings a and b of the exciter generator and winding fd of the main generator are connected together, while winding c of the exciter generator is floating. Applying KVL, we get the following set of equations:

$$\dot{\lambda}_a = r_a i_a + v_a \tag{17}$$

$$\dot{\lambda}_b = r_b i_b + v_b \tag{18}$$

$$\dot{\lambda}_c = r_c i_c + v_c \tag{19}$$

$$\dot{\lambda}_{kq} = -r_{kq} i_{kq} \tag{20}$$

$$\dot{\hat{i}}_a - \dot{i}_{fd} = 0 \tag{21}$$

$$\dot{\lambda}_{kd} = -r_{kd} i_{kd} \tag{22}$$

$$\dot{\hat{\lambda}}_a - \dot{\hat{\lambda}}_b - \dot{\lambda}_{fd} = (\hat{r}_a + \hat{r}_b + r_{fd})\hat{i}_a \tag{23}$$

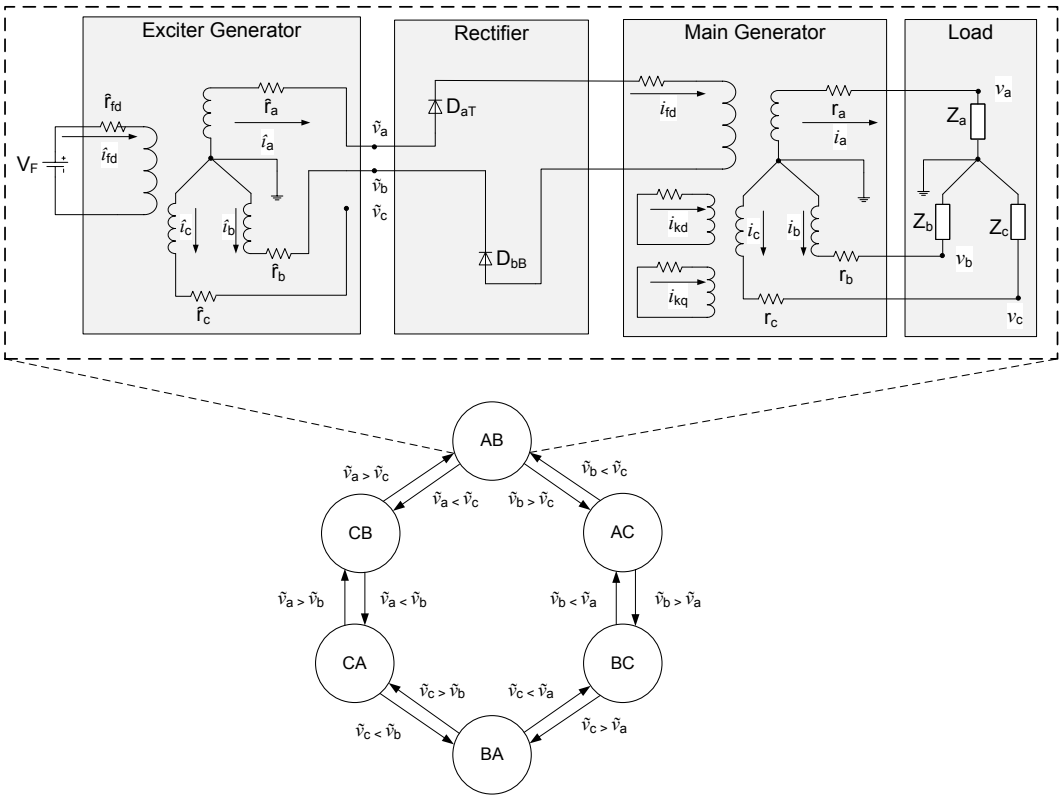

Figure 21: Brushless generator system automaton. The dashed box shows the electrical schematic diagram when the system is in mode AB, where windings a and b of the exciter generator, and winding fd of the main generator are connected together, while winding c of the exciter generator is floating.

$$\dot{\hat{i}}_a + \dot{\hat{i}}_b = 0 \tag{24}$$

$$\dot{\hat{i}}_c = 0 \tag{25}$$

$$\dot{\hat{\lambda}}_{fd} = -\hat{r}_{fd}\hat{i}_{fd} + V_F \tag{26}$$

$$\dot{\omega} = \frac{P}{2J}\left(T_m - T_e - \hat{T}_e - D\omega\right) \tag{27}$$

$$\dot{\theta}_r = w \tag{28}$$

T_e and $\hat{T}_e$ denote the electric (load) torque of the main and exciter generators, respectively, and are given by [92]:

$$
\begin{aligned}
T_e = {} & \frac{P(L_{mq}-L_{md})}{6}\left[i_a^2-0.5(i_b+i_c)^2-i_a(i_b+i_c)\right]\sin(2\theta_r) \\
& + \frac{PL_{md}}{3}\left(\frac{N_{fd}}{N_s}i_{fd}+\frac{N_{kd}}{N_s}i_{kd}\right)\left[i_a-0.5i_b-0.5i_c\right]\cos(\theta_r) \\
& + \frac{\sqrt{3}P(L_{mq}-L_{md})}{8}\left(i_b^2+i_c^2-2i_ai_b+2i_ai_c\right)\cos(2\theta_r) \\
& + \frac{P(L_{mq}-L_{md})}{2}i_bi_c\sin(2\theta_r)+\frac{PL_{md}}{2\sqrt{3}}\left[i_b-i_c\right]\sin(\theta_r) \\
& - \frac{N_{kq}P}{3N_s}L_{mq}i_{kq}\left[i_a-0.5i_b-0.5i_c\right]\sin(\theta_r)+\frac{N_{kq}P}{2\sqrt{3}N_s}L_{mq}i_{kq}\left[i_b-i_c\right]\cos(\theta_r)
\end{aligned} \tag{29}
$$

$$
\begin{aligned}
\hat{T}_e = {} & \frac{P(\hat{L}_{mq}-\hat{L}_{md})}{6}\left[\hat{i}_a^2-0.5(\hat{i}_b^2+\hat{i}_c)^2-\hat{i}_a(\hat{i}_b+\hat{i}_c)\right]\sin(2\theta_r) \\
& + \frac{\sqrt{3}P(\hat{L}_{mq}-\hat{L}_{md})}{8}\left(\hat{i}_b^2+\hat{i}_c^2-2\hat{i}_a\hat{i}_b+2\hat{i}_a\hat{i}_c\right)\cos(2\theta_r)+\frac{\hat{N}_{fd}P}{2\sqrt{3}\hat{N}_s}\left[\hat{i}_b-\hat{i}_c\right]\sin(\theta_r) \\
& + \frac{P(\hat{L}_{mq}-\hat{L}_{md})}{2}\hat{i}_b\hat{i}_c\sin(2\theta_r)+\frac{\hat{N}_{fd}P}{3\hat{N}_s}\hat{L}_{md}\hat{i}_{fd}\left[\hat{i}_a-0.5\hat{i}_b-0.5\hat{i}_c\right]\cos(\theta_r)
\end{aligned} \tag{30}
$$

There are 12 state variables, representing the currents in the different windings, in addition to the angular displacement θ_r, and angular velocity ω. From (21), (24), and (25), we have four dependent currents, which reduces the state variables to nine. However, we use the twelve state variables to keep the model representation consistent between the different modes, and also to facilitate model implementation.

We define the following vectors:

$$
\boldsymbol{\lambda} = \begin{bmatrix} \lambda_a & \lambda_b & \lambda_c & \lambda_{kq} & \lambda_{fd} & \lambda_{kd} \end{bmatrix}^T
$$

$$
\mathbf{i} = \begin{bmatrix} i_a & i_b & i_c & i_{kq} & i_{fd} & i_{kd} \end{bmatrix}^T
$$

$$
\hat{\boldsymbol{\lambda}} = \begin{bmatrix} \hat{\lambda}_a & \hat{\lambda}_b & \hat{\lambda}_c & \hat{\lambda}_{fd} \end{bmatrix}^T
$$

$$
\hat{\mathbf{i}} = \begin{bmatrix} \hat{i}_a & \hat{i}_b & \hat{i}_c & \hat{i}_{fd} \end{bmatrix}^T
$$

$$
\mathbf{R} = \begin{bmatrix} r_a & r_b & r_c & -r_{kq} & 0 & -r_{kd} & \hat{r}_a+\hat{r}_b+r_{fd} & 0 & 0 & -r\hat{f}_d \end{bmatrix}
$$

$$
\mathbf{u} = \begin{bmatrix} v_a & v_b & v_c & 0 & 0 & 0 & 0 & 0 & 0 & V_F \end{bmatrix}^T
$$

We have the following $\lambda - i$ relationship for the main generator:

$$\boldsymbol{\lambda} = \mathbf{L}\mathbf{i} \quad \Rightarrow \quad \dot{\boldsymbol{\lambda}} = \mathbf{L}\dot{\mathbf{i}} + \dot{\mathbf{L}}\mathbf{i} \tag{31}$$

and for the exciter generator:

$$\hat{\boldsymbol{\lambda}} = \hat{\mathbf{L}}\hat{\mathbf{i}} \quad \Rightarrow \quad \dot{\hat{\boldsymbol{\lambda}}} = \hat{\mathbf{L}}\dot{\hat{\mathbf{i}}} + \dot{\hat{\mathbf{L}}}\hat{\mathbf{i}} \tag{32}$$

where $\mathbf{L}$ and $\hat{\mathbf{L}}$ are the inductance matrices for the main and exciter generators, respectively. The matrices are time-varying, depending on the angular displacement θ_r, and their expressions are given in the appendix. Combining (17)-(32) together, and using the notation $\mathbf{L}_2$ to designate row 2 of matrix $\mathbf{L}$, and $\mathbf{1}_{nm}^{i_1 j_1, i_2 j_2, \cdots}$ to designate an $n \times m$ matrix with all zero elements except elements $(i_1, j_1), (i_2, j_2), \ldots$, we get:

$$\mathbf{M}\begin{bmatrix} \dot{\mathbf{i}} \\ \dot{\hat{\mathbf{i}}} \end{bmatrix} = (\mathbf{N} + \mathbf{R})\begin{bmatrix} \mathbf{i} \\ \hat{\mathbf{i}} \end{bmatrix} + \mathbf{u}$$

where:

$$\mathbf{M} = \begin{bmatrix} \mathbf{L}_1 & \mathbf{L}_2 & \mathbf{L}_3 & \mathbf{L}_4 & -\mathbf{1}_{16}^{15} & \mathbf{L}_6 & -\mathbf{L}_5 & \mathbf{0} & \mathbf{0} & \mathbf{0} \\ \mathbf{0} & \mathbf{0} & \mathbf{0} & \mathbf{0} & \mathbf{1}_{14}^{11} & \mathbf{0} & \hat{\mathbf{L}}_1 - \hat{\mathbf{L}}_2 & \mathbf{1}_{14}^{11,12} & \mathbf{1}_{14}^{13} & \hat{\mathbf{L}}_4 \end{bmatrix}^T \tag{33}$$

$$\mathbf{N} = \begin{bmatrix} -\dot{\mathbf{L}}_1 & -\dot{\mathbf{L}}_2 & -\dot{\mathbf{L}}_3 & -\dot{\mathbf{L}}_4 & \mathbf{0} & -\dot{\mathbf{L}}_6 & \dot{\mathbf{L}}_5 & \mathbf{0} & \mathbf{0} & \mathbf{0} \\ \mathbf{0} & \mathbf{0} & \mathbf{0} & \mathbf{0} & \mathbf{0} & \mathbf{0} & \dot{\hat{\mathbf{L}}}_2 - \dot{\hat{\mathbf{L}}}_1 & \mathbf{0} & \mathbf{0} & -\dot{\hat{\mathbf{L}}}_4 \end{bmatrix}^T \tag{34}$$

where $\mathbf{0}$ and $\mathbf{1}$ are column vectors of 0 and 1, respectively, with appropriate dimensions. The state-space model for the complete system is then given by:

$$\begin{bmatrix} \dot{\mathbf{i}} \\ \dot{\hat{\mathbf{i}}} \end{bmatrix} = \mathbf{M^{-1}}(\mathbf{N}+\mathbf{R}) \begin{bmatrix} \mathbf{i} \\ \hat{\mathbf{i}} \end{bmatrix} + \mathbf{M^{-1}}\mathbf{u}$$

$$\dot{\omega} = \frac{P}{2J}\left(T_m - T_e - \hat{T}_e - D\omega\right) \tag{35}$$

$$\dot{\theta}_r = w$$

This represents a nonlinear, time-varying system. It should be highlighted that the state space model given by (35) is not a complete system description, since the main generator terminal voltages have to be defined in terms of the state variables, i.e., the winding currents. For example, if we assume a resistive load R_a, R_b, R_c, then the complete state space model is still given by (35) with the following definition for $\mathbf{R}$ and $\mathbf{u}$:

$$\mathbf{R} = \text{diag}(R_a + r_a, R_b + r_b, R_c + r_c, -r_{kq}, 0,$$

$$- r_{kd}, \hat{r}_a + \hat{r}_b + r_{fd}, 0, 0, -\hat{r_{fd}}) \tag{36}$$

$$\mathbf{u} = \begin{bmatrix} 0 & 0 & 0 & 0 & 0 & 0 & 0 & 0 & 0 & V_F \end{bmatrix}^T \tag{37}$$

The model presented in this section is implemented in Matlab/Simulink®, and the nominal behavior of the machine is discussed in Section III.6.1. The nominal behavior is also summarized in Figure 25.

III.4 Modeling Main Field Winding Faults

Generator winding faults can be classified into one of two main categories: parametric faults and structural faults [121]. Parametric faults are characterized by a change in the magnitude of one (or more) system model parameters. These faults do not affect the structure of the system, and, therefore, the system model is still a valid representation for the actual system. Structural faults change the system configuration and cannot be captured by a magnitude change in the system

parameters. The system model under these faults is no longer valid, and a new model representing the new configuration is necessary to generate the system behavior.

Parametric faults can be further classified into abrupt and incipient faults, where abrupt faults describe a sudden change in system parameters, while incipient faults describe a degradation that evolves continuously with time. An example of an abrupt fault is the sudden increase of a winding resistance, or the sudden decrease in the number of windings, due to shorted turns. An example of an incipient fault is the gradual increase of winding resistance due to overheating of the rotating part.

Parametric faults can be represented easily using the hybrid model presented in Section III.3. The structure of the model remains the same, including the discrete modes and the continuous dynamics equations, although the continuous dynamics for every discrete mode will be different depending on the new parameter values.

Structural faults can be classified into external and internal faults. External faults are the ones that happen outside the machine terminals, and although they do not change the structure of the machine, the overall system model changes. An example is a phase to phase short circuit fault. Internal faults are intrinsic to the machine itself (within the machine boundary). An example of an internal fault that changes the structure of the system is a phase to ground short circuit. The short circuit from the winding to the ground creates a new loop with voltage equal to 0 [122]. The machine with the short circuit fault could be modeled in a similar way to the one presented in Section III.3, by including the new loop. The number of discrete modes will remain the same, since it is related to the rectifier circuit, but the continuous dynamics inside every discrete mode will be different. The situation becomes more complex when there is a dual fault from two phases to the ground.

Field winding faults generally evolve over time, and structural faults are usually caused by persistent, small parametric faults. For example, a small number of shorted turns may cause overheating in the magnetic core of the generator, which after a period of time causes structural winding to ground faults. Therefore, we consider only parametric faults for the field winding. As pointed

out before, structural faults could be simulated by extending the hybrid model, with the added complexity represented by the increased system order.

An example of a single parametric fault, an abrupt increase in the main generator field winding resistance r_{fd}, is simulated. The results are discussed in Section III.6.3, and the behavior is summarized in Figure 28.

III.5 Modeling Rectifier Diode Faults

In this section, we exploit the hybrid model presented in Section III.3 to model the brushless generator with different combinations of diode faults. We first identify rectifier circuit fault types, then we present an algorithm to identify the discrete dynamics for the system with any combination of faulty diodes. We give examples for different faults to explain the algorithm implementation.

Studying the rectifier circuit shows that faults could occur in either the diodes or the cables connecting the three phase output of the exciter generator to the rectifier circuit. Diodes fail in one of two ways: failed open or failed short. In practice, shorted diodes often overheat, and burn out causing open circuits. Therefore, we address open circuit diode faults in this work. Cable faults are diverse, and we restrict ourselves in this study to discrete cable faults, where one of the 3-phases of the exciter generator is no longer connected to the rectifier circuit. Figure 22 illustrates the three types of faults, where diode D_{aT} is open, diode D_{cB} is shorted, and phase b is disconnected from the rectifier circuit. It can be easily shown that the loss of one phase is equivalent to two diodes suffering open circuit failures in the vertical branch of the rectifier connected to the faulty phase.

The six discrete modes presented in Table 3 represent the maximum set of modes that the system can be in for any normal or faulty behavior. In other words, the system with rectifier diode faults can be represented with a subset of the set composed of the six discrete modes of the system. An additional OFF mode may be needed for the case of multiple diode faults, representing the rectifier circuit when in off mode (not conducting, i.e., the exciter and main generators are decoupled). Algorithm 1 provides a formal procedure to specify valid system modes and to define

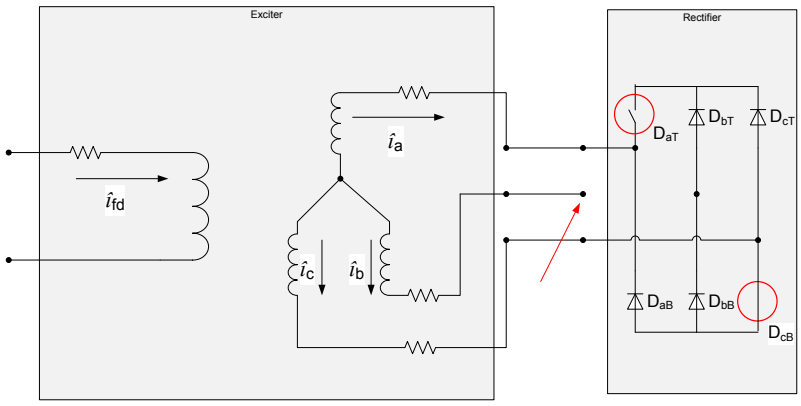

Figure 22: Brushless generator rectifier faults. Diode D_{aT} fails open, diode D_{cB} fails closed, while phase b is disconnected from the rectifier circuit.

system behavior. The algorithm is general and could be applied to single and multiple diode faults, as well as phase faults.

We describe some terminology that is used in Algorithm 1. We designate the set of diodes for the rectifier circuit by $D = \{D_{ij}, i \in P = \{a, b, c\}, j \in \{T, B\}\}$, where i represents the connected phase and j represents the position of the diode (Top or Bottom). The set of faulty diodes is denoted by $F \subset D$. $\Omega = \{AB, AC, BC, BA, CA, CB\}$ is the set of the discrete modes for the brushless hybrid system, and $\Omega_f = \Omega \cup \{OFF\}$ is the set of the discrete modes for the brushless hybrid system, covering both normal and faulty system behavior. The set of valid discrete system modes after a diode fault has occurred is denoted by $M \subset \Omega_f$, and the set of excluded system modes is denoted by $\bar{M} = \Omega_f - M$. Finally, $g : \Omega \mapsto \Omega_f$ is a function mapping defining the replacement for every excluded system mode, i.e. it defines the discrete mode the system resides in during the time period originally allocated to the excluded mode.

In the following, we give examples for single, dual diode, and phase faults. Examples refer to Figure 20 for illustration purposes.

Example III.1 (Single Diode Fault)**.** Assume diode D_{aT} failed in an open circuit position. Following Algorithm 1 with $F = \{D_{aT}\}$:

$$\bar{M}_{aT} = \{AB, AC\}$$
$$\bar{M} = \bar{M}_{aT} = \{AB, AC\}, M = \{BA, CA, CB, BC\}$$

Algorithm 1 Specifying valid system modes and system behavior with rectifier diode faults

Input: F
Output: $M, g(.)$
{define excluded system modes}
for $k \in F$ **do**
  if $j = T$ **then**
    $\bar{M}_k = \{i\bar{i} : \bar{i} = P - i\}$
  else
    $\bar{M}_k = \{\bar{i}i : \bar{i} = P - i\}$
  end if
end for
$\bar{M} = \cup_{k \in F} \bar{M}_k, M = \Omega - \bar{M}$ {set of valid system modes}
{define system behavior and whether OFF state is required}
for $m = p_1 p_2 \in \Omega$ **do**
  if $m \in \bar{M}$ **then**
    $\bar{p} = P - \{p_1, p_2\}$
    $m_1 = p_1\bar{p}, m_2 = \{\bar{p}p_2\}$ {m_1 and m_2 cannot be valid system modes simultaneously, otherwise m will not be an excluded mode.}
    if $m_1 \in M$ **then**
      $g(m) = m_1$
    else if $m_2 \in M$ **then**
      $g(m) = m_2$
    else
      $g(m) = OFF$
      $M = M \cup \{OFF\}$
    end if
  else
    $g(m) = m$
  end if
end for
return $M, g(.)$

$$
\begin{aligned}
m = AB \quad m_1 = AC \text{ (excluded)} \quad m_2 = CB \text{ (valid)} \\
\Rightarrow g(AB) = CB \quad \text{AB time spent in CB} \\
m = AC \quad m_1 = AB \text{ (excluded)} \quad m_2 = BC \text{ (valid)} \\
\Rightarrow g(AC) = BC \quad \text{AC time spent in BC} \\
M = \{BA, CA, CB, BC\} \\
g(\Omega) = \{CB, BC, BC, BA, CA, CB\}
\end{aligned}
$$

Figure III.23(a) illustrates the system automaton under this new condition, with excluded modes and transitions marked with dashed lines. Figure III.23(b) shows the rectifier circuit output voltage (main generator field excitation) with D_{aT} diode fault, as compared to the normal output. The system spends the time of mode AB in mode CB, and the time for mode AC in mode BC. Also, since the rectifier output voltage is the difference between the connected terminal voltages v_a, v_b,

and v_c (according to the active mode), the transition condition from mode CB to mode BC shows that the rectifier output voltage has to return to zero every complete cycle through system modes.

If, on the other hand, diode D_{aB} fails in an open circuit position, then the same argument leads to the exclusion of modes BA and CA. Other single diode failures can be analyzed in a similar way. ■

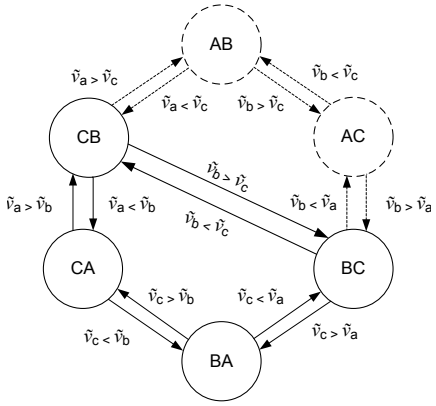

(a) System automaton with rectifier diode D_{aT} open circuit fault. Modes AB and AC are no longer valid system modes, and the system jumps from mode CB directly to mode BC. Time for mode AB is spent in mode CB, and time for mode AC is spent in mode BC.

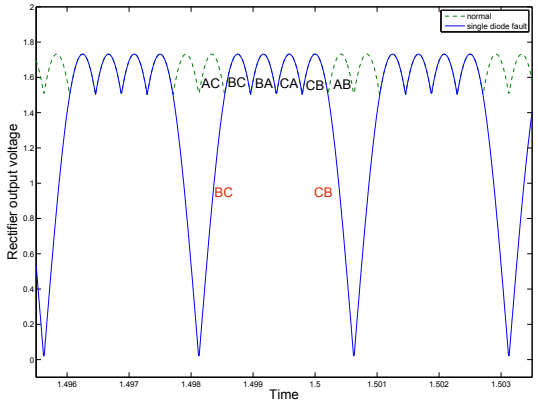

(b) Rectifier output voltage with a single diode fault, for diode D_{aT}. The labels indicate the active system mode during every time period. The dashed curve refers to the normal output voltage, while the solid curve represents the output with diode fault. Modes AC and AB are not valid system modes with D_{aT} fault, and the system moves from mode CB to mode BC directly, causing a return to zero for the rectifier output voltage.

Figure 23: System automaton and rectifier output voltage for a single diode fault.

Example III.2 (Dual Diode Fault)**.** Assume diodes D_{aT} and D_{bB} failed in an open circuit position, then $F = \{D_{aT}, D_{bB}\}$:

$$
\begin{aligned}
\bar{M}_{aT} &= \{AB, AC\} \\
\bar{M}_{bB} &= \{AB, CB\} \\
\bar{M} &= \bar{M}_{aT} \cup \bar{M}_{bB} = \{AB, AC, CB\}, M = \{BA, BC, CA\} \\
m &= AB \quad m_1 = AC(\text{excluded}) \quad m_2 = CB \text{ (excluded)} \\
&\Rightarrow g(AB) = OFF \quad \text{AB time spent in OFF state} \\
M &= \{BA, BC, CA, OFF\} \\
m &= AC \quad m_1 = AB \text{ (excluded)} \quad m_2 = BC \text{ (valid)} \\
&\Rightarrow g(AC) = BC \quad \text{AC time spent in BC} \\
m &= CB \quad m_1 = CA \text{ (valid)} \quad m_2 = AB \text{ (excluded)} \\
&\Rightarrow g(CB) = CA \quad \text{CB time spent in CA} \\
M &= \{BA, BC, CA, OFF\} \\
g(\Omega) &= \{OFF, BC, BC, BA, CA, CA, OFF\}
\end{aligned}
$$

Figure III.24(a) illustrates the resulting system automaton. The system spends the time of mode CB in mode CA, the time of mode AB in mode OFF, and the time of mode AC in mode BC. This gives rise to the rectifier circuit output voltage in Figure III.24(b). ■

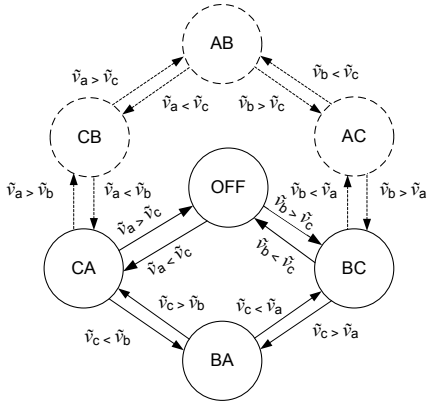

(a) System automaton with rectifier diodes D_{aT} and D_{bB} open circuit fault. Modes CB, AB, and AC are no longer valid system modes. An additional OFF mode is required, representing the case when the rectifier circuit is not conducting, hence the exciter and main generators are decoupled. Time for mode CB is allocated to CA, time for mode AC is allocated to BC, and time for mode AB is allocated to OFF mode.

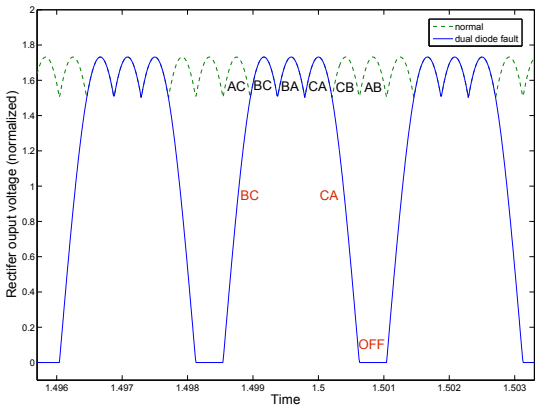

(b) Rectifier output voltage with a dual diode fault, for diode D_{aT} and D_{bB}. The labels indicate the active system mode during every time period. The dashed curve refers to the normal output voltage, while the solid curve represents the output with diode fault. Modes AC, CB, and AB are not valid system modes, and the time for mode AB is allocated to an OFF mode, representing no conduction for the rectifier circuit.

Figure 24: System automaton and rectifier output voltage for a dual diode fault.

For phase faults, a discrete phase fault (loosing one phase connection to the rectifier) is equivalent to two diode faults in the vertical branch connected to the phase. In this case, every phase loss results in an exclusion of four system modes, since every diode results in the exclusion of two modes, and the two diodes, being in one branch, do not have any common modes. Moreover, it can be easily shown that it is always true that there is a valid mode for the system when the transition condition to an excluded mode is satisfied. Therefore, OFF mode is not a valid system mode for phase faults. Phase faults can be modeled in a similar way to Examples III.1 and III.2.

The two types of faults presented in Examples III.1 and III.2 are simulated in this work. The results are discussed in Section III.6.2, and the behavior is summarized in Figures 26 and 27, respectively.

III.6 Simulation Results

The complete mathematical model for the brushless generator, presented in Section III.3, is implemented in Matlab/Simulink ® [123], to generate behaviors under nominal and faulty conditions. A 400 Hz brushless generator, with the equivalent set of parameter values (in SI units) shown in Table 4, is used for simulation. These parameters are in dq0 domain, and transformed to the phase-domain values using the equations shown in Table 5. The transformation is not unique since more than one ratio of the windings may result in the same set of parameter values in the phase domain. The parameter values are used for both the main and exciter generators. Primed parameters are field variables referred to the armature windings.

Table 4: Aircraft generator dq0 model parameters

Parameter	Description	Value
L_{ls}	Leakage inductance, stator winding	0.004527 H
L_{md}	Magnetizing inductance, d winding	0.1086 H
L_{mq}	Magnetizing inductance, q winding	0.05175 H
$\acute{L}_{lkq}$	Leakage inductance, kq winding (referred)	0.01015 H
$\acute{L}_{lfd}$	Leakage inductance, fd winding (referred)	0.01132 H
$\acute{L}_{lkd}$	Leakage inductance, kd winding (referred)	0.007334 H
r_a	resistance, stator winding a	1.62 Ω
r_b	resistance, stator winding b	1.62 Ω
r_c	resistance, stator winding c	1.62 Ω
$\acute{r}_{kq}$	resistance, kq winding	4.772 Ω
$\acute{r}_{fd}$	resistance, fd winding	0.6 $k\Omega$
$\acute{r}_{kd}$	resistance, kd winding	3.142 Ω
N_s	Number of turns, stator winding	100
N_{fd}	Number of turns, fd winding	100
N_{kq}	Number of turns, kq winding	100
N_{kd}	Number of turns, kd winding	100
D	Damping coefficient	0.009 $kg.m^2.s^{-1}$
J	Moment of inertia	0.0923 $kg.m^2$

Table 5: Aircraft generator phase-domain model parameters calculation

Parameter	Description	Expression
L_A	Machine geometrical parameter	$\frac{Lmd+Lmq}{3}$
L_B	Machine geometrical parameter	$\frac{Lmd-Lmq}{3}$
L_{lkq}	Leakage inductance, kq winding	$\left(\frac{2}{3}\right)\left(\frac{N_{kq}}{N_s}\right)^2 \acute{L}_{lkq}$
L_{mkq}	Magnetizing inductance, kq winding	$\left(\frac{2}{3}\right)\left(\frac{N_{kq}}{N_s}\right)^2 L_{mq}$
L_{lfd}	Leakage inductance, fd winding	$\left(\frac{2}{3}\right)\left(\frac{N_{fd}}{N_s}\right)^2 \acute{L}_{lfd}$
L_{lkd}	Leakage inductance, kd winding	$\left(\frac{2}{3}\right)\left(\frac{N_{kd}}{N_s}\right)^2 \acute{L}_{lkd}$
L_{skq}	Mutual inductance, stator-kq windings	$\left(\frac{2}{3}\right)\left(\frac{N_{kq}}{N_s}\right) L_{mq}$
L_{sfd}	Mutual inductance, stator-fd windings	$\left(\frac{2}{3}\right)\left(\frac{N_{fd}}{N_s}\right) L_{md}$
L_{skd}	Mutual inductance, stator-kd windings	$\left(\frac{2}{3}\right)\left(\frac{N_{kd}}{N_s}\right) L_{md}$
L_{fdkd}	Mutual inductance, fd-kd windings	$\left(\frac{N_{fd}}{N_{kd}}\right) L_{mkd}$
r_{kq}	Resistance, kq winding	$\left(\frac{2}{3}\right)\left(\frac{N_{kq}}{N_s}\right)^2 \acute{r}_{kq}$
r_{fd}	Resistance, fd winding	$\left(\frac{2}{3}\right)\left(\frac{N_{fd}}{N_s}\right)^2 \acute{r}_{fd}$
r_{kd}	Resistance, kd winding	$\left(\frac{2}{3}\right)\left(\frac{N_{kd}}{N_s}\right)^2 \acute{r}_{kd}$

III.6.1 Nominal Behavior

The system is simulated with no faults to set up the reference signals for comparison purposes, when studying system behavior with faults. The following signals are observed (Figure 25):

- **Exciter generator winding currents**: according to system dynamics description in Section III.3, every phase current $\hat{i}_a, \hat{i}_b, \hat{i}_c$ is on for the duration of two modes (1/3 the generator output period ≈ 0.83 ms), off for 1/6 of the period, on (with opposite sign) for 1/3 of the period, and off for 1/6 of the period. The field current is steady with superimposed small magnitude oscillations.

- **Rectifier output voltage**: the voltage is a typical output from a 3-phase rectifier, with average DC voltage and superimposed ripples.

- **Main generator winding currents**: phase currents represent the nominal 3-phase sinusoidal output from the generator. Damper winding currents are equal to zero during steady state, with very small ripples. The field winding current signal exhibits the same behavior of its accompanying rectifier output voltage.

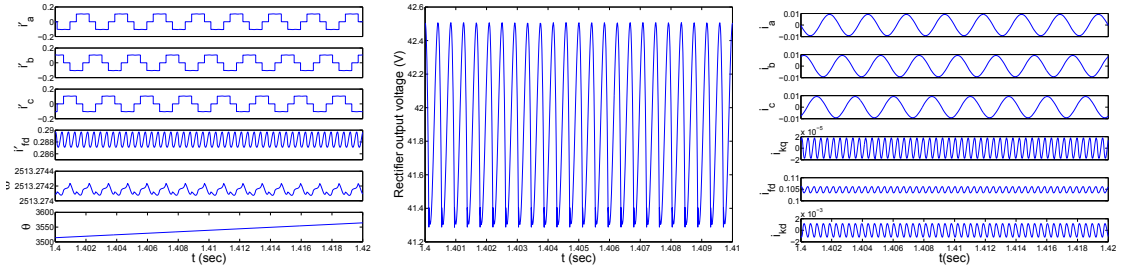

(a) Exciter generator currents, angular velocity, and angular displacement. Phase currents take turns to switch on and off, and the field current has small magnitude oscillations around its steady state value. The angular velocity has very small perturbations due to the PI controller dynamic behavior.

(b) Rectifier output voltage is the typical output from a 3-phase diode rectifier, where sinusoidal ripples are superimposed on the average DC voltage.

(c) Main generator winding currents. 3-phase currents are sinusoidal signals with $\pi/3$ phase shifts, the damper winding currents are effectively zero with very small magnitude oscillations, and the field winding current has the same sinusoidal ripples of the rectifier output voltage, with much smaller magnitude.

Figure 25: Nominal behavior for the brushless generator.

III.6.2 Diode Fault Injection

Single and dual diode faults are simulated. Diode designations are with reference to Figure 20.

Single Diode Fault

The system is simulated with an open circuit fault in diode D_{aT}, injected at time t = 0.5 s. According to Section III.5, this results in the discrete mode set $\{CB, BC, BA, CA\}$, and the automaton in Figure III.23(a). The following signals are observed (Figure 26):

- **Exciter generator winding currents**: because of excluded modes, $\hat{i}_a \leq 0$. $\hat{i}_b$ and $\hat{i}_c$ exhibit similar behavior to their nominal waveform, except that the transition from positive to negative half cycle for $\hat{i}_b$ is smooth with no abrupt return to zero as in the nominal case. The same is applied to $\hat{i}_c$ when switching from negative to positive half cycles. This can be easily explained by following the system automaton in Figure III.23(a). The exciter field winding

current undergoes periodic oscillations with the same waveform as the rectifier output voltage, except that the waveform does not return to zero, but to a value that is > 0 and smaller than its steady state value.

- **Rectifier output voltage**: the voltage returns to zero during modes AB and AC, as explained in Section III.5. The signal does not match Figure III.23(b) as the 3-phase output from the exciter generator is not pure sinusoidal with rectifier diode faults.

- **Main generator winding currents**: the 3-phase currents undergo distortion, which may be detected by harmonic analysis. The field winding signal behavior is very similar to the output voltage. An interesting behavior for damper winding currents is noted, since these currents are almost equal to zero in normal operation. With diodes fault, both currents undergo out of phase spikes at the time of fault injection, then both signals have oscillations with sufficient magnitude that could be exploited for fault detection. Furthermore, the oscillations are out of phase by π degrees rad.

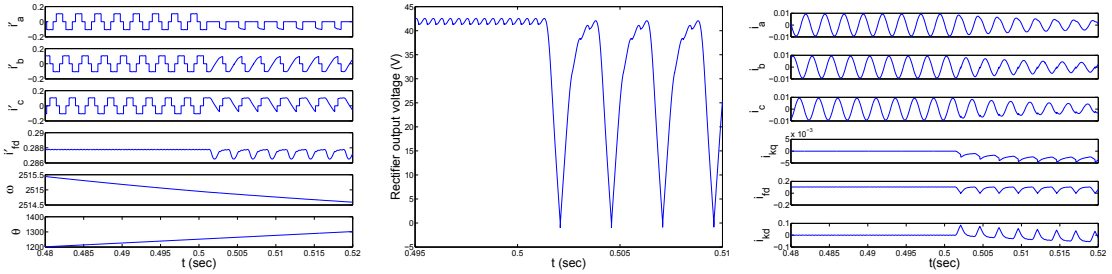

(a) Exciter generator currents, angular velocity, and angular displacement. Phase current $\hat{i}_a \leq 0$ and $\hat{i}_b$ and $\hat{i}_c$ do not transition abruptly from negative to positive and vice versa, respectively. Field current $\hat{i}_{fd}$ has periodic oscillations with the same waveform as the rectifier output voltage. No noticeable effect on the angular velocity.

(b) Rectifier output voltage returns to zero due to the excluded modes AB and AC resulting from the diode fault.

(c) Main generator winding currents. 3-phase currents are slightly distorted. The damper winding currents i_{kq} and i_{kd} have negative and positive spikes, respectively, at the fault injection time, and then undergo periodic oscillations with high magnitude compared to their steady state zero value.

Figure 26: Behavior of the brushless generator with a single diode fault, diode D_{aT} in Figure 20 fails open.

Dual Diode Fault

The system is simulated with an open circuit fault in diodes D_{aT} and D_{bB}, injected at time $t = 0.5$ s, which results in the discrete mode set $\{BC, BA, CA, OFF\}$, and the automaton in Figure III.24(a). The following signals are observed (Figure 27):

- **Exciter generator winding currents**: because of the excluded modes, $\hat{i}_a \leq 0$ and $\hat{i}_b \geq 0$. The exciter field current undergoes periodic oscillations with very similar waveform to the rectifier output voltage.

- **Rectifier output voltage**: the voltage goes to zero for the duration of mode AB (1/6 the output voltage period ≈ 0.42 ms), as explained in Section III.5. The discrepancy with Figure III.24(b) is due to the fact that the 3-phase output from the exciter generator is not pure sinusoidal with rectifier diode faults. The negative spike is an artifact of hybrid systems simulation when switching modes, and is not part of the system dynamics.

- **Main generator winding currents**: slight distortion is noted in phases *abc* output currents, but not with a sufficient magnitude to allow robust fault detection. The field winding signal behavior is very similar to the output voltage. The behavior for damper winding currents is the same as in the case of a single diode fault, namely out of phase spikes, followed by large magnitude periodic oscillations.

It can be shown that other diode faults have similar effects, except for phase differences. As a conclusion, fault signatures for different diode faults are very similar with regard to main generator damper winding and phase currents. The distinguishing signals are the exciter phase winding currents, the main generator field winding current, and the rectifier output voltage. These facts are illustrated by Table 6, which summarizes the system behavior with nominal and different fault types. It represents the fault signature table that could be further exploited to develop fault detection algorithms for different types of faults.

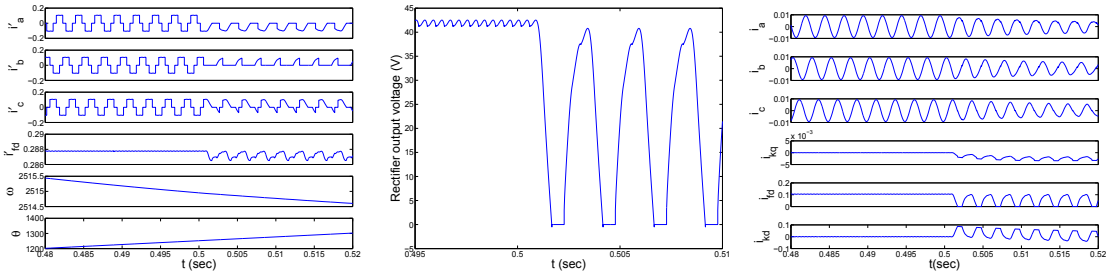

(a) Exciter generator currents, angular velocity, and angular displacement. Phase current $\hat{i}_a \leq 0$ and $\hat{i}_b \geq 0$. Field current $\hat{i}_{fd}$ undergoes oscillations with a waveform very similar to the rectifier output voltage. No noticeable effect on the angular velocity.

(b) Rectifier output voltage returns to zero for the duration of mode AB.

(c) Main generator winding currents. 3-phase currents are slightly distorted. The damper winding currents i_{kq} and i_{kd} have negative and positive spikes, respectively, at the fault injection time, and then undergo periodic oscillations with high magnitude compared to their steady state zero values.

Figure 27: Behavior of the brushless generator with a dual diode fault, diodes D_{aT} and D_{bB} in Figure 20 fail open.

III.6.3 Parametric Faults Injection

We consider an abrupt change in the resistance of the field winding of the main generator, r_{fd}. In practice, this may be caused by winding overheating. A 10% sudden increase in the resistance value is injected at simulation time $t = 0.5$ sec., and the following signals are observed (Figure 28)

- **Exciter generator winding currents**: the only notable behavior is the transient reduction in current magnitude, while no effect is noted on the angular velocity.
- **Rectifier output voltage**: a reduction in the rectifier output voltage is noted, due to the higher input impedance of the main generator field winding. The spike at the time of fault injection is an artifact due to the switching behavior of the hybrid system, and is not part of the system dynamics.
- **Main generator winding currents**: the phase currents undergo sudden decrease of the magnitude. The most notable fault signature is in the damper winding kq current signal, that shows a negative spike and damped oscillations. A very similar behavior is noted for damper winding kd current, but with positive spike.

We conclude that for parametric abrupt faults, only magnitude change is noted, and as long as the fault magnitude is within the control range of the GCU, the GCU will compensate the 3-phase output signal for the fault effect. Therefore, detection of the fault using the 3-phase output signal may be hard if the response time of the GCU is small. On the other hand, monitoring phase currents for the exciter generator and damper winding currents is likely to be more effective for detecting this kind of faults, provided they are measurable or could be estimated using a system observer (see discussion in Section III.7). Table 6 summarizes the resistance fault signatures.

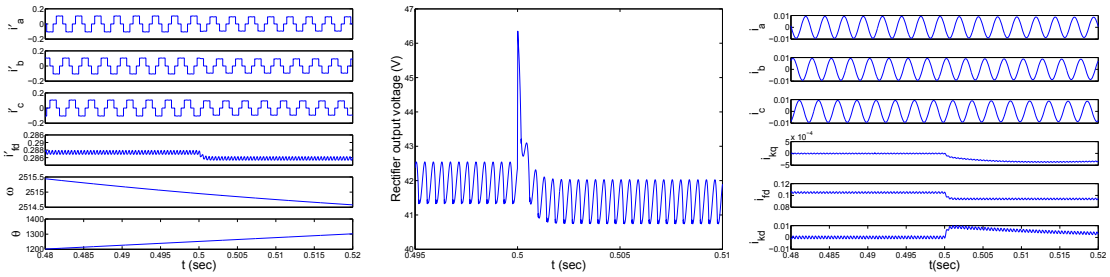

(a) Exciter generator currents, angular velocity, and angular displacement. Transient reduction of current magnitude occurs. No impact on the angular velocity is noted.

(b) Rectifier output voltage decreases due to the higher input impedance of the field winding.

(c) Main generator winding currents. A transient decrease in 3-ph currents is noted. Damper winding currents i_{kq} and i_{kd} show negative and positive spikes, followed by small oscillations and a return to zero.

Figure 28: Behavior of the brushless generator with an abrupt parametric fault in the main generator field winding resistance r_{fd}.

Table 6 summarizes the system behavior with nominal and different fault types discussed in this section. It represents the fault signature table that could be further exploited to develop fault detection algorithms for different types of faults.

III.7 Discussion of Modeling and Simulation Results

The results of the simulation experiments show that fault signatures are mostly notable in the current signals of the rotating windings, namely phase windings of the exciter generator and field/damper windings of the main generator. Fault signature in output phase currents is not easily detectable, especially that phase currents have much higher frequency. Therefore, to detect faults from these waveforms, either faster sensors are required or frequency response analysis is needed. However, and as pointed out before, most of the existing techniques for generator fault detection rely on phase

Table 6: Brushless generator fault signatures

Fault	$\hat{i}_a$	$\hat{i}_b$	$\hat{i}_f$	v_{rec}	$i_a \backslash i_b \backslash i_c$	i_{kq}	i_{kd}
Nominal	$\llcorner$ 0.83 ms $\lrcorner$		DC	3-ph rectified	3-ph sin.	0	0
Single diode fault	≤ 0	$\llcorner$ 2.5 ms $\llcorner$	$\downarrow, \sim$	hits zero every 2.5 ms	$\downarrow -$	$\downarrow, \sim$	$\uparrow, \sim$
Dual diode fault	≤ 0	≥ 0	$\downarrow, \sim$	$\llcorner$ 2.5 ms $\llcorner$	$\Downarrow -$	$\downarrow, \sim$	$\uparrow, \sim$
Resistance fault	$\downarrow\uparrow$	$\downarrow\uparrow$	$\downarrow\uparrow$	$\downarrow\uparrow$	$\downarrow -$	$\downarrow -$	$\uparrow -$

$\uparrow$	signal magnitude increase
$\Uparrow$	signal magnitude increase (qualitatively higher than $\uparrow$)
$\downarrow$	signal magnitude decrease
$\Downarrow$	signal magnitude decrease (qualitatively lower than $\downarrow$)
$-$	signal nominal value
$\sim$	signal oscillations around its nominal value
$\llcorner$	signal returns to zero from positive magnitude, remains zero for 0.42 ms
$\lrcorner$	signal returns to zero from negative magnitude, remains zero for 0.42 ms
$\uparrow\downarrow$	signal magnitude increase, followed by a signal magnitude decrease
$\llcorner\ T\ \llcorner$	signal returns to zero from positive magnitude every T ms, remains zero for 0.42 ms

current measurements and harmonic analysis, making it harder to discriminate between faults. Given these facts, internal winding currents of the exciter and main generators represent potential candidates for detecting diode and parametric faults.

In most practical installations, internal winding current measurements are not directly measurable, since these windings are mounted on the rotating part of the generator, making it unusually hard to install sensors that produce reliable measurements. One way to solve this problem is to estimate the unmeasurable currents using the brushless generator state space model. Some work on the use of observers for damper winding currents to estimate generator parameters has been reported in [124]. However, the authors are not aware of any work that addressed the observer design for the complete brushless generator, which has to be a hybrid observer. The starting point is to use the model presented in Section III.3, perhaps with some relaxing assumptions to simplify the hybrid observer design. One such practical assumption is that the angular velocity of the machine is constant during normal and faulty behavior of the machine operation. The results of our simulation experiment presented in this chapter, in addition to the feedback obtained from our industrial partners, have shown very small effect of the faults considered on the variability of the angular velocity. This assumption has the effect of transforming the system into a linear, but a time-varying (LTV) system, thereby making the observer design much simpler.

The brushless generator hybrid model developed in this chapter can be used for FDI by augmenting it with a bank of hybrid observers; one observer for the nominal system model, and an additional observer with the faulty system model for each fault to be detected. The hybrid observer has, as its input, the brushless generator input $u = [\ V_F \quad T_m\ ]$ and output $y = [\ i_a \quad i_b \quad i_c\ ]$, and is composed of a location observer and a continuous observer. The location observer estimates the current system mode, $\hat{q}$, and the continuous observer estimates the continuous system states, $\hat{\mathbf{x}}$, given the current system mode from the location observer [125]. Detection of faults presented in this chapter is accomplished by comparing the estimated states $\hat{\mathbf{x}}$ from the hybrid observer with the least residual to the signals in Table 6 to discriminate between faults.

Some comments about the brushless generator model presented in this chapter are in order. The model assumes linear magnetic circuits, where there is no saturation in the machine. Most modern generating systems are designed to work in the linear region of the magnetic curve, therefore, this should not be a limiting factor in using the model. However, if the objective is to simulate the machine with overload conditions, or if the fault to be simulated drives the machine into the saturation region, then the model has to be extended to include saturation effect. Also, in some practical designs, a filter capacitor is added to the output of the rectifier circuit to smooth the output voltage that is applied to the main field winding. This capacitor will try to maintain the rectifier output voltage during diode failure, so that the voltage does not return to zero, unlike the simulation results in this chapter. However, the analysis will be similar with the addition of one state variable representing the capacitor voltage.

Finally, as an extension to this study, the model could be evaluated using a laboratory setup akin to the one presented in [103], where different diode faults could be injected. The model implemented in Matlab/Simulink could be simulated offline or in real-time on a personal computer to compare the results. Further, laboratory measurements could be communicated to the model for further analysis and tuning, using Matlab Instrument Control Toolbox and the appropriate input/output digital interface.

III.8 Summary

In this chapter, we have presented a hybrid modeling approach for brushless generators with nominal and faulty conditions. Direct phase-domain (abc domain) modeling is shown to facilitate generator modeling, especially with machine faults, since it avoids unnecessary transformations introduced by the dq0 modeling approach. The hybrid modeling approach presented is an accurate method to model brushless generators with faults in the exciter generator/rectifier parts. It has been shown also that with diode faults, the hybrid modeling approach helps understanding the physics of failure events by defining a framework for modeling and simulation of different combinations of faults.

For different rotor faults, the fault signatures generated have shown that currents in the rotating windings are more appropriate for fault detection and isolation. On the other hand, the 3-phase output currents as well as the excitation current do not show fault signatures different from what has been reported in the literature about other types of machine faults.

Some of the future research problems include the use of the hybrid model in building accurate FDI schemes for the different faults discussed in the chapter. The use of a hybrid observer along with the fault signatures developed to detect and isolate faults is an important research direction. The power of the FDI scheme that is based on the hybrid observer, as compared to existing techniques for brushless generator fault detection, is also of practical interest.

The work in this chapter reveals the complexity of accurate physics-based models. Such models could be hard to utilize in online fault detection and isolation systems. However, physics-based models could be used to generate accurate data sets for the system behavior under a variety of operating conditions. The generated data sets could be used to build statistical models for the machine under different nominal and faulty conditions. Chapter IV presents a fault detection scheme based on such statistical models.

CHAPTER IV

Abrupt and Incipient Fault Detection Using Statistical Models

In Chapter III, we investigated physics-based modeling for aircraft generators. The developed model is a complex nonlinear, time-varying dynamic system. Practical engineering systems, in general, tend to have models as complex as or even more complex than the generator model. Building a Fault Detection and Isolation system using such complex models is a difficult task. The task becomes even more difficult when considering intermittent and incipient fault types. Fortunately, less complex models are often sufficient for the FDI task. In this chapter, we explore the power of statistical modeling in building robust FDI systems. Statistical models rely on the availability of a sufficient data set to describe the system under study in different operating modes. This data set may be obtained either from operating data set of real life systems or from the simulation of physics-based models, akin to the model developed in Chapter III.

In this chapter, we develop a general framework to detect and distinguish between abrupt persistent, abrupt intermittent, and incipient faults. The framework is based on the change detection theory and could be applied to any system as long as a statistical description could be obtained for the system behavior. We specialize the framework to the case of Gaussian noise and exponential fault profile, and obtain closed form expressions for the estimators and a recursive expression for the fault detector. We apply the developed framework to detect different fault types in the NASA ADAPT-Lite Electrical Power System, in the context of the DXC'10 diagnosis competition, and achieve 2nd position [4]. To show how the algorithm could be applied to a general fault model, we apply the developed algorithm on the problem of aircraft generator winding fault detection using differential protection techniques [5].

The rest of the chapter is organized as follows: Section IV.1 is a brief introduction to statistical models. Section IV.2 describes the statistical models for different fault types under consideration. Section IV.3 describes the general FDI system. Section IV.4 describes the detailed detector design.

Section IV.5 derives the estimators for fault parameters. Section IV.6 describes the application of the FDI system on NASA electrical testbed for DXC'10 competition. Section IV.7 describes the application of the detector for the general fault model in the case of aircraft generator winding faults. Section IV.8 proposes an extension to enhance the detector performance. The work is concluded in Section IV.9.

IV.1 Introduction to Statistical Modeling

A statistical model for system measurements is a pair (Y, P), where Y is the random variable representing the measurement, and P is the probability distribution which is thought to generate the observed data. The source of randomness could be sensor noise, system disturbance, system model uncertainty, or some or all of these sources. To detect any change from the nominal system behavior, we need at least a statistical description for the nominal behavior. This model could be described, for a single measurement, on the form:

$$y[n] = s[n] + w[n] \tag{38}$$

where $y[n]$ is the time series of the observations from the sensor, $s[n]$ is a deterministic signal that depends on the measured variable, and $w[n]$ is an additive noise. For each system fault, the observation model could be described similarly as:

$$y[n] = s_{f_i}[n] + w_{f_i}[n] \tag{39}$$

where i is the fault under consideration, $s_{f_i}[n]$ describes the system behavior under fault for this particular observation, and $w_{f_i}[n]$ describes the noise behavior under this fault condition. The nominal signal $s[n]$ is either known from training data, or generated online by an independent system observer. The system observer is built using the nominal system model. In either case, the value $s[n]$ is subtracted from the observation sequence to obtain the residual signal. In addition, the noise behavior is assumed independent of the fault, and considered the same under both nominal

and faulty conditions. Accordingly, the detection problem could be expressed on the form:

$$\begin{aligned} \mathcal{H}_0 : &\quad r[n] = w[n] \\ \mathcal{H}_i : &\quad r[n] = \Delta s_{f_i}[n] + w[n] \qquad i = 1, 2, \ldots, m \end{aligned} \tag{40}$$

where $r[n]$ is the residual signal for the sensor, m is the number of faults, and $\Delta s_{f_i}[n] = s_{f_i}[n] - s[n]$ represents the deviation in the measurement as a result of the fault. $\Delta s_{f_i}[n]$ is usually partially known, with unknown parameters to be estimated from the observations.

Two main approaches exist to detect a change in a data stream: 1) fixed sample size detection, and 2) sequential detection. In fixed sample size detection, a detection window is used to specify the samples that will be used in the detection process. The decision is evaluated at the end of the detection window. This detection window may be sliding, where each new observation replaces the oldest one. In such case, the decision is evaluated each time a new sample arrives. Sequential detection, on the other hand, does not fix the sample size in advance. Instead, data are evaluated as they arrive, and the decision may be declared at any time instant, if the stopping criteria is met [109]. Sequential detection has been shown to be more efficient, on average, in terms of shorter delay for detection [126]. However, the analysis of sequential detection is much harder, and in many cases, no closed form expressions exist for the detector performance. The lack of closed form formulae makes detector tuning a challenging task, and often heuristics are applied to properly tune the detector based on the specific application. Fixed sample size detection, on the other hand, is a well-understood field, and common detectors (e.g. Gaussian noise case) have closed form expressions for the detector performance [10].

In this chapter, we consider sequential detection, since delay for detection is a crucial measure that needs to be minimized, in order to take the necessary action required to protect humans, systems, as well as the environment from any catastrophic consequences of the faults.

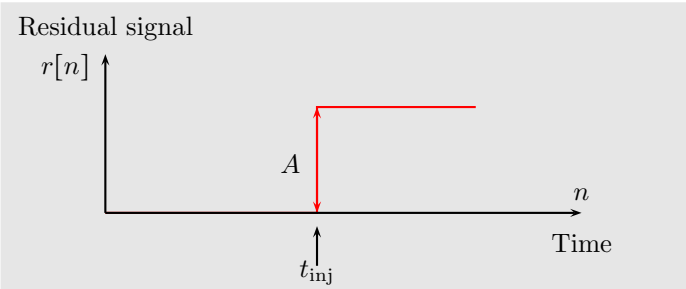

Figure 29: Abrupt persistent fault profile. Noise is removed from the residual signal for clarity.

IV.2 Fault Modeling

We consider three different fault types, and present a statistical model for the residual signal for each fault type.

IV.2.1 Abrupt Persistent Fault

The profile for abrupt persistent faults is shown in Figure 29, without the additive noise. The residual signal for the fault could be expressed as:

$$r[n] = A + w[n], \tag{41}$$

where A is a constant (could be positive or negative), representing the fault magnitude. We assume that $w[n]$ is a stationary Gaussian discrete random process with zero mean and variance σ_n^2. For this fault type, it is required to estimate the fault injection time t_{inj} and the fault magnitude A. We note here that A represents the fault magnitude for the specific signal measured, and not for the faulty component. Any necessary transformations should be applied to estimate the fault magnitude for the system component.

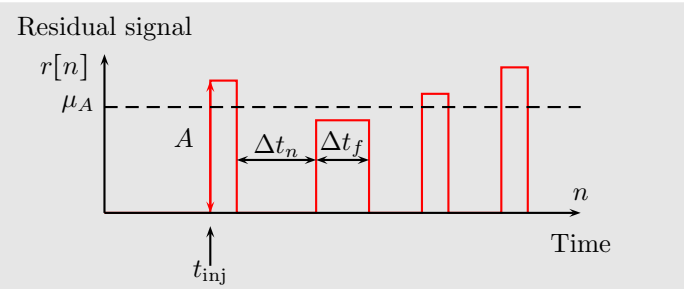

Figure 30: Abrupt intermittent fault profile. Noise is removed from the residual signal for clarity.

IV.2.2 Abrupt Intermittent Fault

The profile for abrupt intermittent faults is shown in Figure 30, without the additive noise. The residual signal for the fault could be expressed as:

$$r[n] = AZ[n] + w[n] \tag{42}$$

A is the fault magnitude, which is assumed different for each occurrence of the fault. We assume here that A is a Gaussian random variable, with mean μ_A and variance σ_A^2. $Z[n]$ is a binary random process representing the existence or absence of the fault, and defined by:

$$Z[n] = \begin{cases} 0 & \text{fault absent} \\ 1 & \text{fault present} \end{cases} \tag{43}$$

A common assumption for $Z[n]$ random process is to define it as a two-state Markov chain, as depicted in Figure 31, where one state represents the no-fault condition, while the other state represents the fault condition [105]. The parameters of the Markov chain are assumed unknown and evaluated from the data samples. The Markov chain assumption leads to an exponential distribution for the inter-arrival time Δt_n and the persistence time Δt_f of the fault [127]. Therefore, $\Delta t_n \sim \texttt{exp}(\mu_n)$, where $\mu_n = \alpha$, and $\Delta t_f \sim \texttt{exp}(\mu_f)$, where $\mu_f = \beta$.

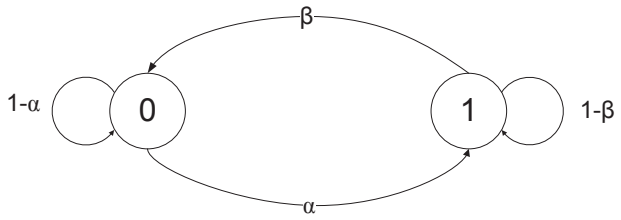

Figure 31: Markov chain modeling for intermittent faults

To summarize, the parameters to be estimated with this fault type are: 1) the fault injection time t_{inj}, 2) the mean fault magnitude μ_A, 3) the mean inter-arrival time for the fault μ_n, and 4) the mean persistence time for the fault μ_f.These parameters are identified in Figure 30.

IV.2.3 Incipient Fault

The profile for incipient faults is shown in Figure 32, without the additive noise. The residual signal for the fault could be expressed as:

$$r[n] = Bn + w[n] \tag{44}$$

where $B = MT_s$, M is a constant representing the slope of the drift, and T_s is the sampling period. The parameters to be estimated with this fault type are t_{inj} and M.

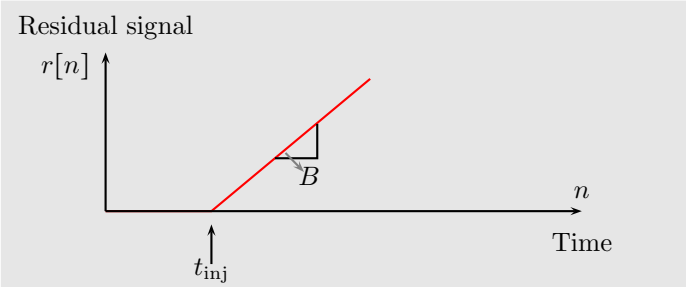

Figure 32: Incipient fault profile. Noise is removed from the residual signal for clarity.

IV.3 Fault Detection and Isolation System

The general block diagram for the FDI system is shown in Figure 33. The main components are summarized below.

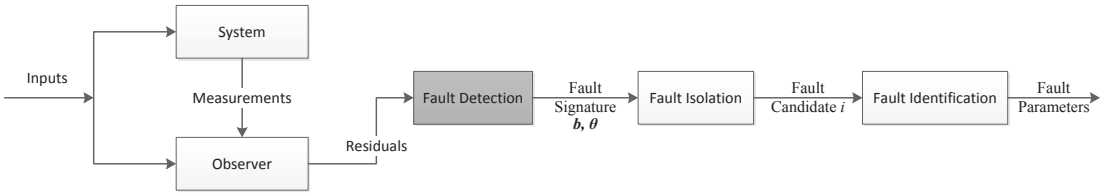

Figure 33: Fault detection and isolation system block diagram. The focus of the study is on the fault detection algorithm.

- **System**. The physical system to be monitored, with its inputs and output measurements available to the observer.

- **Observer**. The observer uses the same inputs applied to the system, as well as the output measurements, to evaluate the residual signals. The observer uses prior information about the system, e.g. a system model akin to the one developed in Chapter III, to estimate the nominal system outputs. The difference between the estimated outputs and the true outputs is the residual vector used by the fault detector.

- **Fault Detection**. The fault detector uses the residual signals to decide if there is a fault in the system. The fault detector has to be robust to measurement noise, system disturbances, as well as model inaccuracies. Some fault detectors are designed as dynamic systems that generate structured residuals which respond to a subset of faults [116]. These types of fault detectors integrate the observer, fault detection, and fault isolation functions in one unit. However, design of such detectors is usually complex except for simple linear systems. Another common approach is to use the residual signals from the observer, and apply statistical techniques to declare if there is a significant change in one or more of the output measurements. The output of the fault detector in this case is a vector of binary variables representing the fault signature

for the system. We adopt this technique in this chapter. In Figure 33, $\boldsymbol{b}$ represents the fault signature vector, where each entry b_i is defined as:

$$b_i = \begin{cases} 0 & \text{no fault} \\ 1 & \text{fault} \end{cases} \tag{45}$$

In addition, the fault detector in our work provides an estimate for the fault parameters relevant to the fault type, as explained in Section IV.5. We designate the vector of estimated fault parameters for each measurement by θ_i.

- **Fault Isolation.** The fault isolator uses the fault signature developed by the detector, to reason about the possible fault candidates, and finally to declare a final decision on which fault(s) exists in the system. The isolator may be as simple as a lookup table, matching the fault signature to the closest fault candidate, or it may device sophisticated diagnosis algorithms to isolate the true fault. The fault isolator also has to deal with uncertainties in the fault signature results, since false alarms and missed detections are unavoidable in any fault detector.

- **Fault Identification**. The fault identifier estimates the fault parameters for the declared fault candidates. The identifier applies any necessary transformations to the estimates generated by the fault detector, in order to estimate the fault magnitude of the failed component in the system. This transformation may not be required if there is a one-to-one correspondence between the measured variable and the faulty component.

In this work, we focus on the design of the fault detector. The fault detector is required to accomplish the following tasks:

1. Decide if there is a change in the nominal behavior of the system.

2. Declare whether the existing fault is an abrupt persistent, abrupt intermittent, or incipient fault.

3. Estimate the relevant fault parameters.

IV.4 Fault Detector Design

Since detection of all fault types described in Section IV.2 could be reformulated into the hypothesis testing problem in (40), we use change detection theory to design the fault detector. Since we have unknown parameters after the change (e.g. fault magnitude), two main algorithms are used to detect the change [109]:

1. Weighted CUSUM algorithm, where the likelihood ratio is weighted (marginalized) w.r.t. all possible values of the unknown parameter. This requires prior information about the unknown parameters and results in an integration that may not be easy to evaluate.

2. Generalized Likelihood Ratio algorithm, where the unknown parameters are replaced by their respective ML estimates.

We choose the GLR algorithm for the detector design. We designate the Log Likelihood Ratio (LLR) for observations r from time j up to time k by:

$$S_j^k(\theta_1) = \sum_{i=j}^{k} \ln \frac{p_{\theta_1}(r[i])}{p_{\theta_0}(r[i])} \tag{46}$$

where θ_0 and θ_1 are the set of parameters that characterize the distribution of observations before and after the change, respectively. θ_0 is assumed known from the nominal system behavior data, while θ_1 is assumed unknown. In addition, the change time is unknown to the detector. These parameters are substituted by their ML estimates, and the test statistic is given by:

$$g_k = \max_{1 \le j \le k} \sup_{\theta_1} S_j^k(\theta_1) \tag{47}$$

If there is a minimum magnitude v_m of the changes of interest to the parameter θ, then the test statistic could be rewritten as:

$$g_k = \max_{1\le j\le k} \sup_{\theta_1:|\theta_1-\theta_0|\ge v_m>0} S_j^k(\theta_1) \tag{48}$$

The detection time t_a is the minimum value of k at which $g_k \ge h$, where h is the detector threshold:

$$t_a = \min\{k| \max_{1\le j\le k} S_j^k \ge h\} \tag{49}$$

The conditional ML estimate for the change time (conditioned on t_a) is the value of j at which the maximum value of g_k is reached. Therefore, the conditional ML estimate for the change magnitude and time are given by:

$$(\hat{t}_0, \hat{\theta}_1) = \arg \max_{1\le j\le t_a} \sup_{\theta_1} \sum_{i=j}^{t_a} \ln \frac{p_{\theta_1}(r[i])}{p_{\theta_0}(r[i])} \tag{50}$$

In the following, we derive the test statistic for each fault type. We note from Section IV.2 that $p_{\theta_0} \sim \mathcal{N}(0, \sigma_n^2)$ for all fault types. In addition, σ_n^2 is assumed known from nominal system data.

IV.4.1 Abrupt Persistent Fault Detection

From (41), $\theta_1 = A$, which is the only unknown parameter after change, in addition to the unknown change time. After straightforward simplifications, the LLR can be written as:

$$S_j^k = \frac{A}{\sigma_n^2} \sum_{i=j}^{k} \left(r[i] - \frac{A}{2} \right) \tag{51}$$

The test statistic in (48) is then given by:

$$g_k = \frac{1}{\sigma_n^2} \max_{1\le j\le k} \sup_{A:|A|\ge v_m>0} \sum_{i=j}^{k} \left[Ar[i] - \frac{A^2}{2} \right] \tag{52}$$

The unconstrained maximization over A produces:

$$\hat{A}_j = \frac{1}{k-j+1} \sum_{i=j}^{k} r[i] \tag{53}$$

Adding the constraint $|A| \geq v_m$ and noting that the maximization is for a quadratic function:

$$|\hat{A}_j| = \left(\frac{1}{k-j+1} \left| \sum_{i=j}^{k} r[i] \right| - v_m \right)^+ + v_m \tag{54}$$

and sign A_j is the same as the sign of $\frac{1}{k-j+1} \sum_{i=j}^{k} r[i]$. The test statistic is then given by:

$$g_k = \frac{1}{\sigma_n^2} \max_{1 \leq j \leq k} \sum_{i=j}^{k} \left[\hat{A}_j r[i] - \frac{\hat{A}_j^2}{2} \right] \tag{55}$$

When $v_m = 0$, the test statistic becomes:

$$\boxed{g_k = \frac{1}{2\sigma_n^2} \max_{1 \leq j \leq k} \frac{1}{k-j+1} \left[\sum_{i=j}^{k} r[i] \right]^2 \underset{\mathcal{H}_0}{\overset{\mathcal{H}_1}{\gtrless}} \gamma} \tag{56}$$

We note that the same result in (56) could be obtained if we substitute for the ML estimator of A, $\hat{A}$, in (51), where $\hat{A}$ is given by:

$$\hat{A} = \frac{1}{k-j+1} \sum_{i=j}^{k} r[i] \tag{57}$$

Accordingly, in subsequent discussions, we assume $v_m = 0$, which allows us to use the ML estimator directly in the LLR expression. If it is desired to have a minimum change for detection v_m, then it could be subtracted from the residual signal before applying the detection algorithm.

IV.4.2 Abrupt Intermittent Fault Detection

From the residual signal expression in (42), we note that when $Z[n] = 1$, i.e. a fault is present, the detection problem is identical to the abrupt persistent fault case, except that the mean under $\mathcal{H}_1$ is different. This is because there is only one realization of the random variable A during any

faulty period. Accordingly, the test statistic is the same for both faults. Since both A for the abrupt persistent fault, and μ_A for the abrupt intermittent fault are unknown, there is no way to differentiate between the two types of faults using only the GLRT test. An obvious discriminatory feature is the frequency of occurrence of the fault over a given time frame. Therefore, the solution we use is to reset the GLRT detector after each time a fault is declared. The detector then uses the estimated fault magnitude $\hat{A}$ as its new baseline and starts sampling from this new reset point. If the fault is persistent, and in the absence of false alarms, no more faults will be detected. On the other hand, if the fault is intermittent, then multiple fault instances will be detected. Each two consecutive faults will have opposite signs for $\hat{A}$. Therefore, we can summarize the fault signature by $\text{sgn}(\hat{A})$, where sgn is the sign function. The fault signature, assuming positive fault magnitude and no false alarms, is given by:

$$\text{sgn}(\hat{A}) = \begin{cases} 1 & \text{Abrupt persistent} \\ 1 \quad -1 \quad 1 \quad -1 \quad 1 \quad \ldots & \text{Abrupt intermittent} \end{cases} \tag{58}$$

A threshold could be set for how many fault instances are required before declaring a fault to be intermittent.

IV.4.3 Incipient Fault Detection

Since the incipient fault is characterized by a continuous increase in the signal magnitude, the application of the LRT for abrupt faults will detect consecutive changes in one direction only. Therefore, the fault signature for incipient faults, assuming positive fault magnitude, is given by:

$$\text{sgn}(\hat{A}) = [\ 1 \quad 1 \quad 1 \quad 1 \quad 1 \quad \ldots\ ] \qquad \text{Incipient fault} \tag{59}$$

Similarly, a threshold could be set for how many fault instances are required before declaring a fault to be incipient. From (58) and (59), we note that each fault type has a distinct signature, enabling us to discriminate between different faults by proper tuning of the detector thresholds. Algorithm

2 summarizes the complete detection algorithm. The parameter γ_p represents the integer threshold on the number of changes to declare an abrupt persistent fault. Ideally, i.e. without false alarm, γ_p should be set to 1. In practice, γ_p should be set > 1 to accommodate for false alarms from the change detector. The threshold γ_{pn} represents the number of samples the algorithm should wait after detecting a change to declare an abrupt persistent fault. This threshold is important in order to avoid a premature decision about the fault type, since the fault may be an intermittent one, with long persistence time. The parameters γ_i and γ_c represent the integer thresholds on the sum of the elements of the fault signature vector, for abrupt intermittent and incipient faults, respectively. For intermittent faults, γ_i should be ideally 0 or 1 (see (58)), while for incipient faults γ_c should be set > 1 (see (59)). Although it is possible to use one threshold in place of γ_i and γ_c, two thresholds give more control on the detector performance, since false alarms in each case could be handled independently. The parameter estimation part of the algorithm is explained in Section IV.5

IV.5 Fault Parameter Estimation

In this section, we present expressions for parameter estimators for each fault type. The results draw directly from classical estimation theory techniques [110].

IV.5.1 Abrupt Persistent Faults

The detection algorithm 2 returns the fault injection time t_{inj} and the fault magnitude $\hat{A}$, which are the only parameters to be estimated with this fault type. Therefore, no additional estimators are required for the abrupt persistent fault case. The estimators are given by:

$$\hat{t}_{\text{inj}} = \mathbf{T}[1] \tag{60}$$

$$\hat{A} = \mathbf{A}[1] \tag{61}$$

IV.5.2 Abrupt Intermittent Faults

The parameters to be estimated are:

Algorithm 2 Change Detection Algorithm

Input: r
Output: $\mathbf{T}, \mathbf{A}, F, \boldsymbol{\theta}$
Initialize: $\mathbf{T} = [], \mathbf{A} = [], F = [], \mathbf{G} = [0], A_0 = 0$
while true **do**
  Read current sample value r
  Expand test statistic vector, subtract fault magnitude if a fault is detected:
  $k = \text{size}(\mathbf{G})$
  for $j = 1 : k$ **do**
    $\mathbf{G}[j] = \mathbf{G}[j] + r - (k - j + 1)A_0$
  end for
  Estimate σ_n^2
  TStatistic $= -\infty$
  for $j = 1 : k$ **do**

    if $\frac{1}{k-j+1}\mathbf{G}^2[j] >$ TStatistic **then**
      TStatistic $= \frac{1}{k-j+1}\mathbf{G}^2[j]$
      $t_f = j$
      $\hat{A} = \frac{1}{k-j+1}\mathbf{G}[j]$
    end if
  end for
  if $\frac{1}{2\sigma_n^2}$TStatistic $> \gamma$ **then**
    fault = true
    $\mathbf{G} = \mathbf{G}[t_f : \text{end}]$
    $A_0 = \hat{A}$
    $\mathbf{A} = \begin{bmatrix} \mathbf{A} & \hat{A} \end{bmatrix}$
    $\mathbf{T} = \begin{bmatrix} \mathbf{T} & t_f \end{bmatrix}$
  end if
  if $1 \leq \text{size}(\mathbf{A}) < \gamma_p$ & $\text{size}(\mathbf{G}) > \gamma_{pn}$ **then**
    F = 'Abrupt Persistent'
    $\hat{t}_{\text{inj}} = \mathbf{T}[1], \quad \hat{A} = \mathbf{A}[1]$
    $\boldsymbol{\theta} = [\ \hat{t}_{\text{inj}} \quad \hat{A}\ ]$
    break
  else if $\text{size}(\mathbf{A}) > \gamma_p$ & $\text{sum}(\text{sgn}(\boldsymbol{A})) < \gamma_i$ **then**
    F = 'Abrupt Intermittent'
    $\hat{t}_{\text{inj}} = \mathbf{T}[1], \quad \hat{\mu}_A = \bar{\mathbf{A}}$
    $\mathbf{T}_n = \mathbf{T}[i+1] - \mathbf{T}[i] \quad i = 2, 4, 6, \ldots, \quad \hat{\mu}_n = \bar{\mathbf{T}}_n$
    $\mathbf{T}_F = \mathbf{T}[i+1] - \mathbf{T}[i] \quad i = 1, 3, 5, \ldots, \quad \hat{\mu}_F = \bar{\mathbf{T}}_f$
    $\boldsymbol{\theta} = [\ \hat{t}_{\text{inj}} \quad \hat{\mu}_A \quad \hat{\mu}_n \quad \hat{\mu}_f\ ]$
    break
  else if $\text{size}(\mathbf{A}) > \gamma_p$ & $\text{sum}(\text{sgn}(\boldsymbol{A})) > \gamma_c$ **then**
    F = 'Incipient'
    $\hat{t}_{\text{inj}} = \mathbf{T}[1]$
    $\hat{B} = \frac{\sum_{n=0}^{N-1} nr[n]}{\sum_{n=0}^{N-1} n^2}$
    $\boldsymbol{\theta} = [\ \hat{t}_{\text{inj}} \quad \hat{B}\ ]$
    break
  end if
  $\mathbf{G} = \begin{bmatrix} \mathbf{G} & 0 \end{bmatrix}$
end while
return $\mathbf{T}, \mathbf{A}, F, \boldsymbol{\theta}$

1. **Fault Injection Time**. The vector $\mathbf{T}$ returned by Algorithm 2 contains all fault injection times. We use the definition of the fault injection time in the case of intermittent faults as the time instant at which the first fault takes place:

$$\hat{t}_{\text{inj}} = \mathbf{T}[1] \tag{62}$$

2. **Mean Fault Magnitude**. The fault magnitude is drawn from a Gaussian distribution. Therefore, the ML estimator for its mean μ_A is just the arithmetic mean of the fault magnitude vector $\boldsymbol{A}$ returned by Algorithm 2 as follows:

$$\hat{\mu}_A = \bar{\mathbf{A}} = \frac{1}{\text{size}(\mathbf{A})} \sum_{i=1}^{\text{size}(\mathbf{A})} A[i] \tag{63}$$

3. **Mean Time Between Faults**. The inter-arrival times can be calculated from the vector $\mathbf{T}$ as:

$$\mathbf{T}_n = \mathbf{T}[i+1] - \mathbf{T}[i] \qquad i = 2, 4, 6, \ldots \tag{64}$$

The inter-arrival time has an exponential distribution. Therefore, the ML estimator for its mean is just the arithmetic mean of $\mathbf{T}_n$:

$$\hat{\mu}_n = \bar{\mathbf{T}}_n = \frac{1}{\text{size}(\mathbf{T}_n)} \sum_{i=1}^{\text{size}(\mathbf{T}_n)} T_n[i] \tag{65}$$

4. **Mean Fault Duration**. Similarly, the fault durations are calculated as follows:

$$\mathbf{T}_f = \mathbf{T}[i+1] - \mathbf{T}[i] \qquad i = 1, 3, 5, \ldots \tag{66}$$

and the ML estimator is given by:

$$\hat{\mu}_f = \bar{\mathbf{T}}_f = \frac{1}{\text{size}(\mathbf{T}_f)} \sum_{i=1}^{\text{size}(\mathbf{T}_f)} T_f[i] \tag{67}$$

IV.5.3 Incipient Faults

The parameters to be estimated are:

1. **Fault Injection Time**. Similar to the case of an abrupt intermittent fault, we define the fault injection time as the time instant at which the first fault takes place:

$$\hat{t}_{\text{inj}} = \mathbf{T}[1] \tag{68}$$

2. **Drift Slope**. We note from (44) that the observations represent a linear model in the unknown parameter B. To show that, we write the vector form of (44) on the form:

$$\mathbf{r} = \mathbf{H}B + \mathbf{w} \tag{69}$$

where $\mathbf{H} = \begin{bmatrix} 0 & 1 & 2 & \dots & N \end{bmatrix}$. We note here that sample 0 corresponds to the time instant t_{inj} and sample N corresponds to the time instant NT_s, where T_s is the sampling period and N is the total number of samples used in the estimation process. The solution of the estimation problem for the linear model in (69) results in the Minimum Variance Unbiased Estimator (MVUE) [110]:

$$\hat{B} = (\mathbf{H}^T\mathbf{H})^{-1}\mathbf{H}^T\mathbf{r} \tag{70}$$

using the expression for $\mathbf{H}$ we obtain:

$$\hat{B} = \frac{\sum_{n=0}^{N-1} nr[n]}{\sum_{n=0}^{N-1} n^2} \tag{71}$$

We note that in Algorithm 2, we assumed that the parameter estimation takes place the moment the fault detector declares the fault type. It may be desired to detect the fault as soon as possible (hence setting the relevant thresholds accordingly). However, the parameter estimation process may be desired to take more time, so that the estimates are more robust. In such scenario, the algorithm will not terminate when the fault is declared. Rather, it will run in an identical way to acquire more samples until the parameter estimation achieves a certain criterion that is defined by the application. The extension of the algorithm to include this scenario is straightforward, and not included here for brevity.

IV.5.4 Measurement Noise Variance

In Section IV.4, we assumed that the measurement noise variance σ_n^2 is known. If the variance is unknown, then it could be estimated from the nominal data using the MVUE for the Gaussian mean and variance:

$$\hat{\mu}_n = \bar{\mathbf{r}} \tag{72}$$

$$\hat{\sigma}_n^2 = \frac{1}{N-1} \sum_{n=0}^{N-1} (r[n] - \hat{\mu}_n)^2 \tag{73}$$

where N is the number of samples used for estimation, and $E[\mu_n] = 0$ for the nominal residual signal. It should be highlighted that this is approximate. The formal method is to substitute for the ML estimate of the noise variance when calculating the LLRT, as in Section IV.4.

IV.6 Case Study I: NASA ADAPT Electrical Testbed

The detection algorithm presented in this chapter was applied to detect different fault types in the NASA ADAPT-Lite Electrical Power System, in the context of the DXC'10 diagnosis competition. The main function of the EPS is to supply power to the Unmanned Aircraft Systems and payloads. The EPS schematic diagram is shown in Figure 34, where a battery is connected to a load bank through a set of switches, circuit breakers, and an inverter. The fault profiles to be detected are identical to the ones presented in this chapter. Examples of faults are load resistance abrupt and

incipient changes, sensor drift, and sensor failure. A complete description of the DXC'10 competition can be found in [4].

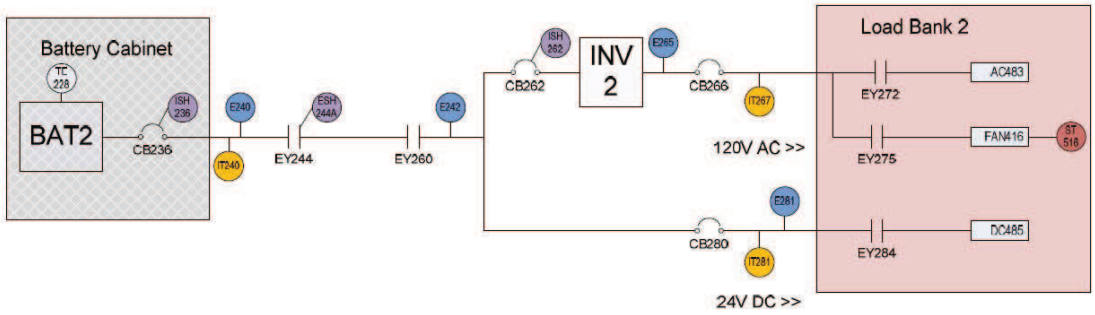

Figure 34: NASA Electrical Power System Schematic Diagram

The DXC'10 competition has 154 fault scenarios. In each scenario, a single fault in one of the system components is injected. The fault types include abrupt, abrupt intermittent, drift, and stuck faults. Figures 35, 36, and 37 plots the data from sensor IT240 for three sample fault scenarios, representing the three fault types. The incipient fault is the most challenging to detect, since the drift slope is very small compared to the noise variance. A comment about the detector performance for incipient faults and possible enhancements is given later in this section.

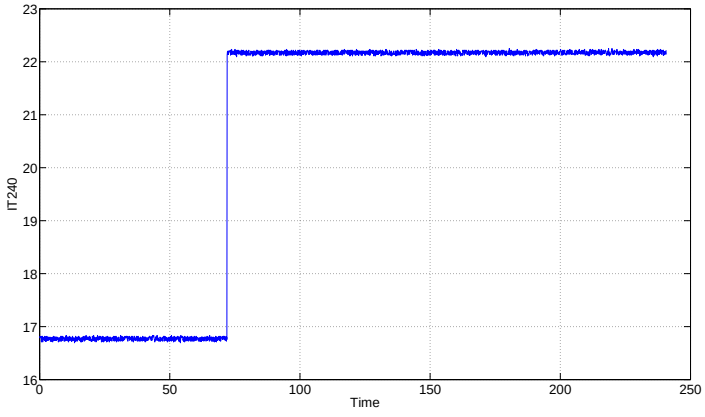

Figure 35: Abrupt persistent fault as manifested in sensor IT240, NASA DXC'10 competition

The performance of the detector is evaluated by reporting the fault type and component correctly, in addition to accurate estimation of the fault parameters. A snapshot of the fault scenarios is shown

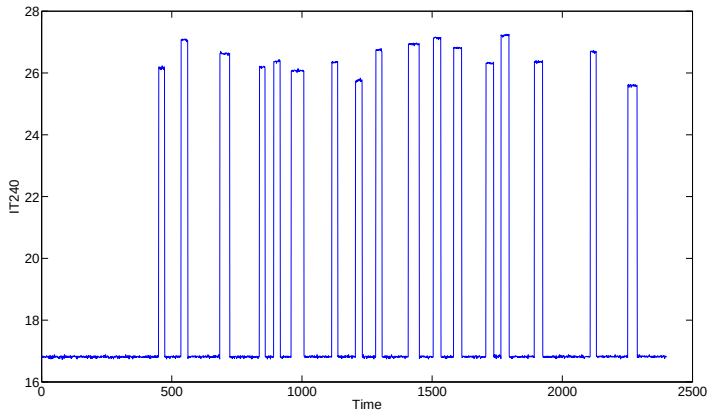

Figure 36: Abrupt intermittent fault as manifested in sensor IT240, NASA DXC'10 competition

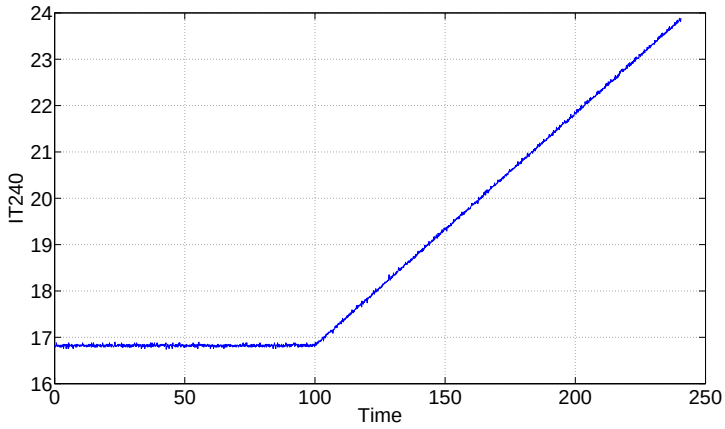

Figure 37: Incipient fault as manifested in sensor IT240, NASA DXC'10 competition

in Table 7. The last column, designated "Action" specifies whether the mission should be aborted or continued (NOP) when such a fault is detected. The specific action is dependent on different factors, including the faulty component, fault type, and fault magnitude.

Table 8 shows the threshold values used for the detector, and Table 9 shows the performance of the detector with the competition scenarios. We note that the detector performed poorly for the incipient faults. The main reason behind that is the way the detector was built to detect this type of faults. We relied on the heuristic approach of multiple change detections in one direction as an incipient fault signature. Since γ_c = 6, this requires six consecutive detected changes in the data stream. Unfortunately, most of the fault scenarios in the competition for incipient faults has very small drift slope. Therefore, the data set was not enough to declare an incipient fault. For this

Component	Fault Type	t_{inj} (sec)	B	$A(\mu_A)$	μ_f (sec)	μ_n (sec)	Action
IT240	Abrupt Persistent	72		5.4			ABORT
IT240	Abrupt Intermittent	45		9.78	2.96	8.44	ABORT
IT267	Abrupt Persistent	192		-0.2			NOP
IT267	Abrupt Intermittent	43		1.52	3.08	6.39	ABORT
IT267	Incipient	40	0.003				ABORT
E240	Stuck	102		23.9			NOP
EY275	Stuck Open	141.899					ABORT

Table 7: A snapshot of fault scenarios, NASA DXC'10 competition.

reason, most of the undetected incipient faults were reported as either abrupt persistent or abrupt intermittent faults, as the number of changes detected was below the threshold γ_c. A sketch for the solution of this problem is introduced in Section IV.8, where an independent LRT is performed for the incipient fault.

The detector performed reasonably well for abrupt persistent faults. Most of the missed detections in this case were because of the improper tuning of the detector. In the fault scenarios presented, different noise levels were associated with the same sensor in different scenarios. Since the detector threshold was fixed, based on the training data set, the detector was not able to cope with the change in variance from one fault scenario to the other. The solution of this problem is to use an adaptive threshold, where the algorithm automatically sets the detector threshold based on the estimated variance value for the incoming data set.

The detector performance for abrupt intermittent faults was worse than for abrupt persistent faults. The performance for intermittent faults cannot be better than persistent faults since missing an abrupt fault leads also to an intermittent fault miss. The excess performance degradation is because the threshold value γ_i was set to 5. That was mainly to accommodate for false alarms from the change detector. This problem could be addressed by lowering the threshold and reducing the false alarm rate simultaneously. The false alarm rate can be reduced by proper detector tuning with the penalty of increased delay for detection.

The remedy actions to enhance the detector performance are summarized in the last column in Table 9.

Threshold	Related Fault	Value
γ	Detector threshold	75
γ_p	Abrupt persistent	5
γ_i	Abrupt intermittent	5
γ_c	Incipient	6

Table 8: Detector thresholds for NASA DXC'10 competition

Fault Type	Total Scenarios	Detected	Undetected	P_D	Remedy
Abrupt Persistent	37	29	8	0.783	Adaptive threshold
Abrupt Intermittent	35	25	10	0.714	Low γ_i
Incipient	37	19	18	0.513	LRT

Table 9: Detector performance, NASA DXC'10 competition.

IV.7 Case Study II: Differential Protection for Aircraft Generator Windings

Differential protection has been successfully used in detecting generator winding faults [99]. It relies on the simple idea of measuring the phase current before and after the protected winding, using current transformers (CTs). When there is a discrepancy between the two measurements, a fault is declared and the generator is shut down as a protective measure. Figure 38 shows the differential protection architecture. The zone between the two current transformers is designated as the *protected zone*, and the current transformers are designated as Differential Protection Current Transformers (DPCTs).

Traditional differential protection relies on differential relays. In normal operation, the DPCT currents are equal, and therefore, they do not operate the relay coil. When there is a winding fault (e.g., a short to ground), a difference current will flow through the relay coil. If the difference current exceeds a certain threshold, the relay trips and the generator is shut down. In practice, a difference current may also be produced due to CT saturation, CT phase angle errors, or noisy measurements. Therefore, to prevent unnecessary tripping of the relay, an adaptive threshold is employed [112].

The traditional protection technique suffers from two drawbacks: (1) it relies on simple averaging techniques with fixed size window, without exploiting the signal information, and (2) it does not take into account the case where faults may be intermittent. This results in a degraded performance in the form of a high probability of false alarm, hence the generator may be shut down unnecessarily,

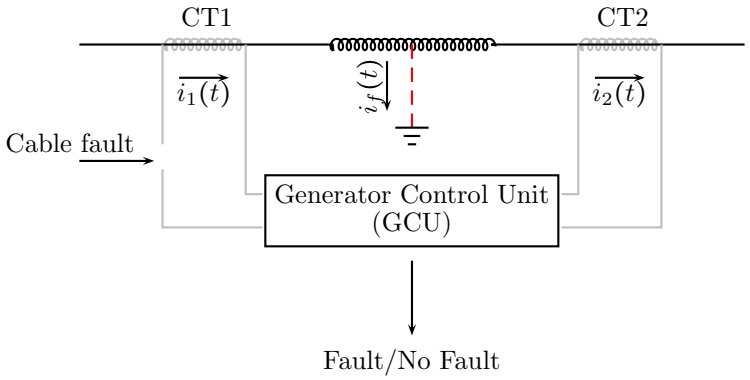

Figure 38: Differential protection for generator windings

or in the form of a high probability of missing a winding fault. In this section, we show that the performance of differential protection systems could be enhanced by deploying more sophisticated signal processing algorithms. These algorithms cannot be implemented on traditional relay-based systems. However, since aircraft AC generators are monitored and controlled by generator digital control units with sufficient computational capabilities, the detection algorithms could be implemented easily with a small percentage utilization of system resources. We consider first fixed-size window detectors, where we can obtain closed forms for the detector performance. We then consider sequential detectors and show how to apply the general detector developed in Section IV.4 on the differential protection problem. We focus our discussion in this section on abrupt faults. Incipient faults could be handled similarly.

IV.7.1 Hypothesis Testing Formulation

We assume that during nominal behavior, the two transformer currents are equal and given by:

$$i_1[n] = i_2[n] = A\cos(2\pi f_0 n + \phi_a), \tag{74}$$

where f_0 is the fundamental frequency, and ϕ_a represents the fault-free phase angle. For a balanced three phase system, the amplitude A is the same for the three phases, and the phases differ by $2\pi/3$ rad.

Assuming no winding fault, the difference current will be only a noise process, i.e., $i[n] = w[n]$. We assume that $w[n]$ is a stationary Gaussian random process with mean zero and variance σ^2. When a short circuit winding fault occurs, $i_1[n]$ and $i_2[n]$ will have different amplitudes from the normal operating value (overload condition):

$$i_1[n] = \tilde{A}\cos(2\pi f_0 n + \tilde{\phi}_a) + w_1[n] \tag{75}$$

$$i_2[n] = C\cos(2\pi f_0 n + \phi_c) + w_2[n] \tag{76}$$

We can express the differential current from Equations (75) and (76) as:

$$i[n] = B\cos(2\pi f_0 n + \phi_b) + w[n], \tag{77}$$

where

$$\begin{aligned} B &= \sqrt{\tilde{A}^2 + C^2 + 2\tilde{A}C\cos(\tilde{\phi}_a + \phi_c)} \\ \phi_b &= \arctan\frac{C\sin(\phi_c) - \tilde{A}\sin(\tilde{\phi}_a)}{C\cos(\phi_c) + \tilde{A}\cos(\tilde{\phi}_a)} \end{aligned}$$

The amplitude B and the phase ϕ_b depend on the magnitude and location of the winding fault, and they are not known a priori. Without prior assumptions about the nature of the fault, not much can be said about B and ϕ_b, except that $\tilde{A} - C \le B \le \tilde{A} + C$, which holds directly from the inequality $-1 \le \cos(x) \le 1$. If we assume that the winding fault is an almost complete short circuit, then C is very small and we can assume $B \approx \tilde{A}$, without knowledge of the phase angles. If, however, C cannot be neglected, which is the case when there is a partial short circuit, then B varies widely depending on the phase angle values.

The above description represents the following composite hypothesis testing problem:

$$\begin{aligned} \mathcal{H}_0 : i[n] &= w[n] \\ \mathcal{H}_1 : i[n] &= B\cos(2\pi f_0 n + \phi_b) + w[n] \end{aligned} \tag{78}$$

where B and ϕ_b are unknown.

IV.7.2 Fixed-Size Window Detection

The optimal detector for the hypothesis test in (78) depends on our knowledge about the sinusoidal signal. Perfect knowledge will produce the best performance. However, the magnitude and phase are usually not known a priori, since they depend on the fault type. Therefore, because the signal parameters are not completely known, we have to accept a performance loss in the detectors. In the following discussion, we compare different detectors, based on the available signal knowledge. The results are drawn directly from classical signal detection theory [10].

We assume that the decision is based on the N-dimensional random vector $\mathbf{i} = [i[0] \quad i[1] \ldots i[N-1]]$. To simplify the notation, we assume that the data samples start at the time instant $n = 0$. The detection for signals with an unknown delay, n_0, can be treated similarly by estimating n_0 from the data samples, with a slight loss in the detection performance. The design of the detector is the determination of the test statistic $T(\mathbf{i})$, as a function of the observation vector $\mathbf{i}$, and the detector threshold γ:

$$T(\mathbf{i}) \underset{\mathcal{H}_0}{\overset{H_1}{\gtrless}} \gamma \tag{79}$$

Sample Average Detector

In this case, no signal knowledge is used, and the detector is given by:

$$T(\mathbf{i}) = \sum_{n=0}^{N-1} i[n] \underset{\mathcal{H}_0}{\overset{H_1}{\gtrless}} \gamma \tag{80}$$

It can be easily shown that the detector Receiver Operating Characteristic (ROC) curve is given by:

$$P_D = Q\left(Q^{-1}(P_F) - \sqrt{\frac{\mathcal{E}_1}{\sigma^2}}\right), \tag{81}$$

where:

$$\mathcal{E}_1 = \frac{B^2}{N}\left[\sum_{n=0}^{N-1}\cos(2\pi f_0 n + \phi_b)\right]^2 \tag{82}$$

and $Q(.)$ is the right-tail probability for the standard normal PDF. Since the signal amplitude, B, is a measure of the fault magnitude, one way to express the detection performance is in terms of the signal to noise ratio, B/σ. From Equations (81) and (82) we get:

$$P_D = Q\left(Q^{-1}(P_F) - \left(\frac{B}{\sigma}\right)\frac{\sum_{n=0}^{N-1}\cos(2\pi f_0 n + \phi_b)}{\sqrt{N}}\right) \tag{83}$$

Known Sinusoidal Signal Detector

If the sinusoidal signal $s_b[n] = B\cos(2\pi f_0 n + \phi_b)$ is completely known, then the optimal detector is the matched filter, given by:

$$T(\mathbf{i}) = \sum_{n=0}^{N-1} i[n]s_b[n] \underset{\mathcal{H}_0}{\overset{H_1}{\gtrless}} \gamma, \tag{84}$$

and the ROC curve is given by:

$$P_D = Q\left(Q^{-1}(P_F) - \sqrt{\frac{\mathcal{E}_2}{\sigma^2}}\right), \tag{85}$$

where:

$$\mathcal{E}_2 = B^2\sum_{n=0}^{N-1}\cos^2(2\pi f_0 n + \phi_b) \tag{86}$$

Accordingly:

$$P_D = Q\left(Q^{-1}(P_F) - \left(\frac{B}{\sigma}\right)\sqrt{\sum_{n=0}^{N-1}\cos^2(2\pi f_0 n + \phi_b)}\right) \tag{87}$$

Unknown Amplitude Detector

If the signal amplitude is not known, the samples are used to calculate the Maximum Likelihood Estimator (MLE) for the amplitude, and the detector is given by:

$$T(\mathbf{i}) = \left[\sum_{n=0}^{N-1} i[n]\cos(2\pi f_0 n + \phi_b)\right]^2 \underset{\mathcal{H}_0}{\overset{H_1}{\gtrless}} \gamma, \tag{88}$$

and the ROC curve is given by:

$$P_D = Q\left(Q^{-1}(\frac{P_F}{2}) - \left(\frac{B}{\sigma}\right)\sqrt{\sum_{n=0}^{N-1}\cos^2(2\pi f_0 n + \phi_b)}\right) + Q\left(Q^{-1}(\frac{P_F}{2}) + \left(\frac{B}{\sigma}\right)\sqrt{\sum_{n=0}^{N-1}\cos^2(2\pi f_0 n + \phi_b)}\right) \tag{89}$$

The performance of this detector can be easily shown to be worse than the matched filter.

Unknown Amplitude and Phase Angle Detector

In practice, when a fault occurs, the resulting sinusoidal signal has unknown amplitude and phase angle. Therefore, this case represents the practical situation with most winding faults, and its performance should be compared with the sample average detector, where no signal knowledge is exploited. The unknown amplitude, B, and the phase angle, ϕ_b, could be estimated from the sample data, using MLE, and the detector is given by:

$$T(\mathbf{i}) = \frac{1}{N}\left[\left(\sum_{n=0}^{N-1} i[n]\cos(2\pi f_0 n)\right)^2 + \left(\sum_{n=0}^{N-1} i[n]\sin(2\pi f_0 n)\right)^2\right] \underset{\mathcal{H}_0}{\overset{H_1}{\gtrless}} \gamma' \tag{90}$$

and the ROC curve is given by:

$$P_D = Q_{\chi_2'^2(N\lambda)}\left(-2\ln P_F\right), \tag{91}$$

where $\lambda = B^2/2\sigma^2$, $P_F = e^{-\gamma'/\sigma^2}$, and $Q_{\chi_2'^2(\lambda)}$ is the right tail probability for the non-central chi-squared PDF with 2 degrees of freedom, and non-centrality parameter λ. If it is desired to constrain

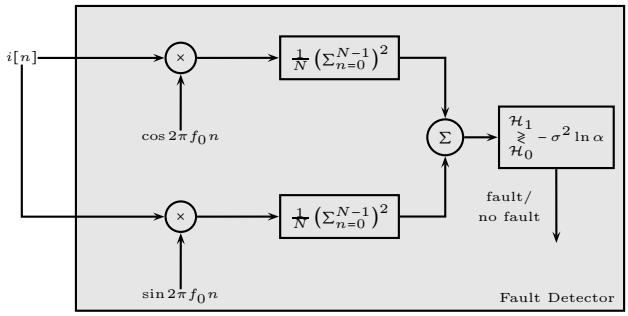

Figure 39: Block diagram for the persistent winding fault detector. The threshold is set to maximize P_D for the constraint $P_F = \alpha$.

P_F to α, then the detector operating point becomes:

$$(P_F, P_D) = (\alpha, Q_{\chi_2'^2(N\lambda)}(-2\ln\alpha))$$

which corresponds to the detector threshold $\gamma\prime = -\sigma^2 \ln \alpha$. Figure 39 shows a detailed block diagram for the detector.

Performance Comparison

Figure 40 illustrates the detection performance for the four detector designs presented. The probability of detection is plotted against the signal to noise ratio B/σ (using a semilog scale). We use the parameter values $N = 10, f_0 = 1/7, \phi_b = 0$, and $P_F = 0.05$. As expected, the best performance is achieved by the matched filter detector, which assumes complete knowledge about the sinusoidal signal. The detector with unknown amplitude has a slight degradation in the performance, and the loss of performance is not significant when, additionally, the phase is not known.

The sample average detector has the worst performance, and not comparable to the other three detectors. This is because the detector does not use any signal information. Traditional differential protection systems rely on this type of detectors, and therefore, using the detector with unknown amplitude and phase outperforms it by a large magnitude. For example, from Figure 40, at signal to noise ratio = 1, the sample average detector achieves $P_D \approx 0.115$, while the detector with unknown

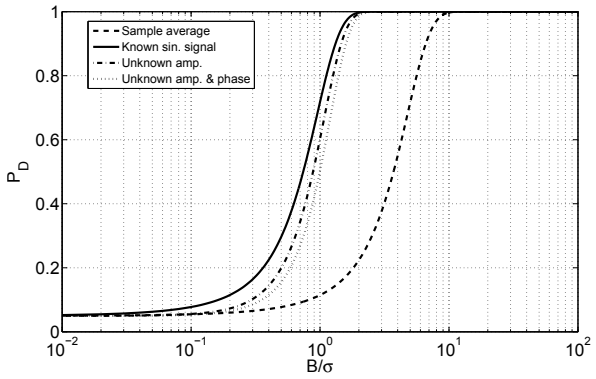

Figure 40: Detection performance for the four persistent winding fault detectors in Section IV.7.2. The sample average detector has the worst performance, since it does not use the available signal information. Slight degradation is noted when the amplitude and phase of the sinusoidal signal are not known.

amplitude and phase achieves $P_D \approx 0.5$. The advantage of the latter detector is that it requires only knowledge about the frequency of the sinusoidal signal.

IV.7.3 Sequential Detection

Fixed-Size window detection has the advantage of a relatively easy tuning. However, the delay for detection is on the average higher than sequential detection. In this section, we apply the sequential detection algorithm developed in Section IV.4 on the differential protection problem. We follow the same procedure in Section IV.4. To find the LRT statistic, we need to find the ML estimator for both B and ϕ_b. It can be shown that the ML estimators could be approximately given by [110]:

$$\hat{B} = \sqrt{\alpha_1^2 + \alpha_2^2} \tag{92}$$

$$\hat{\phi}_b = \arctan\left(\frac{-\alpha_2}{\alpha_1}\right) \tag{93}$$

where

$$\alpha_1 = \frac{2}{k-j+1}\sum_{i=j}^{k} r[i]\cos 2\pi f_0 i \tag{94}$$

$$\alpha_2 = \frac{2}{k-j+1}\sum_{i=j}^{k} r[i]\sin 2\pi f_0 i \tag{95}$$

and the approximation is based on the assumption that f_0 is not near 0 or 1/2. This could be guaranteed by adjusting the sampling frequency of the GCU. Substituting for the ML estimators, we can show that the test statistic is given by:

$$\boxed{g_k = \frac{1}{\sigma^2} \max_{1 \le j \le k} \frac{1}{k-j+1} \left[\left(\sum_{i=j}^{k} r[i] \cos 2\pi f_0 i \right)^2 + \left(\sum_{i=j}^{k} r[i] \sin 2\pi f_0 i \right)^2 \right]} \tag{96}$$

The performance of change detectors is usually measured by numerical simulations, since no closed form solution could be obtained.

IV.8 Detector Enhancement

The incipient fault detection scheme presented in Section IV.4 was based on the heuristic approach of repetitive change detection. This process is suboptimal, since it assumes the data model for the abrupt fault. A more accurate method is to use the incipient fault data model in (44). In this case, we have three hypotheses, one for each fault type, [1] in addition to the nominal case. We cannot formulate this problem as a multi-hypothesis change detection problem, since there is no case where the data model changes from the incipient fault case to the abrupt fault case or vice versa. Alternatively, we can run two binary hypothesis tests in parallel, one for each fault type. In the likely event that both detectors will fire a detection event, an additional LRT is performed between the data models of the abrupt and incipient faults, to decide which fault is the most likely one. The data samples that are used in this LRT are the ones *after* the latest fault is declared, and the length of the data samples used is to be decided based on the required accuracy. This enhanced detection scheme is depicted in Figure 41.

In Figure 41, the abrupt fault detector has the same design as the one presented in this chapter. Now we need to design the incipient fault detector, as well as the fault selector. We start with the

[1] We assume here that the discrimination between abrupt persistent and abrupt intermittent faults is done the same way as in the current detector design. Therefore, the new design is concerned only with the comparison between abrupt persistent and incipient faults.

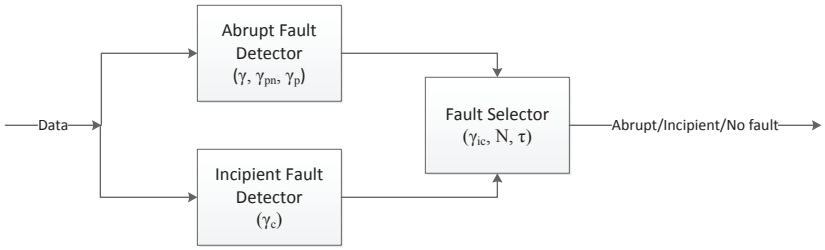

Figure 41: Enhanced detector design for efficient detection of incipient faults

incipient fault detector, where we have the binary composite hypothesis testing problem:

$$\mathcal{H}_0 : r[n] = w[n] \tag{97}$$

$$\mathcal{H}_1 : r[n] = Bn + w[n] \tag{98}$$

We calculate the LLR as in Section IV.4, noting that the ML estimator for B is given by (71). It is straightforward to show that the test statistic is given by:

$$\boxed{g_k = \frac{1}{2\sigma_n^2} \max_{1 \le j \le k} \frac{1}{\sum_{i=j}^{k} (i - j + 1)} \left[\sum_{i=j}^{k} i r[i] \right]^2 \underset{\mathcal{H}_0}{\overset{\mathcal{H}_1}{\gtrless}} \gamma_c} \tag{99}$$

The moment the fault selector receives an alarm from one of the fault detectors, it carries out an LRT between the two fault distributions:

$$\mathcal{H}_0 : r[n] = A + w[n] \tag{100}$$

$$\mathcal{H}_1 : r[n] = Bn + w[n] \tag{101}$$

The LRT produces the following test statistic, after substituting for the ML estimators for A and B:

$$g_k = \frac{1}{2\sigma_n^2}\left[\left(\frac{\left(\sum_{n=0}^{N-1} nr[n]\right)^2}{\sum_{n=0}^{N-1} n^2} - \frac{\left(\sum_{n=0}^{N-1} r[n]\right)^2}{N}\right]\right] \underset{\mathcal{H}_0}{\overset{\mathcal{H}_1}{\gtrless}} \gamma_{ic} \tag{102}$$

The data samples to be included in the test start from the estimated fault injection time $\hat{t}_{\text{inj}}$. An adjustable delay τ, may be introduced also in the fault selector, to take into account the probability that the other fault detector may produce a delayed alarm. In such case, the fault injection time is considered to be the maximum of the two fault injection times reported. The number of samples, N, is adjustable, based on the required probability of detection, for a given probability of false alarm rate.

In the following, we show the performance of the fault selector when A and B are known. The performance in this case has a closed form solution, which gives us an intuition about how to tune the detector and select the number of samples N. In the actual case, A and B have to be estimated from the sample data. This complicates the test statistic, and the performance in this case could be evaluated only numerically using Monte Carlo Simulations. When A and B are known, it can be shown that the ROC curve for the fault selector is given by:

$$P_D = \left[(Q^{-1}(P_{FA}) - \sqrt{\left(\sum_{n=0}^{N-1}(Bn - A)^2\right)/\sigma_n^2}\right] \tag{103}$$

This ROC expression shows that the detection performance increases as the difference between the two fault profiles, normalized by the noise variance, gets higher. This suggests the use of large data samples to distinguish between the two fault profiles, if the slope of the incipient fault is small.

Table 10 summarizes the tunable parameters for the enhanced detector design. These parameters are also marked on Figure 41.

Parameter	Description	Detector
γ	Threshold for abrupt fault LRT	Abrupt detector
γ_{pn}	Number of samples to wait to declare an abrupt persistent fault	Abrupt detector
γ_p	Number of changes to declare an intermittent fault	Abrupt detector
γ_c	Threshold for incipient fault LRT	Incipient detector
γ_{ic}	Threshold for abrupt/incipient faults LRT	Fault selector
N	Number of samples for abrupt/incipient faults LRT	Fault selector
τ	Time delay after a single fault detection to perform an LRT	Fault selector

Table 10: Tunable parameters for the enhanced detector design

IV.9 Summary

Statistical models are powerful in designing fault detectors for physical systems, provided that a data set is available for the nominal system behavior and the set of faults of interest. We presented a general fault detection algorithm, based on change detection theory, which is capable of detecting abrupt, intermittent, and incipient faults. The algorithm was used in the NASA DXC'10 competition and achieved 2nd position. The detector performance could be further enhanced by the proper turning of different thresholds, as well as by running two separate detectors in parallel for the abrupt and incipient faults. To show how the detector could be applied to general fault types, we developed the detector design for aircraft generator winding fault detection using differential protection techniques. Performance evaluation of the differential protection case study was not possible due to the lack of empirical data set for training and evaluation.

The performance of abrupt persistent fault detectors depends on the change magnitude as well as the allowed delay for detection. Since the fault magnitude is not under the designer control, increasing the delay for detection increases the performance, especially for small system changes. The distinction between abrupt and intermittent faults is rather simple if false alarms are not considered. False alarms complicate the problem, as the detection system incorrectly counts the false changes towards the minimum threshold required to declare an intermittent fault. The detector presented in this chapter could be enhanced by adding more sophisticated algorithms to reduce the false alarm rate.

Incipient faults are challenging to detect if the drift slope is small. A long data record is required in this case to accurately detect the fault. In addition, the discrimination between incipient and abrupt faults cannot rely only on counting the number of changes, as presented in the basic algorithm. Counting the number of changes only resulted in a high miss rate for fault detection in the DXC'10 competition, since incipient faults introduced had a very small slope value. We presented a more sophisticated algorithm to enhance the incipient fault detection performance. The new algorithm has to be validated using existing data set from the DXC'10 competition.

Several enhancements are possible for the presented algorithm. An adaptive threshold that changes with the noise variance level could possibly increase the probability of detection. The distinction between abrupt persistent and intermittent faults could be enhanced by reducing the false alarm rate of the change detector, which could be done by increasing the delay for detection. Recursive detection and estimation statistics are also important in practical implementations to speed up the decision process, allowing for early fault declaration and parameter estimation.

In Chapters III and IV, we focused on modeling the physical system, while ignoring the communication network connecting the physical and cyber systems. This assumption is reasonable for the applications introduced, i.e. aircraft generators and power distribution systems where sensors are connected to the cyber system using hard-wired cables. However, in other applications, e.g. decentralized detection with wireless sensor networks, the communication network is an integrated part of the system and its design affects the system performance directly. In the rest of the dissertation, we turn our attention to the integration of the communication network into the design of detection systems. We focus on statistical modeling for the physical system and assume a decision making system using WSNs, where the main purpose is to decide whether there is an abnormal behavior in the monitored physical system.

CHAPTER V

Model-based Detection in Wireless Sensor Networks

In Chapters III and IV, the focus is on modeling the physical system and designing the decision unit. The other system components in Figure 1, especially the communication network, are assumed to be ideal, and hence ignored in the system design. This assumption is valid if the link between system components is accomplished by hard-wired cables. For more recent applications, where sensors and actuators represent data network nodes that are connected by a communication infrastructure, this assumption is no longer valid. The situation is even worse if the communication infrastructure includes wireless channels. Clearly, the communication network has to be incorporated into the design process to better understand the interaction between the different system components, and to be able to obtain an optimized performance for the complete system. In the rest of the dissertation, we focus on the integration of the communication network in the design process, in order to optimize the detection performance. The focus of the study in terms of the CPS block diagram is reproduced in Figure 42. We assume wireless communication networks since they are the least reliable, and consider different network topologies and media access control protocols.

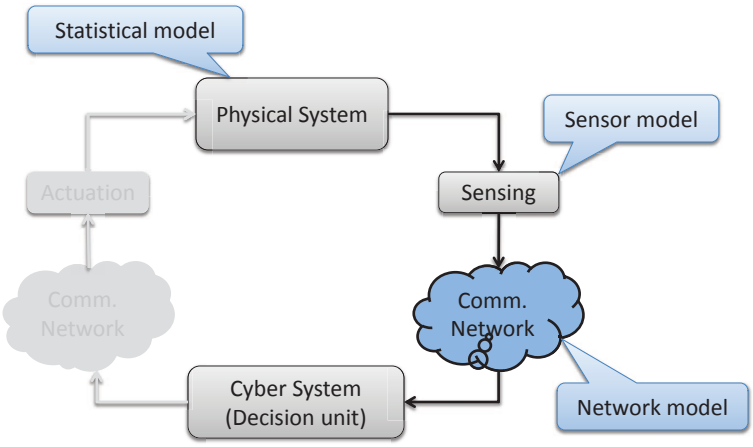

Figure 42: Focus of model-based detection in WSN study.

In this chapter, we outline the design process and explain it with simple examples. This design process is followed in Chapters VI and VII to design single hop networks with slotted ALOHA and TDMA media access protocols, respectively, and in Chapter VIII to design tree networks. The rest of this chapter is organized as follows; Section V.1 presents a motivating example for the design work. Section V.2 explains the design process, and Section V.4 presents a brief overview of the application of the design process on the single hop network with slotted ALOHA, which is treated in depth in Chapter VI.

V.1 Motivating Example

Consider the simple wireless network in Figure 43 that is deployed to detect a change in the environment. specifically, consider the target detection problem, and assume that the communication channel is shared between sensor nodes. The fusion center is required to select the *best* sensor(s) that yield the optimal detection performance. If the Quality of Information at each sensor node is the only criterion, then the fusion center should select sensor S_3 to permanently transmit since it is the nearest to the target location. Sensors S_1 and S_2 have lower QoI and their attempts to gain channel access will interfere with S_3 and lower the detection performance. Now consider the same problem if we considered the Channel State Information as an additional criterion for sensor selection. Although S_3 has the highest QoI, it may have the worst channel quality since it is the farthest from the fusion center. Sensor S_1 is the opposite case; it has the lowest QoI, being the farthest from the target location, however it may have the best channel quality since it is the nearest to the fusion center. S_2 strikes a balance between the two cases, where it is midway from both the target location and the fusion center. The answer to the question of which sensor(s) should transmit becomes not obvious. Now consider adding the additional criterion of Residual Energy Information (REI), which represents the amount of energy reserve in each sensor battery. The problem now becomes more complicated. For example, S_1 may have the best channel condition to the fusion center, but it may have very low energy reserve. The sensor will use low transmission power to prolong its lifetime, hence most of the transmissions maybe lost. Accordingly, the *equivalent* channel quality may not

be the best amongst the other sensors. Clearly, the problem becomes much more complicated. A related question is *what are the communication parameters that will be used by the contributing sensors?*, e.g. the communication rate and the transmission power.

To accurately answer these questions, we need a system model that integrates the different sensor quality measures in addition to the communication parameters. This model has to be related to the performance measure for our detection application, so that the relevant design variables could be optimized to achieve the optimal detection performance. This discussion is formalized in the next section, where the design process is explained.

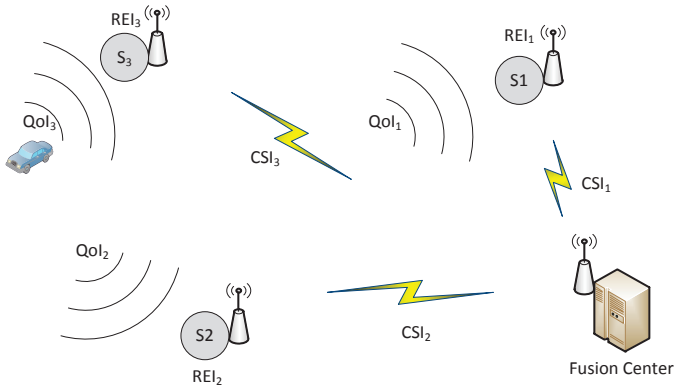

Figure 43: Wireless Sensor Networks in detection applications. QoI is the Quality of Information at each sensor, CSI is the Channel State Information for the link between each sensor and the fusion center, and REI is the Residual Energy Information for each sensor.

V.2 Design Process

Based on the discussion in Section V.1, we formalize our design process as in Figure 44. The design process stages are summarized as follows:

- **Performance Measure**. The process starts with the specification of the performance measure for the application. A careful choice for the performance measure is crucial for the system performance. General performance measures that are not application-specific may lead to a significant loss in the system performance. As an example, a typical performance measure for our detection application is the probability of error. If we consider a generic performance

measure, e.g. fairness or maximum throughput, a performance loss will occur. This case is emphasized with the performance comparison performed in Chapters VI, VII, and VIII. The performance measure represents the objective function in the resulting optimization problem.

- **Quality Measures**. The choice of the quality measures to be included depends on the application and the objective of the study. Choosing quality measures that are irrelevant complicates the system model while leading to negligible performance gain. In our motivating example in Section V.1, the quality measures are QoI, CSI, and REI.

- **Component Models**. The system components to be modeled are chosen based on the quality measures included in the design. For example, the QoI dictates a sensing model for the observations at each sensor node. The CSI requires a model for the physical channel between the sensor node and the fusion center. The REI requires an energy model for the sensor node, and for the whole sensor network if there is a constraint on the total energy budget. The components to be modeled also define the design variables of the system. The decision of whether a system parameter is a design variable or a constraint is application specific. As an example, by modeling the communication channel, possible design variables are the communication rate and transmission power for each sensor.

- **System Model**. The system model integrates the component models in a way that allows the objective function to be expressed in terms of the quality measures and the design variables. The development of the system model is always driven by the performance measure.

- **Optimization Problem**. The outcome of the system model is an optimization problem, where the design variables have to be chosen to optimize the performance. The specific application defines the constraints on the design variables. Depending on the complexity of the application, the optimization problem maybe solved analytically or numerically using different constrained optimization algorithms. Very few optimization problems could be solved analytically. In addition, with the exception of convex optimization problems, obtaining a global maximum (minimum) for the objective function cannot be guaranteed.

- **Performance Comparison**. The last stage in the design process is to measure the performance gain by comparing the proposed design to other design approaches using the same benchmark.

This design process is iterative, and the design may be refined based on the outcome of each iteration. In Section V.3, we given an example for the design process for a simple slotted ALOHA network with identical sensors. Section V.4 provides a more complex design example for the slotted ALOHA sensor network, where multiple quality measures are considered. This later example is a summary for the design case in Chapter VI.

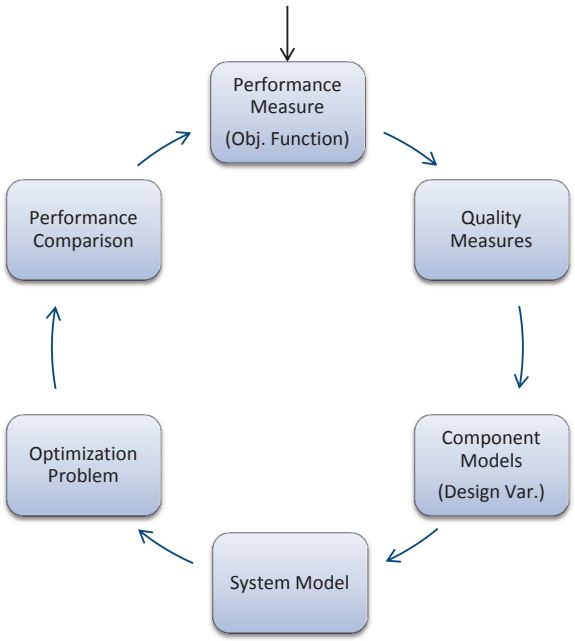

Figure 44: Design process for Wireless Sensor Networks in detection applications

V.3 Design Example-Single-hop Slotted ALOHA WSN with Identical Sensors

We consider the design problem for the single-hop slotted ALOHA sensor network in Figure 45. The network is deployed to detect the presence of an object in a specific geographic area. Sensors collect their observations and transmit them over the shared communication channel to the decision unit.

The decision unit takes a final decision after a fixed time period. In the following, we go through the design process illustrated in Figure 44.

- **Performance Measure**. The detection performance is usually measured by the probability of error or the ROC curve. The probability of detection (for a given fixed probability of false alarm), or the probability of error, represents our objective function.
- **Quality Measures**. We assume the simplest network, where the QoI is the same for all sensors. We ignore the energy constraint, and the physical channel degradation. We consider only the collision phenomenon between sensors.
- **Component Models**. The choice of the QoI dictates a statistical model for the environment, which is the same for all sensors. The choice of the collision state requires a model for the MAC sublayer. Based on these component models, the design variable is the detector threshold only.
- **System Model**. The system model is an expression of the probability of detection (probability of error) as a function of the system quality measures and the design variables.
- **Optimization Problem**. The optimization problem could be expressed in the form:

$$\begin{aligned} \max_{\gamma} \quad & P_D(\gamma;\lambda) \\ \text{subject to} \quad & P_F(\gamma;\lambda) = \alpha \end{aligned}$$

  where γ is the detector threshold and λ is the multiaccess channel parameter.
- **Performance Comparison**. For this simple network, comparison with centralized detection scheme, where all sensors transmit without collision, is sufficient.

The performance analysis for this problem with ROC measure is considered in [128], and the probability of error measure is considered in [129], for simple hypothesis testing problem. The analysis problem with composite hypothesis testing is considered in [130]. The design problem is considered in [131], where the objective is to adapt the threshold according to the quantity of the information received.

V.4 Design Example-Single-hop Slotted ALOHA WSN

We consider a more complex design example for the same single-hop slotted ALOHA sensor network in Figure 45. In this case, the decision unit is required to specify which sensors to transmit, and the communication parameters that are used by each contributing sensor. In the following, we go through the design process illustrated in Figure 44.

- **Performance Measure**. The detection performance is usually measured by the probability of error or the ROC curve. These measures are shown in Chapter VI to produce intractable formulation. This is an outcome of the first iteration through the design process. As a consequence, we adopt the deflection coefficient as our performance measure. The deflection coefficient belongs to the family of *distance measures* that are typically used to achieve tractable results [17]. The deflection coefficient represents our objective function.

- **Quality Measures**. We include the QoI, CSI, and the REI quality measures in the design process. The choice of QoI is motivated by the detection application. The choice of the CSI is motivated by the desire to capture the network effect on the overall system performance. The choice of the REI is motivated by the limited energy budget typically encountered in WSN applications.

- **Component Models**. The choice of the QoI dictates a statistical model for the environment. The choice of the CSI requires a physical channel model that includes the physical layer and the MAC sublayer of the communication network. The choice of the REI requires an energy model for the sensor. Based on these component models, the design variables are specified to be the communication rate, retransmission probability for the MAC sublayer, and the transmission energy for each sensor.

- **System Model**. The system model is an expression of the deflection coefficient as a function of the system quality measures and the design variables.

- **Optimization Problem**. The optimization problem is expressed in the general form:

$$\begin{aligned} \max_{\boldsymbol{x}} \quad & D(\boldsymbol{x}) \\ \text{subject to} \quad & f_i(\boldsymbol{x}) \geq 0 \qquad i = 1, 2, \ldots, m \\ & g_i(\boldsymbol{x}) = 0 \qquad i = 1, 2, \ldots, p \end{aligned}$$

  where D is the deflection coefficient, $\boldsymbol{x}$ is the vector of the design variables, f_i is the set of inequality constraints, and g_i is the set of equality constraints on $\boldsymbol{x}$. In Chapter VI, the optimization problem is shown to be non-convex. In addition, the problem possesses linear inequality constraints only, which could be expressed in the form $A\boldsymbol{x} = b$.

- **Performance Comparison**. Two classical design approaches for sensor networks are (i) decoupled approach, where each system component is designed separately, and (ii) maximum throughput approach, where the objective is to maximize the *quantity* of the information at the fusion center. The benchmark is a sensor network with given layout and sensor characteristics.

The complete design for the system in Figure 45 is presented, along with the performance comparison, in Chapter VI.

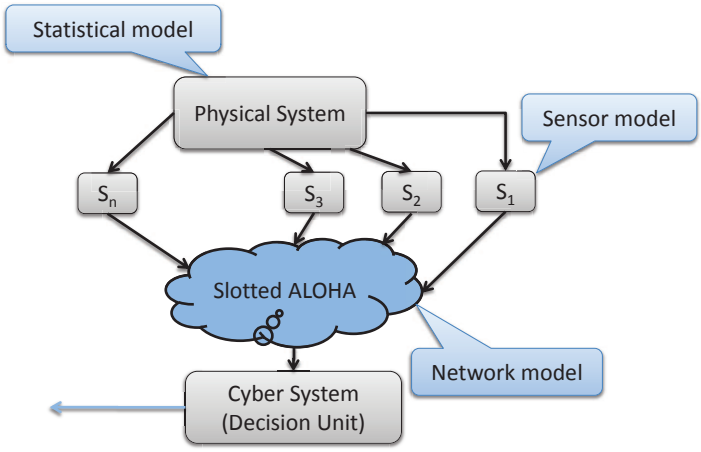

Figure 45: Design example for the single-hop Slotted ALOHA Wireless Sensor Network

CHAPTER VI

Transmission Control Policy Design for Slotted ALOHA Sensor Networks

VI.1 Introduction

In this chapter, we follow the design process outlined in Chapter V for the single-hop sensor network with slotted ALOHA media access control. The single-hop network is feasible when sensor nodes cannot communicate with each other to form a multihop network to the fusion center, e.g., cellular nodes communicating to a base station. Slotted ALOHA is considered for two reasons: (1) the traditional assumption of a dedicated orthogonal channel between each sensor node and the fusion center may not be feasible in practice, and (2) slotted ALOHA forms the basis for many standard protocols (e.g., GPRS in 3G GSM networks). Therefore, tuning of the protocol parameters to optimize the detection performance can be done in practice without a need to redesign the system. As outlined in Section V.4, we adopt the deflection coefficient as our detection performance measure. We choose the QoI, CSI, and REI as our system quality measures. Our design variables are the sensor communication rate, transmission power, and the ALOHA retransmission probability. These design variables collectively define what is called the *Transmission Control Policy* (TCP) for the sensor network.

We explain in depth the last three steps in the design process in Figure 42; namely the system model, the optimization problem, and the performance comparison. We develop an integrated model for the WSN that includes the system, sensing, and different networking aspects. The network component captures the physical layer as well as slotted ALOHA MAC sublayer. We integrate the QoI, CSI, and REI in the design process, and design a complete TCP that maximizes the detection performance. We show that our design results in significant detection performance improvement over the classical design approaches, where either the network is ignored altogether, or designed to satisfy performance measures that are not relevant to the application [8].

The rest of the chapter is organized as follows: we formulate the problem in Section VI.2. The detailed system model is derived in Section VI.3. The solution of the formulated optimization problem to obtain the optimal TCP is given in VI.4. Section VI.5 presents two widely-known detection performance measures, their relationship to the proposed detection measure, and their method of calculation. Section VI.6 summarizes two different design approaches, to be compared to the proposed design approach. Section VI.7 provides an illustrative numerical example. The work is concluded in Section VI.8.

VI.2 Problem Formulation

Figure 46 illustrates the detection system architecture, where a set of N wireless sensors denoted by the set $\mathcal{S} = \{S_1, S_2, \ldots, S_N\}$, and a fusion center denoted by FC, collaborate to detect the phenomenon of interest. We assume that the geographical area is divided into a number of resolution cells, where each cell is monitored by a subset of the sensors. Before the actual detection process takes place, the fusion center needs to specify which sensors will contribute to the detection process for each given cell. To do that, the fusion center broadcasts a message containing the location of the phenomenon (target, smoke,...etc) to be detected. Each sensor responds with the following information: 1) sensor location, 2) the average signal to noise ratio of the measured phenomenon at the sensor location, and 3) the energy reserve in sensor battery. This information could be achieved in practice as follows: 1) the sensor location could be estimated by different localization methods [132]. 2) The average signal to noise ratio of the measured phenomenon could be estimated by the sensor using the distance between the sensor and the phenomenon location, prior information about the phenomenon measured, and the information of the channel state between the sensor and the phenomenon location. 3) Finally, the energy reserve could be easily estimated by the sensor from the battery charging state. The fusion center uses the sensor location, along with channel measurement techniques, to estimate the CSI for the sensor. The signal to noise ratio represents the QoI for the sensor, while the energy reserve represents the REI.

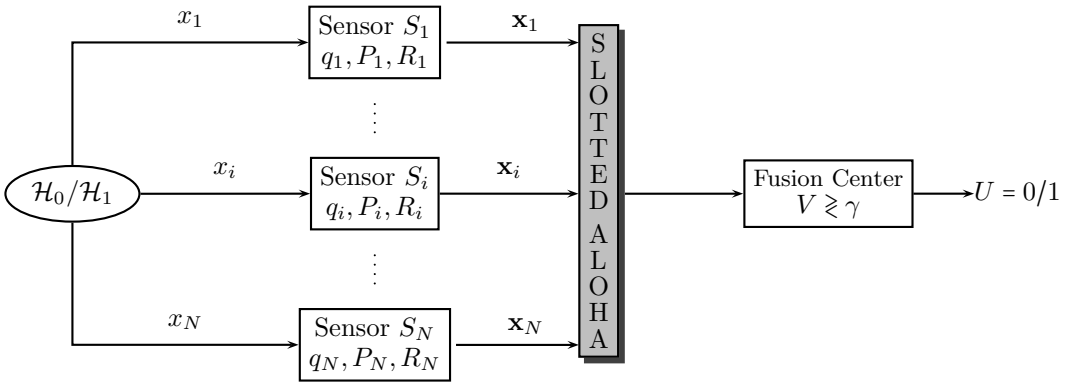

Figure 46: System model for detection in one-hop sensor networks. Sensors communicate periodically their observations to the fusion center over MAC. At the end of the detection window, the fusion center makes a global final decision regarding the true state of nature.

The fusion center uses the three quality measures to calculate the optimal transmission control policy for each sensor by solving an optimization problem. The TCP design variables are then sent back to the relevant sensors. Some sensors may not contribute to the detection process, due to either low quality of information (e.g. phenomenon is too far), low channel state (e.g. high noise or long distance to the fusion center), or not enough energy to transmit to the fusion center (e.g. not enough battery power or long distance to the fusion center combined with bad channel quality). The fusion center transmits the TCP variables only to the sensors which are specified by the optimization algorithm to be reliable to contribute to the detection task. We call this the *selectivity* property of the proposed algorithm. Each sensor keeps locally a lookup table that contains the TCP parameters for each resolution cell in the geographic area. The entries in the lookup table remain valid for the given location as long as the quality measures for each sensor did not change from the last run of the optimization algorithm.

After each sensor receives the optimal values of its TCP variables, the detection process proceeds as follows: the fusion center broadcasts a message to initiate a detection cycle at the local wireless sensors. Each local sensor samples the environment by collecting a number of observations x_i, and then forms a data packet and communicates its message directly to the fusion center over a shared wireless link using the slotted ALOHA multiaccess control scheme, and the TCP variables sent by

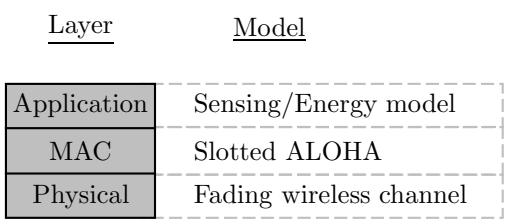

Figure 47: A layered approach to detection system modeling. The design variables are coupled through the system-wide objective function and the energy and delay constraints.

the fusion center. Finally, the fusion center makes a final decision after a fixed amount of time representing the maximum allowed delay for detection.

VI.3 System Model

The detection scheme described above suggests a layered approach to system modeling, as depicted in Figure 47. The physical layer represents the wireless channel model, and defines system parameters such as the communication bit rate and the energy consumed in communicating sensor information to the fusion center. The Media Access Control layer represents the slotted ALOHA protocol model, and defines the protocol-specific parameters such as the transmission probability. Finally, the application layer represents the sensing and energy models, and defines the model of the observations obtained by local sensors, as well as the WSN energy constraints. We seek a cross-layer design approach, where the parameters of system layers are the decision variables that need to be selected to optimize the detection performance. Since WSNs deployed for detection applications work under stringent delay and energy constraints, the parameters of different layers are cross-coupled, and therefore the independent design of each layer does not necessarily result in the optimal detection performance given the constrained resources.

VI.3.1 Wireless Channel Model

We focus on the case where the sensor nodes and the fusion center have minimal movement and the environment changes slowly. Since detection applications typically have low communication rate requirements, the coherence time of the wireless channel could be considered much larger than the

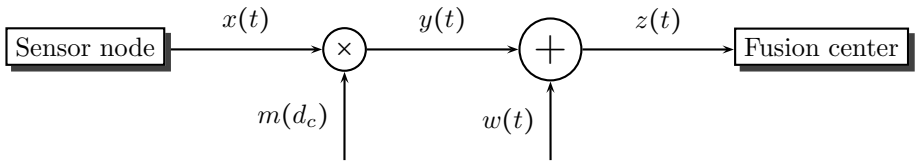

Figure 48: Block diagram for the wireless communication channel. The transmitted signal is subject to large-scale fading and additive white Gaussian noise.

transmission frame length. Accordingly, only the slow fading component of the wireless channel is considered. Figure 48 shows the fading channel model, where the output signal is expressed as:

$$z(t) = m(d_c)x(t) + w(t)$$

$w(t)$ is an additive white Gaussian noise with power spectral density $N_0/2$. The term $m(d_c)$ represents the mean path attenuation for a sensor node at a distance d_c from the fusion center, where the dependence on time t is dropped since slow fading is considered. We use the Hata path-loss model for the mean path attenuation, where the total dB power loss is given by [133]:

$$P_L = \underbrace{20\log\left(\frac{4\pi d_0}{\lambda_p}\right) + 10\rho_c \log(d_c/d_0)}_{\mu_c} + X_{\sigma_c} \qquad \text{dB} \tag{104}$$

where d_0 is a reference distance corresponding to a point located in the far field of the transmit antenna, λ_p is the wavelength of the propagating signal, ρ_c is the path loss exponent, and X_{σ_c} is a zero-mean Gaussian random variable with variance σ_c^2. The power loss (in dB) is therefore a Gaussian random variable with mean μ_c and variance σ_c^2, i.e. $P_L \sim \mathcal{N}(\mu_c, \sigma_c^2)$.

The given wireless channel represents an unreliable bit pipe for the data link layer, with instantaneous Shannon capacity given by:

$$C = W\log_2\left(1 + \frac{P_r}{N_0 W}\right) \quad \text{bps} \tag{105}$$

where W is the channel bandwidth and P_r is the signal power received by the fusion center. Using the result of Shannon coding theorem, the data link layer could achieve arbitrary communication rates R up to the channel capacity using appropriate coding schemes. Given the state of the art coding schemes that approach the Shannon capacity, we can approximately assume that the fusion center can perform error-free decoding for any transmission with bit rate $R < C$. Therefore, the channel is considered "ON" when $R < C$ and "OFF" otherwise, giving rise to the two-state channel model akin to the one presented in [89]. This condition is equivalent to:

$$P_r \underset{\text{OFF}}{\overset{\text{ON}}{\gtrless}} N_0 W \left(2^{\frac{R}{W}} - 1\right) \tag{106}$$

Using (104) and noting that $P_r = P_t 10^{-P_L/10}$, where P_t is the average signal power transmitted by the local sensor, we get:

$$P_L \underset{\text{ON}}{\overset{\text{OFF}}{\lessgtr}} 10 \log \left(\frac{P_t}{N_0 W \left(2^{\frac{R}{W}} - 1\right)} \right) \tag{107}$$

Using the result that $P_L \sim \mathcal{N}(\mu_c, \sigma_c^2)$, we get the probability of the channel being "ON" during a transmission:

$$P[\text{channel is ON}] = \lambda_c = \Phi \left[\frac{1}{\sigma_c} \left(10 \log \frac{P_t}{N_0 W (2^{\frac{R}{W}} - 1)} - \mu_c \right) \right] \tag{108}$$

where $\Phi(.)$ is the cumulative distribution function for the standard normal PDF. We note that the CSI relevant to our model is represented by the statistics σ_c, μ_c, and N_0. These statistics are required to be estimated by each sensor, and no instantaneous channel state information is required for the TCP design. Since we assume fixed nodes and a slowly varying channel, the estimation process could be run less frequently to save sensor node resources. This is particularly important in wireless sensor networks since the estimation of the channel state is both time and power consuming.

Example VI.1. Figure 49 illustrates the results in (107) and (108). The right-hand side of Figure 49 shows the channel "ON" region in the $P_L - R$ two-dimensional space, while the left-hand side

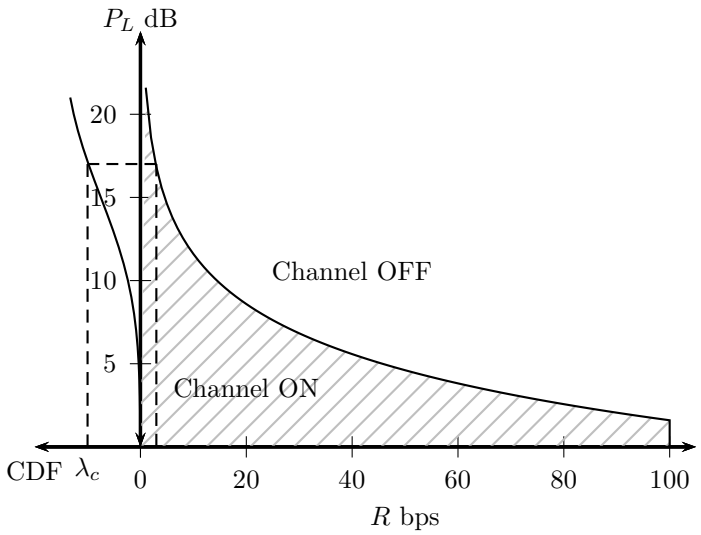

Figure 49: The wireless channel is ON for any operating point (R, P_L) in the hatched region. For any given value of R, the probability that the channel is ON is the Gaussian CDF for the corresponding P_L value on the curve separating the two regions.

shows the cumulative distribution function of P_L. The following parameters are used:

$$f = 916 \text{ MHz} \qquad d_c = 50 \text{ m} \qquad \mu_c = 65 \text{ dB} \quad \sigma_c = 5 \text{ dB}$$

$$N_0 = 10^{-10} \text{ W/Hz} \quad W = 200 \text{ KHz} \quad P_t = 1 \text{ mW}$$

■

The expression in (108) represents the probability of a successful packet transmission from the sensor node to the fusion center, provided that the local sensor node successfully gained the channel access. In Section VI.3.2, we show that this probability is further reduced due to the collisions resulting from the random access to the channel.

VI.3.2 Media Access Control Protocol Model

We assume a slotted ALOHA multiaccess communication protocol, where each packet requires one time slot for the transmission, all time slots have the same length, and all transmitters are synchronized. When it is desired to detect the phenomenon of interest, the fusion center broadcasts a message to all sensors, which triggers the detection cycle at all sensors. The detection cycle,

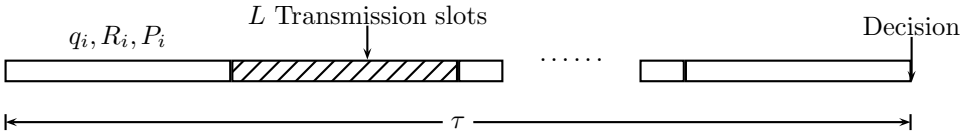

Figure 50: Detection cycle is composed of L slots, where each sensor attempts transmission with probability q_i and bit rate R_i. A final decision is taken by the fusion center at the end of the detection cycle.

demonstrated in Figure 50, has length τ, which defines the *delay for detection*, and is composed of L transmission slots, each of time τ/L. Each local sensor i collects a number of observations n_i and forms an information packet for transmission over the wireless channel. The sensor i then attempts to transmit to the fusion center with probability q_i and communication rate R_i, given by:

$$\boxed{R_i = \frac{bLn_i}{\tau}} \tag{109}$$

where b is the number of encoding bits for each observation. Sensors attempt transmission in every slot during the detection cycle, despite the state of their last transmission. The decision takes place at the end of the detection cycle, using the information received during that detection cycle. The process repeats for every detection request initiated by the fusion center. We note that in the above description for the MAC protocol, we ignored the acknowledgement slots and any protocol specifics required for synchronization or rate negotiation to simplify the analysis. Also, we ignored the packet overhead, which is a reasonable approximation for practical WSN protocols with large packet payload.

Now, we calculate the overall probability of a successful packet transmission. At any given time slot, the probability of a single packet transmission by sensor i is given by $q_i \prod_{j\neq i}(1-q_j)$. Further, this packet will be successfully received by the fusion center if the state of the physical channel between the sensor and the fusion center is "ON" during this time slot. Therefore, using (108), the total probability of a successful packet transmission by sensor i is given by:

$$P[\text{success}] = \lambda_i = q_i \prod_{j\neq i}(1-q_j)\Phi\left[\frac{1}{\sigma_c^i}\left(10\log\frac{P_t^i}{N_0 W(2^{\frac{R_i}{W}}-1)} - \mu_c^i\right)\right] \tag{110}$$

VI.3.3 Energy Model

To formulate the energy model for each sensor, we need first to define the sensor network lifetimes. Different definitions exist in the literature, and the choice of a specific definition is usually governed by the application and/or the tractability of the resulting problem formulation. In the following, we summarize the main network lifetime definitions:

1. *The time taken until the first sensor fails due to battery depletion [134].* This is a pessimistic measure, since the network may continue functioning despite the failure of one or more sensors. Nevertheless, the definition provides a worst-case analysis for the network. This could be expressed as

$$\mathcal{L} = \min(\mathcal{L}_i) \tag{111}$$

   where $\mathcal{L}_i$ is the lifetime of sensor i.

2. *The time taken until the last sensor fails due to battery depletion.* This is an optimistic measure, since the desired performance of the network may not be obtained after the failure of some sensors. It provides an upper bound on the lifetime of the sensor network. This could be expressed as

$$\mathcal{L} = \max(\mathcal{L}_i) \tag{112}$$

3. *The time taken until a fraction of sensors fail [135].* The specification of the fraction value is rather subjective. More often, the average lifetime of sensor nodes is used:

$$\mathcal{L} = \frac{1}{N} \sum_{i=1}^{N} \mathcal{L}_i \tag{113}$$

4. *The time taken until the application performance measure drops below a minimum required value.* Assuming the application performance is measured by the quantity D, and that the

minimum required value is D_0, then the network lifetime could be expressed as:

$$\mathcal{L} = \max\{t : D \geq D_0\} \tag{114}$$

This definition is more practical since it is coupled to the application in hand. However, the resulting problem formulation is generally harder to solve compared with the other lifetime definitions.

A general formula for network lifetime, which applies to any definition of the network lifetime, including the aforementioned ones, is derived in [136]. The definition holds independently of the underlying network model including network architecture and protocol, channel fading characteristics, and energy consumption model. The lifetime formula is given by:

$$\mathcal{L} = \frac{\mathcal{E}^0 - \mathcal{E}^w}{f_r \mathcal{E}^r} = \frac{\sum_{i=1}^{N} (e_i^0 - e_i^w)}{f_r \sum_{i=1}^{N} e_i^r} \tag{115}$$

where $\mathcal{E}^0 = \sum_{i=1}^{N} e_i^0$ is the total initial energy in all sensors at the time of deployment, $\mathcal{E}^w = \sum_{i=1}^{N} e_i^w$ is the total wasted energy remaining in sensor nodes when the network dies, f_r is the average sensor reporting rate defined here as the number of detection cycles per unit time, and $\mathcal{E}^r = \sum_{i=1}^{N} e_i^r$ is the expected reporting energy consumed by all sensors in one detection cycle. We slightly modify the network lifetime definition in (115) to keep the analysis tractable. We assume that the total wasted energy for each sensor is known and equal to the energy remaining in the sensor battery when it is not capable of operating its circuitry. This simplification decouples the total wasted energy from the network lifetime, which results in a linear constraint on the total reporting energy. This allows for efficient solution of the optimization problem. To get an intuition about the network lifetime definition in (115), we express the network lifetime as a function of individual sensor lifetimes:

$$\mathcal{L} = \frac{\sum_{i=1}^{N} \left(e_i^0 - e_i^w\right)}{\sum_{i=1}^{N} \frac{e_i^0 - e_i^w}{\mathcal{L}_i}} \tag{116}$$

where the individual sensor lifetime $\mathcal{L}_i = (e_i^0 - e_i^w)/f_r e_i^r$. Equation (116) is a weighted harmonic mean of the set of individual sensor lifetimes. The weights are the net energies for sensor nodes. For equal weights, the network lifetime resorts to a simple harmonic mean. Since the harmonic mean is known to tend strongly toward the least elements of a set, and hence mitigate the impact of large outliers, this definition strikes a balance between the min definition, where the network is considered dead when the first sensor fails, and the max definition, where the network expires with failure of the last sensor. Given also the nature of detection applications, where the few sensors nearby the detected object carry most of the detection information and hence the detection performance, we see that the given network lifetime definition is appropriate for the given application.

Our objective is to allocate the reporting energy e_i^r for each sensor in such a way that maximizes the detection performance. In the following, we derive the energy constraints for the sensor network.

Total Energy Constraint

In practice, it is desired to have a minimum network lifetime, where sensors can perform the assigned task, i.e. $\mathcal{L} \geq l_t$. Using (115), we get:

$$\boxed{\mathcal{E}^r \leq \frac{\mathcal{E}^0 - \mathcal{E}^w}{f_r l_t} = \frac{\sum_{i=1}^{N} (e_i^0 - e_i^w)}{f_r l_t} = \varepsilon_t} \tag{117}$$

The total energy constraint is thus expressed as:

$$\sum_{i=1}^{N} e_i^r \leq \varepsilon_t \tag{118}$$

Individual Energy Constraints

Since the network lifetime tends towards the least lifetimes of sensor nodes, it is desired to keep a minimum lifetime for each sensor. This prolongs the network lifetime, and also avoids depleting the energy reserve for high quality sensors, resulting in a quick expiry of the sensor network. In addition, depleting sensor energy may result in loss of coverage for the area under surveillance. Therefore, we

impose the following constraint on all sensor nodes:

$$\mathcal{L}_i \geq l \qquad i = 1, 2, \ldots, N \tag{119}$$

accordingly, we get:

$$\boxed{e_i^r \leq \frac{e_i^0 - e_i^w}{f_r l} = \varepsilon_i} \tag{120}$$

where we note that $l < l_t$, i.e. $\varepsilon_t < \sum_{i=1}^{N} \varepsilon_i$. Otherwise, each sensor trivially allocates its maximum energy ε_i. Obviously, the reporting energy ≥ 0, hence the individual energy constraint is summarized as:

$$0 \leq e_i^r \leq \varepsilon_i \qquad i = 1, 2, \ldots, N \tag{121}$$

Finally, we need to relate the transmission power P_t in (110) to the reporting energy e^r in each detection cycle. We note that $P_t = e^r/T$, where T is the total time the sensor is transmitting during a detection cycle. We note that the expected number of transmissions by sensor i during a detection cycle is Lq_i. Therefore, $T = (\tau/L)Lq_i = \tau/q_i$, and we get:

$$P_t = \frac{e^r}{\tau q} \tag{122}$$

The total probability of successful packet transmission is then expressed as:

$$P[\text{success}] = \lambda_i = q_i \prod_{j \neq i} (1 - q_j) \Phi \left[a_i + \left(\frac{10}{\sigma_c^i} \right) \log \frac{e_i^r}{q_i (2^{\frac{R_i}{W}} - 1)} \right] \tag{123}$$

where:

$$a_i = -\frac{1}{\sigma_c^i} \left(10 \log N_0 W \tau + \mu_c^i \right) \tag{124}$$

We note that in the above discussion, we neglected the energy consumed by each sensor to report its quality measures to the fusion center. This energy component could be included in the analysis by subtracting it from the initial sensor energy. However, for slowly-varying environments, where the sensor characteristics need to be updated less frequently, this energy component could be neglected compared to the periodic sensor reporting energy.

VI.3.4 Sensing Model

We focus our work on detection using signal amplitude measurements. Therefore, when there is an object at a specific resolution cell, the observation at sensor i, located at d_i distance from the object, could be expressed as:

$$x_i = \frac{\epsilon}{d_i^{\eta/2}} + w_i \tag{125}$$

where ϵ is the amplitude of the emitted signal at the object, η is a known attenuation coefficient, typically between 2 and 4, and w_i is an additive white Gaussian noise with zero mean and variance $\sigma_s^{i^2}$. We note that the above observation model considers passive sensing. In the active sensing case, the observation model is given by:

$$x_i = \zeta \frac{\epsilon_{tr}}{(2d_i)^{\eta/2}} + w_i \tag{126}$$

where ζ is a known reflection coefficient at the object, ϵ_{tr} is the amplitude of the signal transmitted by the active sensor (illuminating signal), and $2d_i$ is the round trip distance travelled by the signal. We note that the two observation models differ only in the scaling factor $\zeta/2^{\eta/2}$. Therefore, without loss of generality, we assume the passive sensing model in the following discussion.

The detection problem could be defined as the following binary hypothesis testing problem, for each time slot k:

$$\mathcal{H}_0 : x_i[j,k] = w_i[j,k] \qquad j = 1, 2, \ldots, n_i$$

$$\mathcal{H}_1 : x_i[j,k] = \mu^i + w_i[j,k] \qquad j = 1, 2, \ldots, n_i \tag{127}$$

where $\mu^i = \epsilon / d_i^{\eta/2}$, and n_i is the number of IID observations obtained by sensor i at each time slot. We note that noise samples are independent across sensors, i.e., the observations at local sensors are independent across time and space, but not necessarily identically distributed since some sensors may be closer to the measured phenomenon, and noise variances are assumed unequal. In the following, we designate the vector of sensor observations at time slot k by $\mathbf{x}_i[k] = \begin{bmatrix} x_i[1,k] & x_i[2,k] & \ldots & x_i[n_i,k] \end{bmatrix}$. We note that $\mathbf{x}_i[k]$ has the multivariate Gaussian distribution $\mathcal{N}(\mathbf{0}, \mathbf{C})$ under hypothesis $\mathcal{H}_0$ and $\mathcal{N}(\boldsymbol{\mu}, \mathbf{C})$ under hypothesis $\mathcal{H}_1$, where $\boldsymbol{\mu} = \begin{bmatrix} \mu^1 & \mu^2 & \ldots & \mu^N \end{bmatrix}$ and $\mathbf{C} = \sigma_s^{i^2} \boldsymbol{I}$.

Proposition 1. *The optimal test statistic at the fusion center for the slotted ALOHA system is given by:*

$$V = \sum_{k=1}^{L} \sum_{i=1}^{N} \sum_{j=1}^{n_i} \left(\frac{\mu^i}{\sigma_s^{i^2}} \right) r_i[k] x_i[j,k] \tag{128}$$

where $r_i[k]$ is a Bernoulli random process representing the success ($r_i = 1$) or failure ($r_i = 0$) of receiving a packet from sensor i in communication slot k. The sample space and probability measure of r_i are defined as $\Omega_{r_i} = \{0, 1\}$ and $P[r_i = 1] = \lambda_i$, respectively.

Proof. At the fusion center, the LLR ratio is the sum of the individual observations received at each time slot. Therefore, the test could be expressed as:

$$\sum_{k=1}^{L} \sum_{i=1}^{N} r_i[k] l(\mathbf{x}_i[k]) \underset{\mathcal{H}_0}{\overset{\mathcal{H}_1}{\gtrless}} \ln \gamma \tag{129}$$

where:

$$l(\mathbf{x}_i[k]) = \ln \frac{p_{\mathbf{x}_i}(\mathbf{x}_i[k];\mathcal{H}_1)}{p_{\mathbf{x}_i}(\mathbf{x}_i[k];\mathcal{H}_0)} = \ln \frac{\frac{1}{(2\pi)^{N/2}|\mathbf{C}|^{1/2}} \exp\left[-\frac{1}{2}(\mathbf{x}_i[k]-\mu^i\mathbf{1})^T\mathbf{C}^{-1}(\mathbf{x}_i[k]-\mu^i\mathbf{1})\right]}{\frac{1}{(2\pi)^{N/2}|\mathbf{C}|^{1/2}} \exp\left[-\frac{1}{2}\mathbf{x}_i^T[k]\mathbf{C}^{-1}\mathbf{x}_i[k]\right]}$$
$$= \frac{\mu^i}{\sigma_s^{i^2}}\mathbf{1}^T\mathbf{x}_i[k] - \frac{1}{2}\left(\frac{\mu^i}{\sigma_s^i}\right)^2\mathbf{1}^T\mathbf{1} = \frac{\mu^i}{\sigma_s^{i^2}}\sum_{j=1}^{n_i} x_i[j,k] - \frac{1}{2}n_i\left(\frac{\mu^i}{\sigma_s^i}\right)^2 \tag{130}$$

The LLR test then reduces to:

$$V = \sum_{k=1}^{L}\sum_{i=1}^{N}\sum_{j=1}^{n_i}\left(\frac{\mu^i}{\sigma_s^{i^2}}\right) r_i[k]x_i[j,k] \quad \underset{\mathcal{H}_0}{\overset{\mathcal{H}_1}{\gtrless}} \quad \frac{1}{2}\sum_{k=1}^{L}\sum_{i=1}^{N} n_i r_i[k]\left(\frac{\mu^i}{\sigma_s^i}\right)^2 + \ln\gamma$$
$$= \frac{1}{2}\sum_{i=1}^{N} z_i n_i\left(\frac{\mu^i}{\sigma_s^i}\right)^2 + \ln\gamma = \gamma\prime \tag{131}$$

where $z_i = \sum_{k=1}^{L} r_i[k]$ indicates the number of times sensor i successfully transmitted to the fusion center in L time slots. We note that the random vector $\mathbf{z} = \begin{bmatrix} z_1 & z_2 & \dots & z_N & z_e \end{bmatrix}$, where $z_e = L - \sum_{i=1}^{N} z_i$, is multinomially distributed with probability vector $\mathbf{p} = \begin{bmatrix} \lambda_1 & \lambda_2 & \dots & \lambda_N & \lambda_e \end{bmatrix}$, where the probability of collision or idle slot $\lambda_e = 1 - \sum_{i=1}^{N}\lambda_i$, and the sample space $\mathcal{Z}$ represents all possible combinations of z_i such that $z_e + \sum_{i=1}^{N} z_i = L$. ■

We adopt the deflection coefficient as a detection performance measure, defined as [10]:

$$D^2 = \frac{\left(E[V;\mathcal{H}_1] - E[V;\mathcal{H}_0]\right)^2}{\mathrm{var}[V;\mathcal{H}_0]} \tag{132}$$

which provides more tractable results in our study. The deflection coefficient is also closely related to other performance measures, e.g. Receiver Operating Characteristics (ROC) curve and the probability of error. In general, the detection performance monotonically increases with increasing the deflection coefficient.

Proposition 2. *The deflection coefficient for the detector in (128) is given by:*

$$\boxed{D^2 = L\sum_{i=1}^{N} n_i\lambda_i\left(\frac{\mu^i}{\sigma_s^i}\right)^2} \tag{133}$$

Proof. To calculate the deflection coefficient for the detector in (128), we use the fact that both $r_i[k]$ and $x_i[j,k]$ are strict-sense stationary random processes (being IID) and independent of each other. Therefore:

$$E[V;\mathcal{H}_0] = L\sum_{i=1}^{N} n_i E[r_i]E[x_i]\left(\frac{\mu^i}{\sigma_s^{i^2}}\right) = 0 \tag{134}$$

$$E[V;\mathcal{H}_1] = L\sum_{i=1}^{N} n_i \lambda_i \left(\frac{\mu^i}{\sigma_s^i}\right)^2 \tag{135}$$

$$\begin{aligned}
\mathrm{var}[V;\mathcal{H}_0] &= L\mathrm{var}\left[\sum_{i=1}^{N}\sum_{j=1}^{n_i} r_i x_i[j]\left(\frac{\mu^i}{\sigma_s^{i^2}}\right)\right] \\
&= LE\left[\left(\sum_{i=1}^{N}\sum_{j=1}^{n_i}\left(\frac{\mu^i}{\sigma_s^{i^2}}\right) r_i x_i[j]\right)^2\right] - L\left(E\left[\sum_{i=1}^{N}\sum_{j=1}^{n_i}\left(\frac{\mu^i}{\sigma_s^{i^2}}\right) r_i x_i[j]\right]\right)^2 \\
&= L\sum_{i_1=1}^{N}\sum_{i_2=1}^{N}\sum_{j_1=1}^{n_{i_1}}\sum_{j_2=1}^{n_{i_2}} E\left[\left(\frac{\mu^{i_1}\mu^{i_2}}{\sigma_s^{i_1{}^2}\sigma_s^{i_2{}^2}}\right) r_{i_1} r_{i_2} x_{i_1}[j_1] x_{i_2}[j_2]\right] - L\left(\sum_{i=1}^{N}\sum_{j=1}^{n_i}\left(\frac{\mu^i}{\sigma_s^i}\right) E\left[r_i x_i[j]\right]\right)^2
\end{aligned}$$

and noting that $E[r_{i_1} r_{i_2}] = 0$ for $i_1 \neq i_2$, and that $E[r_i^2] = \lambda_i$, we get:

$$\begin{aligned}
\mathrm{var}[V;\mathcal{H}_0] &= L\sum_{i=1}^{N}\sum_{j_1=1}^{n_{i_1}}\sum_{j_2=1}^{n_{i_2}}\left(\frac{\mu^i}{\sigma_s^{i^2}}\right)^2 \lambda_i E\left[x_i[j_1]x_i[j_2]\right] \\
&= L\sum_{i=1}^{N}\sum_{j=1}^{n_i}\left(\frac{\mu^i}{\sigma_s^{i^2}}\right)^2 \lambda_i E[x_i^2[j]] + L\sum_{i=1}^{N}\sum_{j_1=1}^{n_{i_1}}\sum_{\substack{j_2=1 \\ j_2\neq j_1}}^{n_{i_2}}\left(\frac{\mu^i}{\sigma_s^{i^2}}\right)^2 \lambda_i E[x_i[j_1]]E[x_i[j_2]] \\
&= L\sum_{i=1}^{N} n_i \lambda_i \left(\frac{\mu^i}{\sigma_s^i}\right)^2
\end{aligned} \tag{136}$$

From (134), (135), and (136), we get:

$$D^2 = L\sum_{i=1}^{N} n_i \underbrace{\left(\frac{\mu^i}{\sigma_s^i}\right)^2}_{c_i} \lambda_i \tag{137}$$

■

We note that the quantity $D_i = n_i \left(\frac{\mu^i}{\sigma_s^i}\right)^2$ represents the signal to noise ratio at sensor i, and we adopt it as a measure of the sensor Quality of Information (QoI). From (133), we note that the overall deflection coefficient at the fusion center is simply a weighted sum of the individual deflection coefficients for each sensor, where the weights are the probabilities of successful packet transmission for each sensor, and the deflection coefficient in case of a collision is set to 0.

Combining (109), (123), and (133) we obtain the objective function:

$$\boxed{D^2 = \frac{\tau}{b} \sum_{i=1}^{N} c_i R_i q_i \prod_{j \neq i} (1 - q_j) \Phi \left[a_i + \left(\frac{10}{\sigma_c^i} \right) \log \frac{e_i^r}{q_i (2^{\frac{R_i}{W}} - 1)} \right]} \tag{138}$$

The trade-off in selecting the communication rate for each sensor is reflected in (138). Increasing the communication rate R results in higher QoI while reducing the probability of successful packet transmission.

One note about the effect of the amplitude of the emitted signal at the object is in order. We note that $c_i = \epsilon^2 / \sigma_s^{i^2} d_i^{\eta}$, therefore the signal amplitude at the object to be detected appears as a scaling factor only in the objective function. This means that the signal amplitude does not affect the optimal operating point for the system. However, the amplitude does affect the detection performance, as intuitively expected. We further note that the objective function does not depend directly on L and n_i. Rather, from the optimal communication rates and (109), L and n_i could be arbitrarily chosen such that:

$$L n_i = \frac{\tau R_i}{b} \tag{139}$$

We note that for any non-zero communication rate, i.e. $R_i > 0$, $n_i \geq 1$, and consequently $L \leq \frac{\tau R_i}{b}$.

Table 11 lists the model parameters and their description. The third column classifies each parameter according to its method of calculation as either given from the application knowledge, estimated online, calculated, or as a design parameter. The fourth column highlights the parameters that are a measure of the REI, CSI, or QoI for each sensor. The last column classifies each parameter

according to its relevant layer in the system model. A complete nomenclature for the system model is shown in Table 12.

Parameter	Description	Calculation	Notes	Layer
W	Channel bandwidth	G		Physical Layer
N_0	Noise power spectral density	E	CSI	
μ_c	Mean path loss	C (104)	CSI	
σ_c^2	Path loss variance	E (channel meas.)	CSI	
e^r	**Reporting energy**	D		
R	**Communication bit rate**	D		
L	**Number of communication slots**	C (109)		MAC Layer
b	Number of encoding bits/observation	G		
q	**Retransmission probability**	D		
τ	Delay for detection	G		Application Layer
l_t	Network lifetime	G		
l	Sensor lifetime	G		
n	**Number of observations**	C (109)		
$c = (\mu/\sigma_s)^2$	Signal to noise ratio	G	QoI	
$e^0 - e^w$	Net sensor useful energy	G	REI	
f_r	Sensor reporting rate	G		

E: Estimated, G: Given, C: Calculated, D: Design

Table 11: Model Parameters for the ALOHA sensor network

VI.4 TCP Design for Optimal Detection

The optimization problem could be summarized as follows:

$$\max \quad \frac{\tau}{b}\sum_{i=1}^{N} c_i R_i q_i \prod_{j\neq i}(1-q_j)\Phi\left[a_i + \left(\frac{10}{\sigma_c^i}\right)\log\frac{e_i^r}{q_i\left(2^{\frac{R_i}{W}}-1\right)}\right] \tag{140}$$

$$\text{subject to} \quad 0 \le q_i \le 1 \tag{141}$$

$$0 \le R_i \tag{142}$$

$$0 \le e_i^r \le \varepsilon_i \qquad i = 1, 2, \ldots, N \tag{143}$$

$$\sum_{i=1}^{N} e_i^r \le \varepsilon_t \tag{144}$$

where:

$$a_i = \frac{-1}{\sigma_c^i}\left(10\log N_0 W\tau + \mu_c^i\right) \tag{145}$$

Param.	Description
λ_p	Wavelength of the propagating signal
d_c	Distance between sensor and fusion center
ρ_c	Channel path loss exponent
μ_c^i	Mean path loss for sensor i
σ_c^i	Path loss std. deviation for sensor i
W	Communication channel bandwidth
P_t^i	Transmission power for sensor i
P_r^i	Signal power received at the fusion center from sensor i
N_0	Noise power spectral density
R_i	Communication rate for sensor i
b	Number of encoding bits/observation
L	Number of transmission slots
n_i	Number of observations sampled by sensor i
τ	Delay for detection
λ_i	Successful packet transmission probability for sensor i
q_i	Retransmission probability for sensor i
$\mathcal{L}$	Sensor network lifetime
e_i^0	Initial energy in sensor i battery
e_i^w	Wasted energy remaining in sensor i battery
e_i^r	Reporting energy for sensor i
f_r	Reporting frequency for the sensor network
α	Percentage of net useful energy used in reporting
ϵ	Amplitude of emitted signal at detected object
d_i	Distance between sensor i and the object
η	Attenuation coefficient for object signal
ζ	Reflection coefficient at the object
$x_i[j,k]$	Observation number j at time slot k for sensor i
$c^i = (\mu^i/\sigma_s^i)^2$	Detected object signal to noise ratio at sensor i
V	Test statistic at the fusion center
N	Total number of wireless sensors
$r_i[k]$	Success or failure of sensor i transmission in slot k
D^2	Deflection coefficient

Table 12: Nomenclature for the ALOHA sensor network

We denote the decision variables by:

$$\boldsymbol{x} = [\ q_1 \quad q_2 \quad \dots \quad q_N \quad R_1 \quad R_2 \quad \dots \quad R_N \quad e_1^r \quad e_2^r \quad \dots \quad e_N^r\ ] \tag{146}$$

where $\boldsymbol{x} \in \boldsymbol{R}^{3N}$, and the objective function by $J(\boldsymbol{x})$. The optimization problem could be rewritten on the form:

$$\begin{aligned} \min_{\boldsymbol{x}} \quad & -J(\boldsymbol{x}) \\ \text{subject to} \quad & A\boldsymbol{x} \geq \boldsymbol{b} \end{aligned} \tag{147}$$

where

$$A = \begin{bmatrix} I & -I & \mathbf{0} & \mathbf{0} & \mathbf{0} & \mathbf{0} \\ \mathbf{0} & \mathbf{0} & I & \mathbf{0} & \mathbf{0} & \mathbf{0} \\ \mathbf{0} & \mathbf{0} & \mathbf{0} & I & -I & -\mathbf{1} \end{bmatrix}^T, \qquad \boldsymbol{b} = -\begin{bmatrix} \mathbf{0} & \mathbf{1} & \mathbf{0} & \mathbf{0} & \boldsymbol{\varepsilon} & \varepsilon_t \end{bmatrix}^T \tag{148}$$

I is the identity matrix, $\mathbf{0}(\mathbf{1})$ is the vector/matrix of all zeros (ones), with appropriate dimensions, and $\boldsymbol{\varepsilon} = \begin{bmatrix} \varepsilon_1 & \varepsilon_2 & \dots & \varepsilon_N \end{bmatrix}$. Although the objective function is not convex, we note that the inequality constraints are linear. Therefore, the Karush-Kuhn-Tucker (KKT) conditions represent a necessary condition for a local maximizer of the objective function [137]. We first form the Lagrangian:

$$L(\boldsymbol{x}, \boldsymbol{\nu}) = -J(\boldsymbol{x}) - \boldsymbol{\nu}^T (A\boldsymbol{x} - \boldsymbol{b}) \tag{149}$$

where $\boldsymbol{\nu}$ is the vector of Lagrange multipliers, defined as:

$$\boldsymbol{\nu}^T = \begin{bmatrix} \nu_{q_1^0} & \dots & \nu_{q_N^0} & \nu_{q_1^1} & \dots & \nu_{q_N^1} & \nu_{R_1} & \dots & \nu_{R_N} & \nu_{e_1^0} & \dots & \nu_{e_N^0} & \nu_{e_1} & \dots & \nu_{e_N} & \nu_{e_T} \end{bmatrix} \tag{150}$$

where $\nu_{q_i^0}$ and $\nu_{q_i^1}$ are the Lagrange multipliers for the constraints in (141), ν_{R_i} is the Lagrange multiplier for the constraint in (142), $\nu_{e_i^0}$ and ν_{e_i} are the Lagrange multipliers for the constraints in 143), and ν_{e_T} is the Lagrange multiplier for the constraint in (144). We denote the primal and dual

optimal points by $\boldsymbol{x}^*$ and $\boldsymbol{\nu}^*$, respectively. The KKT conditions are thus given by:

$$-\nabla J(\boldsymbol{x}^*) - A^T\boldsymbol{\nu}^* = \mathbf{0} \qquad \text{(Stationarity)} \tag{151}$$

$$\boldsymbol{\nu}^{*^T}(A\boldsymbol{x}^* - \boldsymbol{b}) = 0 \qquad \text{(Complementary slackness)} \tag{152}$$

$$(A\boldsymbol{x}^* - \boldsymbol{b}) \succeq \mathbf{0} \qquad \text{(Primal feasibility)} \tag{153}$$

$$\boldsymbol{\nu}^* \succeq \mathbf{0} \qquad \text{(Dual feasibility)} \tag{154}$$

$$-Z^T\nabla^2 J(\boldsymbol{x}^*)Z \succeq 0 \tag{155}$$

where Z is a null-space matrix for the matrix of active constraints at $\boldsymbol{x}^*$, and $\succeq$ represents componentwise inequality for vectors and positive-semidefiniteness for matrices. Further, the KKT conditions are sufficient for a strict local maximizer if the following condition holds:

$$-Z_+^T\nabla^2 J(\boldsymbol{x}^*)Z_+ \succ 0 \tag{156}$$

where Z_+ is a null-space matrix for the matrix of *nondegenerate* active constraints at $\boldsymbol{x}^*$, i.e. constraints with Lagrange multipliers $\neq 0$.

This optimization problem could be solved efficiently using a variety of constrained optimization algorithms, e.g. the interior-point method. However, the result may be a local maximum. To guarantee a global maximum over the function domain, we need to enumerate all possible combinations of the active and inactive constraints, which becomes infeasible for large number of sensors. However, by exploiting the problem nature, the number of combinations can be reduced considerably. The following proposition limits the number of candidate points for a local maximum.

Proposition 3. *The maximum value of the objective function in (140) occurs when:*

1. *one sensor transmits with probability one ($q = 1$) and maximum energy ($e_i^r = \varepsilon_i$), while all other sensors remain silent. The optimal communication rate is given by:*

$$R_i^* = \arg\max_{R_i} R_i\Phi\left[a_i + \left(\frac{10}{\sigma_c^i}\right)\log\frac{\min(\varepsilon,\varepsilon_t)}{\left(2^{\frac{R_i}{W}}-1\right)}\right] \tag{157}$$

2. *a subset of the sensors, defined by the index set $\mathcal{S}_\varepsilon$, transmit with their maximum energy, while all other sensors remain silent. Optimal design variables for the active sensors are at the stationary point of the objective function, i.e. at $\boldsymbol{x}^*$ where $\nabla J(\boldsymbol{x}^*) = \mathbf{0}$. The unallocated energy is equal to $\varepsilon_t - \sum_{i \in \mathcal{S}_\varepsilon} \varepsilon_i$.*

3. *a subset of the sensors, defined by the index set S_ε, transmit with their maximum energy, another subset S_1 transmit with $0 < e_i^r < \varepsilon_i$, and all other sensors remain silent. Optimal design variables for the active sensors are at the point $\boldsymbol{x}^*$, where:*

$$\nabla J_{q_i}(\boldsymbol{x}^*) = 0 \tag{158}$$

$$\nabla J_{R_i}(\boldsymbol{x}^*) = 0 \tag{159}$$

$$\nabla J_{e_i^r}(\boldsymbol{x}^*) = \nabla J_{e_j^r}(\boldsymbol{x}^*) \qquad i, j \in \mathcal{S}_1 \tag{160}$$

$$\nabla J_{e_i^r}(\boldsymbol{x}^*) \leq \min_{j \in \mathcal{S}_\varepsilon} \nabla_{e_j^r} J(\boldsymbol{x}^*)|_{e_j^r = \varepsilon_j} \qquad i \in \mathcal{S}_1 \tag{161}$$

$$\sum_{i \in \mathcal{S}_1} e_i^r = \varepsilon_t - \sum_{j \in \mathcal{S}_\varepsilon} \varepsilon_j \tag{162}$$

[this condition shows that sensors cannot be allocated less than their maximum energy if the total energy constraint is inactive, i.e. energy budget is not fully consumed.]

Design variables for the silent sensors are $q_i = R_i = e_i^r = 0$

Proof. All of the results are a direct consequence of the KKT conditions. Therefore, the complete proof could be reasoned using only the KKT conditions. However, for case 1, it is much easier to reason directly from the objective function. The stationarity condition could be expressed as:

$$\frac{\tau}{b}\left[c_i R_i \prod_{j \neq i}(1-q_j)\left(\Phi(\rho_i) - \frac{10}{\sqrt{2\pi}\sigma_c^i \ln 10}\exp(-\rho_i^2/2)\right) - \sum_{j \neq i} c_j R_j q_j \prod_{k \neq i,j}(1-q_k)\Phi(\rho_j)\right] + \nu_{q_i^0} - \nu_{q_i^1} = 0 \tag{163}$$

$$\frac{\tau}{b}\left[c_i q_i \prod_{j \neq i}(1-q_j)\left(\Phi(\rho_i) - \frac{10\ln 2}{\sqrt{2\pi}W\sigma_c^i \ln 10}\left(\frac{R_i}{1-2^{-R_i/W}}\right)\exp(-\rho_i^2/2)\right)\right] + \nu_{R_i} = 0 \tag{164}$$

$$\frac{\tau}{b}c_i R_i q_i \prod_{j\neq i}(1-q_j)\frac{10}{\sqrt{2\pi}\sigma_c^i \ln 10}\frac{\exp(-\rho_i^2/2)}{e_i^r} + \nu_{e_i^0} - \nu_{e_i^1} - \nu_{e_T} = 0 \tag{165}$$

where

$$\rho_i = a_i + \left(\frac{10}{\sigma_c^i}\right)\log\frac{e_i^r}{q_i\left(2^{\frac{R_i}{W}}-1\right)} \tag{166}$$

For silent sensors, $i \in \mathcal{S}_0$, it could be easily shown, by direct substitution, that $q_i = R_i = e_i^r = 0$ satisfies the KKT conditions. Therefore, This point is a candidate for a local maximizer. The following proof addresses the active sensors.

1. When sensor i transmits with probability one, i.e. $q_i = 1$, if $q_j \neq 0$ for any other sensor $j \neq i$, then a collision is guaranteed when sensor j attempts transmission. Therefore, the fusion center will not receive any information from sensor j. Clearly, q_j should be set to 0 $\quad \forall j \neq i$, i.e. all other sensors have to be silent. The same result could also be obtained by direct inspection of the objective function; when $q_i = 1$, the objective function reduces to:

$$D^2 = \frac{\tau}{b}c_i R_i q_i \prod_{j\neq i}(1-q_j)\Phi\left[a_i + \left(\frac{10}{\sigma_c^i}\right)\log\frac{e_i^r}{q_i\left(2^{\frac{R_i}{W}}-1\right)}\right] \tag{167}$$

   Any value of $q_j \neq 0$ will cause the objective function value to decrease. Therefore, $q_j = 0$. Since R_j and e_j^r do not affect the objective function, we arbitrarily set $R_j = 0$. e_j^r should be set to 0 to save the energy budget for the contributing sensor. The solution $q_j = R_j = e_j^r = 0$ for $j \neq i$ could be shown to satisfy the KKT conditions by direct substitution.

   From (167), the objective function monotonically increases with e_i^r. Therefore, e_i^r should be set to its maximum value, i.e. $e_i^r = \min(\varepsilon, \varepsilon_t)$. Finally, optimal R_i is set to maximize the objective function in (167):

$$R_i^* = \arg\max_{R_i} R_i \Phi\left[a_i + \left(\frac{10}{\sigma_c^i}\right)\log\frac{\min(\varepsilon,\varepsilon_t)}{\left(2^{\frac{R_i}{W}}-1\right)}\right] \tag{168}$$

We conclude that we have a set of N candidate points, $(q_i = 1, q_j = 0, j \neq i)$, for a local maximum.

2. For the active sensors, $0 < q_i < 1$. This case corresponds to the case when the total energy constraint is inactive, i.e. $\nu_{e_T} = 0$. If $e_i^r < \varepsilon_i$, then from the complementary slackness condition $\nu_{e_i^0} = \nu_{e_i^1} = 0$. From the stationarity condition we get $\nabla_{e_i^r} J = 0$, but $\nabla_{e_i^r} J = 0$ if and only if $e_i^r = 0$, a contradiction. Therefore, the only left option is $e_i^r = \varepsilon_i$. In this case, the constraint $e_i^r \leq \varepsilon_i$ is active, hence $\nu_{e_i^0} = 0$. From the stationarity condition we get $\nabla_{e_i^r} J|_{e_i^r = \varepsilon_i} = \nu_{e_i^1}$, which satisfies the dual feasibility condition, since the left hand side is ≥ 0. Therefore, this point is a candidate for a local maximizer.

   We conclude that all active sensors in this case should transmit with maximum energy. Since all other constraints are inactive, all Lagrange multipliers are $= 0$, and therefore, from the stationarity condition, the optimal values for q and R are equal to the stationary point $\boldsymbol{x}^*$ where $\nabla J(\boldsymbol{x}^*) = \mathbf{0}$.

3. In this case, the total energy budget is allocated, and therefore $\nu_{e_T} \geq 0$. From the stationarity condition, we get for $j \in \mathcal{S}_\varepsilon$, $\nabla_{e_j^r} J = \nu_{e_i^1} + \nu_{e_T}$, and since $\nu_{e_i^1} \geq 0$, we get:

$$\nu_{e_T} \leq \nabla_{e_j^r} J|_{e_j^r = \varepsilon_j} \tag{169}$$

   for sensors $i \in \mathcal{S}_1$, we have $e_i^r < \varepsilon_i$, and from the stationarity condition we get:

$$\nabla_{e_i^r} J = \nu_{e_T} \tag{170}$$

   Combining the last two equations, we get (160) and (161). Finally, since the total energy budget is allocated, the energy allocated to the sensors $\in \mathcal{S}_1$ is simply the difference between the total energy budget and the maximum energy allocated to the sensors in $\mathcal{S}_\varepsilon$, giving rise to (162).

■

We note that in Proposition 3, case 3 is the most general case. If $\mathcal{S}_1$ is empty, then this reduces to case 2. If $\mathcal{S}_1$ is empty and $|\mathcal{S}_\varepsilon| = 1$, then this reduces to case 1. Further, we note that case 1 could be checked easily in N time steps (since we have N such candidate points), in addition to the computations required to find the optimal communication rate, which could be implemented efficiently for a single variable function. Unfortunately, the number of combinations in cases 2 and 3 are prohibitively large, and grows exponentially with the number of sensors. Therefore, the proposition cannot guarantee obtaining the global maximum. However, the proposition is still useful for the following reasons: 1) it avoids the case where the optimization algorithm may terminate at the local maxima $q_i = 1, q_j = 0$, while a better local maxima maybe at one of the stationary points, and 2) it provides some information about the choice of the initial point for the optimization algorithm, where initial points near the corner points $q_i = 1, q_j = 0$ have to be avoided. The solution of the optimization problem is summarized in Algorithm 3. In the numerical example, we use the interior-point algorithm, as the optimization algorithm stated in Algorithm 3. To speed up the optimization algorithm, the gradient of the objective function is supplied, which is given by:

$$\frac{\partial J}{\partial q_i} = \frac{\tau}{b}\left[c_i R_i \prod_{j\neq i}(1-q_j)\left(\Phi(\rho_i) - \frac{10}{\sqrt{2\pi}\sigma_c^i \ln 10}\exp(-\rho_i^2/2)\right) - \sum_{j\neq i} c_j R_j q_j \prod_{k\neq i,j}(1-q_k)\Phi(\rho_j)\right] \quad (171)$$

$$\frac{\partial J}{\partial R_i} = \frac{\tau}{b}\left[c_i q_i \prod_{j\neq i}(1-q_j)\left(\Phi(\rho_i) - \frac{10\ln 2}{\sqrt{2\pi}W\sigma_c^i \ln 10}\left(\frac{R_i}{1-2^{-R_i/W}}\right)\exp(-\rho_i^2/2)\right)\right] \quad (172)$$

$$\frac{\partial J}{\partial e_i^r} = \frac{\tau}{b} c_i \frac{R_i}{e_i^r}\prod_{j\neq i}(1-q_j)\frac{10}{\sqrt{2\pi}\sigma_c^i \ln 10}\exp(-\rho_i^2/2) \quad (173)$$

VI.5 Alternative Detection Performance Measures

It is worth mentioning that other performance criteria could be used to measure the detection performance. We introduce two widely-used measures in the following.

Algorithm 3 Optimization Problem Solution

Input: system parameters as in Table 11
Output: optimal decision variables $\boldsymbol{x}^*$, objective function $J(\boldsymbol{x}^*)$
set $q_i = 1/N \quad \forall i, R_i = R_0, e_i^r = \varepsilon_t/N$ {initial point $\boldsymbol{x}_0$ for the optimization algorithm}
$\boldsymbol{x}^*, J(\boldsymbol{x}^*) = \text{OptAlg}(J(\boldsymbol{x}), \boldsymbol{x}_0, \text{constraints})$ {call optimization algorithm}
for $i = 1$ to N **do**
  set $q_i = 1, e_i^r = \varepsilon_i, R_j, e_j^r = 0 \quad \forall j \neq i$
  find $R_i^* = \arg\max_{R_i} J_i(R_i), \quad J_i(R_i) = R_i \Phi\left[a_i + \left(\frac{10}{\sigma_c^i}\right) \log \frac{\min(\varepsilon, \varepsilon_t)}{\left(2^{\frac{R_i}{W}} - 1\right)}\right]$
  calculate $J_i(\boldsymbol{x}_i), \quad \boldsymbol{x}_i = [q_i, \mathbf{0}, R_i, \mathbf{0}, e_i^r, \mathbf{0}]$
  if $J_i(\boldsymbol{x}_i) > J(\boldsymbol{x}^*)$ **then**
    $J(\boldsymbol{x}^*) = J_i(\boldsymbol{x}_i)$ {compare obj. function values}
    $\boldsymbol{x}^* = \boldsymbol{x}_i$
  end if
end for
return $\boldsymbol{x}^*, J(\boldsymbol{x}^*)$

VI.5.1 Receiver Operating Characteristics (ROC) Curve

The curve relates the probability of detection P_D to the probability of false alarm P_{FA} for different threshold values γ for the detector. The expressions for P_D and P_{FA} could be derived as follows:

$$P_D = P[V > \gamma\prime; \mathcal{H}_1] = \sum_{\mathbf{z} \epsilon \mathcal{Z}} P[V > \gamma\prime | \mathbf{z}; \mathcal{H}_1] p[\mathbf{z}] = \sum_{\mathbf{z} \epsilon \mathcal{Z}} \int_{\gamma\prime}^{\infty} p(v|\mathbf{z}; \mathcal{H}_1) p(\mathbf{z}) dv$$

We note from (128) that $v|\mathbf{z}$ is a Gaussian random variable with $\mu_{v|\mathbf{z};\mathcal{H}_0} = 0, \mu_{v|\mathbf{z};\mathcal{H}_1} = \sigma^2_{v|\mathbf{z}} = \sum_{i=1}^N z_i n_i \left(\frac{\mu^i}{\sigma_s^i}\right)^2$. Accordingly:

$$P_D = \sum_{\mathbf{z} \epsilon \mathcal{Z}} Q\left[\frac{\gamma\prime - \sum_{i=1}^N z_i n_i \left(\frac{\mu^i}{\sigma_s^i}\right)^2}{\sqrt{\sum_{i=1}^N z_i n_i \left(\frac{\mu^i}{\sigma_s^i}\right)^2}}\right] \frac{L!}{z_1! z_2! \ldots z_N! z_e!} \lambda_1^{z_1} \lambda_2^{z_2} \ldots \lambda_N^{z_N} \lambda_e^{z_e} \tag{174}$$

where $Q[.] = 1 - \Phi[.]$ is the complementary cumulative distribution function. From (131) we get:

$$P_D = \sum_{\mathbf{z} \epsilon \mathcal{Z}} Q\left[\frac{\ln \gamma - \frac{1}{2} \sum_{i=1}^N z_i n_i \left(\frac{\mu^i}{\sigma_s^i}\right)^2}{\sqrt{\sum_{i=1}^N z_i n_i \left(\frac{\mu^i}{\sigma_s^i}\right)^2}}\right] \frac{L!}{z_1! z_2! \ldots z_N! z_e!} \lambda_1^{z_1} \lambda_2^{z_2} \ldots \lambda_N^{z_N} \lambda_e^{z_e} \tag{175}$$

Similarly, the probability of false alarm is given by:

$$P_{FA} = \sum_{\mathbf{z}\epsilon\mathcal{Z}} Q\left[\frac{\ln\gamma + \frac{1}{2}\sum_{i=1}^{N} z_i n_i \left(\frac{\mu^i}{\sigma_s^i}\right)^2}{\sqrt{\sum_{i=1}^{N} z_i n_i \left(\frac{\mu^i}{\sigma_s^i}\right)^2}}\right] \frac{L!}{z_1!z_2!\ldots z_N!z_e!}\lambda_1^{z_1}\lambda_2^{z_2}\ldots\lambda_N^{z_N}\lambda_e^{z_e} \tag{176}$$

VI.5.2 Probability of Error

Defines the probability of committing an error, and given by:

$$P_e = P[\text{decide } \mathcal{H}_0, \mathcal{H}_1 \text{ true}] + P[\text{decide } \mathcal{H}_1, \mathcal{H}_0 \text{ true}] = \pi_1(1 - P_D) + \pi_0 P_{FA} \tag{177}$$

where π_0 and π_1 are the prior probabilities for $\mathcal{H}_0$ and $\mathcal{H}_1$, respectively, and the detector threshold $\gamma = \pi_0/\pi_1$. Assuming equal prior probabilities, and using the identity $Q(-x) = 1 - Q(x)$, we get from (175) and (176):

$$P_e = \sum_{\mathbf{z}\epsilon\mathcal{Z}} Q\left[\left(\frac{1}{2}\right)\sqrt{\sum_{i=1}^{N} z_i n_i \left(\frac{\mu^i}{\sigma_s^i}\right)^2}\right] \frac{L!}{z_1!z_2!z_e!\ldots z_N!}\lambda_1^{z_1}\lambda_2^{z_2}\ldots\lambda_N^{z_N}\lambda_e^{z_e} \tag{178}$$

From (175), (176), and (178), it is clear why we adopt the deflection coefficient as a detection performance measure. The number of possible combinations for the vector $\mathbf{z}$ could be calculated using the occupancy problem formulation [138], and is shown to be $\binom{N+L}{L}$. Therefore, the number of terms in (175), (176), and (178) grows exponentially with the number of sensors and/or the number of slots. In addition, the product of λ_i that appears in all the equations, which includes all system design parameters, makes the optimization very difficult. This is clearly an intractable problem that is not of a practical interest. Therefore, our choice is to optimize the deflection coefficient, which results in a more tractable problem. The design variables are then substituted back in (175), (176), and (178) to calculate P_D, P_{FA}, and P_e, respectively. The designer then could choose the desired operating point on the ROC curve, or the desired probability of error, which corresponds to a pre-calculated values for the design parameters. In this work, we resort to simulations to calculate the ROC curve and the probability of error. This is because we use a large number of sensors to

simulate practical sensor networks. With 100 sensors and 25 time slots, the number of terms in (175), (176), and (178) $\approx 1.3005 \times 10^{26}$, which is hard to evaluate even after knowing the system design parameters.

VI.6 Performance Comparison

We compare our design approach with two other design approaches commonly used to design the transmission control policy for a sensor network. We call our approach Cross Layer Design (CLD) hereafter, since it integrates the physical, MAC, and application layers. In both approaches, we assume equal energy allocation scheme, where the energy is divided equally across sensor nodes. This allocation scheme is typically used when sensor quality measures are not integrated in the design, and therefore, all sensors are treated equally. Sensor energy is thus given by:

$$e_i^r = \frac{\varepsilon_t}{N} \tag{179}$$

This allocation scheme is feasible if $\varepsilon_t/N \leq \varepsilon_i$. Otherwise, ε_i is allocated to each sensor, i.e.:

$$\boxed{e_i^r = \min(\varepsilon_t/N, \varepsilon_i)} \tag{180}$$

For the special case when all sensors have the same initial and wasted energies, i.e. $e^0 - e^w$ is the same, we have from (117) and (120):

$$\varepsilon_t = \frac{N(e^0 - e^w)}{f_r l_t} = \left(\frac{l}{l_t}\right) N\varepsilon_i \tag{181}$$

where ε_i is the same for all sensors. Since $l < l_t$, we have $\varepsilon_t/N < \varepsilon_i$, and therefore the equal energy allocation is feasible in this case. This case is the one considered in the numerical example in Section VI.7

VI.6.1 Max. Throughput Design

The throughput for the given ALOHA sensor network is given by:

$$T = \sum_{i=1}^{N} R_i q_i \prod_{j \neq i} (1 - q_j) \Phi \left[a_i + \left(\frac{10}{\sigma_c^i} \right) \log \frac{e_i^r}{q_i \left(2^{\frac{R_i}{W}} - 1 \right)} \right] \tag{182}$$

In Max. throughput designs, the design variables R_i and q_i are chosen to maximize the throughput in (182). The Max. throughput design thus does not consider the QoI for each sensor. This is clearly shown by comparing (182) to (138), where we note that the Max. throughput design is equivalent to the CLD if all sensors have the same Quality of Information.

VI.6.2 Decoupled Design

In the conventional slotted ALOHA, The MAC sublayer is designed to minimize the probability of collision, without regard to the QoI or CSI of each node. Minimum probability of collision occurs at $q_i = 1/N$. The physical layer is designed to guarantee a minimum probability of successful packet transmission, λ, i.e.:

$$\Phi \left[a_i + \left(\frac{10}{\sigma_c^i} \right) \log \frac{N e_i^r}{2^{\frac{R_i}{W}} - 1} \right] = \lambda \tag{183}$$

Accordingly, R_i is given by:

$$R_i = W \log_2 \left(1 + 10^{\left[0.1 \sigma_c^i (a_i - \Phi^{-1}[\lambda]) + \log N e^r \right]} \right) \tag{184}$$

and using (138), the deflection coefficient is given by:

$$D^2 = \frac{\tau \lambda W}{bN} \left(1 - \frac{1}{N} \right)^{N-1} \sum_{i=1}^{N} c_i \log_2 \left(1 + 10^{\left[0.1 \sigma_c^i (a_i - \Phi^{-1}[\lambda]) + \log N e^r \right]} \right) \tag{185}$$

In practice, λ is pre-determined from the application. However, to make a fair comparison, we use the value of λ that maximizes the deflection coefficient in (185), i.e.:

$$\lambda = \arg\max_{\lambda} D^2 \qquad 0 \leq \lambda \leq 1 \tag{186}$$

We note that the deflection coefficient is smaller for both small and large values of λ. For small λ values, not enough observations are transmitted, while for large values of λ, more collisions occur, hence less observations are received at the fusion center. The gradient of the objective function in (185) is given by:

$$\nabla D^2 = \frac{\tau W}{bN} \sum_{i=1}^{N} c_i \left(\log_2 \left(1 + y(\lambda)\right) - \frac{0.8327 \sigma_c^i y(\lambda) \exp([\Phi^{-1}(\lambda)]^2/2)}{1 + y(\lambda)} \right) \tag{187}$$

$$y(\lambda) = 10^{\left[0.1\sigma_c^i (a_i - \Phi^{-1}[\lambda]) + \log N\right]} \tag{188}$$

The gradient is useful to speed up the optimization algorithm that solves the optimization problem in (186).

VI.7 Simulation Results

In this section, we compare the proposed CLD approach to the classical approaches summarized in Section VI.6 via a numerical example. We assume 70 sensors ($N = 70$) deployed for detection. We cluster sensors into seven 10-sensors groups, and generate the system parameters for each group using a different uniform random number generator. In practice, each group may represent a set of sensors deployed in the same vicinity, and therefore, their system parameter values, e.g. signal to noise ratio and mean path loss, will be similar. Table 13, which replicates the structure of Table 11 for easy reference, shows the system parameter values, including the minimum and maximum values of the uniform random number generator for each group of sensors. We perform the comparison both numerically and through Monte Carlo Simulation (MCS) experiments:

- **Numerical study**. We use the interior-point algorithm with Algorithm 3 to calculate the optimal solution for the CLD in (138) and the Max. throughput design in (eq:Max-Throughput-Objective-Function), and to find the optimal probability of successful packet transmission for the decoupled design in (185).

- **Simulation study**. We use the optimal analytical solution for the design variables to set up a simulator for the wireless network. Using the appropriate random number generators, we simulate the local sensor observations, sensors collisions, and the wireless channel state. We run the MCS experiment 5000 times for each delay for detection/network lifetime value, to obtain accurate results. The output from the simulation is an estimate of the deflection coefficient, probability of error, and the system ROC curve.

Parameter	Description	Value
W	Channel bandwidth	10^3 Hz
N_0	Noise PSD	10^{-9} W/Hz
μ_c	Mean path loss	$[40,45],[45,50],[50,55],[55,60],[60,65]$ dB $[65,70],[70,75]$ dB
σ_c	Path loss std. dev.	$\left[5,8\right]$ dB
e^r	**Transmission Energy**	Design variable
R	**Comm. bit rate**	Design variable
L	**Num. of comm. slots**	$Ln_i = \tau R_i/b$
b	Number of bits/packet	16 bits
q	**Retransmission prob.**	Design variable
τ	Delay for detection	1:150 sec.
l_t	Network lifetime	100:500 days
l	Sensor lifetime	0.7*l_t
n_i	**Num. of observations**	$Ln_i = \tau R_i/b$
c	Signal to noise ratio	$[2,3.2],[2.5,3.5],[0.06,0.08],[1,1.4],[0.5,0.7]\times 10^{-3}$ $[0.12,0.16],[0.03,0.04]\times 10^{-3}$
$e^0 - e^w$	Net sensor useful energy	10^4 J
f_r	Sensor reporting rate	200 cycles/day

Table 13: Model Parameters for the numerical example, ALOHA sensor network

VI.7.1 Deflection Coefficient

Figure 51 shows the performance surface for the slotted ALOHA sensor network for the proposed CLD approach, for different delay and network lifetime values. For a fixed network lifetime, the deflection coefficient increases with the delay for detection, as more observations are expected at

the fusion center. For a fixed delay for detection, the deflection coefficient decreases with network lifetime. This is mainly because the energy budget allocated for each detection cycle decreases to prolong the network lifetime. Decreasing the energy budget reduces the probability of successful packet transmission, hence causing less observations at the fusion center.

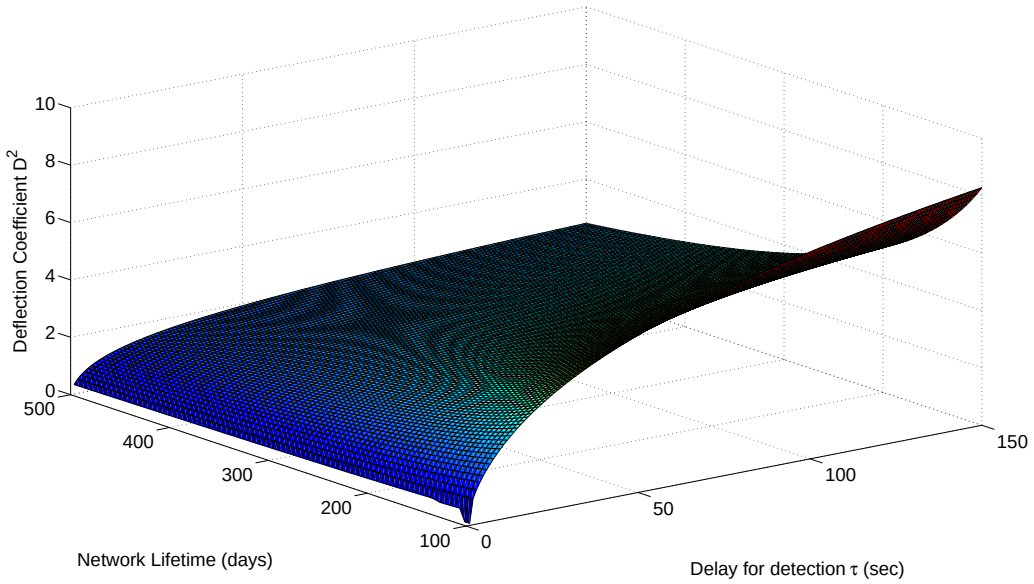

Figure 51: Deflection coefficient as it varies with the network lifetime and delay for detection for ALOHA sensor networks.

Figure 52 shows a contour plot for the deflection coefficient, where each curve corresponds to the set of pair values (Delay for detection, network lifetime) that gives rise to the indicated value of the deflection coefficient. It is shown that to keep the deflection coefficient constant while increasing the network lifetime, the delay for detection has to increase also, so that more observations could be received in each detection cycle, hence compensating for the energy decrease as a result of a prolonged network lifetime.

We resort to two dimensional plots to compare between the different design approaches. Figure 53 shows the deflection coefficient versus the delay for detection for the three design approaches, where network lifetime is set to 250 days. The decoupled design approach has the worst performance, even when choosing the optimal value for the probability of successful transmission λ. This is mainly because the parameters at each layer are specified independently, without regard to the application. The max. throughput design has a better performance since it seeks to maximize the quantity of

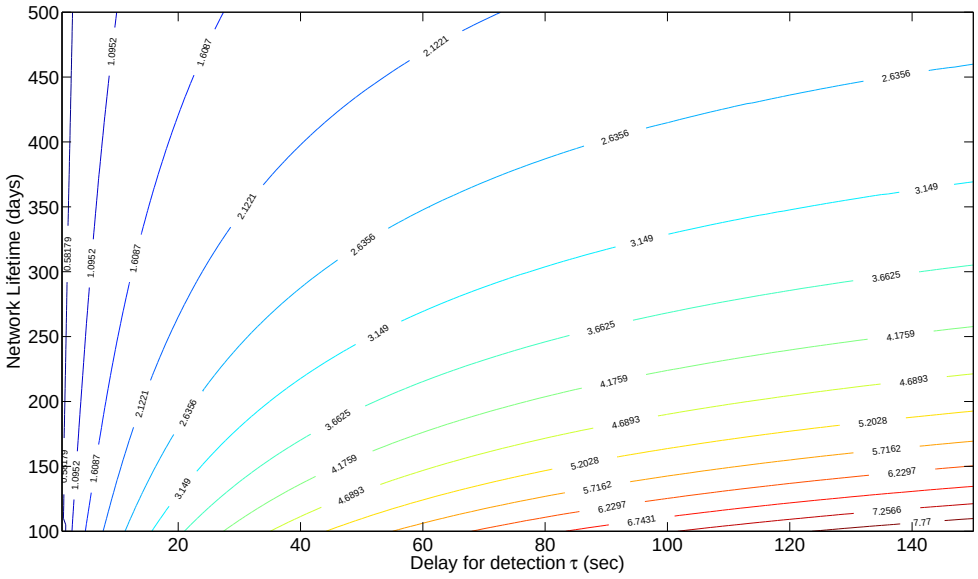

Figure 52: Contour plot for the deflection coefficient for ALOHA sensor networks. Each curve corresponds to the set of pairs (delay, lifetime) that leads to the indicated value of the deflection coefficient.

the information at the fusion center, by integrating the physical and MAC layers. However, since increasing the *quantity* of the information is not equivalent to increasing the information *quality*, as sensors have different QoI, the max. throughput is outperformed by the proposed CLD approach. The performance of the proposed design represents an upper bound on the max. throughput performance. This upper bound is achieved if all sensors have the same QoI. The MCS results are superimposed on the numerical curves. The simulated results coincide with the numerical results (apart from MCS accuracy), hence verifying the correctness of the analysis.

Figure 54 shows the deflection coefficient as it varies with the network lifetime, where delay for detection is set to 50 sec. The results are similar to the delay for detection study, where the proposed CLD approach outperforms the max. throughput and decoupled design approaches. Equivalently, for the same deflection coefficient, the network lifetime with the CLD is longer. The MCS results are superimposed on the numerically-obtained curves, verifying the correctness of the analysis.

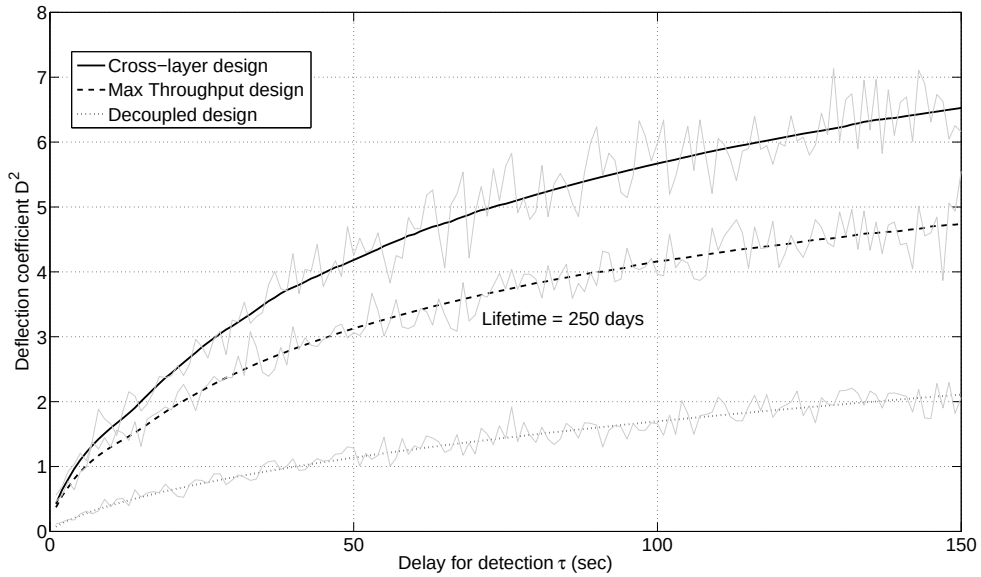

Figure 53: Deflection coefficient as it varies with the delay for detection. The CLD outperforms the decoupled and Max throughput approaches. Max. throughput is always upper-bounded by CLD.

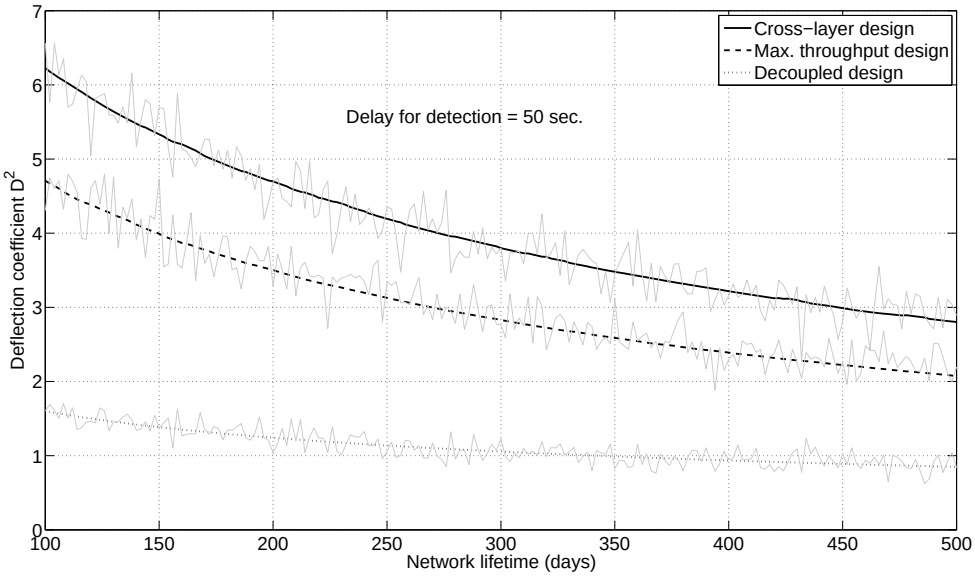

Figure 54: Deflection coefficient as it varies with the network lifetime. The CLD approach outperforms the decoupled and Max. throughput approaches. Max. throughput is always upper-bounded by the CLD for all values of the network lifetime.

VI.7.2 ROC Curves

For the probability of error and the ROC curves, we resort to MCS experiments to obtain the performance curves. Figure 55 shows the probability of error versus the delay for detection, where

network lifetime = 250 days. Since the probability of error is directly proportional to the deflection coefficient, we obtain the same relative performance, i.e. the proposed CLD approach outperforms the other two approaches while the max. throughput approach outperforms the decoupled design one. The same results are obtained for the probability of error as it varies with the network lifetime, for a fixed delay for detection, which is shown in Figure 56.

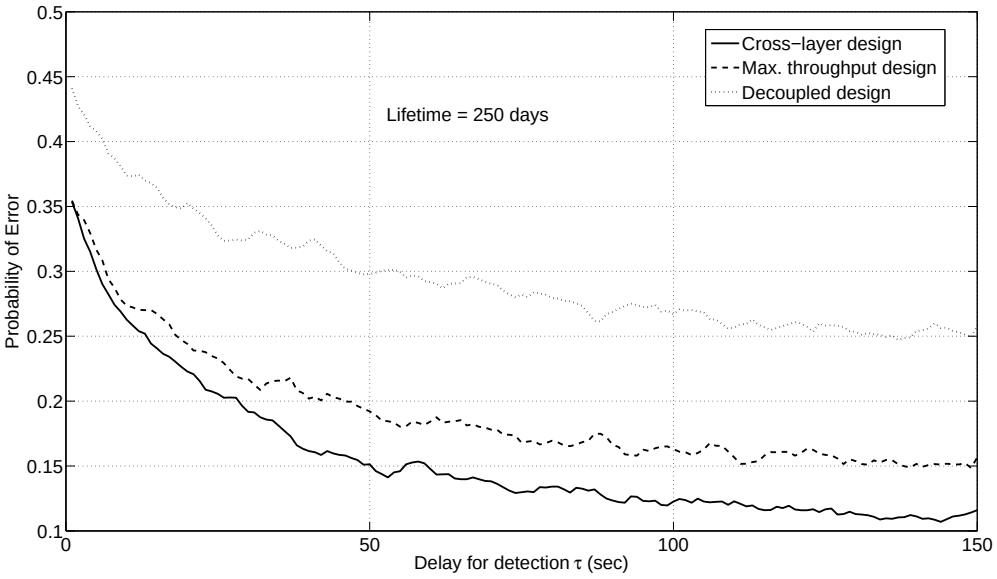

Figure 55: Probability of error for different values of the delay for detection (MCS curves smoothed out for better presentation)

Figure 57 shows the simulated ROC curve for τ = 50 seconds and lifetime = 250 days, and for different values of the threshold $\gamma \in [0, \infty)$. The figure shows the performance enhancement using the CLD approach. In practice, a family of these ROC curves are provided for different values of the delay for detection and network lifetimes. The operating point is located on a specific ROC curve, and the relevant values of the detector threshold and the WSN design variables are set accordingly.

VI.8 Summary

In this chapter, we pursued a model-based approach to design a single-hop slotted ALOHA wireless sensor network deployed for detection applications. We developed an integrated model for the detection system that includes the communication network, sensing, and energy models. We considered the QoI, CSI, and REI quality measures in the design process. We designed a complete transmission

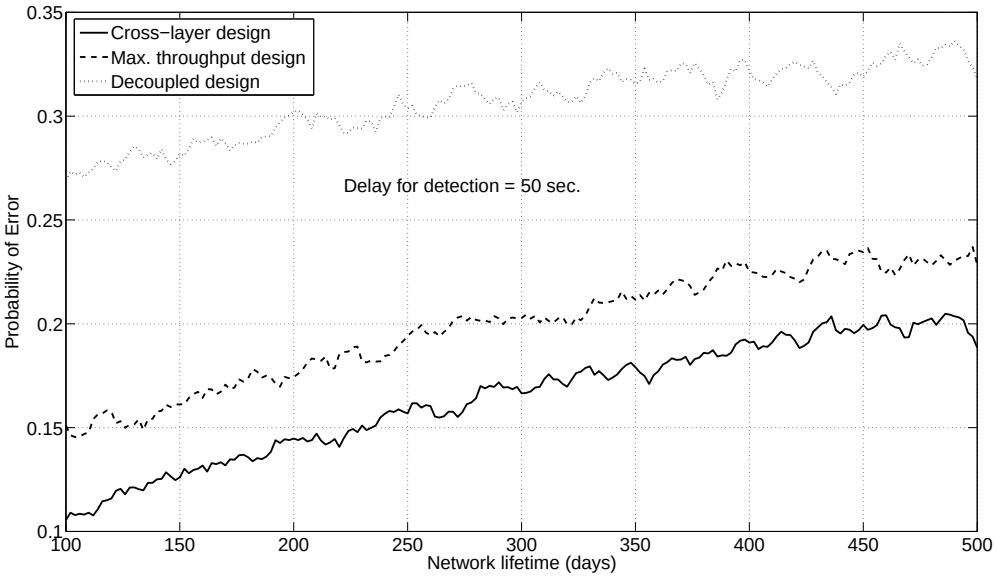

Figure 56: Probability of error for different values of the network lifetime (MCS curves smoothed out for better presentation)

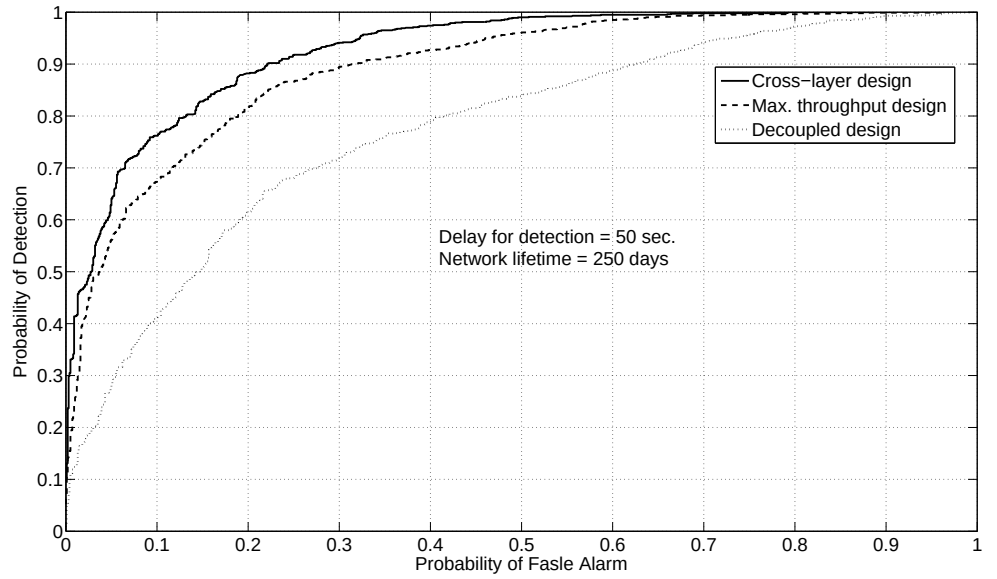

Figure 57: ROC curve for delay τ = 50 seconds and l = 250 days. Different points on each curve correspond to different threshold value for the detector.

control policy that includes the transmission probabilities, communication rate, and energy allocation for each sensor. We showed a significant performance increase over the decoupled and Max. throughput design approaches with equal energy allocation scheme.

The model-based approach results in significant performance increase. However, the resulting model is in general complex, and it maybe required to go through the design process several times to refine the assumptions in order to obtain a tractable model. This complexity is justified when the system resources are limited. The decoupled approach maybe justified for systems with large resources such that the performance loss could be compensated by more resource allocation.

In this chapter, we considered slotted ALOHA as the media access control method for the sensor network. In Chapter VII, we consider the model-based detection problem for TDMA sensor networks, where each sensor is scheduled to transmit in pre-designated time slots, hence eliminating the collision problem. We compare the slotted ALOHA and TDMA networks, and show the conditions under which each access scheme outperforms the other.

CHAPTER VII

Transmission Control Policy Design for TDMA Sensor Networks

VII.1 Introduction

In Chapter VI, we addressed the problem of TCP design for sensor networks communicating using the slotted ALOHA multi-access communication scheme. In this chapter, we study the same problem for Time Division Multiple Access sensor networks. TDMA is a multi-access scheme that eliminates collisions between sensors by scheduling the transmission of all sensors. In fixed assignment TDMA, which we consider in this chapter, transmission slots are preassigned to sensor nodes so that at each time slot only one sensor is allowed to transmit. We follow the same modeling approach in Chapter VI to design the TCP for the TDMA sensor network in order to optimize the detection performance. We also compare the proposed design with two other classical approaches to design TDMA sensor networks. We show that our design improves the detection performance over the classical design approaches, where either the network is ignored altogether, or designed to satisfy performance measures that are not relevant to the application

One important question to be answered here is whether the TDMA scheme is superior to slotted ALOHA for our detection application. On one hand, elimination of collisions results in energy saving and guaranteed transmission for sensor data (conditioned on the physical channel being in state "ON"). On the other hand, TDMA scheme treats all sensors equally, as it assigns each sensor a time slot despite its quality measures. In Section VII.7, we compare the optimal TDMA design approach to its slotted ALOHA counterpart. We show the conditions under which each transmission scheme outperforms the other.

The rest of the chapter is organized as follows: the system model is derived in Section VII.2. The solution of the formulated optimization problem to obtain the optimal TCP is given in VII.3. Section VII.4 presents the ROC and probability of error detection measures, their relationship to the deflection coefficient, and their method of calculation. Section VII.5 summarizes the decoupled

and max. throughput design approaches, to be compared to the proposed design approach. Section VII.6 provides an illustrative numerical example. Section VII.7 presents the TDMA-Slotted ALOHA comparison. The work is concluded in Section VII.8.

VII.2 System Model

We follow the same modeling approach in Chapter VI. We present the full derivation for the new results only, while showing the final result if the component being modeled is the same.

VII.2.1 Wireless Channel Model

The physical channel model is the same as in VI.3.1. The probability of the channel begin "ON" during a transmission is given by:

$$P[\text{channel is ON}] = \lambda_c = \Phi\left[\frac{1}{\sigma_c}\left(10\log\frac{P_t}{N_0 W(2^{\frac{R}{W}}-1)} - \mu_c\right)\right] \tag{189}$$

VII.2.2 Media Access Control Protocol Model

We assume a slotted multiaccess communication scheme, where each packet requires one time slot for the transmission, all time slots have the same length, and all transmitters are synchronized. Each local sensor i collects a number of observations n_i and forms an information packet for transmission over the wireless channel. The sensor transmits to the fusion center only in its dedicated time slot, assigned using the fixed assignment TDMA scheme, with communication rate R_i given by:

$$R_i = \frac{bLn_i}{\tau} \tag{190}$$

where b is the number of encoding bits for each observation. Without loss of generality, we assume that $L = mN$, where m is a positive integer, i.e. at each detection cycle, all sensors transmit the same number of times. This assumption facilitates the comparison with the slotted ALOHA scheme, since the objective function does not depend on the value of L. This is also the case for the TDMA system, as will be shown in Section VII.2.4. Finally, the decision takes place at the end of the

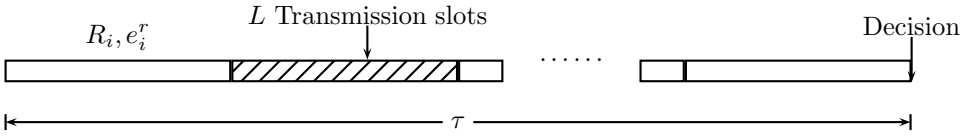

Figure 58: Detection cycle for the TDMA sensor network. The cycle is composed of L slots, where each sensor transmits in its assigned time slots only, with bit rate R_i, and power $e_i^r N/\tau$. A final decision is taken by the fusion center at the end of the detection cycle.

detection cycle, using the information received during that detection cycle. The process repeats for every detection request initiated by the fusion center.

Since collisions are eliminated in the TDMA scheme, the probability of successful packet transmission depends solely on the physical channel condition, as given by (189).

VII.2.3 Energy Model

The energy constraints are identical to Section VI.3.3. We repeat here the network lifetime definition:

$$\mathcal{L} = \frac{\mathcal{E}^0 - \mathcal{E}^w}{f_r \mathcal{E}^r} = \frac{\sum_{i=1}^{N} (e_i^0 - e_i^w)}{f_r \sum_{i=1}^{N} e_i^r} \tag{191}$$

Total Energy Constraint

The following constraint guarantees a minimum network lifetime l_t:

$$\sum_{i=1}^{N} e_i^r \leq \varepsilon_t \tag{192}$$

where

$$\boxed{\varepsilon_t = \frac{\sum_{i=1}^{N} e_i^0 - e_i^w}{f_r l_t}} \tag{193}$$

Individual Energy Constraint

The following constraint guarantees a minimum sensor lifetime l:

$$0 \leq e_i^r \leq \varepsilon_i \tag{194}$$

where

$$\boxed{\varepsilon_i = \frac{e_i^0 - e_i^w}{f_r l}} \tag{195}$$

Finally, we need to relate the transmission power P_t to the reporting energy e^r in each detection cycle. We note that $P_t = e^r/T$, where T is the total time the sensor is transmitting during a detection cycle. Since we assume $L = mN$, each sensor transmits m times. Given time slot length of τ/L, we get:

$$P_t = \frac{N}{\tau} e^r \tag{196}$$

VII.2.4 Sensing Model

Assuming signal amplitude sensors, as in Section VI.3.4, we get the following test statistic and deflection coefficient:

Proposition 4. *The optimal test statistic at the fusion center for the TDMA system is given by:*

$$V = \sum_{k=1}^{m} \sum_{i=1}^{N} \sum_{j=1}^{n_i} \left(\frac{\mu^i}{\sigma_s^{i^2}} \right) r_i[k] x_i[j,k] \tag{197}$$

where $r_i[k]$ is a Bernoulli random process representing the success ($r_i = 1$) or failure ($r_i = 0$) of receiving a packet from sensor i in communication slot k. The sample space and probability measure of r_i are defined as $\Omega_{r_i} = \{0, 1\}$ and $P[r_i = 1] = \lambda_i$, respectively.

Proof. The proof is the same as in Proposition 1, except that L is replaced by m, since each sensor transmits in its m designated time slots only. ■

Proposition 5. *The deflection coefficient for the detector in (197) is given by:*

$$D^2 = m \sum_{i=1}^{N} n_i \underbrace{\lambda_i \left(\frac{\mu^i}{\sigma_s^i} \right)^2}_{c_i} \tag{198}$$

where λ_i is given by (189), and system parameter definition is as in Table 12.

Proof. The proof follows the one for Proposition 2, with L replaced by m. ■

VII.3 TCP Design for Optimal Detection

Using (189), (190), (196), and (198), the complete optimization problem could be expressed as:

$$\max \quad \frac{\tau}{bN} \sum_{i=1}^{N} c_i R_i \Phi \left[a_i + \left(\frac{10}{\sigma_c^i} \right) \log \frac{e_i^r}{2^{\frac{R_i}{W}} - 1} \right] \tag{199}$$

$$\text{subject to} \quad 0 \le R_i \tag{200}$$

$$0 \le e_i^r \le \varepsilon_i \qquad i = 1, 2, \ldots, N \tag{201}$$

$$\sum_{i=1}^{N} e_i^r \le \varepsilon_t \tag{202}$$

where:

$$a_i = \frac{1}{\sigma_c^i} \left(10 \log \frac{N}{N_0 W \tau} - \mu_c^i \right) \tag{203}$$

We denote the decision variables by:

$$\boldsymbol{x} = [\ R_1 \quad R_2 \quad \ldots \quad R_N \quad e_1^r \quad e_2^r \quad \ldots \quad e_N^r\ ] \tag{204}$$

where $\boldsymbol{x} \in \boldsymbol{R}^{2N}$, and the objective function by $J(\boldsymbol{x})$. The optimization problem could be rewritten on the form:

$$\begin{aligned} \min_{\boldsymbol{x}} \quad & -J(\boldsymbol{x}) \\ \text{subject to} \quad & A\boldsymbol{x} \geq \boldsymbol{b} \end{aligned} \tag{205}$$

where

$$A = \begin{bmatrix} I & \mathbf{0} & \mathbf{0} & \mathbf{0} \\ \mathbf{0} & I & -I & -\mathbf{1} \end{bmatrix}^T, \qquad \boldsymbol{b} = -\begin{bmatrix} \mathbf{0} & \mathbf{0} & \boldsymbol{\varepsilon} & \varepsilon_t \end{bmatrix}^T \tag{206}$$

I is the identity matrix, $\mathbf{0}(\mathbf{1})$ is the vector/matrix of all zeros (ones), with appropriate dimensions, and $\boldsymbol{\varepsilon} = \begin{bmatrix} \varepsilon_1 & \varepsilon_2 & \dots & \varepsilon_N \end{bmatrix}$. This optimization problem also has linear constraints. Therefore, the KKT conditions still provide a necessary condition for a local maximizer of the objective function. We define the vector of Lagrange multipliers in this case as:

$$\boldsymbol{\nu}^T = \begin{bmatrix} \nu_{R_1} & \dots & \nu_{R_N} & \nu_{e_1^0} & \dots & \nu_{e_N^0} & \nu_{e_1} & \dots & \nu_{e_N} & \nu_{e_T} \end{bmatrix} \tag{207}$$

where ν_{R_i} is the Lagrange multiplier for the constraint in (200), $\nu_{e_i^0}$ and ν_{e_i} are the Lagrange multiplier for the constraint in (201), and ν_{e_T} is the Lagrange multiplier for the constraint in (202). We denote the primal and dual optimal points by $\boldsymbol{x}^*$ and $\boldsymbol{\nu}^*$, respectively. The KKT conditions are thus given by the same equations in (155).

This optimization problem could be solved efficiently using a variety of constrained optimization algorithms, e.g. gradient-based algorithms. In the comparative study, we solve it using the interior-point method. To speed up the optimization algorithm, the gradient of the objective function is supplied, which is given by:

$$\nabla J_{R_i} = \frac{\tau c_i}{bN}\left[(\Phi(\rho_i) - \frac{10\ln 2}{\sqrt{2\pi}W\sigma_c^i \ln 10}\left(\frac{R_i}{1-2^{-R_i/W}}\right)\exp(-\rho_i^2/2)\right] \tag{208}$$

$$\nabla J_{e_i} = \frac{\tau c_i}{bN}\frac{10}{\sqrt{2\pi}\sigma_c^i \ln 10}\left(\frac{R_i}{e_i^r}\right)\exp(-\rho_i^2/2) \tag{209}$$

VII.4 Alternative Detection Performance Measures

VII.4.1 ROC Curve

Each sensor is allowed to send exactly m times, with success probability λ. Therefore, the probability of getting z_i out of m successes is binomially distributed. The probability of detection is hence given by:

$$P_D = \sum_{\mathbf{z}\in\mathcal{Z}} Q\left[\left(\frac{1}{2}\right)\frac{\ln\gamma - \sum_{i=1}^N z_i n_i\left(\frac{\mu^i}{\sigma_s^i}\right)^2}{\sqrt{\sum_{i=1}^N z_i n_i\left(\frac{\mu^i}{\sigma_s^i}\right)^2}}\right]\binom{m}{z_1}\binom{m}{z_2}\ldots\binom{m}{z_N}\lambda^{\sum_{i=1}^N z_i}(1-\lambda)^{L-\sum_{i=1}^N z_i} \tag{210}$$

where $z_i \in \{0,1,\ldots,m\}$ and $\mathcal{Z} = \{0,1,\ldots,m\}^N$. Similarly:

$$P_{FA} = \sum_{\mathbf{z}\in\mathcal{Z}} Q\left[\left(\frac{1}{2}\right)\frac{\ln\gamma + \sum_{i=1}^N z_i n_i\left(\frac{\mu^i}{\sigma_s^i}\right)^2}{\sqrt{\sum_{i=1}^N z_i n_i\left(\frac{\mu^i}{\sigma_s^i}\right)^2}}\right]\binom{m}{z_1}\binom{m}{z_2}\ldots\binom{m}{z_N}\lambda^{\sum_{i=1}^N z_i}(1-\lambda)^{L-\sum_{i=1}^N z_i} \tag{211}$$

VII.4.2 Probability of Error

Assuming equal prior probabilities, we get from (210) and (211):

$$P_e = \sum_{\mathbf{z}\in\mathcal{Z}} Q\left[\left(\frac{1}{2}\right)\sqrt{\sum_{i=1}^N z_i n_i\left(\frac{\mu^i}{\sigma_s^i}\right)^2}\right]\binom{m}{z_1}\binom{m}{z_2}\ldots\binom{m}{z_N}\lambda^{\sum_{i=1}^N z_i}(1-\lambda)^{L-\sum_{i=1}^N z_i} \tag{212}$$

Similar to the slotted ALOHA sensor network, we resort to MCS to evaluate the ROC curve and the probability of error. This is mainly because we use a large number of sensors and the number of terms in each expression grow exponentially with the network size.

VII.5 Performance Comparison

Similar to the slotted ALOHA sensor network, we compare our design approach with two other design approaches commonly used to design the transmission control policy for a sensor network. We still call our approach the Cross Layer Design, since it integrates the physical, MAC, and application layers. In both approaches, we assume equal energy allocation scheme, where the energy is divided equally across sensor nodes. This allocation scheme is typically used when sensor quality measures are not integrated in the design, and therefore, all sensors are treated equally. Sensor energy is thus given by:

$$e_i^r = \frac{\varepsilon_t}{N} \tag{213}$$

VII.5.1 Max. Throughput Design

The throughput for the given TDMA sensor network is given by:

$$T = \sum_{i=1}^{N} R_i \lambda_i = \sum_{i=1}^{N} R_i \Phi \left[a_i + \left(\frac{10}{\sigma_c^i} \right) \log \frac{e_i^r}{2^{\frac{R_i}{W}} - 1} \right] \tag{214}$$

In Max. throughput designs, the design variables R_i are chosen to maximize the throughput in (214). The Max. throughput design thus does not consider the QoI for each sensor. This is clearly shown by comparing (214) to (199), where we note that the Max. throughput design is equivalent to the CLD if all sensors have the same Quality of Information.

VII.5.2 Decoupled Design

In this design approach, the communication rate for each sensor is typically determined to guarantee a minimum probability of successful packet transmission λ, i.e.:

$$\Phi \left[a_i + \left(\frac{10}{\sigma_c^i} \right) \log \frac{e_i^r}{2^{\frac{R_i}{W}} - 1} \right] = \lambda \tag{215}$$

Accordingly, R_i is given by:

$$R_i = W \log_2 \left(1 + 10^{\left[0.1\sigma_c^i (a_i - \Phi^{-1}[\lambda]) + \log e^r\right]}\right) \tag{216}$$

and using (199), the deflection coefficient is given by:

$$D^2 = \frac{\tau W \lambda}{bN} \sum_{i=1}^{N} c_i \log_2 \left(1 + 10^{\left[0.1\sigma_c^i (a_i - \Phi^{-1}[\lambda]) + \log e^r\right]}\right) \tag{217}$$

In practice, λ is pre-determined from the application. However, to make a fair comparison, we use the value of λ that maximizes the deflection coefficient in (217), i.e.:

$$\lambda = \arg\max_{\lambda} \sum_{i=1}^{N} \lambda c_i \log_2 \left(1 + 10^{\left[0.1\sigma_c^i (a_i - \Phi^{-1}[\lambda]) + \log e^r\right]}\right) \tag{218}$$

VII.6 Simulation Results

In this section, we compare the proposed CLD approach to the two design approaches summarized in Section VII.5. We assume the same example network as in Chapter VI for comparison purposes. Table 14 repeats the system parameter values for the given example. We perform the comparison both numerically and through MCS experiments. The numerical results are obtained using the interior point method, and the optimal design variables are used in the MCS experiment. We run MCS 1000 times for each pair of the delay for detection and network lifetime values.

VII.6.1 Deflection Coefficient

Figure 59 shows the performance surface for the TDMA sensor network for the CLD approach, for different delay for detection and network lifetime values. The deflection coefficient increases with increasing the delay for detection. This is because increasing the delay allows for more observations to be received at the fusion center. However, because the energy budget is limited, increasing the delay beyond a certain limit does not lead to performance increase, as the energy has to be distributed over transmission slots, hence less energy is allocated for each slot and the probability

Parameter	Description	Value
W	Channel bandwidth	10^3 Hz
N_0	Noise PSD	10^{-9} W/Hz
μ_c	Mean path loss	$[40,45],[45,50],[50,55],[55,60],[60,65]$ dB $[65,70],[70,75]$ dB
σ_c	Path loss std. dev.	$\big[5,8\big]$ dB
e^r	**Transmission Energy**	Design variable
R	**Comm. bit rate**	Design variable
L	**Num. of comm. slots**	$Ln_i = \tau R_i/b$
b	Number of bits/packet	16 bits
τ	Delay for detection	1:100 sec.
l_t	Network lifetime	100:400 days
l	Sensor lifetime	$0.7l_t$
n_i	**Num. of observations**	$Ln_i = \tau R_i/b$
c	Signal to noise ratio	$[2,3.2],[2.5,3.5],[0.06,0.08],[1,1.4],[0.5,0.7]\times10^{-3}$ $[0.12,0.16],[0.03,0.04]\times10^{-3}$
$e^0 - e^w$	Net useful energy	10^4 J
f_r	Sensor reporting rate	200 cycles/day

Table 14: Model Parameters for the numerical example, TDMA sensor network

of successful packet transmission decreases. For the same reason, increasing the network lifetime leads to degraded performance, as less energy is allocated for each detection cycle to preserve energy and prolong the network lifetime. The drop in the deflection coefficient at around 60 sec. delay and 100 days network lifetime is due to local convergence of the optimization algorithm. This point represents a local maximum, and a point with larger deflection coefficient could be obtained by varying the initial point of the optimization algorithm.

Figure 60 shows a contour plot for the deflection coefficient, where each curve corresponds to the set of pair values (Delay for detection, network lifetime) that gives rise to the indicated value of the deflection coefficient. It is shown that to keep the deflection coefficient constant while decreasing the delay for detection, the network lifetime has to decrease also, so that more energy could be allocated for each detection cycle, hence compensating for decreasing the detection cycle length.

To compare between the different design approaches, we resort to two dimensional plots for clarity. Figure 61 shows the deflection coefficient versus the delay for detection for the three design approaches, where network lifetime = 250 days. The decoupled design approach shows the worst performance as it does not integrate any quality measure into the design process. The max. throughput approach integrates the physical channel layer and the MAC sublayer into the design.

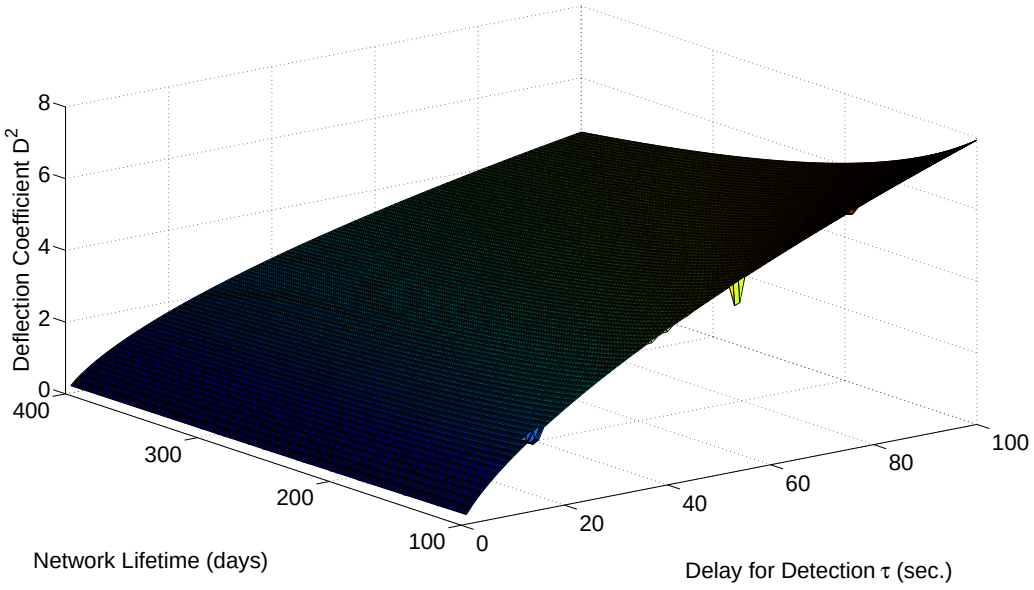

Figure 59: Deflection coefficient as it varies with the network lifetime and delay for detection for TDMA sensor networks.

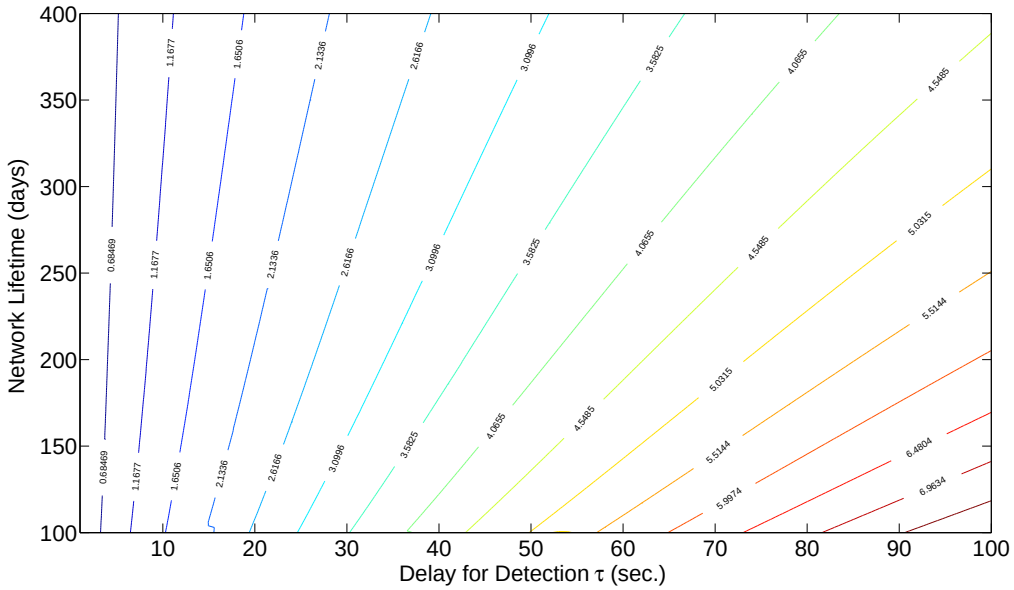

Figure 60: Contour plot for the deflection coefficient for TDMA sensor networks. Each curve corresponds to the set of pairs (delay, lifetime) that leads to the indicated value of the deflection coefficient.

Therefore, it outperforms the decoupled approach. However, since the max. throughput approach ignores the quality of information for each sensor, it shows degraded performance compared to the proposed approach. The cross layer approach outperforms the two other approaches since it integrates the QoI, REI, and CSI into the design process. The CLD represents an upper bound on the

max. throughput approach that is reached only when all sensors have the same QoI. Figure 61 also shows the MCS results for the cross layer approach, superimposed on the curve obtained from the numerical results. Apart from MCS accuracy, the simulated deflection coefficient coincides with the numerical results, verifying the correctness of the analysis. We omit the MCS curves for the other design approaches to avoid cluttering the figure.

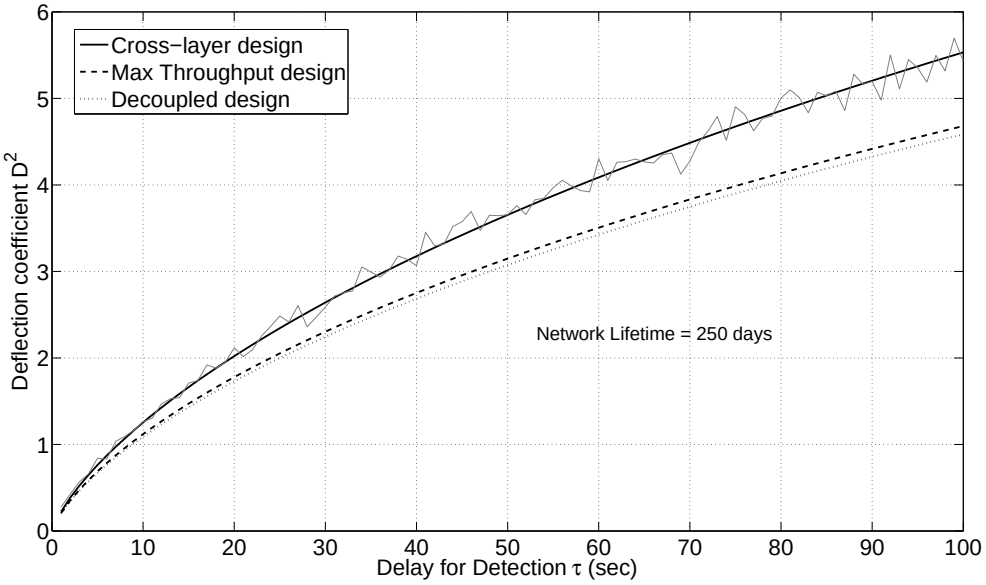

Figure 61: Deflection coefficient for TDMA sensor networks, as it varies with the delay for detection, for fixed network lifetime.

Figure 62 shows the deflection coefficient versus the network lifetime for the three design approaches, where delay for detection = 50 sec. Similarly, the proposed CLD approach outperforms the two other approaches considerably, due to the integration of different system layers and the inclusion of different quality measures into the design process.

VII.6.2 ROC Curves

Similar to the slotted ALOHA sensor network, obtaining the ROC and probability of error curves numerically is intractable. Therefore, we resort to MCS experiments to obtain the performance curves. Figure 63 shows the probability of error versus the delay for detection for lifetime = 250 days. Since probability of error and deflection coefficient are inversely proportional, the probability of error decreases with increasing the delay. Similar to the deflection coefficient, the cross-layer

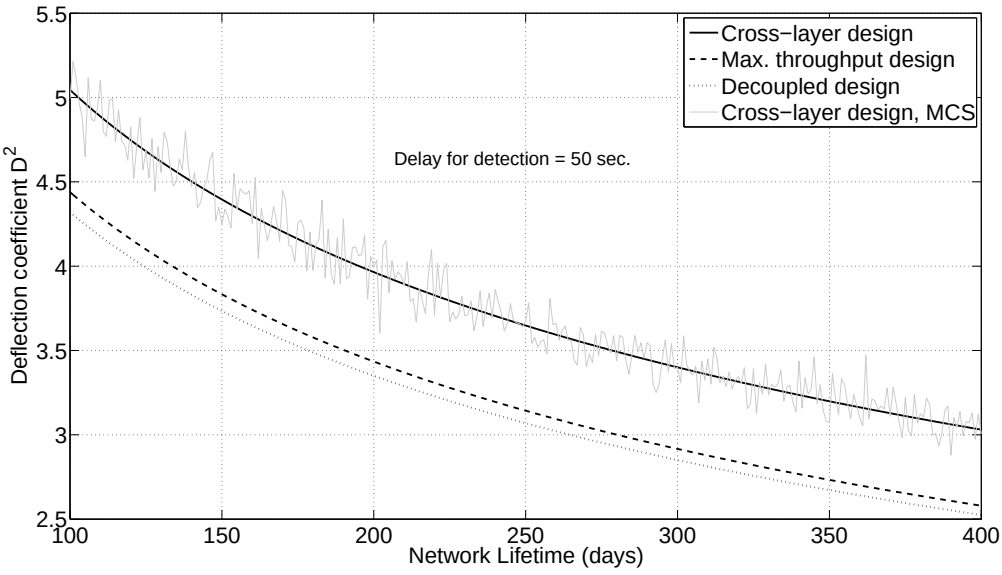

Figure 62: Deflection coefficient for TDMA sensor networks, as it varies with the network lifetime, for fixed delay for detection.

approach outperforms the other two approaches. The difference between the decoupled design and the max throughput designs is not noticed in the figure due to MCS accuracy. Figure 64 shows the probability of error versus the network lifetime when delay = 50 sec. As the network lifetime increases, less energy is allocated to each detection cycle, resulting in higher probability of error. The figure also shows the superiority of the proposed cross layer design.

Figure 65 shows the ROC curve for lifetime = 250 days and delay = 50 sec. Different values on each ROC curve correspond to different threshold values for the detector. For the same probability of false alarm, the proposed cross layer approach results in higher probability of detection than the other approaches. Therefore, by integrating different system layers and quality measures in the design process, we obtain performance enhancement that would not be possible without increasing the delay and/or shortening the network lifetime. Figure 66 shows a log plot for the ROC curve for the typical region of interest for the false alarm probability, $P_F \in [0.01, 0.1]$.

VII.7 Slotted ALOHA-TDMA Comparison

In this section, we compare the performance of the slotted ALOHA and TDMA sensor networks, based on the numerical example in Sections VI.7 and VII.6. Figure 67 shows the deflection coefficient

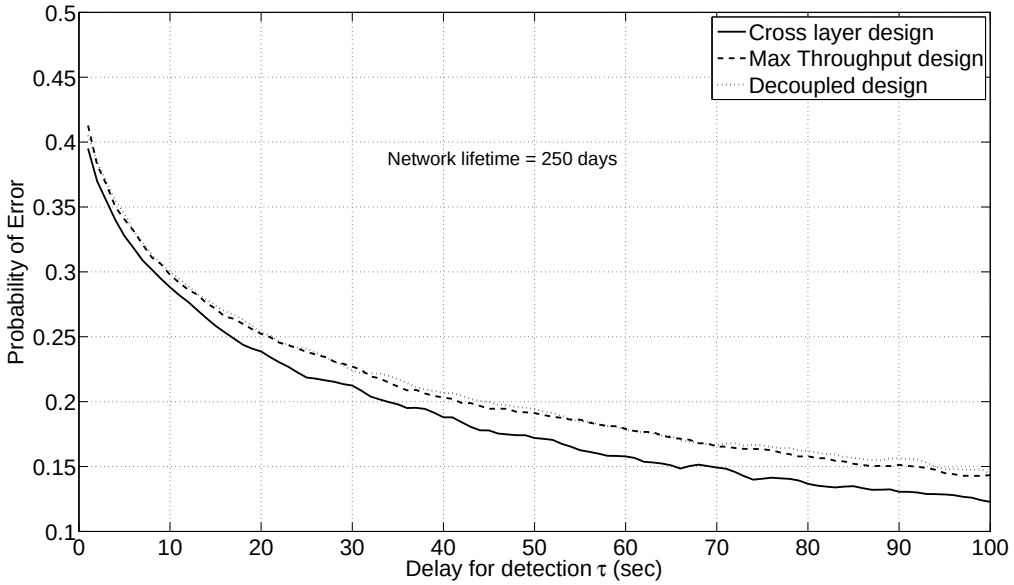

Figure 63: Probability of error for different values of the delay for detection (MCS curves smoothed out for better presentation)

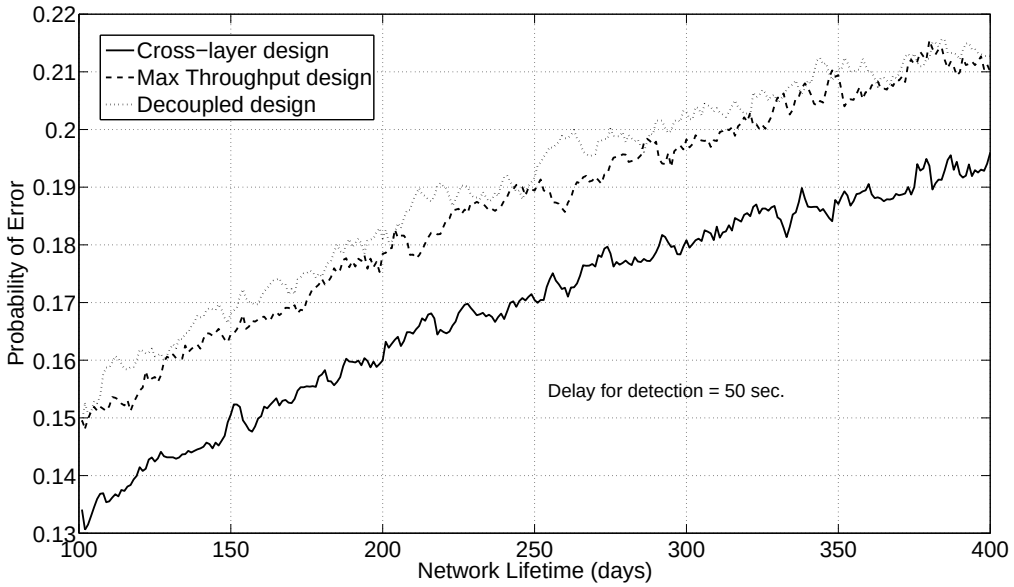

Figure 64: Probability of error for different values of the network lifetime (MCS curves smoothed out for better presentation)

for different delay constraints. We note that the ALOHA network outperforms TDMA if the delay is below a threshold value, τ_{th}. If the delay is increased further, TDMA outperforms the ALOHA network. For $\tau < \tau_{\text{th}}$, the ALOHA network outperforms because of its *selectivity* property, where sensors with relatively lower quality measures compared to other sensors are excluded from the

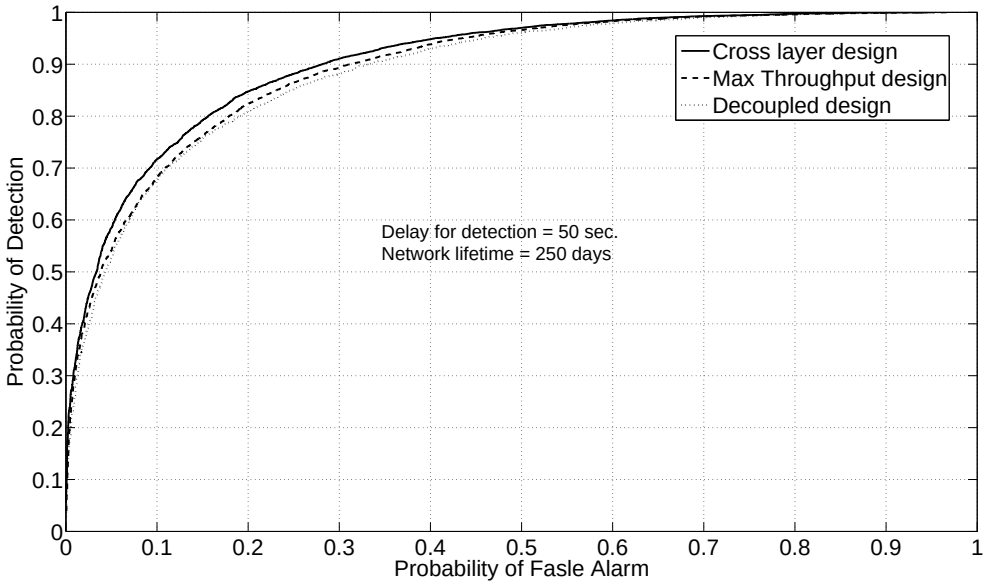

Figure 65: ROC curve for lifetime = 250 days and delay=50 sec. Different points on each curve correspond to different threshold values for the detector.

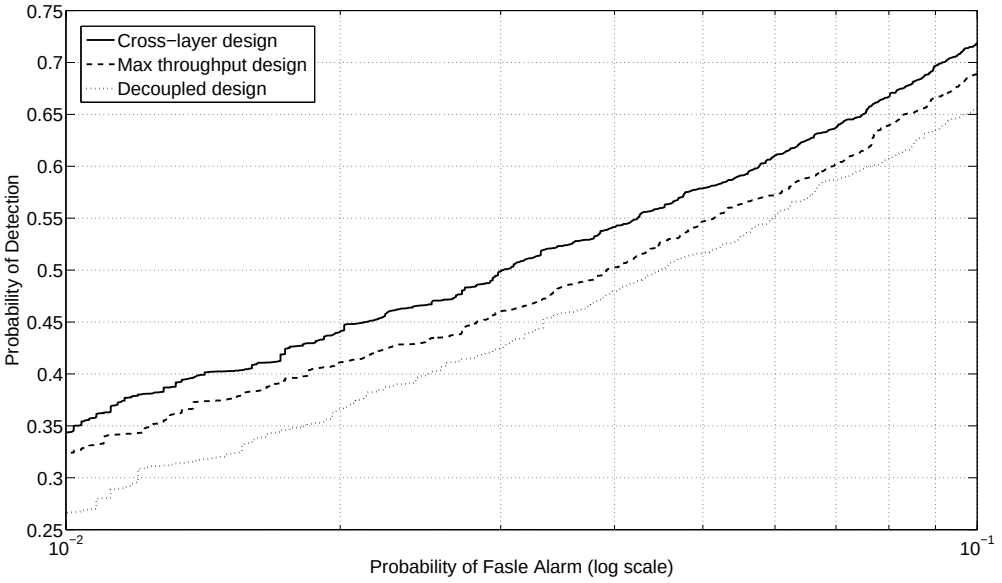

Figure 66: ROC curve for lifetime = 250 days and delay=50 sec. The region of interest is $P_F \in [0.01, 0.1]$

detection task. This *selectivity* property is lacking in the TDMA network, where all sensors are treated equally and scheduled to transmit their observations, regardless of their quality measures. For $\tau > \tau_{\text{th}}$, TDMA outperforms ALOHA, mainly because the average energy per detection cycle (average power) decreases with increasing the delay. Therefore, transmission attempts for each

sensor for the ALOHA network have to be lowered to conserve energy wasted in probable collisions. On the other hand, TDMA does not suffer from collisions. Therefore, even with very small energy per detection cycle, sensors may be able to transfer their information to the fusion center, and therefore, the detection performance will be higher. In general, the delay threshold τ_{th} gets higher as the reporting energy per detection cycle for each sensor, e^r, increases. For the given example, the delay threshold $\tau_{\text{th}} \approx 120$ sec. Since detection applications are delay-sensitive, the ALOHA network would be the choice for network design. However, for scarce energy applications, with very low energy per sensor, TDMA maybe a viable alternative.

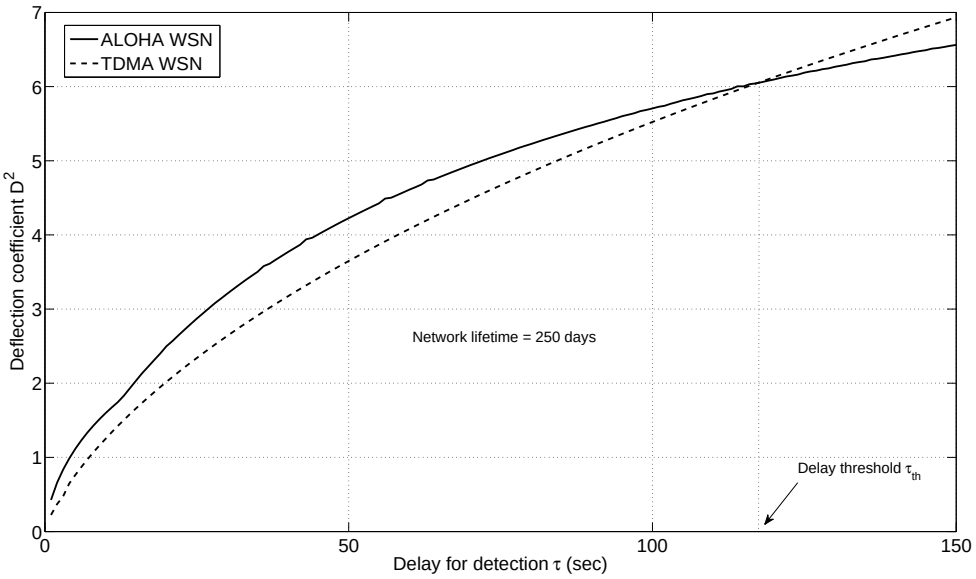

Figure 67: ALOHA-TDMA Comparison for different delay constraints. TDMA outperforms the ALOHA network for delays greater than the delay threshold

Figure 68 shows the deflection coefficient for different lifetime values. Similarly, the TDMA outperforms the ALOHA for lifetime values greater than the threshold lifetime $\mathcal{L}_{th}$. The threshold lifetime gets higher as the delay for detection decreases. For the given numerical example, the threshold lifetime $\mathcal{L}_{th} \approx 285$ days. Since the performance degrades with increasing network lifetime, the deflection coefficient at the threshold lifetime may be below the minimum design value, and therefore, TDMA may not be a feasible design option. For example, in Figure 68, the minimum detection performance is specified by $D^2 = 6$, and therefore, the ALOHA is the design option. At the threshold lifetime, $D^2 \approx 5.2$, which is below the minimum design requirement, and therefore,

TDMA cannot be used with such design requirements. However, for scarce energy applications, the threshold lifetime gets smaller, so that TDMA maybe the only viable design option to extend the network lifetime, on the expense of degraded detection performance.

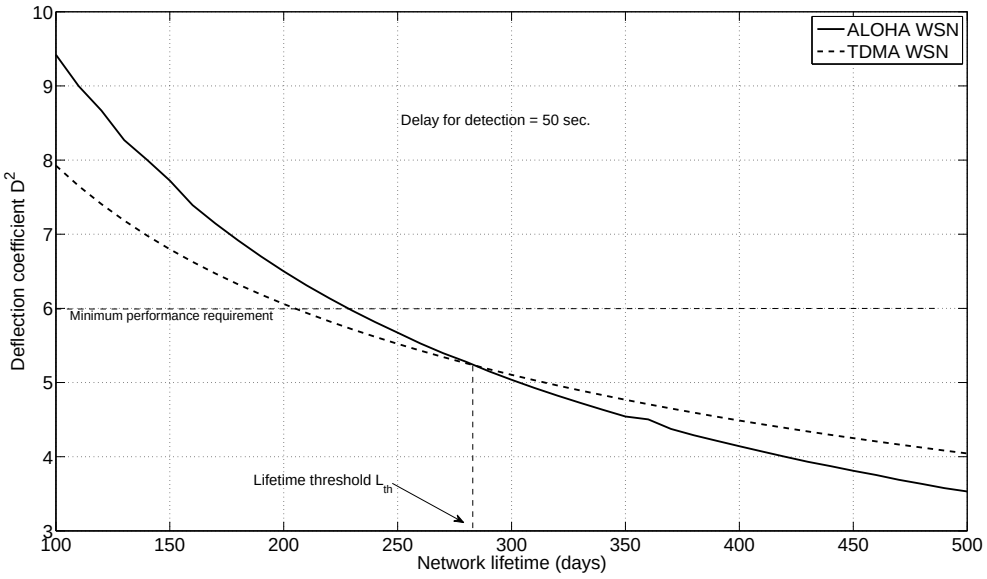

Figure 68: ALOHA-TDMA Comparison for different lifetime constraints. TDMA outperforms the ALOHA network for network lifetime greater than the lifetime threshold

Figure 69 summarizes the performance comparison in the delay-lifetime two dimensional space. The curve represents the boundary between the ALOHA and TDMA regions. For any pair of (delay, lifetime) in the ALOHA region, the ALOHA sensor network has a superior performance, and similarly for the TDMA region. The figure could be augmented by the contour lines for the deflection coefficient for both ALOHA and TDMA, to show the performance measure value. Using the deflection coefficient values, the designer can check whether the selected operating point satisfies the minimum performance requirement. Figure 70 shows the performance regions with the contour lines for the ALOHA region.

VII.8 Summary

In this chapter, we developed an integrated model for the single-hop TDMA sensor network deployed for detection. We designed the transmission control policy for each sensor such that the detection performance is maximized. We showed the performance gain relevant to other classical design

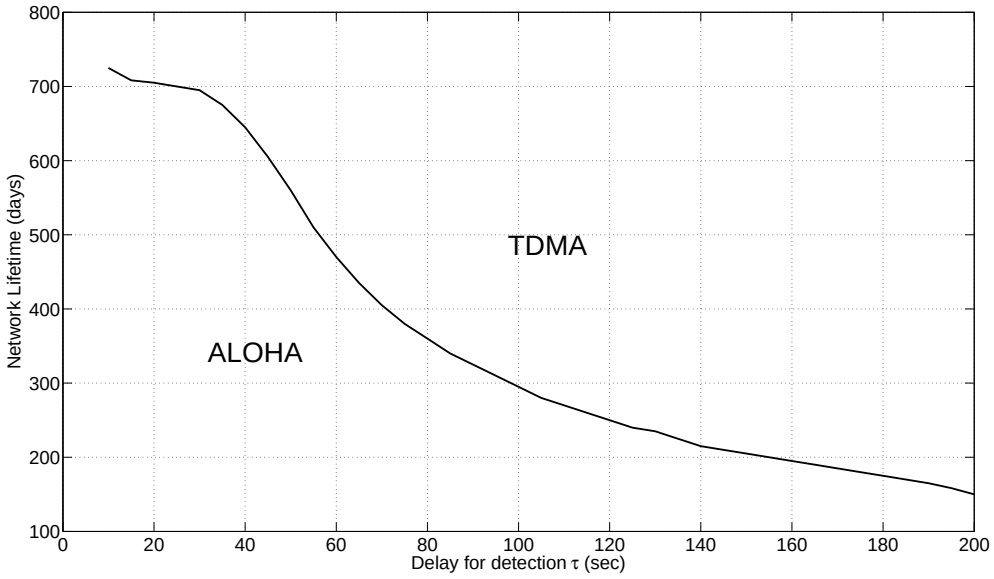

Figure 69: Performance regions for ALOHA and TDMA sensor networks. The chosen operating point is feasible if the performance measure value exceeds the minimum design requirement.

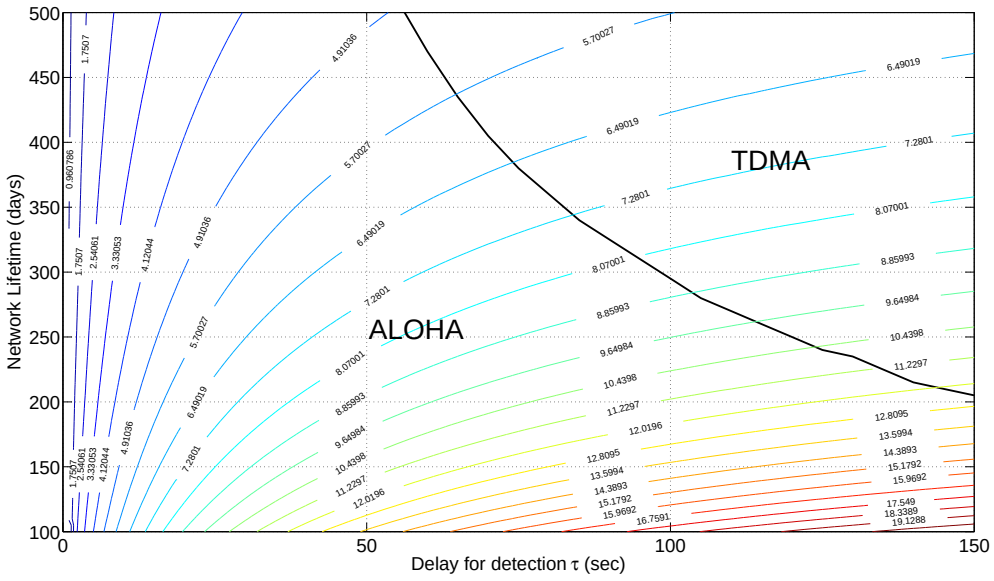

Figure 70: Performance regions for ALOHA and TDMA sensor networks. The ALOHA contour lines show the objective function value in the relevant region.

approaches. The model-based approach results in a no-cost performance increase, since the designer obtains a performance increase for the same delay and lifetime constraints.

The TDMA sensor network is easier to design than the ALOHA network, since one of the design variables is omitted (retransmission probability). However, we showed in this chapter that

the ALOHA network outperforms TDMA for small to moderate delays. For large delays, TDMA outperforms the ALOHA network unless the network lifetime is reduced. The designer chooses the best option based on the delay and lifetime constraints, in addition to the minimum allowed performance measure.

This chapter concludes our work on single-hop networks in this dissertation. It is worth noting that other single-hop sensor network architectures are used in practice, e.g. FDMA. However, the network design is very similar, and could be performed easily by following the design process outlined in Chapter V. In the next chapter, we consider the design of tree sensor networks.

CHAPTER VIII

Transmission Control Policy Design for Tree-Topology Sensor Networks

In Chapters VI and VII, we considered single-hop sensor networks. These networks are feasible when sensor nodes cannot communicate with each other to form a multihop network to the fusion center, e.g., cellular nodes communicating to a base station. However, for large distances between sensor nodes and the fusion center, the parallel topology suffers from two main drawbacks: (i) large energy consumption to communicate directly with the fusion center, and (ii) high probability of packet loss due to the degraded channel state caused by the long distance. Tree networks provide a solution for these two drawbacks. Sensor nodes cooperate in a multi-hop fashion to deliver the information to the fusion center. Therefore, each sensor has to communicate to its nearest neighbor only, hence saving energy and ensuring a better quality communication channel.

In this chapter, we design the transmission control policy for sensor nodes arranged in a tree topology for detection applications. We assume that the tree is already formed based on some given criterion. Therefore, the routing problem is not considered in this work. We assume slotted ALOHA multi-access scheme for each set of nodes sharing the same parent. We still follow the design process in Figure 42. The performance and quality measures are identical to the discussion in Chapters VI and VII, namely deflection coefficient as a performance measure, and QoI, CSI, and REI as quality measures.

In Chapters VI and VII, we assume direct transmission scheme, where information is transmitted without preprocessing to the fusion center. Although the direct transmission scheme results in no loss of detection performance at the fusion center, it may not be appropriate in tree networks since observations build-up at each intermediate node. Therefore, in addition to the direct transmission scheme, we study in this chapter the in-network processing scheme, where observations are locally quantized before transmission. We compare the two schemes and study the conditions where each scheme outperforms.

We summarize the contributions of our work as follows [9]: (1) We develop an integrated model for the detection system, that captures the physical channel, MAC protocol, the detection application models, and their interactions. The model also incorporates the QoI, CSI, and REI measures for each sensor. (2) We design a complete transmission control policy for the tree topology for a finite number of sensors, rather than asymptotically. The TCP variables include retransmission probabilities and communication rates for sensor nodes. (3) We show that the proposed design approach has a significant improvement in the detection performance over the classical decoupled and maximum throughput approaches. (4) We study the design problem when local observations are quantized, and show the conditions under which the local quantization scheme outperforms the direct transmission scheme.

The rest of the chapter is organized as follows: we formulate the problem in Section VIII.1. The detailed system model is derived in Section VIII.2. The solution of the optimization problem to obtain the optimal TCP is given in VIII.3. Section VIII.4 describes the decoupled and maximum throughput design approaches, to be compared to the proposed design. Section VIII.5 provides the performance comparison using a numerical example. The work is concluded in Section VIII.7.

VIII.1 Problem Formulation

Figure 71 illustrates the detection system architecture, where a set of N wireless sensors, and a fusion center denoted by FC, are arranged in a tree structure, and collaborate to detect the phenomenon of interest. We assume the tree structure is pre-specified, possibly based on sensor locations, and therefore the routing problem is not considered. Initially, the fusion center broadcasts a message containing the location of the phenomenon to be detected, soliciting information from different sensors. Each sensor responds to its parent with the following information: (1) sensor location, (2) the average signal to noise ratio of the measured phenomenon at the sensor location, and (3) the energy the sensor will devote to the detection process.

Two approaches are possible to calculate the optimal transmission control policy. The global approach, where the fusion center receives the information from all sensors (through their respective

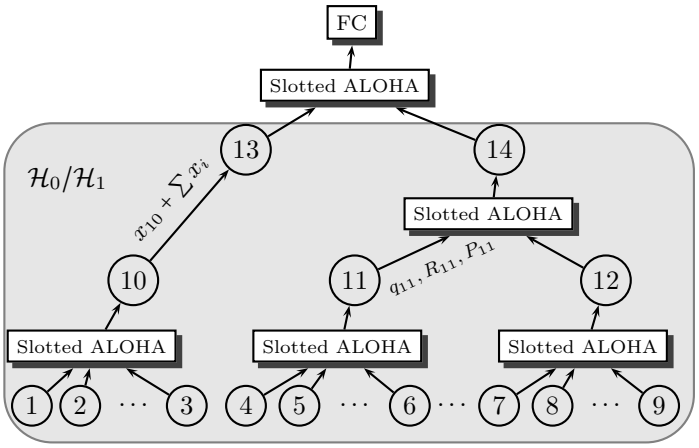

Figure 71: Detection architecture for tree-topology WSN. Sensors communicate their observations in a multihop fashion over slotted ALOHA multiaccess channels to the fusion center.

parents), calculates the optimal transmission control policy for each sensor by solving a constrained nonlinear optimization problem, and transmits the values of the TCP variables back to the relevant sensors. This global approach may not be feasible in large sensor networks as it is not scalable with the network size, in addition to the fact that the design parameters have to be propagated back from the fusion center down to all network nodes. A more practical approach is the local approach, where each parent node solves a smaller local optimization problem to specify the *locally* optimal TCP variables for its child nodes.

Some sensors may not contribute to the detection process, due to either low quality of information, low channel state, or not enough energy to transmit to the parent node (e.g. not enough battery power or long distance to the parent node combined with bad channel quality). The fusion center (global approach) or the parent nodes (local approach) transmit the TCP variables only to the sensors which are specified by the optimization algorithm to be reliable to contribute to the detection task. The resulting values of the TCP variables remain valid for the given location as long as the quality measures for each sensor did not change from the last run of the optimization algorithm.

After each sensor receives the optimal values of the TCP variables, the detection process proceeds as follows: the fusion center broadcasts a message to initiate a detection cycle at the local wireless sensors. Each local sensor samples the environment by collecting a number of observations, and then forms a data packet and communicates its message to the parent node over a shared wireless link

using the slotted ALOHA multiaccess control scheme. Parent nodes relay the information of the child nodes, in addition to their own information, through the tree network until reaching the fusion center. Finally, the fusion center makes a final decision after a fixed amount of time representing the maximum allowed delay for detection.

VIII.2 System Model

In this section, we present the system model for the tree detection network. Some parts of the model resemble the parallel detection network described in Section VI.3. These parts will be briefly mentioned in the following discussion for reference purposes.

VIII.2.1 Wireless Channel Model

The model of the wireless channel between each parent-child pair in the tree network is identical to the model presented in Section VI.3. The probability that the channel is "ON" during a transmission is then given by:

$$P[\text{channel is ON}] = \lambda_c = \Phi\left[\frac{1}{\sigma_c}\left(10\log\frac{P_t}{N_0 W(2^{\frac{R}{W}}-1)} - \mu_c\right)\right] \tag{219}$$

where R is the communication rate of the child node during a transmission to the parent node.

VIII.2.2 Media Access Control Protocol Model

We assume a slotted ALOHA multi-access communication protocol between each parent node and its child nodes, where each packet requires one time slot for the transmission, all time slots have the same length, and all transmitters are synchronized. Furthermore, we assume that the sub-trees composed of each parent and its immediate children do not interfere with each other. This could be achieved in practice by using different wireless channels for transmission, or it may be as a result of the physical separation between sub-trees such that sub-tree transmissions get attenuated before interfering with other transmissions.

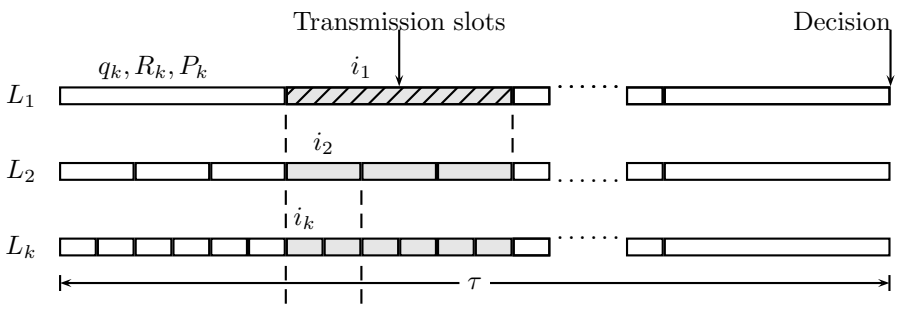

Figure 72: Detection cycle of length τ is divided into L_1 slots for nodes at depth 1 that have the same parent, L_2 slots for nodes at depth 2, and so on. The number of slots at each depth is an integer multiple of the number of slots at the previous depth. Inside each slot, each sensor attempts transmission with the indicated TCP parameters.

The detection cycle, demonstrated in Figure 72, has length τ, which defines the *delay for detection*. The detection cycle is divided into a number of transmission slots L_i, for nodes at the same depth i of the tree, and sharing a common parent. The relationship between the number of slots for consecutive depths is given by $L_{i+1} = m_i L_i$, where m_i is a positive integer. In the following discussion, we designate the set of all child nodes for sensor k by $\mathcal{C}_k$, and the set of all siblings (excluding sensor k) by $\mathcal{B}_k$.

At the beginning of every time slot, each local sensor k collects a number of observations n_k and forms an information packet for transmission over the wireless channel. The sensor then attempts to transmit to its parent with probability q_k, transmission power P_k, and communication rate R_k. The sensor attempts transmission at each time slot, despite the status of its previous transmission attempts. The final decision is taken at the fusion center using the information received during the detection cycle. The process repeats for every detection request initiated by the fusion center.

The communication rate for sensor k at tree depth i could be expressed with the aid of Figure 73 as follows:

$$R_k = \frac{bL_i n_k}{\tau} + \frac{1}{m_i} \sum_{v \in \mathcal{C}_k} Z_v R_v, \qquad \sum_{v \in \mathcal{C}_k} Z_v = m_i \tag{220}$$

where b is the number of encoding bits for each observation, and Z_v is the number of times the child sensor v successfully transmitted during the m_i time slots. The first term in (220) represents the

information collected by the sensor node, and vanishes if the node functions as a relay node for its child nodes. The second term represents the information received from the child nodes and vanishes for leaf nodes.

Now, we calculate the overall probability of a successful packet transmission, including the wireless channel effect. We note from (220) that the communication rate of intermediate nodes is a random variable, being dependent on the information received from its child nodes. Accordingly, accurate formulation for the problem requires modification of (219) to include the randomness of the communication rate. Unfortunately, no closed form solution could be obtained for the channel ON probability in this case. Even If we approximated the sum in the second term of (220) by a Gaussian random variable using the Central Limit Theorem, and used the approximation of R to derive the new probability of success, we would obtain, after some manipulations, a sum of two Log Normal random variables, which does not have a closed-form probability distribution. Therefore, to keep the analysis tractable, we resort to a suboptimal solution, where the communication rate for each node is represented by its expected value. Accordingly, Equation (219) is still applicable, where R represents the average communication rate. Now, at any given time slot, the probability of a single packet transmission by sensor k is given by $q_k \prod_{v \in \mathcal{B}_k} (1 - q_v)$. Further, this packet will be successfully received by the parent node if the state of the physical channel between the child node k and the parent node is "ON" during this time slot. Therefore, using (219), the total probability

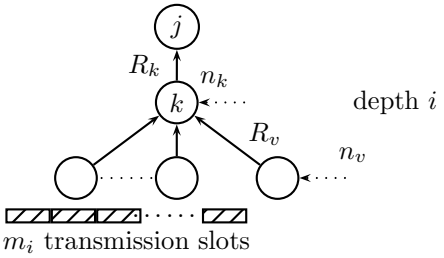

Figure 73: The communication rate for node k at tree depth i is the sum of the communication rate required to send its local observations and the communication rates of its child nodes that successfully transmitted during the previous m_i time slots.

of a successful packet transmission by sensor k is given by:

$$\lambda_k = q_k \left[\prod_{v \in \mathcal{B}_k} (1 - q_v) \right] \Phi \left[\frac{10}{\sigma_c^k} \log \frac{P_t^k}{N_0 W (2^{\frac{\bar{R}_k}{W}} - 1)} - \frac{\mu_c^k}{\sigma_c^k} \right] \tag{221}$$

where $\bar{R}_k$ is obtained by taking the expected value for (220) and noting that Z_v is a binomially distributed random variable with $E[Z_v] = m_i \lambda_v$

$$\bar{R}_k = \frac{b L_i n_k}{\tau} + \sum_{v \in \mathcal{C}_k} \lambda_v \bar{R}_v \tag{222}$$

VIII.2.3 Energy Model

We repeat the expression of the network lifetime introduced earlier in Chapter VI:

$$\mathcal{L} = \frac{\mathcal{E}^0 - \mathcal{E}^w}{f_r \mathcal{E}^r} \tag{223}$$

Similar to Chapters VI and VII, we can include the energy allocation problem in our formulation, i.e. finding optimal e_i^r values for all sensors that maximize the detection performance while guaranteeing a minimum network lifetime. In this work, however, we focus on the optimal TCP problem, and therefore we resort to a simpler energy formulation. First, we assume that e_i^w is the energy remaining in the sensor battery when the sensor is not capable of operating its electronic circuits for computations and communication, which is fixed and known for each sensor. Second, we assume that the reporting energy for each sensor e_i^r is a fixed percentage of its net useful energy at the time of sensor deployment, i.e.:

$$e_i^r = \alpha_e (e_i^0 - e_i^w) \tag{224}$$

and using (223), it can be shown that:

$$\mathcal{L}_i = \mathcal{L} = \frac{1}{f_r \alpha_e} \tag{225}$$

In other words, the individual sensors' lifetime and the network lifetime are equal, i.e. all nodes die together. This formulation has the advantage that we do not need to worry about the situation where the relay node dies before its children, hence rendering its whole subtree not used.

The energy consumed by each sensor in one detection cycle is thus given by:

$$e_k^r = \frac{e_k^0 - e_k^w}{f_r \mathcal{L}} \qquad \forall k \tag{226}$$

which could be calculated for any desired network lifetime $\mathcal{L}$. The total energy consumed by each sensor is divided between transmission and reception (except for leaf nodes). By assuming that the energy consumed in the reception process is proportional to the detection cycle time with proportionality constant α, and by noting that the expected number of transmissions by sensor k during a detection cycle is $L_i q_k$, we get:

$$P_t^k = \frac{(e_k^r/\tau) - \alpha}{q_k} = \frac{1}{q_k}(p_k - \alpha) \tag{227}$$

where $p_k = e_k^r/\tau$ is the average transmission power over one detection cycle, which summarizes the Residual Energy Information (REI) for each sensor. Using (227) in (221), we get:

$$\lambda_k = q_k \left[\prod_{v \in \mathcal{B}_k} (1 - q_v) \right] \Phi \left[a_k - \left(\frac{10}{\sigma_c^k} \right) \log q_k \left(2^{\frac{\bar{R}_k}{W}} - 1 \right) \right] \tag{228}$$

where $a_k = \frac{1}{\sigma_c^k} \left(10 \log \frac{p_k - \alpha}{N_0 W} - \mu_c^k \right)$. We note that $\alpha < p_k$ for the sensor to be able to transmit the information. In addition, $\alpha = 0$ for leaf nodes.

VIII.2.4 Sensing Model

We focus our work on detection using signal amplitude measurements. We use the same sensing model as in Chapter VI:

$$x_k = \frac{\epsilon}{d_k^{\eta/2}} + w_k \tag{229}$$

where ϵ is the amplitude of the emitted signal at the object, η is a known attenuation coefficient, typically between 2 and 4, and w_k is an additive white Gaussian noise with zero mean and variance $\sigma_s^{k^2}$.

The detection problem could be defined as the following binary hypothesis testing problem, for each time slot i:

$$\begin{aligned} &\mathcal{H}_0 : x_k[j,i] = w_k[j,i] && j = 1,2,\ldots,n_k \\ &\mathcal{H}_1 : x_k[j,i] = \mu^k + w_k[j,i] && j = 1,2,\ldots,n_k \end{aligned} \tag{230}$$

where $\mu^k = \epsilon/d_k^{\eta/2}$, and n_k is the number of observations obtained by sensor k at each time slot. We note that noise samples are independent across sensors, i.e., the observations at local sensors are independent across time and space, but not necessarily identically distributed since some sensors may be closer to the measured phenomenon, and noise variances are assumed unequal.

Definition 6. *The slot sequence $i_1 i_2 \ldots i_k$ represents slot i_k at tree depth k, which is a subslot of slot i_{k-1} at tree depth $k-1$, and all the way up to slot i_1 at tree depth 1. This is illustrated in Figure 72.*

Definition 7. *$r_{v_j}[i_1 i_2 \ldots i_j]$ is a random variable representing the success or failure of transmitting a packet from sensor v_j to its parent, in the slot sequence $i_1 i_2 \ldots i_j$. r_{v_j} is Bernoulli-distributed with sample space $\Omega = \{0,1\}$ and probability measure as in (228).*

Proposition 8. *The optimal test statistic at the fusion center for the slotted ALOHA tree network with depth l is given by:*

$$V = \sum_{i_1=1}^{L_1} \sum_{v_1 \in \mathcal{C}_f} \sum_{j_1=1}^{n_{v_1}} r_{v_1}[i_1] \Bigg[\left(\frac{\mu^{v_1}}{\sigma_s^{v_1^2}} \right) x_{v_1}[j_1, i_1] + \sum_{i_2=1}^{m_1} \sum_{v_2 \in \mathcal{C}_{v_1}} \sum_{j_2=1}^{n_{v_2}} r_{v_2}[i_1 i_2] \Bigg[\left(\frac{\mu^{v_2}}{\sigma_s^{v_2^2}} \right) x_{v_2}[j_2, i_1 i_2] + \ldots + \sum_{i_l=1}^{m_{l-1}} \sum_{v_l \in \mathcal{C}_{v_{l-1}}} \sum_{j_l=1}^{n_{v_l}} r_{v_l}[i_1 \ldots i_l] \left(\frac{\mu^{v_l}}{\sigma_s^{v_l^2}} \right) x_{v_l}[j_l, i_l i_2 \ldots i_l] \Bigg] \ldots \Bigg] \tag{231}$$

Proof. At the fusion center, the Log Likelihood Ratio is an optimal test. Using the independence assumption of sensor observations, the LLR could be expressed as a sum of the individual sensor LLRs provided that the information is transmitted successfully to the fusion center. The information transmitted by sensor v_l at tree depth l and time slot i_l will be received at the fusion center if all transmissions in the slot sequence $i_1 \dots i_l$ were successful, i.e. $r_{v_1}[i_1] r_{v_2}[i_1 i_2] \dots r_{v_l}[i_1 \dots i_l] = 1$. Using this fact, the LLR test could be expressed as:

$$\sum_{i_1=1}^{L_1} \sum_{v_1 \in \mathcal{C}_f} r_{v_1}[i_1] L\left(\boldsymbol{x}_{v_1}[i_1]\right) + \sum_{i_1=1}^{L_1} \sum_{v_1 \in \mathcal{C}_f} \sum_{i_2=1}^{m_1} \sum_{v_2 \in \mathcal{C}_{v_1}} r_{v_1}[i_1] r_{v_2}[i_1 i_2] L\left(\boldsymbol{x}_{v_2}[i_1 i_2]\right) + \dots + \sum_{i_1=1}^{L_1} \sum_{v_1 \in \mathcal{C}_f} \dots \sum_{i_l=1}^{m_{l-1}} \sum_{v_l \in \mathcal{C}_{v_{l-1}}} r_{v_1}[i_1] \dots r_{v_l}[i_1 \dots i_l] L\left(\boldsymbol{x}_{v_l}[i_1 \dots i_l]\right) \underset{\mathcal{H}_0}{\overset{\mathcal{H}_1}{\gtrless}} \ln \gamma \tag{232}$$

where the LLR could be derived as in (130):

$$L\left(\boldsymbol{x}_{v_l}[i_1 \dots i_l]\right) = \frac{\mu^{v_l}}{{\sigma_s^{v_l}}^2} \sum_{j_l=1}^{n_{v_l}} x_{v_l}[j_l, i_1 \dots i_l] - \frac{1}{2} n_{v_l} \left(\frac{\mu^{v_l}}{\sigma_s^{v_l}}\right)^2 \tag{233}$$

Using (233) in (232) and factoring out, the LLR test is then given by:

$$\begin{aligned} V = & \sum_{i_1=1}^{L_1} \sum_{v_1 \in \mathcal{C}_f} \sum_{j_1=1}^{n_{v_1}} r_{v_1}[i_1] \left[\left(\frac{\mu^{v_1}}{{\sigma_s^{v_1}}^2} \right) x_{v_1}[j_1, i_1] + \sum_{i_2=1}^{m_1} \sum_{v_2 \in \mathcal{C}_{v_1}} \sum_{j_2=1}^{n_{v_2}} r_{v_2}[i_1 i_2] \left[\left(\frac{\mu^{v_2}}{{\sigma_s^{v_2}}^2} \right) x_{v_2}[j_2, i_1 i_2] + \right.\right. \\ & \left.\left. \dots + \sum_{i_l=1}^{m_{l-1}} \sum_{v_l \in \mathcal{C}_{v_{l-1}}} \sum_{j_l=1}^{n_{v_l}} r_{v_l}[i_1 \dots i_l] \left(\frac{\mu^{v_l}}{{\sigma_s^{v_l}}^2} \right) x_{v_l}[j_l, i_l i_2 \dots i_l] \right] \dots \right] \underset{\mathcal{H}_0}{\overset{\mathcal{H}_1}{\gtrless}} \\ & \frac{1}{2} \sum_{i_1=1}^{L_1} \sum_{v_1 \in \mathcal{C}_f} r_{v_1}[i_1] \left[n_{v_1} \left(\frac{\mu^{v_1}}{\sigma_s^{v_1}} \right)^2 + \sum_{i_2=1}^{m_1} \sum_{v_2 \in \mathcal{C}_{v_1}} r_{v_2}[i_1 i_2] \left[n_{v_2} \left(\frac{\mu^{v_2}}{\sigma_s^{v_2}} \right)^2 + \right.\right. \\ & \left.\left. \dots + \sum_{i_l=1}^{m_{l-1}} \sum_{v_l \in \mathcal{C}_{v_{l-1}}} r_{v_l}[i_1 \dots i_l] n_{v_l} \left(\frac{\mu^{v_l}}{\sigma_s^{v_l}} \right)^2 \right] \dots \right] + \ln \gamma \end{aligned} \tag{234}$$

■

The expression in (231) is simply a weighted sum of the observations received at the fusion center. The complexity of the equation comes from the fact that successful reception of the observations of child nodes at the fusion center depends on the success of the transmission of all parent nodes up to the fusion center.

Proposition 9. *The deflection coefficient for the detector in (231) is given by:*

$$D^2 = L_1 \sum_{v_1 \in \mathcal{C}_f} \lambda_{v_1} \left[n_{v_1} c_{v_1} + m_1 \sum_{v_2 \in \mathcal{C}_{v_1}} \lambda_{v_2} \left[n_{v_2} c_{v_2} + \ldots + m_{d-1} \sum_{v_l \in \mathcal{C}_{v_{l-1}}} \lambda_{v_l} n_{v_l} c_{v_l} \right] \ldots \right] \tag{235}$$

where $c_v = (\mu^v / \sigma_s^v)^2$.

Proof. We use the definition of the deflection coefficient in (132). We use the fact that $r_i[k]$ and $x_i[j,k]$ are both IID and independent. In addition, r_{v_i} and r_{v_j} are independent for $i \neq j$, and $E[r_{v_i}] = \lambda_{v_i}$

$$\begin{aligned} E[V;\mathcal{H}_0] = \sum_{i_1=1}^{L_1} \sum_{v_1 \in \mathcal{C}_f} \sum_{j_1=1}^{n_{v_1}} E\left[r_{v_1}[i_1]\right] \Bigg[\left(\frac{\mu^{v_1}}{{\sigma_s^{v_1}}^2} \right) E\left[x_{v_1}[j_1, i_1]; \mathcal{H}_0\right] + \\ \ldots + \sum_{i_l=1}^{m_{l-1}} \sum_{v_l \in \mathcal{C}_{v_{l-1}}} \sum_{j_l=1}^{n_{v_l}} E\left[r_{v_l}[i_1 \ldots i_l]\right] \left(\frac{\mu^{v_l}}{{\sigma_s^{v_l}}^2} \right) E\left[x_{v_l}[j_l, i_l i_2 \ldots i_l]; \mathcal{H}_0\right] \Bigg] = 0 \end{aligned} \tag{236}$$

$$\begin{aligned} E[V;\mathcal{H}_1] &= \sum_{i_1=1}^{L_1} \sum_{v_1 \in \mathcal{C}_f} \sum_{j_1=1}^{n_{v_1}} E\left[r_{v_1}[i_1]\right] \Bigg[\left(\frac{\mu^{v_1}}{{\sigma_s^{v_1}}^2} \right) E\left[x_{v_1}[j_1, i_1]; \mathcal{H}_1\right] + \\ &\quad \ldots + \sum_{i_l=1}^{m_{l-1}} \sum_{v_l \in \mathcal{C}_{v_{l-1}}} \sum_{j_l=1}^{n_{v_l}} E\left[r_{v_l}[i_1 \ldots i_l]\right] \left(\frac{\mu^{v_l}}{{\sigma_s^{v_l}}^2} \right) E\left[x_{v_l}[j_l, i_l i_2 \ldots i_l]; \mathcal{H}_1\right] \Bigg] \\ &= L_1 \sum_{v_1 \in \mathcal{C}_f} \lambda_{v_1} \left[n_{v_1} \left(\frac{\mu^{v_1}}{\sigma_s^{v_1}} \right)^2 + m_1 \sum_{v_2 \in \mathcal{C}_{v_1}} \lambda_{v_2} \left[n_{v_2} \left(\frac{\mu^{v_2}}{\sigma_s^{v_2}} \right)^2 + \ldots m_l \sum_{v_l \in \mathcal{C}_{v_l}} \lambda_{v_l} n_{v_l} \left(\frac{\mu^{v_l}}{\sigma_s^{v_l}} \right)^2 \right] \ldots \right] \end{aligned} \tag{237}$$

To find $\mathrm{var}[V;\mathcal{H}_0]$, we expand the test statistic, noting that transmissions in different slots are IID:

$$\begin{aligned} \mathrm{var}[V;\mathcal{H}_0] = L_1 \mathrm{var} \Bigg[& \sum_{v_1 \in \mathcal{C}_f} \sum_{j_1=1}^{n_{v_1}} r_{v_1}[i_1] \left(\frac{\mu^{v_1}}{{\sigma_s^{v_1}}^2} \right) x_{v_1}[j_1, i_1] \\ & + L_1 m_1 \sum_{v_1 \in \mathcal{C}_f} \sum_{v_2 \in \mathcal{C}_{v_1}} \sum_{j_1=1}^{n_{v_1}} \sum_{j_2=1}^{n_{v_2}} r_{v_1}[i_1] r_{v_2}[i_1 i_2] \left(\frac{\mu^{v_2}}{{\sigma_s^{v_2}}^2} \right) x_{v_2}[j_2, i_1 i_2] + \ldots \\ & + \sum_{i_1=1}^{L_1} \sum_{v_1 \in \mathcal{C}_f} \cdots \sum_{i_l=1}^{m_{l-1}} \sum_{v_l \in \mathcal{C}_{v_{l-1}}} r_{v_1}[i_1] \ldots r_{v_l}[i_1 \ldots i_l] \left(\frac{\mu^{v_l}}{{\sigma_s^{v_l}}^2} \right) x_{v_l}[j_l, i_1 \ldots i_l] \Bigg] \end{aligned} \tag{238}$$

We use the identity:

$$\mathrm{var}\left(\sum_{i=1}^{N} X_i\right) = \sum_{i=1}^{N}\sum_{j=1}^{N} \mathrm{COV}(X_i, X_j) = \sum_{i=1}^{N}\sum_{j=1}^{N} E[X_i X_j] - E[X_i]E[X_j] \tag{239}$$

The second term in (239) vanishes for all terms in (238) since the observations have zero mean under $\mathcal{H}_0$. In addition, the first term vanishes except when $i = j$. Accordingly:

$$\begin{aligned}\mathrm{var}[V;\mathcal{H}_0] = {} & L_1 \sum_{v_1\in\mathcal{C}_f} n_{v_1} E[(r_{v_1})^2]E[(x_{v_1})^2;\mathcal{H}_0]\left(\frac{\mu^{v_1}}{\sigma_s^{v_1{}^2}}\right)^2 \\ & + L_1 m_1 \sum_{v_1\in\mathcal{C}_f}\sum_{v_2\in\mathcal{C}_{v_1}} n_{v_2} E[(r_{v_1})^2]E[(r_{v_2})^2]E[(x_{v_2})^2;\mathcal{H}_0]\left(\frac{\mu^{v_2}}{\sigma_s^{v_2{}^2}}\right)^2 + \dots \\ & + L_1 m_1 \dots m_l \sum_{v_1\in\mathcal{C}_f} \dots \sum_{v_l\in\mathcal{C}_{v_{l-1}}} E[(r_{v_1})^2]\dots E[(r_{v_l})^2]E[(x_{v_l})^2;\mathcal{H}_0]\left(\frac{\mu^{v_l}}{\sigma_s^{v_l{}^2}}\right)^2\end{aligned} \tag{240}$$

We note that $E[(r_v)^2] = \lambda_v$ and $E[(x_v)^2] = \sigma_s^{v^2}$. Accordingly:

$$\begin{aligned}\mathrm{var}[V;\mathcal{H}_0] = {} & L_1 \sum_{v_1\in\mathcal{C}_f} n_{v_1}\lambda_{v_1}\left(\frac{\mu^{v_1}}{\sigma_s^{v_1}}\right)^2 + L_1 m_1 \sum_{v_1\in\mathcal{C}_f}\sum_{v_2\in\mathcal{C}_{v_1}} n_{v_2}\lambda_{v_1}\lambda_{v_2}\left(\frac{\mu^{v_2}}{\sigma_s^{v_2}}\right)^2 + \dots \\ & + L_1 m_1 \dots m_l \sum_{v_1\in\mathcal{C}_f} \dots \sum_{v_l\in\mathcal{C}_{v_{l-1}}} \lambda_{v_1}\dots\lambda_{v_1}\left(\frac{\mu^{v_l}}{\sigma_s^{v_l}}\right)^2\end{aligned} \tag{241}$$

and factoring out, we get:

$$\mathrm{var}[V;\mathcal{H}_0] = L_1 \sum_{v_1\in\mathcal{C}_f} \lambda_{v_1}\left[n_{v_1}\left(\frac{\mu^{v_1}}{\sigma_s^{v_1}}\right)^2 + m_1 \sum_{v_2\in\mathcal{C}_{v_1}} \lambda_{v_2}\left[n_{v_2}\left(\frac{\mu^{v_2}}{\sigma_s^{v_2}}\right)^2 + \dots m_l \sum_{v_l\in\mathcal{C}_{v_l}} \lambda_{v_l} n_{v_l}\left(\frac{\mu^{v_l}}{\sigma_s^{v_l}}\right)^2\right]\dots\right] \tag{242}$$

From (235), (236), (237), and (242), and by defining $c_v = (\mu^v/\sigma_s^v)^2$, we obtain (235) ∎

We note that the quantity $n_v c_v$ is a measure of the QoI for each sensor. Using (222) in (235), we obtain our objective function:

$$D^2 = \frac{\tau}{b}\sum_{v_1\in\mathcal{C}_f} \lambda_{v_1}\left[\bar{R}_{v_1} c_{v_1} + \sum_{v_2\in\mathcal{C}_{v_1}} \lambda_{v_2}\left[\bar{R}_{v_2}(c_{v_2} - c_{v_1}) + \dots + \sum_{v_l\in\mathcal{C}_{v_{l-1}}} \lambda_{v_l}\bar{R}_{v_l}(c_{v_l} - c_{v_{l-1}})\right]\dots\right] \tag{243}$$

A complete nomenclature for the system model is shown in Table 15

Param.	Description
μ_c^i	Mean path loss for sensor i
σ_c^i	Path loss std. deviation for sensor i
W	Communication channel bandwidth
P_t^i	Transmission power for sensor i
p_i	Average transmission power for sensor i over one detection cycle
N_0	Noise power spectral density
R_i	Average Communication rate for sensor i
b	Number of encoding bits/observation
L_i	Number of transmission slots at tree depth i
m_i	Number of subslots at tree depth $i+1$ for each slot at tree depth i
n_i	Number of observations sampled by sensor i
l	Tree depth
τ	Delay for detection
λ_i	Successful packet transmission probability for sensor i
q_i	Retransmission probability for sensor i
$\mathcal{L}$	Sensor network lifetime
$\mathcal{L}_i$	Sensor i lifetime
e_i^0	Initial energy in sensor i battery
e_i^w	Wasted energy remaining in sensor i battery
e_i^r	Reporting energy for sensor i
f_r	Reporting frequency for the sensor network
α_e	Percentage of net useful energy used in reporting
α	Proportionality constant for receiving energy
ϵ	Amplitude of emitted signal at detected object
d_i	Distance between sensor i and the object
η	Attenuation coefficient for object signal
$x_i[j,k]$	Observation number j at time slot k for sensor i
$c^i = (\mu^i/\sigma_s^i)^2$	Detected object signal to noise ratio at sensor i
V	Test statistic at the fusion center
N	Total number of wireless sensors
$r_i[k]$	Success or failure of sensor i transmission in slot k
D^2	Deflection coefficient
$\mathcal{C}_k$	Set of all child nodes for sensor k
$\mathcal{B}_k$	Set of all sibling nodes for sensor k

Table 15: Nomenclature for the ALOHA Tree sensor network

VIII.3 TCP Design for Optimal Detection

The optimization problem could be summarized as follows:

$$\max_{\boldsymbol{q},\bar{\boldsymbol{R}}} \frac{\tau}{b} \sum_{v_1 \in \mathcal{C}_f} \lambda_{v_1} \left[\bar{R}_{v_1} c_{v_1} + \sum_{v_2 \in \mathcal{C}_{v_1}} \lambda_{v_2} \left[\bar{R}_{v_2} (c_{v_2} - c_{v_1}) + \ldots + \sum_{v_l \in \mathcal{C}_{v_{l-1}}} \lambda_{v_l} \bar{R}_{v_l} (c_{v_l} - c_{v_{l-1}}) \right] \ldots \right]$$

$$\text{s.t. } 0 \le q_i \le 1$$

$$\bar{R}_i \ge \sum_{v \in \mathcal{C}_i} \lambda_v \bar{R}_v \qquad i = 1 : N \tag{244}$$

where:

$$\lambda_v = q_v \left[\prod_{k \in \mathcal{B}_v} (1 - q_k) \right] \Phi \left[a_v - \left(\frac{10}{\sigma_c^v} \right) \log q_v \left(2^{\frac{\bar{R}_v}{W}} - 1 \right) \right] \tag{245}$$

$$a_v = \frac{1}{\sigma_c^v} \left(10 \log \frac{p_v - \alpha}{N_0 W} - \mu_c^v \right) \tag{246}$$

$$c_v = \left(\frac{\mu^v}{\sigma_s^v} \right)^2 \tag{247}$$

The last constraint guarantees that intermediate nodes can at least relay the observations of their children nodes. This constraint reduces to $\bar{R}_i \ge 0$ for leaf nodes. Although this problem could be solved by existing algorithms (e.g. interior point method) for a local maximum, we note that the objective function in (243) gets more complicated as the tree depth increases. Adding the fact that all design variables have to be propagated back to tree nodes, a more practical approach is clearly needed. If we look at the objective function expression in (243), we note that it reflects the tree hierarchy, i.e. the last term in the expression represents the contribution of the leaf nodes, preceded by the contribution of the parents of the leaf nodes, and so on, until reaching the sensor nodes at the top level of the tree (depth=1). This could be shown by expressing the objective function using the following recursive equation:

$$D^2 = \frac{\tau}{b} J_{FC}$$

$$J_k = \sum_{v \in \mathcal{C}_k} \lambda_v \left[\bar{R}_v (c_v - c_k) + J_v \right] \tag{248}$$

where $J_v = 0$ for leaf nodes and $c_k = 0$ for the fusion center node. This structure of the objective function suggests a local optimization approach for the problem, where we start by optimizing J_v for sensors at depth $l-1$ and continue the local optimization recursively using (248), until reaching the fusion center. This approach is practical since the solution of each local optimization problem could be carried out locally at each parent node. The solution approach is illustrated in Figure 74.

By substituting (228) in (248), we can express the local optimization problem at parent node k as follows:

$$\max_{\boldsymbol{q}, \bar{\boldsymbol{R}}} \sum_{v \in \mathcal{C}_k} q_v \left[\prod_{i \in \mathcal{B}_v} (1 - q_i) \right] \left[\bar{R}_v (c_v - c_k) + J_v \right] \Phi \left[a_v - \left(\frac{10}{\sigma_c^v} \right) \log q_v \left(2^{\frac{\bar{R}_v}{W}} - 1 \right) \right]$$

$$\text{s.t. } 0 \le q_v \le 1$$

$$\bar{R}_v \ge \sum_{u \in \mathcal{C}_v} \lambda_u \bar{R}_u = r_v \tag{249}$$

We note that J_v and r_v are fixed values, obtained from solving the local optimization problems at lower levels in the hierarchy. The notation for the local optimization problem is illustrated in Figure 75.

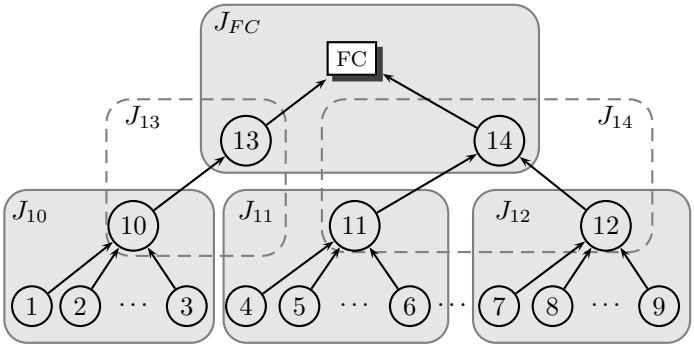

Figure 74: Hierarchical optimization for the TCP design problem. Sub-trees are locally optimized starting from the leaf nodes.

Let the number of child nodes for sensor k is N_k, and denote the decision variables by $\boldsymbol{x} = \begin{bmatrix} q_1 & q_2 & \dots & q_{N_k} & \bar{R}_1 & \bar{R}_2 & \dots & \bar{R}_{N_k} \end{bmatrix}$, where $\boldsymbol{x} \in \mathbb{R}^{2N_k}$, and the objective function by $J(\boldsymbol{x})$, then the optimization problem could be rewritten on the form:

$$\begin{aligned} &\min_{\boldsymbol{x}} \quad -J(\boldsymbol{x}) \\ &\text{subject to } A\boldsymbol{x} \geq \boldsymbol{b} \end{aligned} \tag{250}$$

where

$$A = \begin{bmatrix} I & -I & \mathbf{0} \\ \mathbf{0} & \mathbf{0} & I \end{bmatrix}^T, \qquad \boldsymbol{b} = \begin{bmatrix} \mathbf{0} & -\mathbf{1} & \boldsymbol{r} \end{bmatrix}^T \tag{251}$$

I is the identity matrix, $\mathbf{0}(\mathbf{1})$ is the vector/matrix of all zeros (ones) with appropriate dimensions, and $\boldsymbol{r} = \begin{bmatrix} r_1 & r_2 & \dots & r_{N_k} \end{bmatrix}^T$. This problem is similar to the optimization problem considered in Chapter VI, except that the energy is already allocated among sensors. Therefore, we present the following result without proof. The proof is very similar to Proposition 3.

Proposition 10. *The maximum value of the objective function in (249) occurs either when one sensor transmits with probability one and all other sensors remain silent, or at a stationary point of the objective function, i.e. at* $\boldsymbol{x}^*$ *where* $\nabla J(\boldsymbol{x}^*) = 0$.

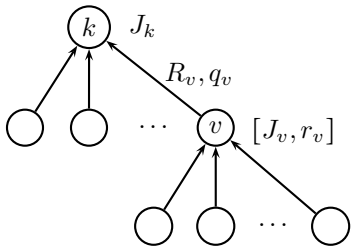

Figure 75: Notation for the local optimization problem for the tree sensor network, with direct transmission of local sensor data. The local optimization runs at sensor node k to calculate the design variables for sensor nodes $v \in \mathcal{C}_k$. J_v and r_v are calculated from running the local optimization algorithm at sensor node v.

Since we may have multiple stationary points in the interior of the objective function domain, the proposition does not guarantee obtaining the global maximum. However, the proposition is still useful for the following reasons: 1) it avoids the case where the optimization algorithm may terminate at the local maximum $q_i = 1, q_j = 0$, while a better local maximum maybe at one of the stationary points, and 2) it provides information about the choice of the initial point for the optimization algorithm, where initial points near the corner points $q_i = 1, q_j = 0$ have to be avoided.

VIII.4 Performance Comparison

We compare our design approach to the classical decoupled and maximum throughput design approaches. We still consider the local approach for system design and optimization, since global optimization is not of practical interest.

VIII.4.1 Decoupled design

In this approach, each layer is designed separately. In the conventional slotted ALOHA, the MAC sublayer is designed to minimize the probability of collision, without regard to the QoI or CSI of each node. For the sub-tree composed of node k and the set of its immediate children, $\mathcal{C}_k$, Minimum probability of collision occurs at $q_v = 1/N_k$, where $N_k = |\mathcal{C}_k|$, and consequently $P_t^k = (p_k - \alpha)/N_k$. The physical layer is designed to guarantee a minimum probability of successful packet transmission, λ_v. Using (219), we obtain:

$$\bar{R}_i = W \log_2 \left(1 + 10^{\lceil 0.1\sigma_c^i (a_i - \Phi^{-1}[\lambda_v]) + \log N_k \rceil}\right) \tag{252}$$

and using (248), the deflection coefficient is given by:

$$\begin{aligned} D^2 &= \frac{\tau}{b} J_{FC} \\ J_k &= \frac{\lambda_v}{N_k} \left(1 - \frac{1}{N_k}\right)^{N_k - 1} \sum_{v \in \mathcal{C}_k} \left[J_v + (c_v - c_k)\bar{R}_i\right] \end{aligned} \tag{253}$$

To make a fair comparison, we do not assume a pre-set value of λ_k. Rather, we optimize λ_k values to yield the maximum deflection coefficient. Therefore, the local optimization problem in (249) could be written on the form:

$$\begin{aligned}
&\max_{\lambda_v} \frac{\lambda_v}{N_k}\left(1-\frac{1}{N_k}\right)^{N_k-1} \sum_{v\in\mathcal{C}_k}\left[\bar{R}_v(c_v-c_k)+J_v\right] \\
&\text{s.t. } \bar{R}_v \geq \sum_{u\in\mathcal{C}_v} \lambda_u \bar{R}_u = r_v
\end{aligned} \tag{254}$$

and using (252) for $\bar{R}_v$, we obtain:

$$\begin{aligned}
&\max_{\lambda_v} \frac{W\lambda_v}{N_k}\left(1-\frac{1}{N_k}\right)^{N_k-1} \sum_{v\in\mathcal{C}_k}\left[\log_2\left(1+10^{\left[0.1\sigma_c^v(a_v-\Phi^{-1}[\lambda_v])+\log N_k\right]}\right)(c_v-c_k)+J_v\right] \\
&\text{s.t. } \lambda_v \leq \min_{v\in\mathcal{C}_k} \Phi\left[a_v-\left(\frac{10}{\sigma_c^v}\right)\left\{\log\left(2^{\frac{\sum_{u\in\mathcal{C}_v}\lambda_u\bar{R}_u}{W}}-1\right)-\log N_k\right\}\right]
\end{aligned} \tag{255}$$

VIII.4.2 Max Throughput Design

The throughput of any relay node k is defined as:

$$T_k = \sum_{v\in\mathcal{C}_k} \lambda_v \bar{R}_v = \sum_{v\in\mathcal{C}_k} \bar{R}_v q_v \prod_{i\in\mathcal{B}_v}(1-q_i)\Phi\left[a_v-\left(\frac{10}{\sigma_c^v}\right)\log q_v\left(2^{\frac{\bar{R}_v}{W}}-1\right)\right] \tag{256}$$

The objective is to choose the design variables q_v and R_v to locally maximize the throughput. The constraint on the communication rate of node v could be expressed in terms of its throughput as $\bar{R}_v \geq T_v$, where $T_v = 0$ for leaf nodes. The optimization problem could be formulated as:

$$\begin{aligned}
&\max_{\boldsymbol{q}_v,\bar{\boldsymbol{R}}_v} \sum_{v\in\mathcal{C}_k} \bar{R}_v q_v\left[\prod_{i\in\mathcal{B}_v}(1-q_i)\right]\Phi\left[a_v-\left(\frac{10}{\sigma_c^v}\right)\log q_v\left(2^{\frac{\bar{R}_v}{W}}-1\right)\right] \\
&\text{s.t. } 0\leq q_v\leq 1 \\
&\quad \bar{R}_v \geq \sum_{u\in\mathcal{C}_v}\lambda_u\bar{R}_u
\end{aligned} \tag{257}$$

where λ_u and $\bar{R}_u$ are obtained from solving the local optimization problems at the lower level for each node v, as indicated in Figure 75. The optimal design variables could then be substituted back in (248) to evaluate the deflection coefficient.

VIII.5 Numerical Example

We consider the tree network in Figure 76, with system parameters as indicated on the tree edges. We use $W = 2 \times 10^3$ Hz, $N_0 = 10^{-10}$ W/Hz, and $b = 16$ bits. We use the interior-point algorithm to calculate the optimal solution in each case.

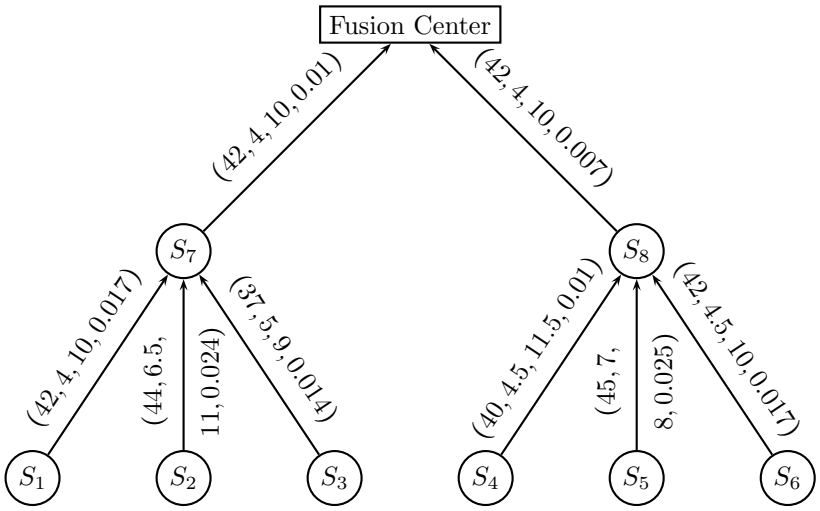

Figure 76: Tree detection network for the example problem. Labels on each edge represent μ_c, σ_c, e (in mJ), and Signal to noise ratio, respectively, for each source sensor.

Figure 77 shows the performance surface for the slotted ALOHA tree network in Figure 76, for the proposed design approach. The surface plots the deflection coefficient for different delay and network lifetime values. The system exhibits a similar behavior to the single hop ALOHA network studied in Chapter VI; for a fixed network lifetime, the deflection coefficient increases with the delay for detection, as more observations are expected at the fusion center. For a fixed delay for detection, the deflection coefficient decreases with network lifetime, as the energy budget allocated for each detection cycle decreases to prolong the network lifetime. Decreasing the energy budget reduces the probability of successful packet transmission, hence causing less observations at the fusion center.

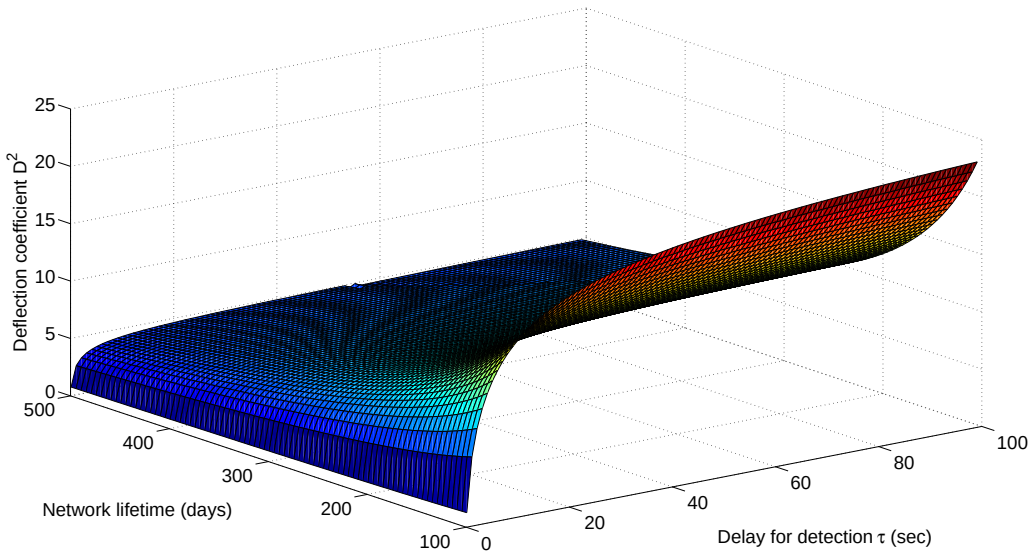

Figure 77: Deflection coefficient as it varies with the network lifetime and delay for detection for the ALOHA tree sensor network.

Figure 78 shows a contour plot for the deflection coefficient, where each curve corresponds to the set of pair values (Delay for detection, network lifetime) that gives rise to the indicated value of the deflection coefficient. Similar to the single hop case, to keep the deflection coefficient constant while increasing the network lifetime, the delay for detection has to increase also, so that more observations could be received in each detection cycle. This compensates for the energy decrease as a result of a prolonged network lifetime.

We resort to two dimensional plots to compare between the different design approaches. Figure 79 shows the deflection coefficient versus the delay for detection, where the network lifetime is set to 250 days. The decoupled design approach shows the worst performance, since it does not take into account the application layer, in addition to the decoupling between the physical and MAC layers. The max throughput design outperforms the decoupled design, since it integrates both the physical and MAC layers. The proposed cross-layer design approach outperforms the two other approaches, by integrating the application layer (quality of the sensors) into the design process. This performance enhancement comes with no additional complexity since the optimization problem is very similar in the cross-layer and the max throughput design approaches. Therefore, for any value of the delay for detection, the detection performance is the highest for the cross-layer design. As another

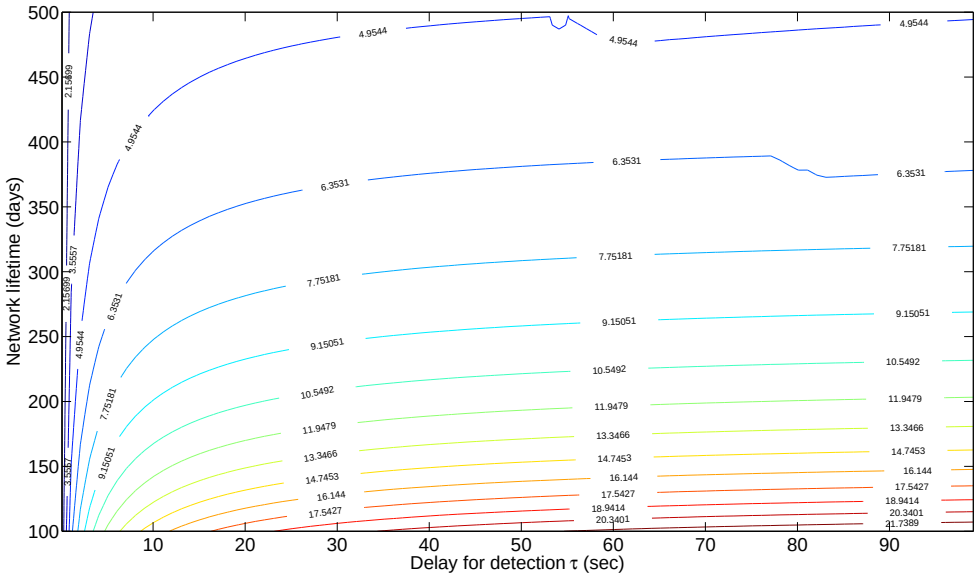

Figure 78: Contour plot for the deflection coefficient for the ALOHA tree sensor network. Each curve corresponds to the set of pairs (delay, lifetime) that leads to the indicated value of the deflection coefficient.

interpretation, to obtain the same detection performance from the other designs as in the cross-layer approach, the delay for detection has to increase significantly. Some values of the deflection coefficient may not be achievable by the other design approaches for any arbitrary value of the delay for detection, due to saturation of the deflection coefficient, as shown asymptotically in Figure 79.

Figure 79 also shows the deflection coefficient resulting from solving the global optimization problem in (244). We note that there is no loss of optimality for using the local optimization approach for very small delay for detection. As the delay increases, the local optimization results in a degraded performance. However, we note that the degradation is not significant. More importantly, the degradation does not increase significantly with further increase in the delay. Therefore, the local optimization approach has saved the system resources, with a small loss in the performance. We note that this result is particular to the given example network and system parameters. The degradation in performance due to local optimization has to be assessed based on the given system and constraints.

Figure 80 shows the deflection coefficient as it varies with the network lifetime, where delay for detection is set to 50 sec. The results are similar to the delay for detection study, where the

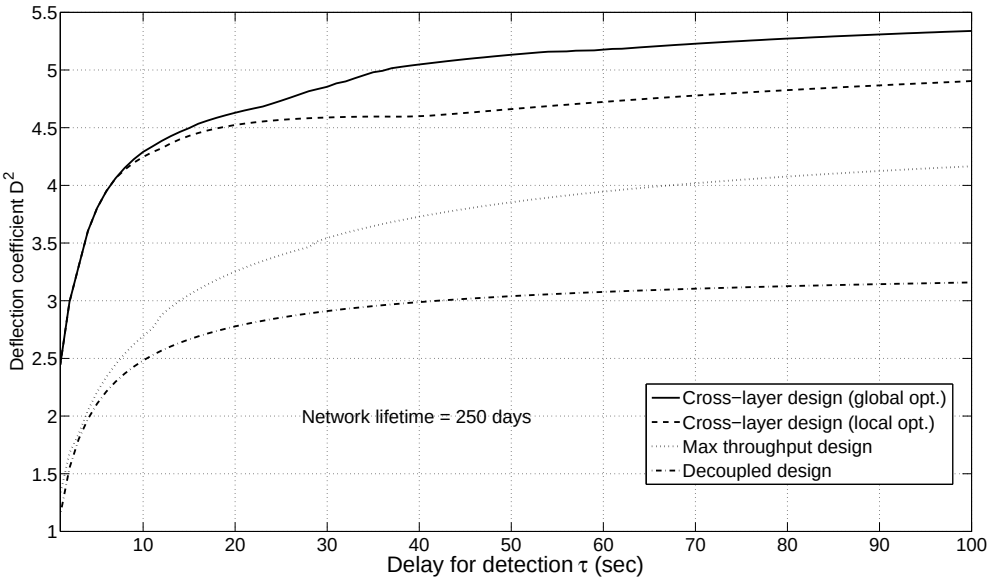

Figure 79: Deflection coefficient as it varies with the delay for detection. The proposed cross-layer design approach outperforms both the Max. throughput and decoupled design approaches for all values of the delay for detection. The performance loss due to local optimization is not significant.

proposed cross-layer approach outperforms the max. throughput and decoupled design approaches. Equivalently, for the same deflection coefficient, the network lifetime with the cross-layer design is longer. Similarly, performance degradation due to local optimization gets larger with increasing the network lifetime, but insignificant when compared to the saving in system resources.

VIII.6 In-Network Processing

Transmission of raw observations guarantees no loss of detection performance at the fusion center. On the down side, observations build-up and accumulate through the tree network. Therefore, the communication rate at relay nodes up in the tree hierarchy has to increase to cope with the volume of data coming from child nodes. This causes higher probability of information loss due to the high communication rate. Since higher relay nodes carry most of the information, losing such packets causes the loss of most of the information transmitted through the network. Another design approach is to perform in-network processing, thereby reducing the communication rate and increasing the probability of successful transmission. On the down side, this approach suffers from performance degradation due to the irrecoverable loss caused by the in-network processing. In

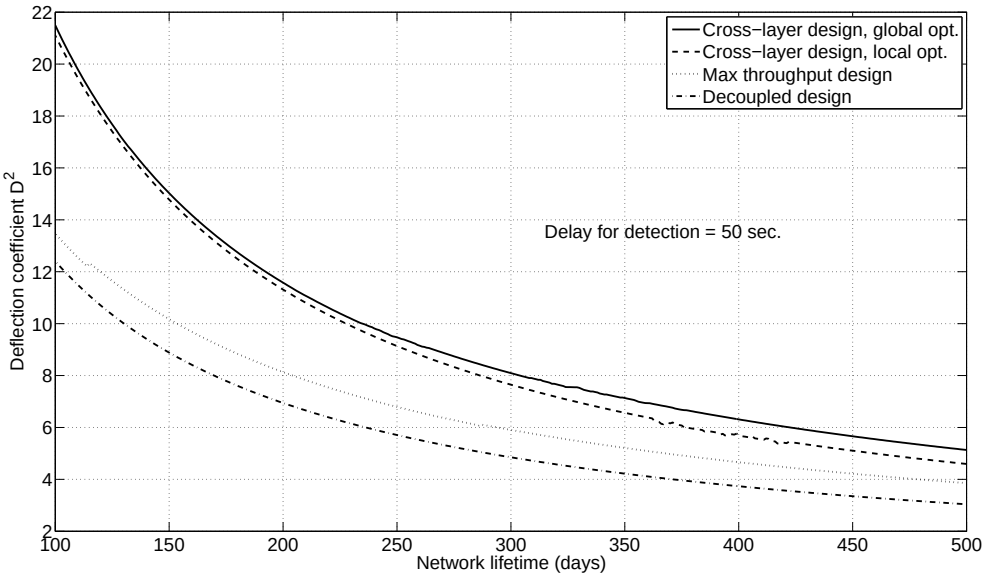

Figure 80: Deflection coefficient as it varies with the network lifetime. The CLD approach outperforms the decoupled and Max. throughput approaches. Max. throughput is always upper-bounded by the CLD for all values of the network lifetime. The performance loss due to local optimization is not significant.

this section, we formulate the in-network processing design problem and compare it to the direct transmission approach presented earlier in this chapter. We explain only the differences from the direct transmission design to avoid repetition.

VIII.6.1 Media Access Control Protocol Model

The MAC protocol is identical to the one presented in Section VIII.2.2, with one exception; after each sensor k collects its n_k observations in slot i, it calculates its LLR:

$$z_k = \frac{\mu^k}{{\sigma_s^k}^2} \sum_{j=1}^{n_k} x[j,i] \tag{258}$$

where x is a Gaussian random variable with $\mathcal{N}(0, {\sigma_s^k}^2)$ under $\mathcal{H}_0$ and $\mathcal{N}(\mu_k, {\sigma_s^k}^2)$ under $\mathcal{H}_1$. Z accordingly is a Gaussian random variable with $\mathcal{N}(0, n_k(\mu_k/\sigma_s^k)^2)$ under $\mathcal{H}_0$ and $\mathcal{N}(n_k(\mu_k/\sigma_s^k)^2, n_k(\mu_k/\sigma_s^k)^2)$ under $\mathcal{H}_1$. There is no loss of optimality in this process, since the LLR is optimal at the fusion center as observations are independent across sensors [67]. The LLR is then quantized using b_k bits, to

obtain the discrete random variable y_k:

$$y_k = Q(z_k; b_k) \tag{259}$$

This quantized version is transmitted to the parent node in the tree structure. Each sensor node forwards the quantized LLR of its descendants without further quantization, in addition to its own quantized LLR, to the next parent node. The process repeats until all observations arrive at the fusion center. Similar to (222), the communication rate for each sensor is given by:

$$\bar{R}_k = \frac{b_k L_i}{\tau} + \sum_{v \in \mathcal{C}_k} \lambda_v \bar{R}_v \tag{260}$$

We note here that the number of quantization bits is a design variable, different from one sensor to the other. The decision on how many quantization bits will be used is dependent on the sensor quality measures. Large number of quantization bits reduces the loss in the signal to noise ratio yet increases the probability of packet loss.

VIII.6.2 Sensing Model

We choose the following test statistic to be implemented at the fusion center:

$$V = \sum_{i_1=1}^{L_1} \sum_{v_1 \in \mathcal{C}_f} r_{v_1}[i_1] \left[y_{v_1} + \sum_{i_2=1}^{m_1} \sum_{v_2 \in \mathcal{C}_{v_1}} r_{v_2}[i_1 i_2] \left[y_{v_2}[j_2, i_1 i_2] + \ldots + \sum_{i_l=1}^{m_{l-1}} \sum_{v_l \in \mathcal{C}_{v_{l-1}}} r_{v_l}[i_1 \ldots i_l] y_{v_l}[j_l, i_l i_2 \ldots i_l] \right] \ldots \right] \tag{261}$$

This test statistic is sub-optimal. To obtain the optimal one, we need to take the LLR for the discrete random variables Y_i at the fusion center. Unfortunately, this problem does not have a closed form solution, and the detector performance is usually approximated using different statistical techniques [34]. We resort to the suboptimal statistic in (261), as it is similar to the one in (231) for the direct observation system, which facilitates the performance comparison. Now, to find the deflection coefficient for the statistic in (261), we need to calculate the expectation of V under both

$\mathcal{H}_0$ and $\mathcal{H}_1$, in addition to its variance under $\mathcal{H}_0$. We first need to define the quantization function in (259). We adopt the following quantizer:

$$Q(z) = \Delta\left(\left\lfloor \frac{z}{\Delta} \right\rfloor + \frac{1}{2}\right) \tag{262}$$

where Δ is the quantizer step size. We have the following proposition.

Proposition 11. *The deflection coefficient of the test statistic in (261), with the quantizer in (262), is given by:*

$$D^2 = \frac{\left(L_1 \sum_{v_1 \in \mathcal{C}_f} \lambda_{v_1} \left[n_{v_1} \left(\frac{\mu^{v_1}}{\sigma_s^{v_1}}\right)^2 + \delta_{v_1} + m_1 \sum_{v_2 \in \mathcal{C}_{v_1}} \lambda_{v_2} \left[n_{v_2} \left(\frac{\mu^{v_2}}{\sigma_s^{v_2}}\right)^2 + \delta_{v_2} \ldots m_l \sum_{v_l \in \mathcal{C}_{v_l}} \lambda_{v_l} n_{v_l} \left(\frac{\mu^{v_l}}{\sigma_s^{v_l}}\right)^2 + \delta_{v_l} \right] \ldots \right]\right)^2}{L_1 \sum_{v_1 \in \mathcal{C}_f} \lambda_{v_1} \left[n_{v_1} \left(\frac{\mu^{v_1}}{\sigma_s^{v_1}}\right)^2 + \delta'_{v_1} + m_1 \sum_{v_2 \in \mathcal{C}_{v_1}} \lambda_{v_2} \left[n_{v_2} \left(\frac{\mu^{v_2}}{\sigma_s^{v_2}}\right)^2 + \delta'_{v_2} + \ldots m_l \sum_{v_l \in \mathcal{C}_{v_l}} \lambda_{v_l} n_{v_l} \left(\frac{\mu^{v_l}}{\sigma_s^{v_l}}\right)^2 + \delta'_{v_l} \right] \ldots \right]} \tag{263}$$

where

$$\begin{aligned}
\delta &= \frac{\Delta}{\pi} \sum_{k=1}^{\infty} \frac{1}{k} \sin\left[\frac{2\pi k n}{\Delta} \left(\frac{\mu}{\sigma_s}\right)^2 \right] e^{-2\left(\frac{\pi k}{\Delta}\right)^2 n \left(\frac{\mu}{\sigma_s}\right)^2} \\
\delta' &= \left(\frac{\Delta}{\pi}\right)^2 \left[\sum_{k_1=1}^{\infty} \sum_{k_2=1}^{\infty} \frac{1}{2k_1 k_2} \left(\cos\left[\frac{2\pi(k_1 - k_2) n}{\Delta} \left(\frac{\mu}{\sigma_s}\right)^2 \right] e^{-2\left(\frac{\pi(k_1-k_2)}{\Delta}\right)^2 n \left(\frac{\mu}{\sigma_s}\right)^2} \right.\right. \\
&\quad \left.\left. - \cos\left[\frac{2\pi(k_1 + k_2) n}{\Delta} \left(\frac{\mu}{\sigma_s}\right)^2 \right] e^{-2\left(\frac{\pi(k_1+k_2)}{\Delta}\right)^2 n \left(\frac{\mu}{\sigma_s}\right)^2} \right) \right]
\end{aligned} \tag{264}$$

Proof. First we obtain the statistics of the quantized random variable Y. From (259) and (262):

$$E[Y] = \Delta\left(E\left[\left\lfloor \frac{Z}{\Delta} \right\rfloor\right] + \frac{1}{2}\right) \tag{265}$$

and using the series expansion of the floor function:

$$\lfloor x \rfloor = x - \frac{1}{2} + \frac{1}{\pi} \sum_{k=1}^{\infty} \frac{\sin(2\pi k x)}{k} \tag{266}$$

we get:

$$E[Y] = E[Z] + \frac{\Delta}{\pi}\sum_{k=1}^{\infty}\frac{1}{k}E\left[\sin\left(\frac{2\pi k}{\Delta}Z\right)\right] \tag{267}$$

Denote $\theta_k = 2\pi k/\Delta$, and using the expansion $\sin(x) = (e^{jx} - e^{-jx})/2$ to find the expectation for the second term:

$$\begin{aligned} E[Y] &= \mu_Z + \frac{\Delta}{\pi}\sum_{k=1}^{\infty}\frac{1}{k}\frac{1}{2j}\left(E\left[e^{j\theta_k Z}\right] - E\left[e^{-j\theta_k Z}\right]\right) \\ &= \mu_Z + \frac{\Delta}{\pi}\sum_{k=1}^{\infty}\frac{1}{k}\frac{1}{2j}\left(e^{j\theta_k\mu_z}E\left[e^{j\theta_k(Z-\mu_z)}\right] - e^{-j\theta_k\mu_z}E\left[e^{-j\theta_k(Z-\mu_z)}\right]\right) \end{aligned} \tag{268}$$

Using the exponential function expansion and noting that the odd central moments for the Gaussian distribution are equal to zero, we obtain:

$$\begin{aligned} E[Y] &= \mu_Z + \frac{\Delta}{\pi}\sum_{k=1}^{\infty}\frac{1}{k}\sin\left(\theta_k\mu_Z\right)e^{-\theta_k^2\sigma_Z^2} \\ &= \mu_Z + \frac{\Delta}{\pi}\sum_{k=1}^{\infty}\frac{\Delta}{k}\sin\left(\frac{2\pi k}{\Delta}\mu_Z\right)e^{-2\left(\frac{\pi k}{\Delta}\right)^2\sigma_Z^2} \end{aligned} \tag{269}$$

and using the distribution of Z in (258), we obtain:

$$E[Y;\mathcal{H}_0] = 0 \tag{270}$$

$$\begin{aligned} E[Y;\mathcal{H}_1] &= n\left(\frac{\mu}{\sigma_s}\right)^2 + \frac{\Delta}{\pi}\sum_{k=1}^{\infty}\frac{1}{k}\sin\left[\frac{2\pi kn}{\Delta}\left(\frac{\mu}{\sigma_s}\right)^2\right]e^{-2\left(\frac{\pi k}{\Delta}\right)^2 n\left(\frac{\mu}{\sigma_s}\right)^2} \\ &= n\left(\frac{\mu}{\sigma_s}\right)^2 + \delta \end{aligned} \tag{271}$$

For the variance:

$$\begin{aligned} \mathrm{var}[Y;\mathcal{H}_0] &= E[Y^2;\mathcal{H}_0] \\ &= \Delta^2 E\left[\left(\left\lfloor\frac{z}{\Delta}\right\rfloor + \frac{1}{2}\right)^2\right] \\ &= \sigma_Z^2 + \left(\frac{\Delta}{\pi}\right)^2 E\left[\left(\sum_{k=1}^{\infty}\frac{1}{k}\sin\left[\frac{2\pi k}{\Delta}Z\right]\right)^2\right] + \frac{2\Delta}{\pi}E\left[Z\sum_{k=1}^{\infty}\frac{1}{k}\sin\left(\frac{2\pi k}{\Delta}Z\right)\right] \end{aligned} \tag{272}$$

Similar to the derivation for the expected value, the last term vanishes since all moments are odd. Therefore:

$$\begin{aligned}\mathrm{var}[Y;\mathcal{H}_0] &= \sigma_Z^2 + \left(\frac{\Delta}{\pi}\right)^2 E\left[\sum_{k_1=1}^{\infty}\sum_{k_2=1}^{\infty}\frac{1}{k_1k_2}\sin\left[\frac{2\pi k_1}{\Delta}Z\right]\sin\left[\frac{2\pi k_2}{\Delta}Z\right]\right] \\ &= \sigma_Z^2 + \left(\frac{\Delta}{\pi}\right)^2 E\left[\sum_{k_1=1}^{\infty}\sum_{k_2=1}^{\infty}\frac{1}{k_1k_2}\left(\cos\left[\frac{2\pi(k_1-k_2)}{\Delta}Z\right] - \cos\left[\frac{2\pi(k_1+k_2)}{\Delta}Z\right)\right]\right] \end{aligned} \tag{273}$$

Similar to the expected value derivation, we use $\cos x = (e^{jx} - e^{-jx})/2$, and after some algebraic manipulations we obtain:

$$\begin{aligned}\mathrm{var}[Y;\mathcal{H}_0] &= n\left(\frac{\mu}{\sigma_s}\right)^2 + \left(\frac{\Delta}{\pi}\right)^2\left[\sum_{k_1=1}^{\infty}\sum_{k_2=1}^{\infty}\frac{1}{2k_1k_2}\left(\cos\left[\frac{2\pi(k_1-k_2)n}{\Delta}\left(\frac{\mu}{\sigma_s}\right)^2\right]e^{-2\left(\frac{\pi(k_1-k_2)}{\Delta}\right)^2 n\left(\frac{\mu}{\sigma_s}\right)^2}\right.\right. \\ &\quad \left.\left. - \cos\left[\frac{2\pi(k_1+k_2)n}{\Delta}\left(\frac{\mu}{\sigma_s}\right)^2\right]e^{-2\left(\frac{\pi(k_1+k_2)}{\Delta}\right)^2 n\left(\frac{\mu}{\sigma_s}\right)^2}\right)\right] \\ &= n\left(\frac{\mu}{\sigma_s}\right)^2 + \delta' \end{aligned} \tag{274}$$

Similar to the derivation of Proposition (9), we take the expectation and variance of (261), and using (270), (271), and (274), we obtain:

$$D^2 = \frac{\left(L_1\sum_{v_1\in\mathcal{C}_f}\lambda_{v_1}\left[n_{v_1}\left(\frac{\mu^{v_1}}{\sigma_s^{v_1}}\right)^2 + \delta_{v_1} + m_1\sum_{v_2\in\mathcal{C}_{v_1}}\lambda_{v_2}\left[n_{v_2}\left(\frac{\mu^{v_2}}{\sigma_s^{v_2}}\right)^2 + \delta_{v_2}\ldots m_l\sum_{v_l\in\mathcal{C}_{v_l}}\lambda_{v_l}n_{v_l}\left(\frac{\mu^{v_l}}{\sigma_s^{v_l}}\right)^2 + \delta_{v_l}\right]\ldots\right]\right)^2}{L_1\sum_{v_1\in\mathcal{C}_f}\lambda_{v_1}\left[n_{v_1}\left(\frac{\mu^{v_1}}{\sigma_s^{v_1}}\right)^2 + \delta'_{v_1} + m_1\sum_{v_2\in\mathcal{C}_{v_1}}\lambda_{v_2}\left[n_{v_2}\left(\frac{\mu^{v_2}}{\sigma_s^{v_2}}\right)^2 + \delta'_{v_2} + \ldots m_l\sum_{v_l\in\mathcal{C}_{v_l}}\lambda_{v_l}n_{v_l}\left(\frac{\mu^{v_l}}{\sigma_s^{v_l}}\right)^2 + \delta'_{v_l}\right]\ldots\right]} \tag{275}$$

■

The expression for the deflection coefficient in (275) is hard to optimize. However, we note from the proof that both the mean and variance degrade exponentially with the quantizer step size Δ. Since Δ is inversely proportional to the number of quantization bits, b_k, we can approximate the degradation in the signal to noise ratio for each sensor k by:

$$S = n_k\left(\frac{\mu_k}{\sigma^{k^2}}\right)^2\left(1 - 2^{-\beta b_k}\right) \tag{276}$$

where β specifies the decay rate, and depends on the range of the quantizer as well as the quantizer design. Now, we use the degraded SNR in (276) to define our approximate deflection coefficient as follows:

$$D^2 = L_1 \sum_{v_1 \in \mathcal{C}_f} \lambda_{v_1} \left[n_{v_1} c'_{v_1} + m_1 \sum_{v_2 \in \mathcal{C}_{v_1}} \lambda_{v_2} \left[n_{v_2} c'_{v_2} + \ldots + m_{d-1} \sum_{v_l \in \mathcal{C}_{v_{l-1}}} \lambda_{v_l} n_{v_l} c'_{v_l} \right] \ldots \right] \tag{277}$$

where:

$$c'_v = \left(\frac{\mu^v}{\sigma_s^v} \right)^2 \left(1 - 2^{-\beta b_v} \right) \tag{278}$$

For comparison purposes with the direct transmission approach, we use the same number of observations for each sensor, and the same number of slots, as in the direct transmission case. From (222), we obtain:

$$L_i n_{v_i} = \frac{\tau}{b} \left(\bar{R}_{v_i} - \sum_{v_j \in \mathcal{C}_{v_i}} \lambda_{v_j} \bar{R}_{v_j} \right) = \frac{\tau}{b} \left(\bar{R}_{v_i} - r_{v_i} \right) = \frac{\tau}{b} u_{v_i} \tag{279}$$

where $\bar{R}_{v_i}$ is the average communication rate for sensor v_i, r_{v_i} is the average communication rate for $\mathcal{C}_{v_i}$, and b is the number of quantization bits in the direct transmission case. The values of these three quantities are obtained from the solution of the optimization problem in the direct transmission case. The objective function could be expressed as:

$$D^2 = \frac{\tau}{b} \sum_{v_1 \in \mathcal{C}_f} \lambda_{v_1} \left[u_{v_1} c'_{v_1} + \sum_{v_2 \in \mathcal{C}_{v_1}} \lambda_{v_2} \left[u_{v_2} c'_{v_2} + \sum_{v_3 \in \mathcal{C}_{v_2}} \lambda_{v_3} \left[u_{v_3} c'_{v_3} + \sum_{v_4 \in \mathcal{C}_{v_3}} \ldots + \sum_{v_l \in \mathcal{C}_{v_{l-1}}} \lambda_{v_l} u_{v_l} c'_{v_l} \right] \right] \ldots \right] \tag{280}$$

VIII.6.3 Optimal Detection with In-Network Processing

We note that the objective function in (280) has the same recursive structure as the direct transmission design. Specifically, we can express the objective function using the following recursive

equations:

$$D^2 = \frac{\tau}{b} J_{FC} \tag{281}$$

$$J_k = \sum_{v \in \mathcal{C}_k} \lambda_v \left[u_v c_v' + J_v \right] \tag{282}$$

$$\lambda_v = q_v \left[\prod_{k \in \mathcal{B}_v} (1 - q_k) \right] \Phi \left[a_v - \left(\frac{10}{\sigma_c^v} \right) \log q_v \left(2^{[b_v (L_i/\tau) + g_v]/W} - 1 \right) \right] \tag{283}$$

$$g_k = \sum_{v \in \mathcal{C}_k} \lambda_j \left[\frac{b_v L_i}{\tau} + g_v \right] \tag{284}$$

where $J_v = 0$ and $g_v = 0$ for leaf nodes, and:

$$a_v = \frac{1}{\sigma_c^v} \left(10 \log \frac{p_v - \alpha}{N_0 W} - \mu_c^v \right) \tag{285}$$

$$c_v' = \left(\frac{\mu^v}{\sigma_s^v} \right)^2 \left(1 - 2^{-\beta b_v} \right) \tag{286}$$

$$u_v = \bar{R}_v - r_v \tag{287}$$

and $r_v = 0$ for leaf nodes. Accordingly, we adopt the same local approach presented in (VIII.3) to solve for the optimal design variables. The local optimization problem at parent node k is expressed as:

$$\begin{aligned} \max_{\boldsymbol{q}, \boldsymbol{b}} \; & \sum_{v \in \mathcal{C}_k} q_v \left[\prod_{i \in \mathcal{B}_v} (1 - q_i) \right] \Phi \left[a_v - \left(\frac{10}{\sigma_c^v} \right) \log q_v \left(2^{[b_v (L/\tau) + g_v]/W} - 1 \right) \right] \left[u_v \left(\frac{\mu^v}{\sigma_s^v} \right)^2 \left(1 - 2^{-\beta b_v} \right) + J_v \right] \\ \text{s.t.} \; & 0 \le q_v \le 1 \\ & b_v \in \mathbb{N} \end{aligned} \tag{288}$$

We note that J_v and g_v are fixed values, obtained from solving the local optimization problems at lower levels in the hierarchy. The notation for the local optimization problem with in-network processing is illustrated in Figure 81.

We denote the decision variables by $\boldsymbol{x} = \begin{bmatrix} q_1 & q_2 & \dots & q_{N_k} & b_1 & b_2 & \dots & b_{N_k} \end{bmatrix}$ where $N_k = |\mathcal{C}_k|$ and $\boldsymbol{x} \in \mathbb{R}^{2N_k}$. Let the local objective function be denoted $J(\boldsymbol{x})$, and ignoring the fact that b is

integer-valued to avoid the discrete optimization problem, then the optimization problem could be rewritten on the form:

$$\begin{aligned} &\min_{\boldsymbol{x}} \quad -J(\boldsymbol{x}) \\ &\text{subject to } A\boldsymbol{x} \geq \boldsymbol{b} \end{aligned} \tag{289}$$

where

$$A = \begin{bmatrix} I & -I & \mathbf{0} \\ \mathbf{0} & \mathbf{0} & I \end{bmatrix}^T, \qquad \boldsymbol{b} = \begin{bmatrix} \mathbf{0} & -\mathbf{1} & \mathbf{0} \end{bmatrix}^T \tag{290}$$

I is the identity matrix, and $\mathbf{0}(\mathbf{1})$ is the vector/matrix of all zeros (ones) with appropriate dimensions. We present the following proposition without proof, which is very similar to Proposition (10), since the two optimization problems have the same structure.

Proposition 12. *The maximum value of the objective function in (289) occurs either when one sensor transmits with probability one and all other sensors remain silent, or at a stationary point of the objective function, i.e. at* $\boldsymbol{x}^*$ *where* $\nabla J(\boldsymbol{x}^*) = 0$.

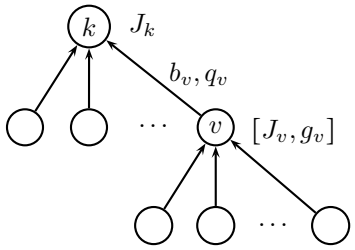

Figure 81: Notation for the local optimization problem for the tree sensor network with in-network processing. The local optimization runs at sensor node k to calculate the design variables for sensor nodes $v \in \mathcal{C}_k$. J_v and g_v are calculated from running the local optimization algorithm at sensor node v.

VIII.6.4 Comparison to the Direct Transmission Approach

For comparison, we used the example network in Figure 76. We use the same system parameters and assume that $\beta = 0.003$ for the local quantizer. Figure 82 compares the deflection coefficient for the direct transmission and in-network processing designs for different delay for detection values. We note that the direct transmission design outperforms the design with local quantization for all delay for detection values below a threshold value τ_{th}. Increasing the delay for detection further causes the in-network processing design to outperform. The first region, i.e. $\tau < \tau_{\text{th}}$ is where the signal processing aspect of the system dominates. In this region, the loss due to quantization cannot be compensated since the delay allowed is small and not enough measurements can be collected to compensate for the quantization loss. The direct transmission scheme outperforms since information is transmitted without prior processing (assuming large number of quantization bits so that quantization error is neglected). In addition, shorter delay allows the reporting energy to be concentrated over a smaller duration, resulting in higher power for each sensor. The high power mitigates the channel impairments and therefore the communication network aspect is not dominant. The situation is reversed when $\tau > \tau_{\text{th}}$. In this region, energy is distributed over longer period, which results in low sensor transmission power and hence the channel impairment is dominant in determining the system performance. The in-network processing design requires lower communication rate thereby mitigating the channel impairment. On the other hand, the direct transmission design requires higher communication rate, resulting in packet loss and degraded system performance.

The delay threshold depends mainly on the quantizer design, summarized by the parameter β, in addition to the signal to noise ratio for each sensor and the energy allocated for the detection process. Figure 83 shows the variation in the delay threshold with the quantizer design parameter β. As β increases, the exponential decay rate for quantization effect is much faster, hence the threshold is lower.

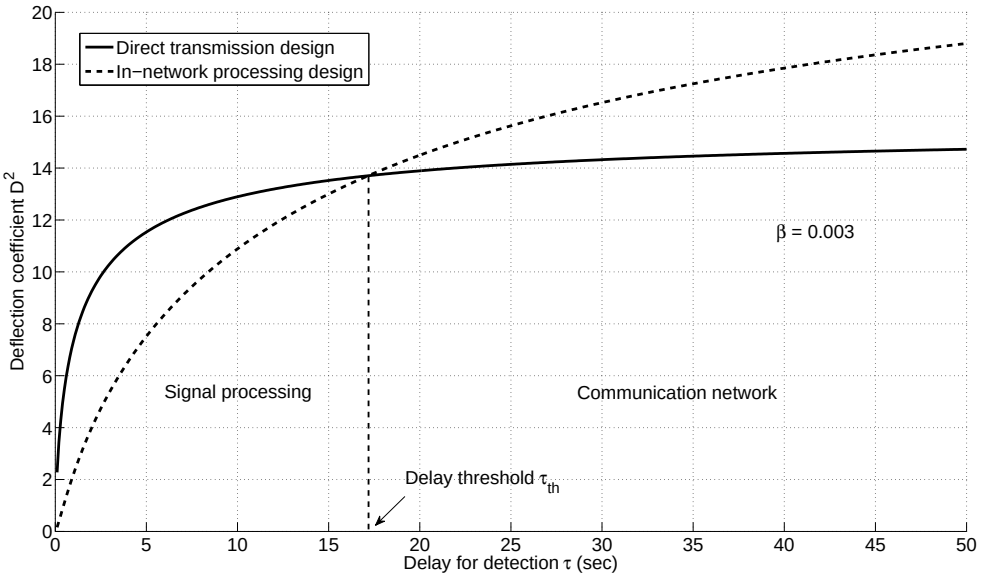

Figure 82: Deflection coefficient for direct transmission and in-network processing designs. The direct transmission design outperforms for delays $< \tau_{\text{th}}$ where the signal processing aspect dominates. The in-network processing design outperforms for delays $> \tau_{\text{th}}$ where the communication network aspect dominates.

VIII.7 Summary

In this chapter, we continued to apply the model-based approach to design a tree-structured, slotted ALOHA sensor network, for detection applications. We developed an integrated model for the detection system and integrated the QoI, REI, and CSI quality measures into the design process. We designed the communication rate and transmission probability for each tree node.

The proposed model-based approach shows significant performance gain over the classical decoupled and maximum throughput approaches commonly adopted to design sensor networks. This performance enhancement comes with no additional complexity since the optimization problem is very similar to the Max. throughput design case.

For applications with stringent delay requirements, we show that system design with direct transmission of sensor observations results in better performance since the channel impairment is unlikely to play a major role. If the application can tolerate longer delays, then the design with in-network processing results in better detection performance, as the communication network becomes a dominant factor in determining the system performance.

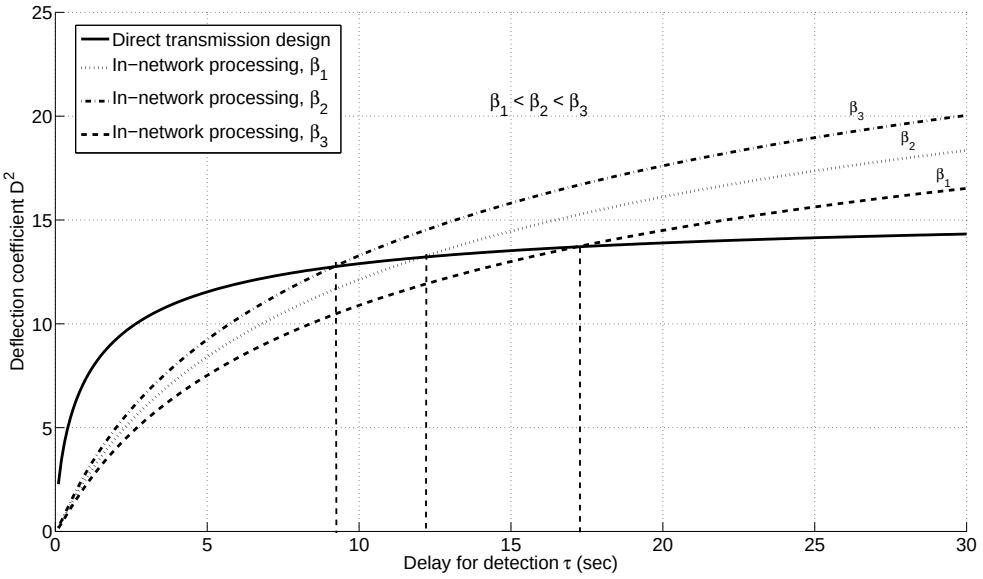

Figure 83: Variation of detection threshold with quantizer design parameter. As β increases, the exponential decay rate for the quantization loss is higher, hence lower detection threshold.

Several extensions are possible for the work presented in this chapter. We assumed that the energy is preallocated to each sensor based on its energy reserve. Optimal energy allocation to maximize the detection performance, akin to Chapters VI and VII, is one possible extension. The network lifetime definition, as well as the energy constraints, are not entirely trivial, as care should be taken that the energy of relay nodes is not depleted before its descendants. Another possible extension is the design of TDMA tree networks, where all transmissions are pre-scheduled, and the performance comparison to the ALOHA network presented in this chapter. The performance comparison with the one-hop sensor network under energy constraint is also of practical interest.

CHAPTER IX

Conclusions

In this dissertation, we pursued a model-based approach for detection in Cyber-Physical Systems. We explored the power of different modeling approaches to represent component behaviors as well as the interactions between different system components. We used the physics-based modeling approach to develop an accurate model for aircraft power generators. We showed the model power in representing nominal as well as different faulty behaviors of the system. We then explored statistical modeling approaches, and developed an algorithm to detect intermittent and incipient faults in physical systems. Finally, we explored the power of integrating the models of system components, in order to optimize detection systems, while simultaneously achieving efficient resource utilization to meet the imposed resource constraints on the system.

IX.1 Summary of Contributions

The main goal of this dissertation work is to enhance the performance of detection systems, by the proper choice of: (1) the system components to be modeled, (2) the modeling paradigm for each system component, and (3) the types of component interactions to be captured in the integrated system model. We achieved this goal by considering different modeling paradigms and system components for different detection problems. In the following, we list our contributions for each class of detection problems addressed.

IX.1.1 Physics-based Modeling for Fault Detection

We have developed a novel physics-based model for the complete brushless AC generator. The model incorporates the exciter generator, rectifier circuit, and the main generator in one hybrid dynamical model. The developed model captures both the continuous and discrete dynamics of the system. We developed the model using the actual machine variables without applying any transformations.

Therefore, the model is a general representation for the machine under both nominal and faulty behaviors. We showed that any combination of open-circuit diode faults could be modeled with a subset of the system hybrid automaton states. We developed an algorithm to identify the valid states for each combination of diode faults. We implemented the model such that any fault profile in any of the system parameters could be simulated at run time. The simulation results also showed the power of the rotating part winding currents in discriminating between diode faults.

IX.1.2 Statistical Modeling for Intermittent and Incipient Fault Detection

We developed a general detection algorithm to detect and distinguish between abrupt persistent, abrupt intermittent, and incipient faults. The detector has a number of thresholds to control different performance measures according to the given application. The detector also returns an estimate for the fault parameters, to assist in the subsequent decision making process. Since the detector is based on the GLRT, it is not limited to the fault profiles presented in this dissertation. In fact, the detection algorithm could be applied to any fault profile, provided that the test statistic is replaced by the one calculated for the new fault profile. We used this algorithm in NASA DXC'10 diagnostics competition and placed 2nd.

IX.1.3 Model-based detection in Wireless Sensor Networks

We developed a unified design process, where the designer can choose the subsystem components to be modeled, and the model attributes, based on the performance and quality measures of the application. The design process is general and could be applied to any CPS application, not only detection applications. Following the design framework, we developed an integrated model for the wireless sensor network in detection applications. The model includes the system, sensing, and different networking aspects. The network component captures the physical layer as well as slotted ALOHA and TDMA MAC sublayers. The model also encompasses different quality measures that are typically treated separately in the literature. We used the developed model to design a complete transmission control policy for the sensor network that includes the communication rate, transmission power, and medium access control parameters for each sensor. We carried out the

design process for both the classical single hop network (parallel topology), as well as the tree topology network, and showed that our design approach results in significant detection performance improvement over the classical design approaches, where either the network is ignored altogether, or designed to satisfy performance measures that are not relevant to the application. In addition, we conducted a comparative study between TDMA and slotted ALOHA, and showed the conditions under which each protocol achieves a better detection performance over the other. These conditions provide a guideline for the designer to choose between the two protocols based on the available system resources and design constraints. Finally, we considered the design problem with in-network processing, where local observations are quantized before transmission. We compared the in-network processing scheme to the direct transmission scheme, and showed the conditions under which each scheme outperforms.

IX.2 Conclusions and Future Directions

Although the studies considered in this dissertation show the power of different modeling approaches, as well as the impact of integrating system components in one unified model on the system performance, the dissertation work also highlights some future research directions, as well as limitations that could be addressed in future research. We highlight some of these possible research directions in the following.

IX.2.1 Physics-based Modeling

We showed the power of physics-based modeling in the developed generator model. Such detailed models are indispensable in understanding the machine behavior under both nominal and faulty conditions. However, building such models is very hard and time consuming. In addition, it may not be efficient for real-time simulations. For example, although the developed generator model was accurate and scalable, it was inefficient from the simulation time aspect. That is mainly because at each time step, the simulator has to calculate the value of different matrices in addition to calculating the inverse of a large 12×12 matrix, which is a computationally expensive task. Since

typical engineering systems have a large number of components with complex interactions, including all components and interactions makes the modeling task intractable. Therefore, the model should include only the components and interactions relevant to the objective of the study. This requires that the modeling objective should be as clear as possible before starting the modeling task. As an example, in the generator study, if the objective is to understand the behavior of the system with only the main generator faults, then abstract modeling for the exciter generator and the rectifier circuit would be sufficient. If diode faults are the objective of the study, then a detailed model is necessary for the exciter generator, and the main generator model maybe abstracted. On the other hand, if the objective of the model is the run-time system simulation, then a thorough study for the system components to be included, and their modeling paradigm, is needed.

Since modeling is an iterative process, it is possible to start with a complex model and simplify it by close examination of the system behavior under nominal and faulty conditions. One example is the aircraft generator, where the angular velocity was found to be approximately constant under a variety of faulty conditions. Using this observation, the angular velocity could be assumed constant, resulting in a linear system, which is easier to model and simulate.

Even with sophisticated models, some fault types are hard to model, either because of the complexity of the physical phenomena associated with the fault, or because the consequences of the fault are unknown. An example is short circuit winding faults in synchronous generators. In such scenarios, physics-based modeling will be of limited use in fault detection and isolation studies. An alternative approach is to use statistical models if faulty data could be obtained from real life experiments. A hybrid detection scheme, where physics-based models and statistical models augment each other, is an interesting research direction.

One limitation of the developed generator model is that it represents the complete system using a single unified state space model. This was required in the study to build a hybrid observer that is capable of estimating the hidden system states. Therefore, a complete mathematical model was needed. However, changes in any system component will require a re-derivation of the complete mathematical model. This approach may not be practical for studies where the main objective is

to simulate and compare different design alternatives. In such cases, component-based modeling gives the flexibility to model each system component separately, and to interchange components during the design process. Although the simulation solver transfers the component-based model into a state space model for the complete system, this process is transparent to the designer and is done automatically without user intervention. Automating the design process is important in modern systems design, and we will revisit this idea when discussing future research for model-based detection in sensor networks.

IX.2.2 Statistical Modeling

Statistical modeling is a powerful approach to detect and isolate faults in complex engineering systems. It provides a solution for some engineering problems where physics-based modeling approaches have limited use. However, the detection performance relies heavily on the underlying observation model. Many factors affect the choice of the observation model, including: (1) prior knowledge about the system behavior, (2) existing data from real-life systems, and (3) model tractability, among others. Often times, it is not easy to validate the assumed model. As an example, intermittent faults were assumed to follow a Markov Chain stochastic model. This assumption is very hard to verify in practice. Intermittent faults tend to take place spontaneously in the system, and in many cases, it is not known if what happened is really an intermittent fault. On the other hand, injecting an intermittent fault in the system will not lead to accurate information about the fault profile since the fault injection process itself has to follow a pre-defined stochastic model, which defeats the purpose of the study. We envision that the solution to this problem is to focus on the robustness of the signal processing algorithms with respect to the data model parameters, rather than trying to verify that the data model is an accurate representation for the system. The challenge here is to select a model that is a good representation of the system, yet robust, *to a certain degree*, to modeling and noise inaccuracies.

In this dissertation, we assumed Gaussian statistical models, where the measurements are assumed to follow a Gaussian distribution. This assumption may not be valid in some detection

problems, and building detectors that are robust to noise variations may not be possible if the noise profiles vary considerably. Even with the Gaussian assumption, we have shown in this dissertation that tuning the sequential detectors does not follow rigorous rules due to the lack of closed form expressions for the detector performance. In all these cases, suboptimal numerical detection algorithms that are adaptive based on the online conditions represent an interesting research direction.

The detection of an intermittent fault, and the estimation of the fault parameters, represent the first steps in the health management process. After fault detection and isolation, the health management system has to decide on the proper action to protect the monitored system. The appropriate action should depend, not only on the faulty component, but also on several other factors. Among these factors are: (1) the magnitude of the fault, (2) fault average persistence time, (3) fault average recurrence rate, (4) criticality level of the function performed by the faulty component, and (5) severity level of the impact of the component failure on the system, environment, and human life. The inclusion of such information in the decision-making process prevents premature decisions that may unnecessarily abort the system mission for a fault that occurred spontaneously in the system. To the best of our knowledge, there are no standard measures for each system component that could be used to define a mapping from the fault information to an appropriate decision based on the faulty component. The definition of such standard measures, as well as the development of standard design processes, with associated software tools, where such measures are incorporated, is an important research direction.

IX.2.3 Model-based detection in Wireless Sensor Networks

We showed in this dissertation that the detection performance could be enhanced considerably by integrating the communication functions into the design process. Although the approach is quite general, some of our assumptions have limitations and could be relaxed in future research work. For example, we assumed fixed sensors, where the relative positions between the sensor nodes and the fusion center do not change. This assumption may be violated in some practical systems for either the sensors, the fusion center, or both. As an example scenario, the fusion center may be fixed and

remotely located at a decision center, while sensors are moving around a surveillance area, either randomly or according to a pre-defined route. In another scenario, the sensors may be fixed, while the fusion center is located on a moving vehicle, e.g. aircraft, that approaches the surveillance area to interrogate information from the dropped sensors. In both of these scenarios, the stationarity assumption is violated. The work could be extended to include the effect of mobility, e.g. small scale fading in the communication channel, but the analysis would be much more involved.

We considered in this dissertation the decentralized scheme, where the fusion center is responsible for the optimization as well as the decision-making task. This scheme becomes impractical when the sensor network size becomes large. As an example, we showed in this dissertation how the optimization problem for the tree network grows rapidly with the network size. We resorted to a suboptimal solution where the optimization problem is solved locally at each parent node. This approach could be generalized to consider distributed detection, where there is no central node to make a final decision. Rather, sensors have limited communication with its neighbours, and the objective is to reach a consensus about the final decision. Consensus algorithms in the context of decentralized detection have been considered recently, but the inclusion of different quality measures, similar to the work in this dissertation, represents a future research direction.

In the process of developing an integrated system model, we made some simplifications, as well as abstractions, in the protocol description. The main reason was to obtain a tractable solution that gives us an insight into the problem. However, compared to practical sensor network protocols, this may be an oversimplification for the network functions. An experimental setup, where existing communication protocols are used, e.g. Zigbee, is an important extension to our work, that may lead to more insight and/or new research directions.

The work presented in this dissertation revealed the complexity of the design process when integrating different system components. Practical engineering systems tend to be much more complex than the detection systems described in this dissertation. With such systems, it is extremely hard to model and optimize the system using analytical techniques. For the model-based approach to be

effective in practice, software tools need to be developed to automate the design process. In a typical design scenario, the designer will define the performance measures, quality measures, component models, and the design variables. The integration process may be accomplished by a simulator, and a numerical optimizer will return the design variables. The software tools will allow also much faster iterations through the design process.

BIBLIOGRAPHY

[1] E. A. Lee, "Cyber physical systems: Design challenges," in *International Symposium on Object/Component/Service-Oriented Real-Time Distributed Computing (ISORC)*, May 2008, invited Paper. [Online]. Available: http://chess.eecs.berkeley.edu/pubs/427.html

[2] President's Council of Advisors on Science and Technology, "Designing a digital future: Federally funded research and development in networking and information technology," Executive Office of the President, PCAST, Tech. Rep., 2010.

[3] A. A. I. B. AAIB, "Report on the serious incident to Airbus A319-111, registration G-EZAC near Nantes, France, on 15 september 2006," AAIB, Tech. Rep., August 2009. [Online]. Available: www.aaib.gov.uk

[4] T. Kurtoglu, S. Narasimhan, S. Poll, D. Garcia, L. Kuhn, J. de Kleer, and A. Feldman, "Second International Diagnostic Competition (DXC'10), Industrial Track, Diagnostic Problem Description," NASA Ames Research Center, Tech. Rep., 2010, https://www.phmsociety.org/competition/dxc/10.

[5] A. Tantawy, X. Koutsoukos, and G. Biswas, "Robust differential protection with intermittent cable faults for aircraft AC generators." Annual Conference of the Prognostics and Health Management Society, PHM09, 2009.

[6] ——, "Aircraft Generators: Hybrid Modeling and Simulation for Fault Detection," *IEEE Transactions on Aerospace and Electronic Systems*, Accepted for publication.

[7] T. Batzel and D. Swanson, "Prognostic health management of aircraft power generators," *IEEE Transactions on Aerospace and Electronic Systems*, vol. 45, no. 2, pp. 473–482, April 2009.

[8] A. Tantawy, X. Koutsoukos, and G. Biswas, "Transmission Control Policy Design for Decentralized Detection in Sensor Networks," in *IEEE International Conference on Distributed Computing in Sensor Systems, DCOSS 2011*, Barcelona, Spain, June 27-29 2011.

[9] ——, "Transmission Control Policy Design for Decentralized Detection in Tree Topology Sensor Networks," in *14th International Conference on Information Fusion, Fusion 2011*, Chicago, IL, July 5-8 2011.

[10] S. M. Kay, *Fundamentals of Statistical Signal Processing, Volume 2: Detection Theory*, ser. Prentice Hall Signal Processing Series, A. V. Oppenheim, Ed. Prentice Hall PTR, 1998.

[11] T. K. Moon and W. C. Stirling, *Mathematical Methods and Algorithms for Signal Processing*. Prentice Hall, Upper Saddle River, NJ, 2000.

[12] Z. Chair and P. Varshney, "Distributed Bayesian hypothesis testing with distributed data fusion," *IEEE Transactions on Systems, Man and Cybernetics*, vol. 18, no. 5, pp. 695–699, Sep/Oct 1988.

[13] B. Chen, L. Tong, and P. K. Varshney, "Channel-aware distributed detection in wireless sensor networks," *IEEE Signal Processing Magazine*, July 2006.

[14] C. Bisdikian, L. Kaplan, M. Srivastava, D. Thornley, D. Verma, and R. Young, "Building principles for a quality of information specification for sensor information," *12th International Conference on Information Fusion, FUSION '09.*, pp. 1370 –1377, July 2009.

[15] I. Hoballah and P. Varshney, "An information theoretic approach to the distributed detection problem," *IEEE Transactions on Information Theory*, vol. 35, no. 5, pp. 988–994, Sep 1989.

[16] D. J. C. MacKay, *Information Theory, Inference, and Learning Algorithms*. Cambridge University Press, 2003.

[17] S. M. Ali and S. D. Silvey, "A general class of coefficients of divergence of one distribution from another," *Journal of the Royal Statistical Society, Series B (Methodological)*, vol. 28, no. 1, pp. 131–142, 1966.

[18] T. M. Cover and J. A. Thomas, *Elements of Information Theory*, 2nd ed. Wiley-Interscience, 2006.

[19] J. N. Tsitsiklis, "Decentralized detection," *Advances in Signal Processing*, vol. 2, pp. 297–344, 1993.

[20] P. K. Varshney, *Distributed Detection and Data Fusion*. Springer, 1996.

[21] L. K. Ekchian and R. R. Tenney, "Detection networks," *21st IEEE Conference on Decision and Control*, vol. 21, pp. 686–691, Dec. 1982.

[22] S. Alhakeem and P. Varshney, "A unified approach to the design of decentralized detection systems," *IEEE Transactions on Aerospace and Electronic Systems*, vol. 31, no. 1, pp. 9–20, Jan 1995.

[23] W. P. Tay, J. Tsitsiklis, and M. Win, "Data fusion trees for detection: Does architecture matter?" *IEEE Transactions on Information Theory*, vol. 54, no. 9, pp. 4155–4168, Sept. 2008.

[24] ——, "On the impact of node failures and unreliable communications in dense sensor networks," *IEEE Transactions on Signal Processing*, vol. 56, no. 6, pp. 2535–2546, June 2008.

[25] ——, "Bayesian detection in bounded height tree networks," *IEEE Transactions on Signal Processing*, vol. 57, no. 10, pp. 4042–4051, Oct. 2009.

[26] W. Li and H. Dai, "Energy-efficient distributed detection via multihop transmission in sensor networks," *IEEE Signal Processing Letters*, vol. 15, pp. 265–268, 2008.

[27] Y. Yang, R. Blum, and B. Sadler, "Energy-efficient routing for signal detection in wireless sensor networks," *IEEE Transactions on Signal Processing*, vol. 57, no. 6, pp. 2050 –2063, June 2009.

[28] Z. M. Charbiwala, S. Zahedi, Y. Kim, Y. H. Cho, and M. B. Srivastava, "Toward quality of information aware rate control for sensor networks," *Fourth International Workshop on Feedback Control Implementation and Design in Computing Systems and Networks, San Francisco*, April 2009.

[29] P. Swaszek and P. Willett, "Parley as an approach to distributed detection," *IEEE Transactions on Aerospace and Electronic Systems*, vol. 31, no. 1, pp. 447 –457, Jan. 1995.

[30] P. S. Fiske, *Put Your Science to Work: The Take-Charge Career Guide for Scientists*, 2nd ed. American Geophysical Union, 2000.

[31] V. V. Veeravalli and J.-F. Chamberland, "Detection in sensor networks," in *Wireless Sensor Networks: Signal Processing and Communications Perspectives*, A. Swami, Q. Zhao, Y.-W. Hong, and L. Tong, Eds. John Wiley & Sons, Ltd, 2007, ch. 6, pp. 119–148.

[32] Q. Zhao, A. Swami, and L. Tong, "The interplay between signal processing and networking in sensor networks," *IEEE Signal Processing Magazine*, vol. 23, no. 4, pp. 84–93, July 2006.

[33] X. Zhang, P. Vincent, and M. Chiang, "Optimal power allocation for distributed detection over MIMO channels in wireless sensor networks," *IEEE Transactions on Signal Processing*, vol. 56, no. 9, pp. 4124 –4140, Sept. 2008.

[34] B. Chen, R. Jiang, T. Kasetkasem, and P. K. Varshney, "Channel aware decision fusion in wireless sensor networks," *IEEE Transactions on Signal Processing*, vol. 52, no. 12, pp. 3454–3458, Dec. 2004.

[35] K. Liu, H. El Gamal, and A. Sayeed, "Decentralized inference over multiple-access channels," *IEEE Transactions on Signal Processing*, vol. 55, no. 7, pp. 3445–3455, July 2007.

[36] T. Duman and M. Salehi, "Decentralized detection over multiple-access channels," *IEEE Transactions on Aerospace and Electronic Systems*, vol. 34, no. 2, pp. 469–476, Apr 1998.

[37] S. C. A. Thomopoulos and L. Zhang, "Distributed decision fusion with networking delays and channel errors," *Inform. Sci.*, vol. 66, pp. 91–118, 1992.

[38] A. Reibman and L. Nolte, "Optimal design and performance of distributed signal detection systems with faults," *IEEE Transactions on Acoustics, Speech and Signal Processing*, vol. 38, no. 10, pp. 1771–1782, Oct 1990.

[39] R. R. Tenney and N. R. Sandell, "Detection with distributed sensors," *IEEE Transactions on Aerospace and Electronic Systems*, vol. AES-17, no. 4, pp. 501–510, July 1981.

[40] I. Hoballah and P. Varshney, "Distributed Bayesian signal detection," *IEEE Transactions on Information Theory*, vol. 35, no. 5, pp. 995–1000, Sep 1989.

[41] A. Reibman and L. Nolte, "Optimal detection and performance of distributed sensor systems," *IEEE Transactions on Aerospace and Electronic Systems*, vol. AES-23, no. 1, pp. 24–30, Jan. 1987.

[42] ——, "Design and performance comparison of distributed detection networks," *IEEE Transactions on Aerospace and Electronic Systems*, vol. AES-23, no. 6, pp. 789–797, Nov. 1987.

[43] Z.-B. Tang, K. Pattipati, and D. Kleinman, "An algorithm for determining the decision thresholds in a distributed detection problem," *IEEE Transactions on Systems, Man and Cybernetics*, vol. 21, no. 1, pp. 231–237, Jan/Feb 1991.

[44] C. Helstrom, "Gradient algorithm for quantization levels in distributed detection systems," *IEEE Transactions on Aerospace and Electronic Systems*, vol. 31, no. 1, pp. 390–398, Jan 1995.

[45] J. N. Tsitsiklis, "On threshold rules in decentralized detection," vol. 25, pp. 232–236, Dec. 1986.

[46] M. Cherikh and P. Kantor, "Counterexamples in distributed detection," *IEEE Transactions on Information Theory*, vol. 38, no. 1, pp. 162–165, Jan 1992.

[47] J. N. Tsitsiklis, "Decentralised detection with a large number of sensors," *Mathematics of Control, Signals, and Systems*, vol. 1, pp. 167–182, 1988.

[48] M. Longo, T. Lookabaugh, and R. Gray, "Quantization for decentralized hypothesis testing under communication constraints," *IEEE Transactions on Information Theory*, vol. 36, no. 2, pp. 241–255, Mar 1990.

[49] C.-C. Lee and J.-J. Chao, "Optimum local decision space partitioning for distributed detection," *IEEE Transactions on Aerospace and Electronic Systems*, vol. 25, no. 4, pp. 536–544, Jul 1989.

[50] Z. Chair and P. Varshney, "Optimal data fusion in multiple sensor detection systems," *IEEE Transactions on Aerospace and Electronic Systems*, vol. AES-22, no. 1, pp. 98–101, Jan. 1986.

[51] E. Drakopoulos and C.-C. Lee, "Optimum multisensor fusion of correlated local decisions," *IEEE Transactions on Aerospace and Electronic Systems*, vol. 27, no. 4, pp. 593–606, Jul 1991.

[52] W. Chang and M. Kam, "Asynchronous distributed detection," *IEEE Transactions on Aerospace and Electronic Systems*, vol. 30, no. 3, pp. 818–826, Jul 1994.

[53] Z. B. Tang, "Optimization of detection networks," Ph.D. dissertation, University of Connecticut, 1990.

[54] J. D. Papastavrou, "Decentralized decision making in a hypothesis testing environment," Ph.D. dissertation, MIT, 1990.

[55] J. Papastavrou and M. Athans, "On optimal distributed decision architectures in a hypothesis testing environment," *IEEE Transactions on Automatic Control*, vol. 37, no. 8, pp. 1154–1169, Aug 1992.

[56] Z.-B. Tang, K. Pattipati, and D. Kleinman, "Optimization of detection networks. II. Tree structures," *IEEE Transactions on Systems, Man and Cybernetics*, vol. 23, no. 1, pp. 211–221, Jan/Feb 1993.

[57] L. K. Ekchian, "Optimal design of distributed networks," Ph.D. dissertation, MIT, 1982.

[58] S. Alhakeem and P. Varshney, "Decentralized bayesian detection with feedback," *IEEE Transactions on Systems, Man and Cybernetics, Part A: Systems and Humans*, vol. 26, no. 4, pp. 503–513, Jul 1996.

[59] S. Thomopoulos, R. Viswanathan, and D. Bougoulias, "Optimal distributed decision fusion," *IEEE Transactions on Aerospace and Electronic Systems*, vol. 25, no. 5, pp. 761–765, Sep 1989.

[60] G. S. Lauer and N. R. Sandell, "Distributed detection of known signal in correlated noise," *Rep. ALPHATECH, Burlington*, Mar. 1982.

[61] J. N. Tsitsiklis and M. Athans, "On the complexity of decentralized decision making and detection problems," *The 23rd IEEE Conference on Decision and Control*, vol. 23, pp. 1638–1641, Dec. 1984.

[62] V. Aalo and R. Viswanathou, "On distributed detection with correlated sensors: two examples," *IEEE Transactions on Aerospace and Electronic Systems*, vol. 25, no. 3, pp. 414–421, May 1989.

[63] R. Viswanathan, S. Thomopoulos, and R. Tumuluri, "Optimal serial distributed decision fusion," *IEEE Transactions on Aerospace and Electronic Systems*, vol. 24, no. 4, pp. 366–376, Jul 1988.

[64] Z. Tang, K. Pattipati, and D. Kleinman, "Optimization of detection networks. I. Tandem structures," *IEEE Transactions on Systems, Man and Cybernetics*, vol. 21, no. 5, pp. 1044–1059, Sep/Oct 1991.

[65] N. Patwari and A. Hero, "Hierarchical censoring for distributed detection in wireless sensor networks," *IEEE International Conference on Acoustics, Speech, and Signal Processing, ICASSP '03*, vol. 4, pp. IV – 848–51 vol.4, April 2003.

[66] F. Cattivelli and A. Sayed, "Distributed detection over adaptive networks based on diffusion estimation schemes," *IEEE 10th Workshop on Signal Processing Advances in Wireless Communications, 2009. SPAWC '09.*, pp. 61 –65, June 2009.

[67] R. Viswanathan and P. Varshney, "Distributed detection with multiple sensors I. fundamentals," *Proceedings of the IEEE*, vol. 85, no. 1, pp. 54–63, Jan 1997.

[68] R. Blum, S. Kassam, and H. Poor, "Distributed detection with multiple sensors II. Advanced topics," *Proceedings of the IEEE*, vol. 85, no. 1, pp. 64–79, Jan 1997.

[69] F. Gini, F. Lombardini, and L. Verrazzani, "Decentralised detection strategies under communication constraints," *IEE Proceedings - Radar, Sonar and Navigation*, vol. 145, no. 4, pp. 199–208, Aug 1998.

[70] S. A. Aldosari and J. M. F. Moura, "Fusion in sensor networks with communication constraints," *Proceedings of the 3rd international symposium on Information processing in sensor networks, IPSN '04*, pp. 108–115, 2004.

[71] J.-J. Xiao and Z.-Q. Luo, "Universal decentralized detection in a bandwidth-constrained sensor network," *IEEE Transactions on Signal Processing*, vol. 53, no. 8, pp. 2617–2624, Aug. 2005.

[72] J.-F. Chamberland and V. Veeravalli, "Decentralized detection in sensor networks," *IEEE Transactions on Signal Processing*, vol. 51, no. 2, pp. 407–416, Feb 2003.

[73] R. Niu, B. Chen, and P. Varshney, "Fusion of decisions transmitted over rayleigh fading channels in wireless sensor networks," *IEEE Transactions on Signal Processing*, vol. 54, no. 3, pp. 1018–1027, March 2006.

[74] V. P. Ying Lin, Biao Chen, "Decision fusion rules in multi-hop wireless sensor networks," *IEEE Transactions on Aerospace and Electronic Systems*, vol. 41, no. 2, pp. 475 – 488, April 2005.

[75] V. Kanchumarthy, R. Viswanathan, and M. Madishetty, "Impact of channel errors on decentralized detection performance of wireless sensor networks: A study of binary modulations, rayleigh-fading and nonfading channels, and fusion-combiners," *IEEE Transactions on Signal Processing*, vol. 56, no. 5, pp. 1761–1769, May 2008.

[76] G. Mergen, V. Naware, and L. Tong, "Asymptotic detection performance of type-based multiple access over multiaccess fading channels," *IEEE Transactions on Signal Processing*, vol. 55, no. 3, pp. 1081–1092, March 2007.

[77] L. Zheng and Y. Yao, "Decentralized detection in relay sensor networks," in *IEEE Military Communications Conference, 2008, MILCOM 2008.*, Nov. 2008, pp. 1 –7.

[78] B. Chen and P. K. Willett, "On the optimality of the likelihood-ratio test for local sensor decision rules in the presence of nonideal channels," *IEEE Transactions on Information Theory*, vol. 51, no. 2, pp. 693–699, Feb. 2005.

[79] H. Chen, B. Chen, and P. Varshney, "Further results on the optimality of the likelihood-ratio test for local sensor decision rules in the presence of nonideal channels," *IEEE Transactions on Information Theory*, vol. 55, no. 2, pp. 828 –832, Feb. 2009.

[80] G. Ferrari and R. Pagliari, "Decentralized binary detection with noisy communication links," *IEEE Transactions on Aerospace and Electronic Systems*, vol. 42, no. 4, pp. 1554–1563, October 2006.

[81] T. Li, "Distributed decision fusion in the presence of link failures," *IEEE Transactions on Aerospace and Electronic Systems*, vol. 32, no. 2, pp. 661 –667, April 1996.

[82] A. Reibman and L. Nolte, "Optimal fault-tolerant signal detection," *IEEE Transactions on Acoustics, Speech and Signal Processing*, vol. 38, no. 1, pp. 179–180, Jan 1990.

[83] J.-F. Chamberland and V. Veeravalli, "Asymptotic results for decentralized detection in power constrained wireless sensor networks," *IEEE Journal on Selected Areas in Communications*, vol. 22, no. 6, pp. 1007 – 1015, Aug. 2004.

[84] J.-F. Chamberland and V. Veercivalli, "The impact of fading on decentralized detection in power constrained wireless sensor networks," *IEEE International Conference on Acoustics, Speech, and Signal Processing, ICASSP '04*, vol. 3, pp. iii–837–40 vol.3, May 2004.

[85] W. Li and H. Dai, "Distributed detection in wireless sensor networks using a multiple access channel," *IEEE Transactions on Signal Processing*, vol. 55, no. 3, pp. 822–833, March 2007.

[86] S. Appadwedula, V. Veeravalli, and D. Jones, "Energy-efficient detection in sensor networks," *IEEE Journal on Selected Areas in Communications*, vol. 23, no. 4, pp. 693 – 702, April 2005.

[87] H.-S. Kim, J. Wang, P. Cai, and S. Cui, "Detection outage and detection diversity in a homogeneous distributed sensor network," *IEEE Transactions on Signal Processing*, vol. 57, no. 7, pp. 2875 –2881, July 2009.

[88] Y. Yuan and M. Kam, "Distributed decision fusion with a random-access channel for sensor network applications," *IEEE Transactions on Instrumentation and Measurement*, vol. 53, no. 4, pp. 1339–1344, Aug. 2004.

[89] L. Liu and J.-F. Chamberland, "Cross-layer optimization and information assurance in decentralized detection over wireless sensor networks," in *Fortieth Asilomar Conference on Signals, Systems and Computers, 2006. ACSSC '06.*, 29 2006-nov. 1 2006, pp. 271 –275.

[90] R. H. Park, "Two-reaction theory of synchronous machines—generalized method of analysis, part i and ii," *American Institute of Electrical Engineers (AIEE) Transactions*, vol. 48, pp. 716–727, 1929.

[91] K. Srivastava and B. Berggren, "Simulation of synchronous machines in phase coordinates including magnetic saturation," *Elsevier Science Electric Power Systems Research*, vol. 56, pp. 177–183, 2000.

[92] P. C. Krause, O. Wasynczuk, and S. D. Sudhoff, *Analysis of Electric Machinery and Drive Systems*. Piscataway, NJ: IEEE Press Power Engineering Series, 2002.

[93] M. Senesky, G. Eirea, and T. J. Koo, "Hybrid modeling and control of power electronics," in *Hybrid Systems: Computation and Control*, ser. Lecture Notes in Computer Science. Springer Berlin / Heidelberg, 2003, vol. 2623/2003, pp. 450–465.

[94] P. J. Antsaklis and X. D. Koutsoukos, "Hybrid systems: Review and recent progress," in *Software-Enabled Control: Information Technology for Dynamical Systems*. Wiley-IEEE, 2003.

[95] H. M. Connally, I. Lodge, R. J. Jackson, and I. Roberts, "Detection of interturn faults in generator rotor windings using airgap search coil," *IEE Conference Publication*, vol. 254, pp. 11–15, 1985.

[96] J. Sottile, F. Trutt, and A. Leedy, "Condition monitoring of brushless three-phase synchronous generators with stator winding or rotor circuit deterioration," *IEEE Transactions on Industry Applications*, vol. 42, no. 5, pp. 1209–1215, Sept.-Oct. 2006.

[97] A. Kulkarni, M. El-Sharkawi, R. Marks, G. Andexler, J. Xing, and I. Kerszenbaum, "Development of a technique for on-line detection of shorts in field windings of turbine-generator rotors: circuit design and testing," *IEEE Transactions on Energy Conversion*, vol. 15, no. 1, pp. 8–13, Mar 2000.

[98] Z. Bo, G. Wang, P. Wang, and G. Weller, "Non-differential protection of generator using fuzzy neural network," *Proceedings of the International Conference on Power System Technology, 1998, POWERCON '98.*, vol. 2, pp. 1072–1076 vol.2, Aug 1998.

[99] W. Breingan, C. Castro, J. Latham, J. Mescua, A. Phadke, J. Postforoosh, E. Schweitzer, W. Strang, F. Tajaddodi, and E. Udren, "Survey of experience with generator protection and prospects for improvements using digital computers," *IEEE Transactions on Power Delivery*, vol. 3, no. 4, pp. 1511–1522, 1988.

[100] J. Penman and H. Jiang, "The detection of stator and rotor winding short circuits in synchronous generators by analysing excitation current harmonics," *International Conference on Opportunities and Advances in International Electric Power Generation*, pp. 137–142, 18-20 Mar 1996.

[101] A. Megahed and O. Malik, "An artificial neural network based digital differential protection scheme for synchronous generator stator winding protection," *IEEE Transactions on Power Delivery*, vol. 14, no. 1, pp. 86–93, Jan 1999.

[102] R. O. Duda, P. E. Hart, and D. G. Stork, *Pattern Classification.* Wiley-Interscience, 2000.

[103] M. McArdle and D. Morrow, "Noninvasive detection of brushless exciter rotating diode failure," *IEEE Transaction on Energy Conversion*, vol. 19, no. 2, pp. 378–383, June 2004.

[104] X.-Y. Li, "A microprocessor-based fault monitor for rotating rectifiers of brushless ac exciters using a pattern-recognition approach," in *Instrumentation and Measurement Technology Conference, 1994. IMTC/94. Conference Proceedings. 10th Anniversary. Advanced Technologies in I & M., 1994 IEEE*, May 1994, pp. 394–397 vol.1.

[105] Y. Malaiya and S. Su, "A survey of methods for intermittent fault analysis," in *National Computer Conference*, New York, June 1979.

[106] R. Abreu, P. Zoeteweij, and A. J. C. van Gemund, "A new Bayesian approach to multiple intermittent fault diagnosis," in *Proceedings of the 21st International Joint Conference on Artificial Intelligence, IJCAI 2009, Pasadena, California, USA, July 11-17, 2009*, 2009, pp. 653–658.

[107] Y. Huang, W.-T. Cheng, C.-J. Hsieh, H.-Y. Tseng, A. Huang, and Y.-T. Hung, "Intermittent scan chain fault diagnosis based on signal probability analysis," in *Design, Automation and Test in Europe Conference and Exhibition, 2004. Proceedings*, vol. 2, feb. 2004, pp. 1072 – 1077 Vol.2.

[108] D. Blough, G. Sullivan, and G. Masson, "Intermittent fault diagnosis in multiprocessor systems," *IEEE Transactions on Computers*, vol. 41, no. 11, pp. 1430 –1441, nov 1992.

[109] M. Basseville and I. V. Nikiforov, *Detection of Abrupt Changes: Theory and Applications*. Prentice Hall, Inc., 1993.

[110] S. M. Kay, *Fundamentals of Statistical Signal Processing, Volume 1: Estimation Theory*, ser. Prentice Hall Signal Processing Series, A. V. Oppenheim, Ed. Prentice Hall PTR, 1993.

[111] Kelly Aerospace Inc., "Alternator FAQ & Troubleshooting," http://www.kellyaerospace.com/alternator_FAQ.html, 2008. [Online]. Available: http://www.kellyaerospace.com/alternator_FAQ.html

[112] Woodward, "Esdr 4 current differential protection relay, manual 37137b," Woodward Governor Company, Tech. Rep., 2007.

[113] Z. Bo, M. Redfern, S. Potts, S. Weller, N. Chin, and F. Jiang, "Non-differential protection of a generator's stator utilizing fault transients," *IEE Seventh International Conference on Developments in Power System Protection*, pp. 503–506, 2001.

[114] P. M. Frank, "Fault diagnosis in dynamic systems using analytical and knowledge-based redundancy–a survey and some new results," *Automatica*, vol. 26, pp. 459–474, 1990.

[115] R. Isermann, "Model-based fault-detection and diagnosis - status and applications," *Annual Reviews in Control*, vol. 29, pp. 71–85, 2005.

[116] J. J. Gertler, *Fault Detection and Diagnosis in Engineering Systems*. Marcel Dekker, Inc., 1998.

[117] S. Narasimhan, P. J. Mosterman, and G. Biswas, "A systematic analysis of measurement selection algorithms for fault isolation in dynamic systems," in *Proceedings of the International Workshop on Diagnosis Principles*, Cape Cod, MA, 1998, pp. 94–101.

[118] P. M. Anderson and A. A. Fouad, *Power System Control and Stability*. Piscataway, NJ: IEEE Press Power Engineering Series, 2005.

[119] E. Mouni, S. Tnani, and G. Champenois, "Comparative study of three modelling methods of synchronous generator," pp. 1551–1556, Nov. 2006.

[120] C. Batard, F. Poitiers, and M. Machmoum, "An original method to simulate diodes rectifiers behaviour with matlab-simulink taking into account overlap phenomenon," *ISIE 2007, IEEE International Symposium on Industrial Electronics, 2007*, pp. 971 –976, June 2007.

[121] A. Tantawy, X. Koutsoukos, and G. Biswas, "Aircraft AC Generators: Hybrid system modeling and simulation," *International Conference on Prognostics and Health Management, PHM08*, 2008.

[122] A. Megahed and O. Malik, "Synchronous generator internal fault computation and experimental verification," *IEE Proceedings-Generation, Transmission and Distribution*, vol. 145, no. 5, pp. 604–610, Sep 1998.

[123] *Simulink 7 Using Simulink*, The MathWorks, Inc., 3 Apple Hill Drive Natick, MA 01760-2098, March 2008.

[124] E. Kyriakides, G. Heydt, and V. Vittal, "On-line estimation of synchronous generator parameters using a damper current observer and a graphic user interface," *IEEE Transactions on Energy Conversion*, vol. 19, no. 3, pp. 499–507, Sept. 2004.

[125] X. Koutsoukos, J. Kurien, and F. Zhao, "Estimation of distributed hybrid systems using particle filtering methods," in *Hybrid Systems: Computation and Control*. Springer Berlin / Heidelberg, 2003, vol. 2623/2003, pp. 298–313.

[126] A. Wald, *Sequential Analysis*. Dover Publications, 2004.

[127] S. Kay, *Intuitive Probability and Random Processes using Matlab*. Springer, 2005.

[128] A. Tantawy, X. Koutsoukos, and G. Biswas, "Detection using intermittent observations for passive wireless sensors," *American Control Conference, ACC2009, St. Louis, Missouri*, 2009.

[129] ——, "Maximum likelihood detection with intermittent observations," *IEEE Conference on Information Sciences and Systems, Johns Hopkins University, Baltimore MD*, 2009.

[130] ——, "Composite hypothesis testing with intermittent observations for passive wireless sensors," *7th IFAC Symposium on Fault Detection, Supervision, and Safety of Technical Processes, Barcelona, Spain*, 2009.

[131] ——, "Optimal performance for detection systems in wireless passive sensor networks," *17th Mediterranean Conference on Control and Automation, MED'09, Thessaloniki, Greece*, 2009.

[132] F. Zhao and L. Guibas, *Wireless Sensor Networks: An Information Processing Approach*. Morgan Kaufmann, 2004.

[133] M. Hata, "Empirical formula for propagation loss in land mobile radio services," *IEEE Transactions on Vehicular Technology*, vol. 29, no. 3, pp. 317 – 325, Aug. 1980.

[134] M. Bhardwaj, T. Garnett, and A. Chandrakasan, "Upper bounds on the lifetime of sensor networks," in *IEEE International Conference on Communications, 2001. ICC 2001.*, vol. 3, 2001, pp. 785 –790 vol.3.

[135] J. Deng, Y. Han, W. Heinzelman, and P. Varshney, "Scheduling sleeping nodes in high density cluster-based sensor networks," *Mobile Networks and Applications*, vol. 10, pp. 825–835, 2005, 10.1007/s11036-005-4441-9. [Online]. Available: http://dx.doi.org/10.1007/s11036-005-4441-9

[136] Y. Chen and Q. Zhao, "On the lifetime of wireless sensor networks," *IEEE Communications Letters*, vol. 9, no. 11, pp. 976 – 978, nov. 2005.

[137] S. Boyd and L. Vandenberghe, *Convex Optimization*. Cambridge University Press, 2004.

[138] H. Stark and J. W. Woods, *Probability and Random Processes with Applications to Signal Processing*, 3rd ed. Prentice Hall, Upper Saddle River, New Jersey, 2002.